GLYCOL NUCLEIC ACIDS AS DUPLEX SCAFFOLD FOR THE DESIGN OF SELF-ASSEMBLED AND SELF-ORGANIZED ARCHITECTURES

A DISSERTATION

in

Chemistry

Presented to the Faculties of Philipps-Universität Marburg in Partial Fulfillment of the Requirements for the Degree of Doctor of Science (Dr. rer. nat.)

Hui Zhou

Hunan, P. R. China

Marburg/Lahn 2011

Department of Chemistry of Philipps-Universität Marburg, accepted as a dissertation on

Supervisor: Prof. Dr. Lilu Zhang

Second reviser: Prof. Dr. Eric Meggers

Date of submission: 07.11.2011

Date of defense: 06.12.2011

Dedicated to my family for their unwavering love and support

Acknowledgments

These past four years in Marburg have been such an incredible experience for me. I have many fond memories of department of chemistry of Philipps-Universität Marburg, and it has been a pleasure to work with so many enthusiastic, bright people during my graduated career. I would like to take this opportunity to express my sincere gratitude to those who have helped me along the way.

First and forest, I would like to thank my research advisor, Prof. Dr. Lilu Zhang, for her enthusiastic support and guidance. Without those, I would not have a thesis to present. She has been a terrific mentor whom I admire greatly for her brilliant creativity, passion of science, and generosity. Some of the things I will remember most about working for Prof. Zhang are that she genuinely cares for her group members. It has been a true honor to work with someone so well respected as both a scientist and an all-around great person. I appreciated Prof. Zhang's patience and understanding over the past years. I wish her and her family all the best and continued success at Philipps-Universität Marburg.

I would also like to thank Prof. Dr. Eric Meggers, the chair of chemical biology of Philipps-Universität Marburg. Prof. Meggers maintains a passion for science that inspires people around him. This passion and all things I learned from Prof. Meggers are important lessons, which will no doubt be helpful in my future career. I wish him and his family all the best and continued success at Philipps-Universität Marburg.

I wish to express my sincere appreciation to my master research advisor, Prof. Dr. Qi Shen at Soochow University, who led me into the field of chemistry. She has been a terrific mentor whom I admire greatly for her passion of science, generosity and great personality. I wish her continued success in her research area and good health.

I would like to thank the facilities directors at Philipps-Universität Marburg because they all maintained excellent facilities. Particularly, Dr. Xiulan Xie and Dr. Uwe Linne who maintained the NMR facility and MS facility, respectively. Without

the hard work and dedication of these people, it would have made my research very difficult.

In the Zhang group, it has been an honor to do my research with lab colleagues. First and foremost, I would like to thank Yonggang Xiang for the generous offering of perylene bismide phosphoramidate that had played a key role in my research. It is an honor to work next to and closely with Yonggang. To be honest, I am not sure how much I would have enjoyed Germany without Yonggang's companionship. I wish him all the best for his Ph.D. study in Marburg.

In the Meggers group, it has been an honor to work with the group members past and present. First and foremost, I must thank Dr. Lei Gong for his help all the time. I wish him and his family all the best and continued success in Xiamen. I would like to thank Dr. Mark Schlegel for helping me to manage the DNA synthesizer and the generous offering of the hydroxypyridone phosphoramidate at the initial time in Marburg. I wish him all the best in his new position. Additionally, I would also like to thank the secretary Ina Pinnschmidt and technician Katja Kräling for their willing help. I am truly thankful to all of the group members of Meggers group, especially to Ph.D. students Sebastian Blank, Sandra Dickmann, Stefan Mollin, Alexander Wilbur, Zhijie Lin and Chen Fu.

During my four years in Marburg, I had the chance to get know some fantastic people, Dong Sun, Min Zhao, Jie Hou, Yumei Lin, Zhiliang You, and Xianzhi Wang. I thank them for bring happiness to me and I wish them all the best.

My family has always been supportive throughout my life, and I would not be where I am today without them. My mother made many sacrifices to give my brother and me the best opportunities possible. I cannot do or say thank you enough for all that she has done for us. I am also thankful to my father for instilling values of a good education and hard work. I would like to express my gratitude to my young brother, Ming, for being an epitome of incredible generosity and support. I thank my future in-laws for their encouragement and understanding while I finished my studies.

Finally, I would like to thank my dear Liu Feng, for filling my life with happiness. I thank her for her love, patience, understanding and support. The past few years have

been such an extraordinary adventure, and I cannot wait to start the next chapter of our lives together.

Table of Contents

List of Schemes

List of Tables

List of Figures

List of Abbreviations

A	adenosine
ACN	acetonitrile
AcOH	acetic acid
aq	aqueous
Ar	aromatic
bp	base pair
br	broad
C	cytosine
Calcd	calculated
CD	circular dichroism
$CDCl_3$	deuterated chloroform
conc	concentrated
CPG	controlled porous glass
d	doublet
dA	2′-deoxyadenpsine
dc	2′-deoxycytosine
DCE	1,2-dichloroethane
DCM	dichloromethane
DDQ	2,3-dichloro-5,6-dicyanobenzoquinone
dG	2′-deoxyguanosine
DMAP	4-dimethylaminopyridine
DMEA	*N*,*N*′-Dimethyl-1,2-ethanediamine
DMF	*N*,*N*-dimethylformamide
DMTr	4,4′-dimethoxytrityl
DMSO	dimethyl sulfoxide

DNA	deoxyribonucleic acid
DSSC	dye sensitised solar cell
EDTA	ethylenediaminetetraacetate acid
eq	equivalent
ESI	electrospray ionization
EtOH	ethanol
G	guanosine
GNA	glycol nucleic acid
GQ	guanosine quadruplex
h	hour(s)
HPLC	high performance liquid chromatography
HRMS	high resolution mass spectrometry
IR	infra-red spectroscopy
L	liters
LNA	locked nucleic acid
LRMS	low resolution mass spectrometry
m	multiplet
M	mol/L
MALDI	matrix assisted laser desorption ionization
MeOH	methanol
min	minute
mL	milliliters
mmol	millimole
NBS	*N*-bromosuccinimide
NMR	nuclear magnetic resonance
ON	oligodeoxynucleotide
PAGE	polyacryamide gel electrophoresis
Ph	phenyl
ppm	parts per million

R_f	retention factor
RT	room temperature
s	singlet
t	triplet
T	thymine
TBAF	tetrabutyl ammonium fluoride
TEAA	triethylammonium acetate
THF	tetrahydrofuran
TLC	thin layer chromatography
T_m	melting temperature
TMPyP	tetrakis[4-(*N*-methylpyridiumyl)]porphyrin
TMS	tetramethylsilane
TNA	L-α-threofuranosyl oligonucleotide
TOF	time of flight
TPP	5,10,15,20-tetraphenylporphyrin
U	uridine
UV-Vis	ultraviolet-visible spectroscopy
μL	microliters
μmol	micromole

Chapter 1 Introduction

Chapter 1.1 Background

Chromophores play important roles as imaging tools in life sciences and as components of industrial dyes and pigments.[1-3] They also participate in natural processes, such as photosynthesis, the processes in circulatory system and so on.[4] Take photosynthesis as an example, the energy conversion of sunlight into chemical material by photosysterms I and II relies on a controlled and defined arrangement of the chlorophyll chromophores, which provides efficient light absorption, energy transfer, and initiation of charge separation.[4] This example demonstrates that the defined chromophore organization is crucial for the performance of an assembly or device. Thus, the design of defined chromophore arrays has been the focus of several studies.

In order to organize chromophores into functional architectures, various approaches for the precise positioning of chromophores have been developed. Among those approaches, DNA constitutes and provides structural scaffolds with unique combinations of properties for the assembly of chromophores[5–7] such as the following: (1) Highly reliable, automated oligonucleotide synthesis enables the solid-phase synthesis of oligonucleotides bearing multiple site-specific modifications; (2) The canonical Watson-Crick base-pairing rule allows the construction of defined helical architectures with high predictability; and (3) The DNA backbone evolves to hold the flat aromatic nucleobases in a well-organized orientation. In the double-helical structure, the nucleobases are nearly perpendicular to the orientation of the backbone and stack on one another. The base-pair distance along the helical axis of B-DNA is 3.4 Å, which provides an ideal basis for the photophysical interactions of chromophores.

However, DNA itself lacks remarkable functionality. Thus, various strategies for generating functionalized nucleic acids have been developed over the last decades. The three general approaches to nucleic acid functionalization are the modifications of the inter-nucleoside phosphate residue, the nucleoside unit, or the DNA termini.[8] Based on aforementioned strategies, chromophores can be incorporated into DNA at

precise sites by following four main aspects: (A) DNA termini modifications, (B) nucleobase replacements, (C) nucleotide replacements, and (D) natural base modifications.

A. DNA termini Modifications.

A large variety of chromophores can be covalently linked to the DNA termini using various methods, such as standard automated oligonucleotide synthesis, post-DNA synthesis and so on. 5′-Terminal modifications are usually achieved by reaction of a phosphitylated modifier with 5′-hydroxyl group, or linking the modification via direct functionalisation of the 5′-position of the ribose moiety (Figure 1.1A).[8a,9] In contrast, the 3′-terminal modifications could be realized by using modified linkers to attach modifications to the 3′-hydroxyl group (Figure 1.1B).[10]

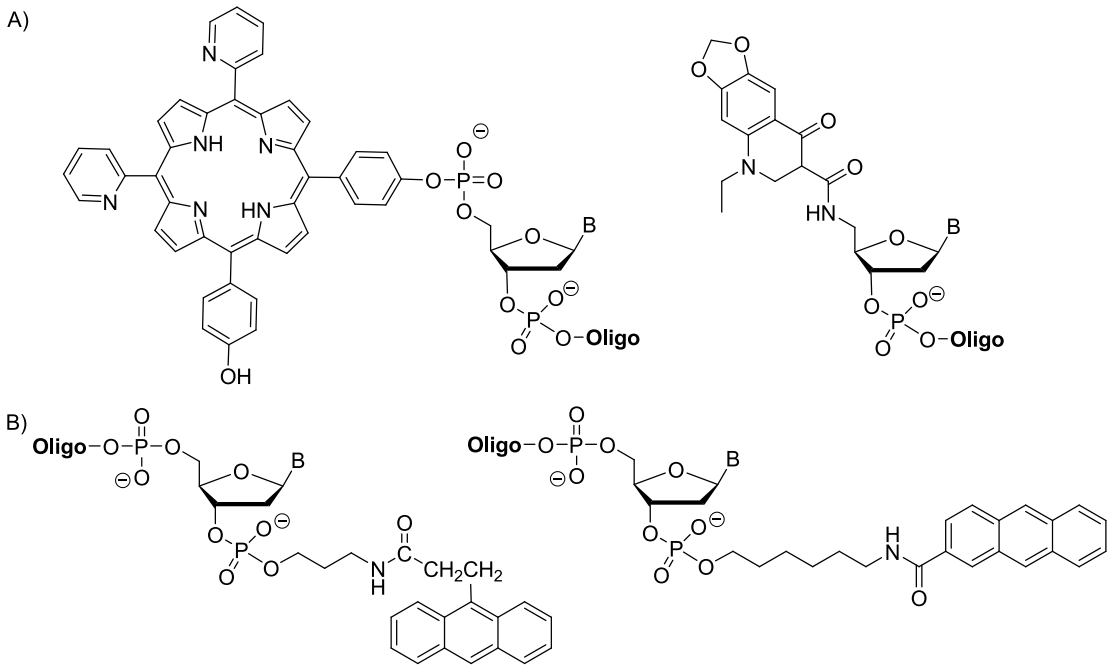

Figure 1.1 Examples of chromophores incorporated into the DNA termini. (A) 5′-terminal modification.[8a,9] (B) 3′-terminal modification.[10]

However, 5′-terminal modifications receive more attention because they are more convenient and commercially feasible compared with 3′-terminal modifications, which have been employed in increasing DNA stability toward enzymatic

degradation,[11] improving duplex thermal stability through capping,[12] enhancing DNA target affinity to facilitate detection,[13] or monitoring DNA structural changes.[9]

B. Nucleobase replacements.

Modification in duplex DNA

The four natural nucleobases represent a set of physicochemical and functional properties but they are limited in numerous aspects, such as polarity, stacking ability, non-fluorescent property, redox potentials and so on. However, the replacement of natural nucleobase with an artificial one provides a wide range of modifications, including but not limited to chromophores.[14] Kool et al. have synthesized a library of fluorescent deoxyribosides based on C-nucleosides and successfully introduced them into DNA (Figure 1.2A), where the natural nucleobases are replaced by chromophores, including pyrene, perylene, terphenyl, terthophene, dimethylaminostilbene, binaphythyl, trinaphthyl, quinacridone and so on. For this strategy, the modifications are incorporated into interior of DNA, namely internal modification.

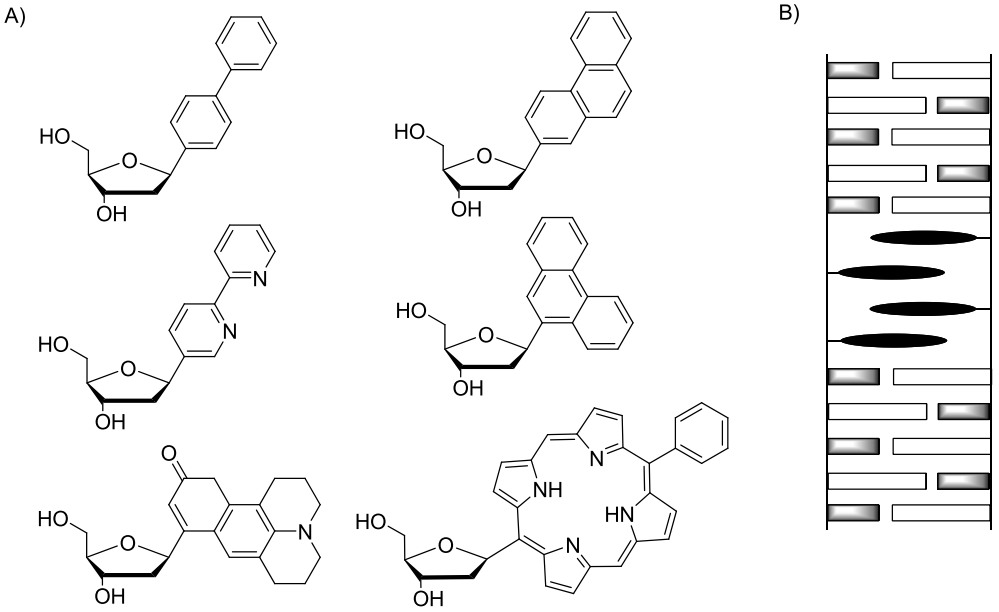

Figure 1.2 (A) A library of fluorescent deoxyribosides was synthesized by Kool et al. Artificial bases replaced the DNA bases. (B) Schematic representation of zipper-like inter-strand stacking within the DNA duplex.[14]

The aromatic nature of chromophores is crucial to forming a stable duplex via π–π stacking. Therefore, chromophores can be designed as artificial nucleobases to stack on one other in a zipper-like fashion (Figure 1.2B).[15,16] Leumann et al. showed that incorporation of multiple biphenyl and/or bipyridyl residues into the middle of duplex can form a zipper-like arrangement array inside the duplex, without perturbing the conformation of DNA duplex. Using this artificial base pairing system, they investigated electron transfer through a stacked phenanthrenyl pair in DNA.[15]

Modification in single strand DNA

Aside from the arrangement of chromophores in duplex DNA, chromophores can be also assembled into a DNA-like single strand, where they interact with each other both physically and electronically like the bases in natural DNA.

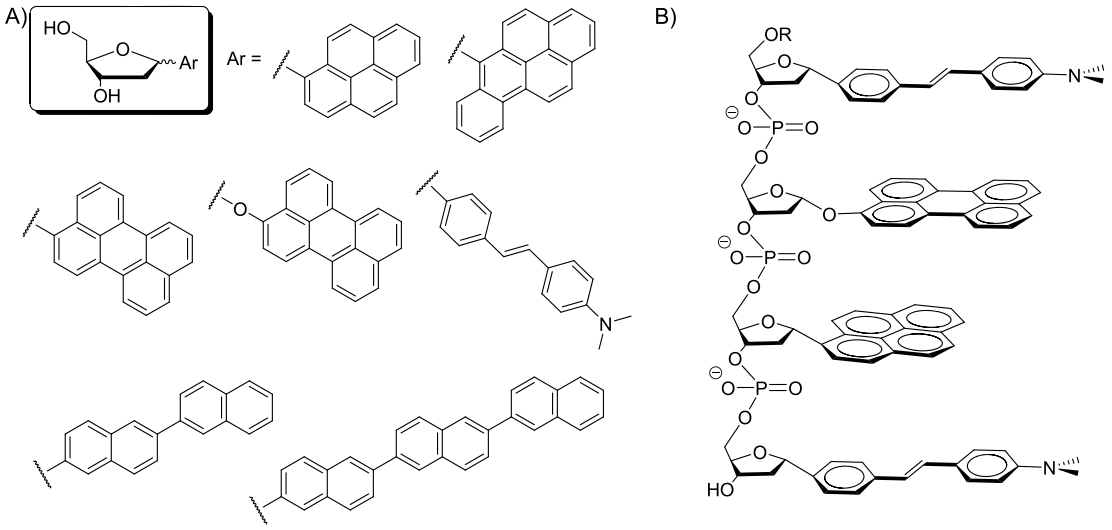

Figure 1.3 (A) Fluorescent deoxyribosides based on C-nucleosides. (B) Structure of one tetrafluor assembled in a DNA backbone.[17,18]

Kool et al. have investigated the interactions of multi-chromophores along the DNA backbone (Figure 1.3).[17,18] The replacement of natural nucleobases with flat aromatic chromophores not only allows them to stack on one other, but also provides water solubility due to the DNA backbone negative charges, thereby mimicking single stranded fluorescent DNA (Figure 1.3B). The coexistence of the different

photophysical interactions within the stacking chromophore array generates interesting optical properties. A 256-member library composed of all combinations of fluorosides bearing quinacridone, pyrene, oxoperylene and dimethylaminostilbene as artificial bases was formed. The tetra-fluorosides displayed remarkably different optical properties from those of individual chromophores, such as high total molar extinction coefficients and large Stockes shifts up to 220 nm.[17] The sequence-dependent fluorescent emission of fluorophores exhibited at least 50 different colors ranging from violet to yellow-orange, and from relatively bright to nearly dark intensities. Subsequently, the study was extended to a 14641-member library composed of 11 fluorosides for the potential application of such tetra-fluorosides to sense UV or visible light exposure with distinct color changes.[18]

Similarly, Inouye et al. synthesized structurally defined fluorosides composed of alkynyl C-nucleosides bearing pyrene, perylene and anthracene as chromophores. Physical and electronic interactions of chromophores were observed and the predominant excimer fluorescence was found to originate not only from homo-oligomers but also from hetero-oligomers.[19]

C. Nucleotide replacements.

Nucleotide replacement involves the complete replacement of an oligonucleotide section (Figure 1.4). In principle, any functional molecule containing two hydroxyl groups can be used to form a building block for DNA automated solid phase synthesis, in which one of the hydroxyl groups is protected by DMTr group, whereas the other one is transformed into phosphoramidite. Generally, two approaches were employed to introduced chromophores into DNA: one is using acyclic linkers based on D- or L-threoninol and so on (Figure 1.4A),[20,21] the other is ro use the chromophore itself as one part of the linker between the phosphodiester functions (Figure 1.4B).[22] By using this method, various self-organization arrays composed of different classes of chromophores, such as methyl red, naphythyl red, perylene bisimide, pyrene, phenanthrene, have been generated by Asanuma,[20] Wagenknecht,[21] Haner[22] et al.

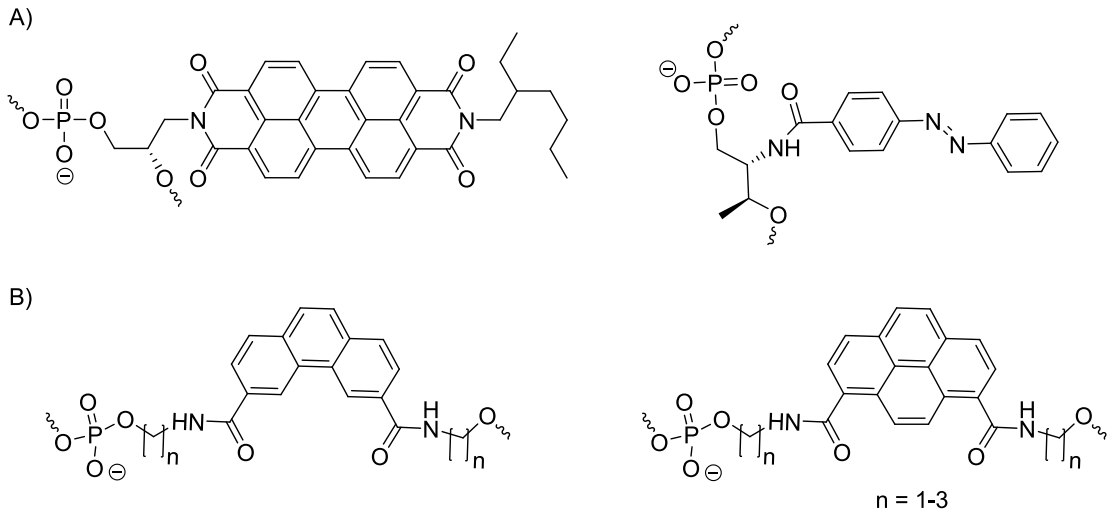

Figure 1.4 Nucleotide replacements. (A) Using acyclic linkers based on D- or L-threoninol.[20,21] (B) Using the chromophore itself as one part of the linker between the phosphodiester functions.[22]

The application of artificial and flexible linkers in the nucleoside analogs is one advantage of this method, which allows the chromophores to intercalate efficiently into DNA. Moreover, the interstrand stacking interactions of chromophores not only stabilize the duplex, but also have a significant influence on the fluorescence properties of duplex. For example, a helically organized chromophore array composed of fourteen pyrenes within DNA, which was resulted from hybridization of two complementary oligopyrene strands each containing seven pyrenes. This modified duplex exhibited a strong enhanced stability (ΔT_m = + 23 ^oC), and a blue shift in the excimer fluorescence when the temperature was decreased.[22]

D. Natural base modifications.

DNA provides an ideal scaffold for introducing chromophores to the outer rim of the DNA and forms a helical array upon duplex hybridization.[23-28] In this aspect, chromophores are located in the grooves of the DNA helix. Thus, this method is so called external modification. Pyrimidines were modified at the 5′-position (Figure 1.5A), and purines were replaced with 7′-deazapurines at the 7′-position (Figure 1.5B) to maintain the helical structure and base pairing. The self-organization of chromophores along the DNA helix without significant perturbation of the canonical

Watson-Crick base-pairing property is one property of this strategy. The major groove is a more commonly chosen site for modification pointing, because it is larger and can accommodate bulky substituents better.

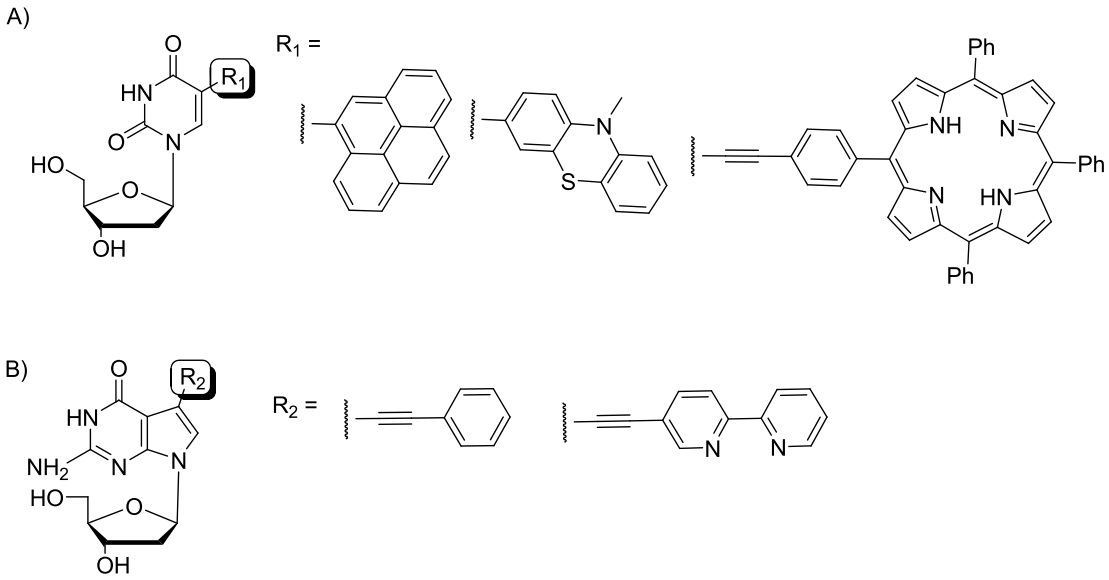

Figure 1.5 DNA natural base modifications. (A) Modification at the 5′-position of pyrimidine.[25,26] (B) Modification at the 7′-position with deazapurine.[24]

A variety of chromophores have been attached with respect to natural nucleoside modification, which may be potentially applied in redox and fluorescence labeling, drug delivery, and nanotechnology. Nevertheless, by helical arranging chromophores, DNA has been used as a scaffold to create photonic and electronic wires. Stulz[25] and Wagenkenecht[26] et al. have shown that chromophores can be covalently bonded to DNA by nucleoside modification, and aligned within the major groove to form helical arrays which exhibit unique optical properties such as solvatochromism or neighbourhood-dependent exciplex-type fluorescence and so on. For example, a zipper-like assembly of eleven porphyrins on the major groove of DNA resulting from the alternating arrangement of chromophores on two complementary strands, which showed a enhanced stability even porphyrins were inserted by Zn(II) ions. Up on annealing of the free and metalated strands, fluorescence of the Zn-porphyrin was partially quenched at the same time fluorescence of the free porphyrin was increased, indicating the efficient energy transfer in this system.[25d] These results represent the

potential of DNA as a scaffold to arrange metal ions on a nanometer scale.

Overall, chromophores can be incorporated into DNA at precise sites by performing terminal, internal, or external modifications, generating defined chromophore arrays in the interior and grooves of duplex DNA or in single DNA-like strands. The chromophore organization proves to exhibit enhanced electronic communication properties and promote various forms of photophysical interactions in the excited state, such as energy transfer, excimer, exciplex, charge-transfer interactions and so on.

Usually, phosphoramidites of modified nucleotides are incorporated into DNA by automated solid phase synthesis, enabling the synthesis of oligonucleotides with more than 100 bases. However, due to the stereocenters in the deoxyribose moiety (especially the anomeric C1′-stereocenter), the synthesis of phosphoramidites of 2′-deoxynucleosides is very time-consuming because it includes long-reaction sequence and chromatographic separation of diastereomers, which is challenging to scale up. Thus, the chemical synthesis of artificial nucleotides is a critical bottleneck for progress in this area of research.

To address the problem of tedious synthesis of nucleotide building blocks and retain the desired base-pairing properties, Meggers et al. developed the glycol nucleic acid (GNA) consisting of a simplified acyclic propylene glycol phosphodiester backbone, which uniquely combines atomic economy, structural simplicity, and high duplex stability (Figure 1.6).[29]

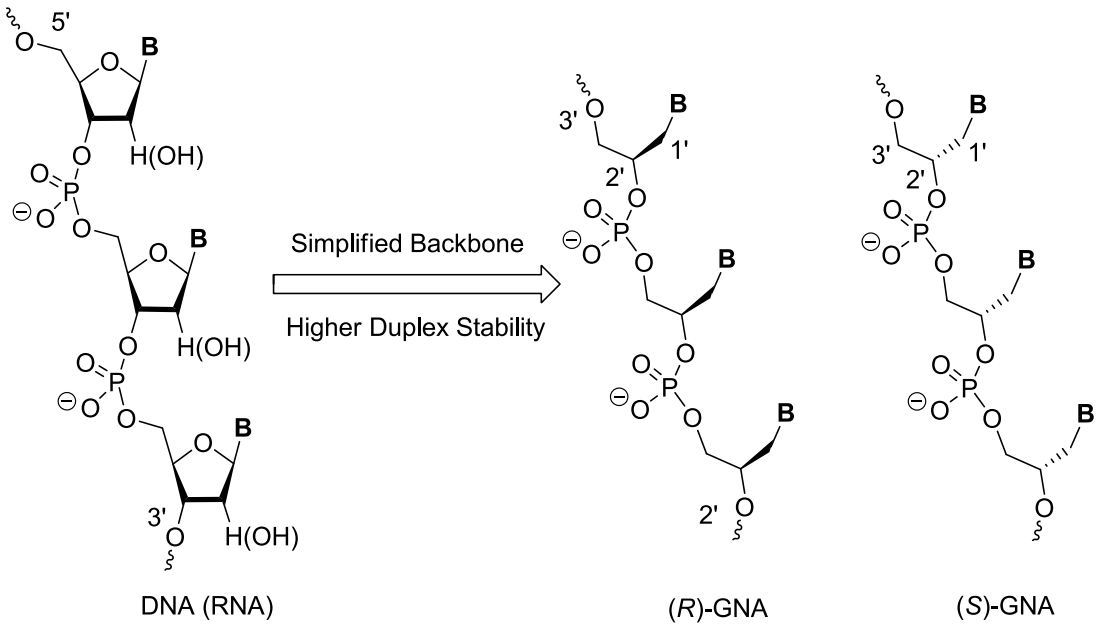

Figure 1.6 Comparison of the constitutions of DNA and RNA, with both enantiomers of GNA.[29]

Chapter 1.2 Previous work with glycol nucleic acids (GNA)

Analogous to DNA and RNA, the homoduplex formation of GNA relies on the Watson-Crick base pairing with antiparallel strand complementarity and 1:1 strand stoichiometry. (*R*)-GNA and (*S*)-GNA do not significantly cross-pair with each other, either in a parallel or antiparallel manner.[29,33] GNA duplexes exhibit high thermal and thermodynamic stabilities, significantly exceeding those of analogous duplexes of DNA and RNA.[29,33,34] For example, in a 18mer GNA is much more stable than DNA and RNA.[29]

Table 1.1 Thermal stabilities of GNA, DNA and RNA duplexes.[29]

System	Sequence	T_m (°C)
GNA	3′-TAAAATTTATATTATTAA-2′ 2′-ATTTTAAATATAATAATT-3′	63
DNA	5′-TAAAATTTATATTATTAA-3′ 3′-ATTTTAAATATAATAATT-5′	41
RNA	5′-TAAAATTTATATTATTAA-3′ 3′-ATTTTAAATATAATAATT-5′	43

Beside the high duplex stability, its straightforward chemical synthesis is another very attractive feature of GNA. Long-reaction sequence and the painstaking separation of anomeric mixtures are not issues for GNA. As shown in Scheme 1.1, propylene glycol nucleotides with natural or artificial bases for automated solid-phase nucleic acid synthesis can be easily obtained through several steps by the regioselective and stereospecific epoxide ring-opening of protected glycidols.[30-32]

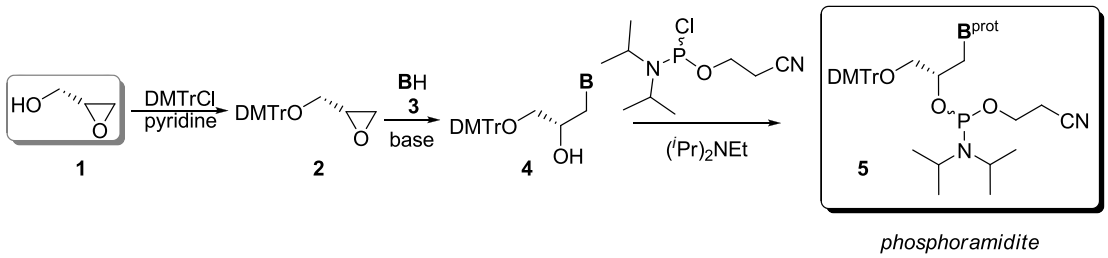

Scheme 1.1 General synthesis of (*S*)-phosphoramidite building blocks for the synthesis of GNA oligonucleotide (**B** represents a natural base or artificial base).[30-32]

The study of a crystal structure of a (*S*)-GNA duplex reveals that the GNA double helix is distinct from canonical A- and B- form nucleic acids, and it may be described as a helical ribbon loosely wrapped around the helical axis (Figure 1.7).[35] (*S*)-GNA undergoes extensive zipper-like interstrand interactions and at the same time possesses a reduced intrastrand base–base stacking interaction because of a large average slide between neighboring base pairs. (*S*)-GNA only displays one large groove, whereas the canonical major groove is a convex surface.

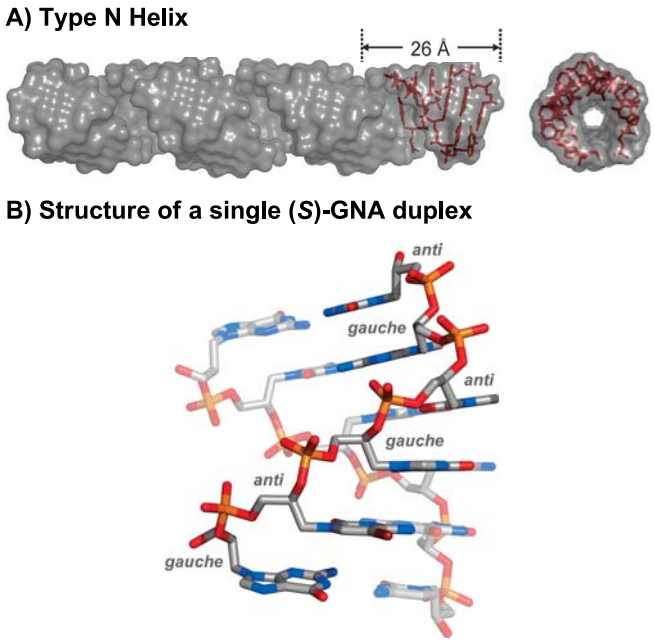

Figure 1.7 (A) Determined structures of (*S*)-GNA duplex: 3′-G^{Br}CGCGC-2′ (Br-GNA). Single duplexes are shown in red sticks. On the right are views along the helical axis. (B) Structure of a single Br-GNA.[35]

Considering the unique combination of high duplex stability, high-base pairing fidelity, and easy synthetic access of GNA nucleotide building blocks, Meggers et al. started investigating the functionalization of GNA by incorporating artificial nucleotides into GNA oligonucleotides. In order to tune the electronic and magnetic properties of nucleic acids, they explored the properties of metal-ion-mediated base pairing in GNA duplexes (Figure 1.8).[36] A nickel(II)-mediated pyridylpurine homobase pair (**P**-Ni-**P**) or a copper(II)-mediated hydroxypyridone homobase pair (**M**-Cu-**M**) was introduced into GNA,[36] which had been developed for metal-mediated base pairing in DNA.[37,89]

The study of the metal ion-dependent duplex formation reveals that the pyridylpurine base pair **P**:**P** in GNA is most strongly stabilized by Ni^{2+} ions among the tested ions.[36] Ni^{2+}-induced stabilization of the pyridylpurine base pair in GNA is comparable with that of the analogous 2′-deoxynucleotide pyridylpurine base pair in the DNA duplex.[38]

In contrast, the hydroxypyridone base pair **M**:**M** is most strongly stabilized by Cu^{2+} ions.[36] The copper(II)-induced stabilization of the hydroxypyridone base pair in

GNA significantly exceeds the stabilization of the analogous 2′-deoxynucleotide hydroxypyridone base pair in DNA, indicating that the Cu^{2+} -mediated **M**:**M** base pair is well-accommodated in the GNA duplex compared with DNA.[37]

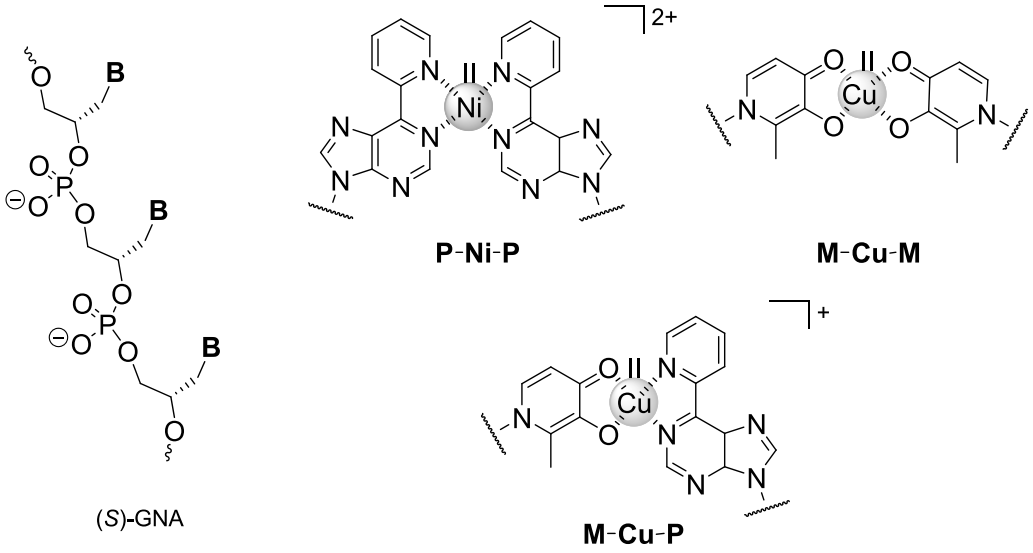

Figure 1.8 Metallo-base pairs investigated in GNA.[36]

Furthermore, the metal-mediated cross-pairing of the hydroxypyridone and pyridylpurine chelates was also investigated in GNA duplexes. The heterobase pair **M**:**P** behaves similarly to the hydroxypyridone homobase pair **M**:**M** in its metal selectivity, and the Cu^{2+}-mediated **M**:**P** base pair exhibits higher stabilization than the Cu^{2+}-mediated **M**:**M** base pair. As far as we know, Cu^{2+}-mediated **M**:**P** is the most stable base pair for GNA to date.

To understand better the metallo-GNA duplex structure, Meggers et al. investigated the crystal structure of a metallo-GNA duplex formed from the Cu^{2+}-mediated pairing of the self-complementary strand 3′-CGHATMCG-2′.[39] The duplex structure reveals that the GNA backbone accommodates the extended size of the metallo-base pair by transforming the conformation of the hydroxypyridone base pair.[36] The crystal structure and high thermal stability of the GNA duplex containing the copper (II)-hydroxypyridone base pair demonstrate that the metallo-base pair fits very well into the overall GNA duplex structure.

With those results in mind, a study was proposed whose main goal was to investigate the properties of chromophore assembly based on GNA backbone.

From the synthesis point of view, the modified GNA nucleotide building blocks are economically accessible starting from commercially available glycidol, which provides a promising straightforward methodology for the incorporation of chromophores into an entire artificial nucleic acid backbone. Thus, the initial goal is to synthesize a library of modified GNA nucleotide building blocks with chromophores as artificial bases for the automated solid-phase nucleic acid synthesis.

From the structure point of view, GNA undergoes extensive zipper-like interstrand interactions and at the same time possesses a reduced intrastrand base–base stacking interaction. Moreover, the GNA backbone can adjust its conformation according to the nature of the artificial base pairs. With the features, GNA duplex architecture may provide challenging opportunities to arrange chromophores in a controlled and unique fashion. Therefore, the next goal is to use GNA as a simplified general duplex scaffold for the design of self-assembled and self-organized functional architectures, and then investigate the properties of assembled chromophores based on GNA backbone.

Furthermore, considering the usefulness of GNA backbone in the economical and convenient synthesis of artificial nucleic acid, functional GNA architectures are expected to evolve into biotechnological tools and used as analogs of DNA in the medicinal and nanotechnological fields.

Chapter 1.3 References

1. Hoeben, F. J.M.; Jonkheijm, P.; Meijer, E.W.; Schenning, A. P. H. J. *Chemical Reviews* **2005**, *105*, 1491.
2. Palermo, V.; Schwartz, E.; Finlayson, C. E.; Liscio, A.; Otten, M. B. J.; Trapani, S.; Müllen,K.; Beljonne, D.; Friend, R. H.; Nolte, R. J. M.; Rowan A. E.; Samori, P. *Advanced Materials* **2010**, *22*, E81.
3. (*a*) Wasielewski, M. R.; *Accounts of Chemical Research* **2009**, *42*, 1910; (*b*) Astruc, D.; Boisselier, E.; Ornelas, C. *Chemical Reviews* **2010**, *110*, 1857; (*c*) Schenning, A. P. H. J.; Meijer, E. W. *Chemical Communication* **2005**, 3245.
4. Schwartz, E.; Gac, S. Le; Cornelissen, J. J. L. M.; Nolte, R. J. M.; Rowan, A. E. *Chemical Society Reviews* **2010**, *39*, 1576.
5. (*a*) Enthart, E. M.; Wagner, C.; Barbaric, J.; Wagenknecht, H.-A. *Tetrahedron*, **2007**, *63*, 3434; (*b*) Wagenknecht, H.-A. *Angewandte Chemie International Edition* **2009,** *48*, 2838; (*c*) Varghese, R.; Wagenknecht, H.-A. *Chemical Communication* **2009**, 2615; (*d*) Gao, J.; Watanabe, S.; Kool, E. T. *Journal of the American Chemical Society* **2004**, *126*, 12748.
6. Malinovskii, V. L.; Wenger, D.; Häner, R. *Chemical Society Reviews* **2010**, *39*, 410.
7. Hannah, K. C.; Armitage, B. A. *Accounts of Chemical Research* **2004**, *37*, 845.
8. (a) Uhlmann, E.; Peyman, A. *Chemical Reviews* **1990**, *90*, 544-584; (b) Varghese, R.; Wagenhnecht, H.-A. *Chemical Communication* **2009**, 2615-2624; (c) Schwartz, E.; Gac, S. L.; Cornelissen, J. J. L. M.; Nolte, R. J. M.; Rowan, A. E. *Chemical Society Reviews* **2010**, *39*, 1576-1599; (d) Bandy, T. J.; Brewer, A.; Burns, J. R.; Marth, G.; Nguyen, T.; Stulz, E. *Chemical Society Reviews* **2011**,*40*,138-148.
9. (a) Balaz, M.; Li, B. C.; Steinkruger, J. D.; Ellestad, G. A.; Nakanishi, K.; Berova, N. *Organic and Biomolecular Chemistry* **2006**, *4*, 1865–1867; (b) mammmana, A.; Pescitelli, G.; Asakawa, T.; Jockusch, S.; Petrovic, A. G.; Monaco, R. R.;

Purrello, R.; Turro, N. J.; Nakanishi, K.; Ellestad, G. A.; Balaz, M.; Berova, N. *Chemistry – A European Journal* **2009**, *15*, 11853-11866.

10. Mukae, M.; Ihara, T.; Tabara, M.; Jyo, A. *Organic and Biomolecular Chemistry* **2009**, *7*, 1349–1354.
11. Winkler, J.; Gilbert, M.; Kocourková, A.; Stessl, M.; Noe, C. R. *ChemMedChem* **2008**, *3*, 101-110.
12. Mokhir, A. A.; Tetzlaff, C. N.; Herzberger, S.; Mosbacher, A.; Richert, C. *Journal of Combinatorial Chemistry* **2001**, *3*, 374-386.
13. Fahlman, R. P.; Sen, D. *Journal of the American Chemical Society* **2002**, *124*, 4610–4616.
14. Kool, E. T. *Accounts of Chemical Research* **2002**, *35*, 936-943.
15. Brotschi, C.; Mathis, G.; Leumann, C. J. *Chemistry – A European Journal* **2005**, *11*, 1911-1923.
16. Hainke, S.; Seitz, O. *Angewandte Chemie International Edition* **2009,** *48*, 8250-8253.
17. (a) Gao, J. M.; Strässler, C.; Tahmassebi, D.; Kool, E. T. *Journal of the American Chemical Society* **2002**, *124*, 11590-11591; (b) Cuppoletti, A.; Cho, Y. J.; Park, J.-S.; Strässler, C.; Kool, E. T. *Bioconjugate chemistry* **2005**, *16*, 528-534; (c) Wilson, J. N.; Cho, Y. J.; Tan, S.; Cuppoletti, A.; Kool, E. T. *ChemBioChem* **2008**, *9*, 279-285; (d) Wilson, J. N.; Gao, J. M.; Kool, E. T. *Tetrahedron*, **2007**, *63*, 3427-3433.
18. Teo, Y. N.; Wilson, J. N.; Kool, E. T. *Journal of the American Chemical Society* **2009**, *131*, 3923-3933.
19. Chiba, J.; Takeshima, S.; Mishima, K.; Maeda, H.; Nanai, Y.; Mizuno, K.; Inouye, M. *Chemistry-A European Journal* **2007**, *13*, 8124-8130.
20. (a) Asanuma, H.; Ahirasuka, K.; Komiyama, M. *Chemical Letter* **2002**, *49*; (b) Kashida, H.; Tanaka, M.; Baba, S.; Sakamoto, T.; kawai, H.; Asanuma, H.; Komiyama, M. *Chemistry – A European Journal* **2006**, *12*, 1911-1923.
21. (a) Wagner, C.; Wagenknecht, H.-A. *Organic Letter* **2006**, *8*, 419; (b) Baumstark, D.; Wagenknecht, H.-A. *Angewandte Chemie International Edition* **2008,** *47*,

2612; (c) Baumstark, D.; Wagenknecht, H.-A. *Chemistry – A European Journal* **2008**, *14*, 6640.

22. (a) Ackermann, D.; Häner, R. Helvetica *Chimica Acta* **2004**, *87*, 2790; (b) Langenegger, S. M.; Häner, R. *ChemBioChem* **2005**, *6*, 2149; (c) Langenegger, S. M.; Häner, R. *Chemical Communcation* **2005**, *6*, 2149; (d) Malinovskii, V. L.; Samain, F.; Häner, R. *Angewandte Chemie International Edition* **2007**, *46*, 4464.
23. (a) Sørensen, M. D.; Petersenb, M.; Wengel, J. *Chemical Communication* **2003**, 2130; (b) Hrdlicka, P. J.; Babu, B. R.; Sørensen, M. D.; Wengel, J. *Chemical Communication* **2004**, 1487.
24. (a) Vrabel, M.; Horakova, P.; Pivonkova, H.; Kalachova, L.; Cernocka, H.; Cahova, H.; Pohl, R.; Sebest, P.; Havran, L.; Hocek, M.; Fojta, M. *Chemistry – A European Journal* **2009**, *15*, 1144-1154; (b) Jager, S.; Rasched, G.; kornreich-Leshem, H.; Engeser, M.; Thum, O.; Famulok, M. *Journal of the American Chemical Society* **2005**, *127*, 15071.
25. (a) Fendt, L.-A.; Bouamaied, I.; Thöni, S.; Amiot, N.; Stulz, E. *Journal of the American Chemical Society* **2007**, *129*, 15319; (b) Bouamaied, I.; Nguyen, T. N.; Rühl, T.; Stulz, E. *Organic & Biomoleculor Chemistry* **2008**, *6*, 3888; (c) Nguyen, T. N.; Brewer, A.; Stulz, E. *Angewandte Chemie International Edition* **2009**, *48*, 1974; (d) Bouamaied, I.; Fendt, L.-A.; Haeussinger, D.; Wiesner, M.; Thoeni, S.; Amiot, N.; Stulz, E. *Nucleotides Nucleic Acids* **2007**, ***26***, 1533.
26. Barbaric, J.; Wagenknecht, H.-A.; *Organic and Biomolecular Chemistry* **2006**, *4*, 2088–2090.
27. Datta, B.; Schuster, G. B. *Journal of the American Chemical Society* **2008**, *130*, 2965.
28. (a) Nakanura, M.; Ohtoshi, Y.; Yamana, K. *Chemical Communication* **2005**, 5163. (b) Nakanura, M.; Shimomura, Y.; Ohtoshi, Y.; Sasa, K.; Hayashi, H.; Nakano, H.; Yamana, K. *Organic and Biomolecular Chemistry* **2007**, *5*, 1945–1951; (c) Nakanura, M.; Murakami, Y.; Sasa, K.; Hayashi, H.; Yamana, K. *Journal of the American Chemical Society* **2008**, *130*, 6904.
29. Zhang, L.; Peritz, A.; Meggers, E. *Journal of the American Chemical Society*

2005, *127*, 4174 –4175.

30. Zhang, L.; Peritz, A. E.; Meggers, E. *Synthesis* **2006**, 645– 653.
31. Schlegel, M. K.; Meggers, E. *Journal of Organic Chemistry* **2009**, *74*, 4615–4618.
32. Schlegel, M. K.; Zhang, L.; Pagano, N.; Meggers, E. *Organic and Biomolecular Chemistry* **2009**, *7*, 476–482.
33. Zhang, L.; Peritz, A.; Meggers, E. *Journal of the American Chemical Society* **2005**, *127*, 4174 –4175.
34. Schlegel, M. K.; Peritz, A. E.; Kittigowittana, K.; Zhang, L.; Meggers, E. *ChemBioChem* **2007**, *8*, 927–932.
35. Schlegel, M. K.; Meggers, E. *Journal of Organic Chemistry* **2009**, *74*, 4615–4618.
36. Schlegel, M. K.; Essen, L.-O.; Meggers, E. *Chemical Communication* **2010**, *46*, 1094–1096.
37. Schlegel, M. K.; Zhang, L.; Pagano, N.; Meggers, E. *Organic and Biomolecular Chemistry* **2009**, *7*, 476–482.
38. Tanaka, K.; Tengeiji, A.; Kato, T.; Toyama, N.; Shiro, M.; Shionoya, M. *Journal of the American Chemical Society* **2002**, *124*, 12494 –12498.
39. Switzer, C.; Sinha, S.; Kim, P. H.; Heuberger, B. D. *Angewandte Chemie International Edition* **2005**, *44*, 1529-1532.
40. Schlegel, M. K.; Essen, L.-O.; Meggers, E. *Journal of the American Chemical Society* **2008**, *130*, 8158 –8159.

Chapter 2 Synthesis of Chromophore Glycol Nucleotides

Chapter 2.1 Introduction

Epoxides are widely used as synthetic intermediates and considered as "spring-loaded" rings for nucleophilic ring-opening reaction.[1] The nucleophilic ring-opening reaction of epoxides provides an efficient approach to convert readily available, inexpensive chemicals into chiral, nonracemic products.[2] A lot of nucleophiles have been employed successfully in ring-opening reactions, including carbon-,[3-8] nitrogen-,[9,10] oxygen-,[11] sulphur-,[12] halogen-based[13] nucleophiles and so on.

Among those reactions, the nucleophilic ring-opening reaction of epoxides by carbon-based nucleophiles provides a useful method, which generates new carbon-carbon σ bonds in a very simple and stereo-defined fashion. Epoxides can be successfully alkylated by various organometallic reagents, such as organomagnesium,[3] organolithium,[4] organocopper,[5] organozinc,[6] organoaluminum,[7] organolanthanide[8] compounds.

It is convenient to start from the enantiomerically enriched terminal epoxides and allow them to react with the necessary carbon nucleophiles in a regioselective fashion to offer enantiopure alcohols. This method has been widely used in the natural products synthesis, where organocopper reagents alkylate enantiopure terminal epoxides to give useful products.[14]

In this study, we describe the synthesis of glycol nucleoside phosphoramidites GNA building blocks of different chromophores, which was based on the nucleophilic ring-opening reaction of dimethoxytritylated (*S*)-glycidol by carbon nucleophiles.

Chapter 2.2 The synthesis of glycol nucleoside phosphoramidites based on the nucleophilic ring-opening of epoxides

Based on the nucleophilic ring-opening reaction of epoxides by carbon nucleophiles, the synthesis of chromophore glycol nucleosides is involved three methods: (1) the application of Grignard reagents, (2) the application of Grignard reagents containing a metallation/transmetallation protocol, (3) the application of organolithium reagents.

1. The application of Grignard reagents

The nucleophilic ring-opening reaction of epoxides by Grignard reagents is a widely used method for generating new carbon-carbon σ bonds.[3] Scheme 2.1 shows the general synthesis of glycol nucleoside phosphoramidites, which was based on the copper(I)-catalyzed reaction of Grignard reagents with epoxide.

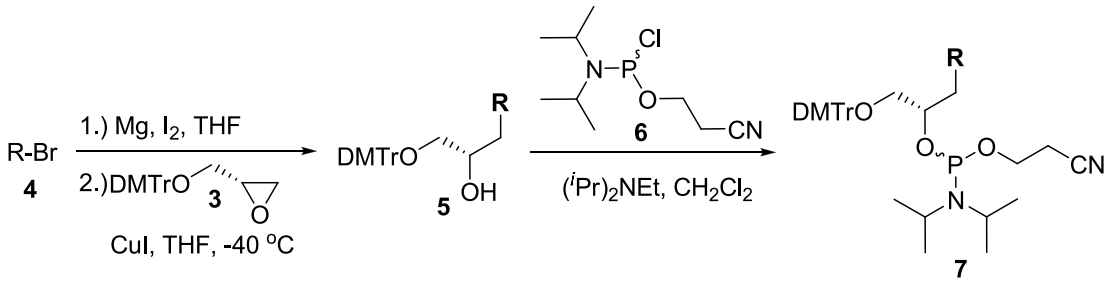

Scheme 2.1 The general synthesis of glycol nucleoside phosphoramidites based on Grignard reagents.

Grignard reagents in this study are formed *via* the reaction of the corresponding aryl bromide with magnesium metal. In the presence of I_2, bromobezene (**4a**), 3-bromobiphyenyl (**4b**), 4-bromobiphyenyl (**4c**), 4-bromonaphthalene (**4d**) and 9-bromophenanthrene (**4e**) were converted into Grignard reagents successfully by reacting with magnesium in THF, respectively. Being catalyzed with CuI, the resulting Grignard reagents underwent a regioselective and stereospecific ring-opening with dimethoxytrityliated (*S*)-glycidol (**3**)[7] at -40 °C to afford the ring

opening products **5a** (85%), **5b** (73%), **5c** (74%), **5d** (61%) and **5e** (65%), respectively. Then, compound **5** followed by the reaction with phosphoramidite reagent **6** in the presence of Hünig's base to afford the phosphoramidite product **7a** (84%), **7b** (85%), **7c** (85%), **7d** (80%) and **7e** (78%), respectively.

Table 2.1 The synthesis of glycol nucleoside phosphoramidites based on Grignard reagents.

Entry	Substrate		Ring-opening product (yield %)	Phosphoramidite product (yield %)
	R-Br	R	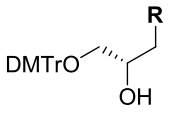	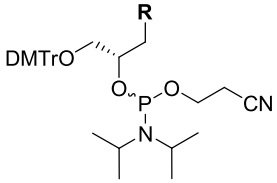
1	4a		5a (85)	7a (84)
2	4b	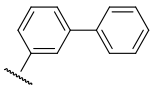	5b (73)	7b (85)
3	4c	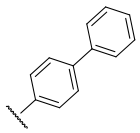	5c (74)	7c (85)
4	4d	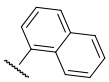	5d (61)	7d (80)
5	4e	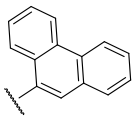	5e (65)	7e (78)

As shown in table 2.1, glycol nucleoside phosphoramidite building blocks of benzene **7a**, biphyenyl **7b**, biphyenyl **7c**, naphthalene **7d** and phenanthrene **7e** were obtained in two steps from dimethoxytritylated (*S*)-glycidol (**3**) with overall yields of 71%, 62%, 63%, 49% and 51%, respectively.

2. The application of Grignard reagents containing a metallation/transmetallation protocol

Although ring-opening reaction of epoxide **3** by Grignard reagents is efficient to produce the precursors of phosphoramidites, there is a few of aryl bromide compounds that could not be converted into Grignard reagents directly by reacting with magnesium metal, such as 2-bromoanthracene or 1-bromopyrene. However, as shown in scheme 2.2, a Grignard reagent could be formed by reacting of organolithium compound and one equivalent of magnesium halide (scheme 2.2).[1] This transmetallation method may provide access to Grignard reagents that are difficult to prepare directly.

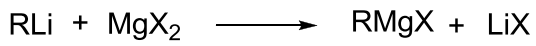

Scheme 2.2 The formation of Grignard reagent by transmetallation reaction.

A protocol containing metallation/transmetallation sequence was applied to produce the desired Grignard reagents of 2-bromoanthracene (**8a**)[16] and 1-bromopyrene (**8b**).[17] Scheme 2.3 shows the general synthesis of glycol nucleoside phosphoramidites based on Grignard reagents containing a metallation/transmetallation sequence.

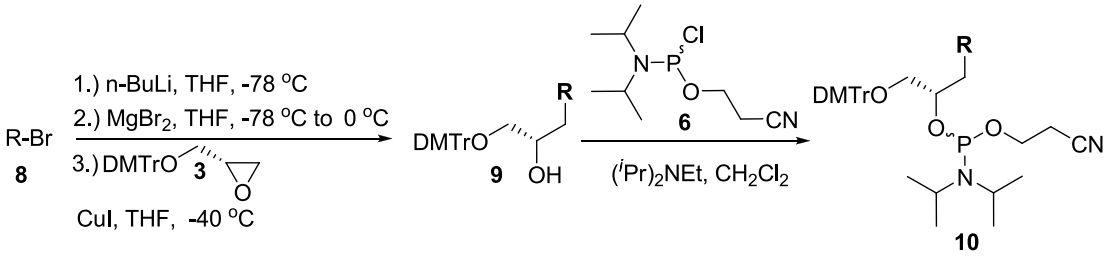

Scheme 2.3 The general synthesis of glycol nucleoside phosphoramidites based on Grignard reagents containing a metallation/transmetallation sequence.

As shown in Scheme 2.3, compound **8** was first converted into lithium species by reacting with *n*-BuLi at -78 °C in THF. The lithium species was subsequently

transmetallated into a Grignard reagent by treatment with freshly prepared $MgBr_2$ (synthesized from Mg turnings and 1, 2-dibromoethane). In the presence of CuI, the resulting solution underwent a regioselective and stereospecific ring-opening reaction with epoxide **3** to afford the compounds **9a** and **9b** in yields of 53% and 50%, respectively. The subsequent reaction with the phosphoramidite reagents **6** in the presence of Hünig's base afforded phosphoramidite products **10a** and **10b** in yields of 69% and 84%, respectively.

Table 2.2 The synthesis of glycol nucleoside phosphoramidites based on Grignard reagents containing a metallation/transmetallation sequence.

Entry	Substrate		Ring-opening product (yield %)	Phosphoramidite product (yield %)
	R-Br	R	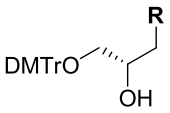	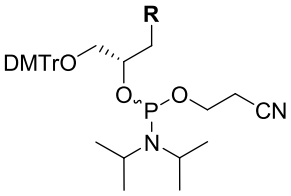
1	8a	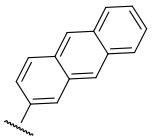	9a (53)	10a (69)
2	8b	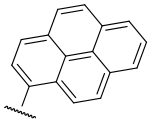	9b (50)	10b (84)

Altogether, through the application of Grignard reagents containing a metallation/transmetallation sequence in the ring-opening reaction, the glycol nucleoside phosphoramidite GNA building blocks of **10a** and **10b** were synthesized in two steps from dimethoxytritylated (*S*)-glycidol (**3**) with overall yields of 37% and 42%, respectively.

3. The application of organolithium reagents

Besides Grignard reagents, organolithium reagents are also frequently used in the nucleophilic ring-opening reaction of epoxides for the synthesis of alcohols, including alkyl-, alkenyl-, alkynyl-, aryllithium and so on. Because of their relatively low reactivity, activation by coordination of a Lewis acid, such as $BF_3 \cdot Et_2O$, to the oxygen atom of the epoxides is required.[1] Furthermore, without the Lewis acid, the ring-opening reaction would be curtailed because of the competing reactions arising from the Lewis acidity or basicity of the organometallic reagent.[18] Scheme 2.4 displays the general synthesis of glycol nucleoside phosphoramidites based on organolithium reagents.

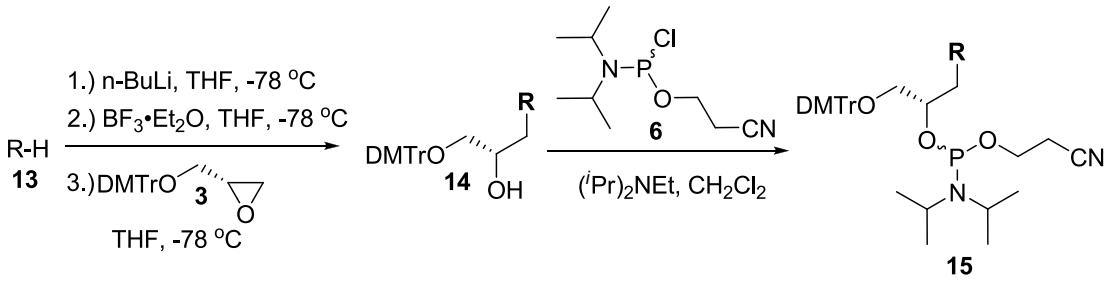

Scheme 2.4 The general synthesis of glycol nucleoside phosphoramidites based on organolithium reagents.

For the synthesis of compound **14a** (table 2.3, entry 1), although the 9-bromoanthracene (**13a**) can be easily converted to Grignard reagent,[13] the resulting Grignard reagent did not react with epoxide to give desired ring-opening product. However, **14a** can be synthesized in 60% yield through the ring-opening reaction of epoxide (**3**) with organolithium reagent, which was prepared by metal-halogen exchange reaction between **13a** and *n*-BuLi at -78 °C in Et_2O. The subsequent reaction with phosphoramidite reagents **6** in the presence of Hünig's base afforded phosphoramidite product **15a** in 74% yield.

Table 2.3 The synthesis of glycol nucleoside phosphoramidites based on organolithium reagents.

Entry	Substrate		Ring-opening Product (yield %)	Phosphoramidite product (yield %)
		R	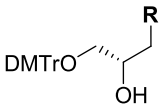	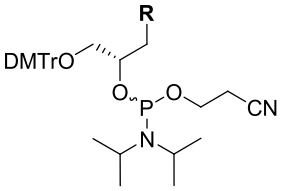
1	13a (R-Br)	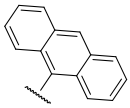	14a (60)	15a (74)
2	13b (R-H)	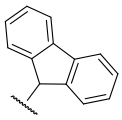	14b (73)	15b (79)

Furthermore, the application of organolithium reagents in ring-opening reaction, including but not limited for halide compounds. The deprotonation of organic compounds with an organolithium species, such as *n*-BuLi, has been widely used as a method for the preparation of organolithium reagent. A few of organic compounds containing acidic proton had been used in the ring-opening reaction of epoxides.

For the synthesis of compound **14b** (table 2.3, entry 2), 9*H*-fluorene (**13b**) was first deprotonated with *n*-BuLi at -78 ^{o}C in THF, the resulting organolithium reagents then reacted with epoxide **3** in the presence of $BF_3 \cdot Et_2O$ at -78 ^{o}C to afford the ring-opening product **14b** in 73% yield. Finally, **14b** reacted with phosphoramidite reagents **6** to afford product **15b** in 79% yield.

Alkynyllithium reagents were also used in the ring-opening reaction of expoxides. Because of their mild acidity, terminal alkynes are easily deprotonated by *n*-BuLi to form alkynyllithium reagent. As shown in table 2.4, 1-ethynylpyrene (**16a**)[19] and 3-ethynylperylene (**16b**)[20] were first deprotonated with *n*-BuLi at -78 ^{o}C in THF. Then, the resulting organolithium reagents reacted with epoxide **3** in the presence of $BF_3 \cdot Et_2O$ at -78 ^{o}C to afford the ring-opening products **17a** and **17b** in yields of 77% and 78%, respectively. Subsequently, these ring-opening products followed by the reaction with phosphoramidite reagent **6** in the presence of Hünig's base to afford the

phosphoramidites **18a** (68%) and **18b** (86%), respectively.

Thus, the compound which can be introduced alkyne group can be used to synthesize glycol nucleoside by this method.

Table 2.4 The synthesis of glycol nucleoside phosphoramidites based on alkynyllithium reagents.

Entry	Substrate		Ring-opening Product (yield %)	Phosphoramidite product (yield %)
	R-H	R	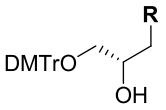	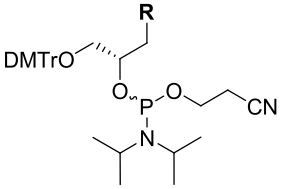
1	16a	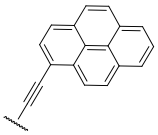	17a (77)	18a (68)
2	16b	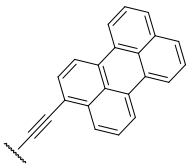	17b (78)	18b (86)
3	16c	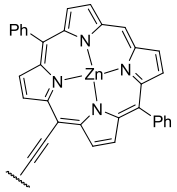	17c (26)	18c (74)

However, by using this method, the ring-opening product **17c** was synthesized in only 26% yield starting from 5-ethynyl-10,20-diphenylporphinatozinc (**16c**), the low yield makes scale up very challenging. This low yield might be resulted from the inefficient formation of alkynyllithium reagent by treating **16c** with *n*-BuLi. The strong base *n*-BuLi may cause the decomposition of **16c**, because the starting material **16c** as well as the corresponding free porphyrin were not separated from the reaction mixture.

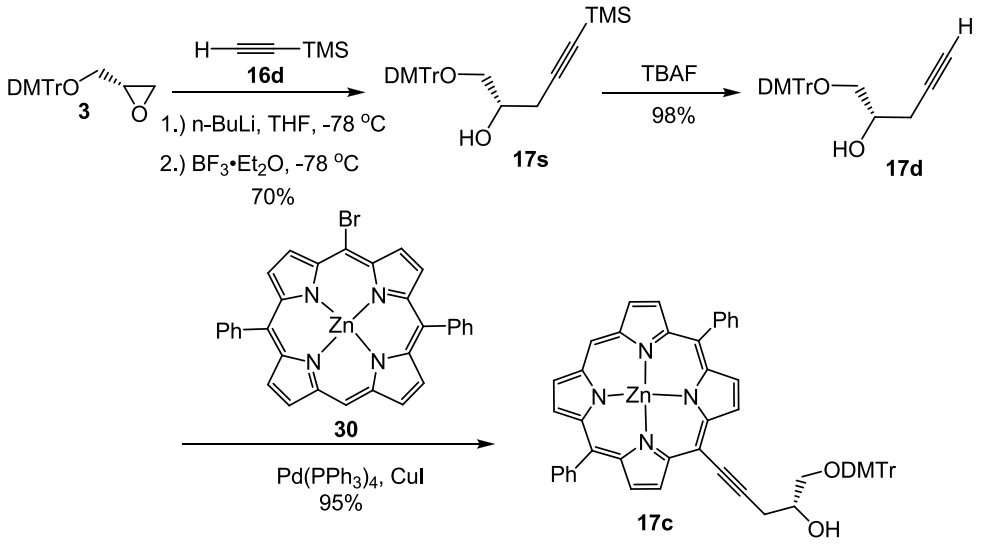

Scheme 2.5 Synthesis of ring-opening compound **17c**.

Another route was also tried to synthesize the compound **17c**. As shown in scheme 2.5, dimethoxytrityliated (*S*)-glycidol (**3**), that was reacted with trimethylsilyl acetylene (**16d**) in the presence of *n*-BuLi and $BF_3 \cdot Et_2O$ to produce the acetylenic alcohol **17s** (70%) in a regioselective and stereospecific epoxide ring-opening fashion. After removal of the TMS group of **17s** with TBAF (98%), a Pd-catalyzed Sonogashira coupling reaction of 5-bromo-10,20-diphenylporphinatozinc (**30**)[21] with compound **17d** afforded compound **17c** smoothly in 95% yield. Further reaction with compound **6** in the presence of Hünig's base yielded the phosphoramidite building block **18c** (74%).

Overall, the fluorene phosphoramidite building block **15a**, 9-substituted anthracene building block **15b**, ethynylpyrene building block **18a** and ethynylperylene building block **18b** were synthesized in two steps from dimethoxytritylated (*S*)-glycidol (**3**) with overall yields of 52%, 58%, 52% and 67%, respectively. Porphyrin acetylide phosphoramidite **18c** was synthesized in four steps from epoxide **3** with an overall yield of 48%.

Chapter 2.3 Conclusions

In this chapter, we presented the synthesis of chromophore glycol nucleotides. The key step of phosphoramidite synthesis was the regioselective and stereospecific ring-opening reaction of dimethoxytrityliated (*S*)-glycidol. The phosphoramidite precursors were synthesized by three efficient methods, namely, the application of Grignard reagents, Grignard reagents containing a metallation/transmetallation protocol and organolithum reagents. Subsequently, the precursors were converted to glycol nucleoside phosphoramidites GNA building blocks in high yields. Thus, we here demonstrated that GNA duplexes are very useful scaffolds for the economical synthesis of modified nucleotide.

Chapter 2.4 Experimental

General procedures and reagents. NMR spectra were recorded on a Brucker AVANCE 300 and Brucker DRX 500. Low-resolution mass spectra were obtained on an LC platform from Agilent using ESI technique. Highresolution mass spectra were obtained on a Thermo Finnigan LTQ FT instrument using APCI ionization. Infrared spectra were recorded on a Brucker "Alpha-P" FT-IR spectrometer. HPLC was performed using an Agilent technologies 1200 series instrument with fraction collection. All non-aqueous operations were carried out under dry nitrogen atmosphere. Solvents and reagents were used as supplied from Aldrich, Alfa Aesar or Acros.

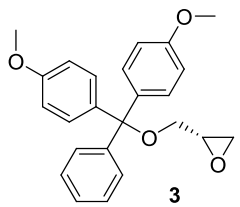

3

Compound 3 To a solution of (*R*)-(+)-glycidol (**1**) (1.21 g, 16.3 mmol) and Et_3N (6.3 mL, 47.5 mmol) in CH_2Cl_2 (47 mL) was added DMTrCl (**2**) (6.64 g, 19.6 mmol). After 12 h, the reaction mixture was poured into sat. aq $NaHCO_3$ (60 mL). The organic layer was envaporated, the residue was dissolved in EtOAc, washed with aq sat. $NaHCO_3$, and purified by chromatography over silica gel eluting with hexanes/EtOAc/Et_3N (10:1:0.01), affording compound **3** as an colorless oil (6.1 g, quantitative yield). ^{1}H NMR (300 MHz, $CDCl_3$): δ = 7.47 (m, 2H), 7.35 (m, 4H), 7.29 (m, 2H), 7.21 (m, 1H), 6.84 (m, 4H), 3.79 (s, 6H), 3.32 (dd, J = 9.9, 2.2 Hz, 1H), 3.17-3.10 (m, 2H), 2.78 (dd, J = 5.0, 4.2 Hz, 1H), 2.63 (dd, J = 5.1, 2.5 Hz, 1H). Spectroscopic data is in agreement with reference.[23]

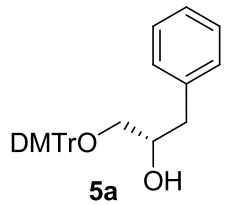

5a

Compound 5a To a suspention of copper iodide (0.04 g, 0.21 mmol) in THF (1 mL) at -40 ^{o}C was added dropwise Grignard reagent [made as follows: to a magnesium turnings (0.04 g, 1.73 mmol) and slurry of I_2 in THF (3.46 mL) was added dropwise bromobenzene (**4a**) (0.17 mL, 1.56 mmol), then the resulting mixture was stirred at room temperature for 30 min]. After stirring for 30 min at -40 ^{o}C, epoxide (0.39 g, 1.05 mmol) in THF (2.1 mL) was added dropwise and stirring was continued at the same temperature for 1 hours. The solution was warmed to 0 ^{o}C, stirred for another 1 hour, and the reaction mixture was poured into saturated $NaHCO_3$ and extracted with CH_2Cl_2 (3 × 50 mL). The combined organic extracts were dried over anhydrous Na_2SO_4, concentrated *in vacuo*, and the resulting oil was purified by chromatography over silica gel eluting with hexanes/ethyl acetate/triethylamine (5:1:0.01), affording compound **5a** as a colorless foam (0.40g, 85%). ^{1}H NMR (300 MHz, $CDCl_3$): δ = 7.35 (d, J = 8.1 Hz, 2H), 7.24 (m, 4H), 7.19-7.08 (m, 6H), 7.04 (m, 2H), 6.74 (d, J = 8.9 Hz, 4H), 7.89 (m, 1H), 3.71 (s, 6H), 3.12 (dd, J = 9.6, 4.3 Hz, 2H), 3.05 (dd, J = 9.5, 6.4 Hz, 2H), 2.70 (m, 2H), 2.17 (d, J = 4.4 Hz, 1H). ^{13}C NMR (75 MHz, $CDCl_3$): δ = 158.53, 144.83, 138.12, 136.03, 130.06, 129.29, 128.35, 128.16, 127.83, 126.82, 126.30, 113.23, 113.14, 86.17, 71.94, 66.58, 55.22, 40.15. IR (thin film): 3058, 3029, 2930, 2835, 1735, 1606, 1581, 1507, 1462, 1444, 1413, 1372, 1299, 1245, 1174, 1154,113, 1072, 1031, 982, 950, 910, 826, 790, 774, 753, 727, 700, 634, 620, 582, 553, and 530 cm^{-1}. HRMS: m/z [M^{+}] calcd for $C_{30}H_{30}O_4$: 454.2139 ; found: 454.2126.

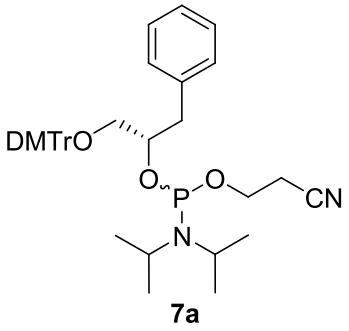

7a

Compound 7a To a solution of **5a** (0.4 g, 0.89 mmol) and *N*,*N*-diisopropylethylamine (0.89 mL, 4.74 mmol) in CH_2Cl_2 (15 mL) was added compound **6** (0.40 mL, 1.78 mmol). After 2 h, the reaction mixture was poured into sat. aq. $NaHCO_3$ (30 mL) and extracted with CH_2Cl_2 (3 × 30 mL). The combined organic layers were evaporated and the residue was purified by chromatography over silica gel eluting with hexanes/ethyl acetate/triethylamine (5:1:0.01), affording **7a** as a colorless foam (0.49 g, 84%). ^{31}P NMR (161.9 MHz, $CDCl_3$): δ = 149.30, 148.12. IR (thin film): 2965, 2931, 2872, 2836, 1607, 1581, 1508, 1462, 1364, 1299, 1248, 1176, 1153, 1125, 1033, 975, 876, 726, 582 and 523 cm^{-1}. HRMS: *m*/*z* [M + H^+] calcd for $C_{39}H_{48}N_2O_5P_1$: 655.3295; found: 655.3269.

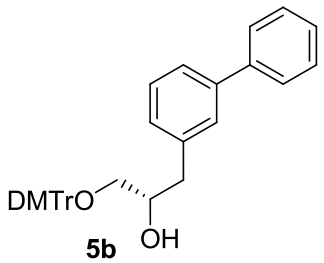

5b

Compound 5b To a suspention of copper iodide (0.05 g, 0.28 mmol) in THF (1 mL) at -40 ^oC was added dropwise Grignard reagent [made as follows: to a magnesium turnings (0.05 g, 2.27 mmol) and slurry of I_2 in THF (4 mL) was added 3-bromobiphenyl (**4b**) (0.35 mL, 2.07 mmol), then the resulting mixture was stirred at room temperature for 30 min]. After stirring for 30 min at -40 ^oC, epoxide (0.52 g, 1.34 mmol) in THF (2.8 mL) was added dropwise and stirring was continued at the same temperature for 1 hours. The solution was warmed to 0 ^oC, stirred for another 1 hour, and the reaction mixture was poured into saturated $NaHCO_3$ and extracted with

CH_2Cl_2 (3 × 50 mL). The combined organic extracts were dried over anhydrous Na_2SO_4, concentrated *in vacuo*, and the resulting oil was purified by chromatography over silica gel eluting with hexanes/ethyl acetate/triethylamine (5:1:0.01), affording compound **5c** as a colorless foam (0.53 g, 73%). ^{1}H NMR (300 MHz, $CDCl_3$): δ = 7.54 (d, J = 8.0 Hz, 2H), 7.45-7.27 (m, 13H), 7.25-7.11 (m, 3H), 6.80 (d, J = 9.0 Hz, 4H), 4.02 (m, 1H), 3.77 (s, 6H), 3.22 (dd, J = 9.4, 4.1 Hz, 1H), 3.15 (dd, J = 9.4, 6.5 Hz, 1H), 2.86 (m, 2H), 2.71 (d, J = 4.4 Hz, 2H). ^{13}C NMR (75MHz, $CDCl_3$): δ = 158.54, 144.88, 144.33, 141.18, 138.63, 136.06, 130.06, 128.78, 128.71, 128.28, 128.17, 127.85, 127.23, 127.19, 126.84, 125.22, 113.16, 86.22, 66.72, 60.40, 55.21, 40.26, 21.04. IR (thin film): 3055, 3033, 2999, 2869, 1606, 1579,1507, 1480, 1462, 1443, 1299, 1246, 1174, 1074, 1031, 982, 902, 826, 755, 726, 698, 582 and 529 cm^{-1}. HRMS: m/z [M + K$^+$] calcd for $C_{36}H_{34}O_4K_1$: 569.2089; found: 569.2085.

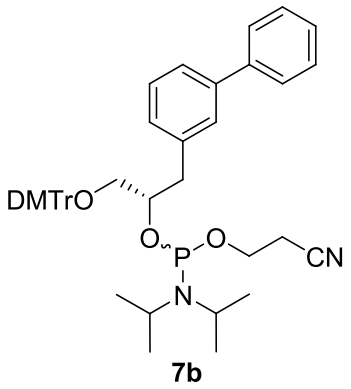

7b

Compound 7b To a solution of **5b** (0.4 g, 0.78 mmol) and *N*,*N*-diisopropylethylamine (0.34 mL, 4.11 mmol) in CH_2Cl_2 (13 mL) was added compound **6** (0.34 mL, 1.56 mmol). After 2 h, the reaction mixture was poured into sat. aq. $NaHCO_3$ (40 mL) and extracted with CH_2Cl_2 (3 × 40 mL). The combined organic layers were evaporated and the residue was purified by chromatography over silica gel eluting with hexanes/ethyl acetate/triethylamine (5:1:0.01), affording **7c** as a colorless foam (0.47 g, 85%). ^{31}P NMR (161.9 MHz, $CDCl_3$): δ = 149.00, 148.40. IR (thin film): 2964, 2930, 2873, 2835, 1607, 1508, 1248, 1176, 1030, 976, 827, 761, 697, 582 and 516 cm^{-1}. HRMS: m/z [M$^+$] calcd for $C_{45}H_{52}N_2O_5P_1$: 731.3608; found: 731.3602.

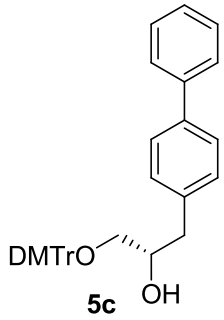

5c

Compound 5c To a suspention of copper iodide (0.09 g, 0.47 mmol) in THF (1 mL) at -40 ^{o}C was added dropwise Grignard reagent [made as follows: to a magnesium turnings (0.09 g, 3.85 mmol) and slurry of I_2 in THF (10 mL) was added 4-bromobiphenyl (**4c**) (0.82 g, 3.50 mmol), then the resulting mixture was stirred at room temperature for 30 min]. After stirring for 30 min at -40 ^{o}C, epoxide (0.88 g, 2.32 mmol) in THF (4.6 mL) was added dropwise and stirring was continued at the same temperature for 1 hours. The solution was warmed to 0 ^{o}C, stirred for another 1 hour, and the reaction mixture was poured into saturated $NaHCO_3$ and extracted with CH_2Cl_2 (3 × 50 mL). The combined organic extracts were dried over anhydrous Na_2SO_4, concentrated *in vacuo*, and the resulting oil was purified by chromatography over silica gel eluting with hexanes/ethyl acetate/triethylamine (5:1:0.01), affording compound **5c** as a colorless foam (0.92 g, 74%). ^{1}H NMR (300 MHz, $CDCl_3$): δ = 7.49 (d, J = 8.0 Hz, 2H), 7.37 (m, 6H), 7.28-7.18 (m, 7H), 7.17-7.09 (m, 3H), 6.75 (d, J = 9.0 Hz, 4H), 3.93 (m, 1H), 3.70 (s, 6H), 3.15 (dd, J = 9.4, 6.4 Hz, 1H), 3.07 (dd, J = 9.4, 6.4 Hz, 1H), 2.75 (m, 2H). ^{13}C NMR (75MHz, $CDCl_3$): δ = 158.57, 144.86, 141.04, 139.26, 137.27, 136.03, 130.11, 129.74, 128.75, 128.20, 127.88, 127.40, 126.87, 113.18, 86.23, 55.22, 39.80. IR (thin film): 3047, 2922, 1585, 1505, 1385, 1304, 1239, 1169, 1078, 1051, 940, 829, 763, 707, and 590 cm^{-1}. HRMS: m/z [M + K^{+}] calcd for $C_{36}H_{34}O_4K_1$: 569.2089; found: 569.2081.

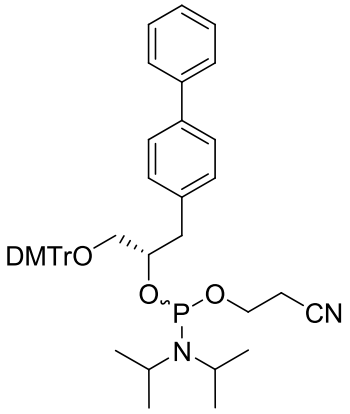

7c

Compound 7c To a solution of **5c** (0.5 g, 0.99 mmol) and *N*,*N*-diisopropylethylamine (0.99 mL, 5.26 mmol) in CH_2Cl_2 (16 mL) was added compound **6** (0.44 mL, 1.98 mmol). After 2 h, the reaction mixture was poured into sat. aq. $NaHCO_3$ (40 mL) and extracted with CH_2Cl_2 (3 × 40 mL). The combined organic layers were evaporated and the residue was purified by chromatography over silica gel eluting with hexanes/ethyl acetate/triethylamine (5:1:0.01), affording **7c** as a colorless foam (0.60 g, 85%). ^{31}P NMR (161.9 MHz, $CDCl_3$): δ = 148.93, 148.84. IR (thin film): 2964, 2930, 2873, 2835, 1607, 1508, 1248, 1176, 1030, 976, 827, 761, 697, 582 and 516 cm^{-1}. HRMS: *m*/*z* [M^+] calcd for $C_{45}H_{52}N_2O_5P_1$: 731.3603; found: 731.3608.

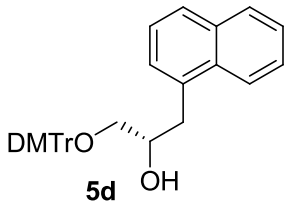

5d

Compound 5d To a suspention of copper iodide (0.09 g, 0.45 mmol) in THF (1 mL) at -40 ^oC was added dropwise Grignard reagent [made as follows: to a magnesium turnings (0.04 g, 1.65 mmol) and slurry of I_2 in THF (4 mL) was added 1-bromonaphthalene (**4d**) (0.31 g, 1.50 mmol), then the resulting mixture was stirred at room temperature for 30 min]. After stirring for 30 min at -40 ^oC, epoxide (0.38 g, 1.00 mmol) in THF (2 mL) was added dropwise and stirring was continued at the same temperature for 1 hours. The solution was warmed to 0 ^oC, stirred for another 1 hour, and the reaction mixture was poured into saturated $NaHCO_3$ and extracted with

CH_2Cl_2 (3 × 50 mL). The combined organic extracts were dried over anhydrous Na_2SO_4, concentrated *in vacuo*, and the resulting oil was purified by chromatography over silica gel eluting with hexanes/ethyl acetate/triethylamine (5:1:0.01), affording compound **5d** as a colorless foam (0.37 g, 64%). ^{1}H NMR (300 MHz, $CDCl_3$): δ = 7.75 (m, 3H), 7.58 (s, 1H), 7.44 (m, 4H), 7.33-7.18 (m, 8H), 6.82 (d, J = 9.1 Hz, 4H), 4.06 (m, 1H), 3.78 (s, 6H), 3.23 (dd, J = 9.4, 4.2 Hz, 1H), 3.17 (dd, J = 9.4, 6.2 Hz, 1H), 2.96 (m, 2H), 2.77 (d, J = 4.5 Hz, 1H). ^{13}C NMR (75MHz, $CDCl_3$): δ = 158.57, 144.95, 144.67, 136.11, 135.78, 134.34, 133.96, 132.18, 130.13, 128.78, 128.23, 127.87, 127.51, 127.21, 126.86, 125.92, 125.54, 125.42, 123.92, 113.18, 86.34, 71.31, 67.00, 60.42, 55.23, 37.45. IR (thin film): 3055, 3000, 2930, 2835, 1734, 1606, 1581, 1507, 1462, 1444, 1413, 1396, 1372, 1299, 1245, 1174, 1154, 1113, 1070, 1030, 981, 951, 908, 826, 790, 776, 754, 726, 701, 635, 618, 582 and 525 cm^{-1}. HRMS: m/z [M^+] calcd for $C_{34}H_{32}O_4$: 504.2295; found: 504.2280.

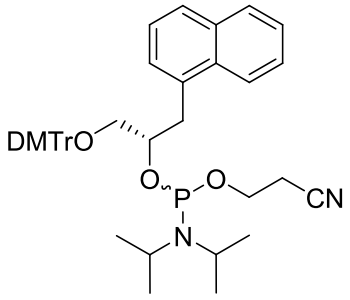

7d

Compound 7d To a solution of **5d** (0.18 g, 0.31 mmol) and *N*,*N*-diisopropylethylamine (0.81 mL, 3.63 mmol) in CH_2Cl_2 (5 mL) was added compound **6** (0.10 mL, 0.46 mmol). After 2 h, the reaction mixture was poured into sat. aq. $NaHCO_3$ (40 mL) and extracted with CH_2Cl_2 (3 × 40 mL). The combined organic layers were evaporated and the residue was purified by chromatography over silica gel eluting with hexanes/ethyl acetate/triethylamine (5:1:0.01), affording **7c** as a colorless foam (0.21 g, 97%). ^{31}P NMR (161.9 MHz, $CDCl_3$): δ = 147.64, 147.15. IR (thin film): 2931, 2874, 2793, 2267, 2237, 2200, 1607, 1581, 1508, 1445, 1396, 1364, 1299, 1248, 1176, 1155, 1073, 1032, 976, 878, 777 and 583 cm^{-1}. HRMS: m/z [M + H^+] calcd for $C_{43}H_{50}N_2O_5P_1$: 705.3452; found: 705.3422.

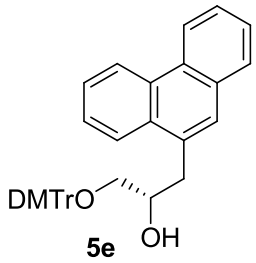

5e

Compound 5e To a suspention of copper iodide (0.05 g, 0.25 mmol) in THF (2.5 mL) at -40 ^{o}C was added dropwise Grignard reagent [made as follows: to a magnesium turnings (0.05 g, 2.08 mmol) and slurry of I_2 in THF (3.8 mL) was added 9-bromophenanthrene (**4e**) (0.49 g, 1.90 mmol), then the resulting mixture was stirred at room temperature for 30 min]. After stirring for 30 min at -40 ^{o}C, epoxide (0.48 g, 1.27 mmol) in THF (2.5 mL) was added dropwise and stirring was continued at the same temperature for 1 hours. The solution was warmed to 0 ^{o}C, stirred for another 1 hour, and the reaction mixture was poured into saturated $NaHCO_3$ and extracted with CH_2Cl_2 (3 × 50 mL). The combined organic extracts were dried over anhydrous Na_2SO_4, concentrated *in vacuo*, and the resulting oil was purified by chromatography over silica gel eluting with hexanes/ethyl acetate/triethylamine (5:1:0.01), affording compound **5e** as a colorless foam (0.46 g, 65%). ^{1}H NMR (300 MHz, $CDCl_3$): δ = 8.73 (d, J = 8.0 Hz, 1H), 8.65 (d, J = 8.2 Hz, 1H), 8.09 (d, J = 7.8 Hz, 1H), 7.78 (d, J = 7.4 Hz, 1H), 7.54-7.70 (m, 5H), 7.47 (d, J = 8.8 Hz, 2H), 7.17-7.37 (m, 6H), 6.80 (d, J = 8.5 Hz, 4H), 4.2 (m, 1H), 3.78 (s, 6H), 3.42 (m, 1H), 3.30 (m, 2H), 3.21 (dd, J = 7.6, 14.0 Hz, 1H). ^{13}C NMR (75 MHz, $CDCl_3$): δ = 158.55, 144.96, 136.01, 132.46, 131.63, 131.25, 130.81, 130.10, 129.90, 128.20, 128,18, 127.96, 127.85, 126.84, 126.60, 126.26, 126.22, 124.53, 123.24, 122.42, 113.16, 86.36, 70.80, 66.98, 55.20, 37.98. IR (thin film): 3412 (br), 2999, 1605, 1506, 1444, 1299, 1245, 1117, 1069, 1030, 901, 826, 747, 725, 700, 582, 526 and 509 cm^{-1}. HRMS: m/z [M + K^{+}] calcd for $C_{38}H_{34}O_4K_1$: 593.2089; found: 593.2084.

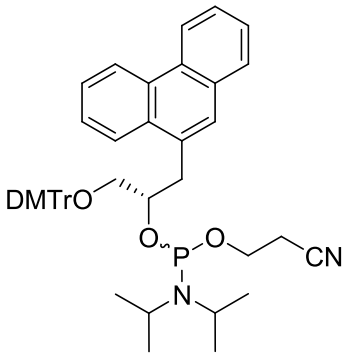

7e

Compound 7e To a solution of **5e** (0.24 g, 0.44 mmol) and *N*,*N*-diisopropylethylamine (0.44 mL, 2.34 mmol) in CH_2Cl_2 (7.2 mL) was added compound **6** (0.20 mL, 0.88 mmol). After 2 h, the reaction mixture was poured into sat. aq. $NaHCO_3$ (40 mL) and extracted with CH_2Cl_2 (3 × 40 mL). The combined organic layers were evaporated and the residue was purified by chromatography over silica gel eluting with hexanes/ethyl acetate/triethylamine (5:1:0.01), affording **7e** as a colorless foam (0.25 g, 78%). ^{31}P NMR (121 MHz, $CDCl_3$): δ = 148.99. 148.42. IR (thin film): 2963, 1606, 1461, 1445, 1363, 1300, 1247, 1175, 1075, 1031, 975, 945, 876, 827, 748, 725, 701, 582, 511 cm^{-1}. HRMS: *m*/*z* [M + H^+] calcd for $C_{47}H_{52}N_2O_5P_1$: 755.3608; found: 755.3601.

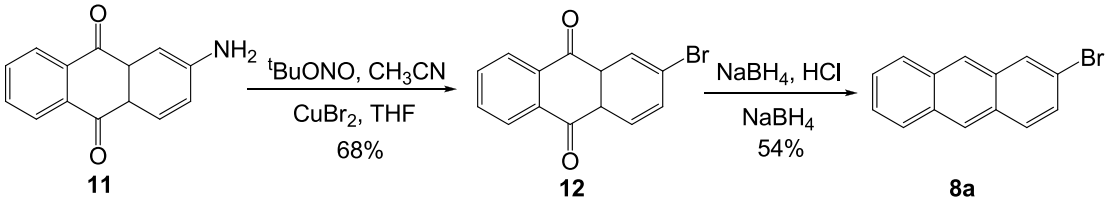

Scheme 2.6 The synthesis of 2-bromoanthracene (**8a**).

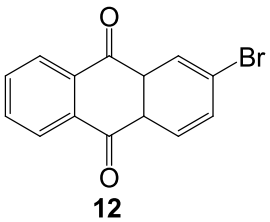

12

Compound 12 Cupric bromide (17.87 g, 80.0 mmol, 2 equiv.) was dissolved in CH_3CN (96 mL) in a 500 mL flask. *tert*-Butyl nitrite (9.64 mL) was added to the

reaction mixture with stirring. 2-Aminoanthraquinone (**11**) (8.92 g, 40.0 mmol) was dissolved in THF (130 mL) and placed in an addition funnel affixed to the reaction flask. The anthraquinone solution was added at 25 ^{o}C over a 20 min period, and the reaction mixture was stirred for 20 h. The reaction mixture was concentrated and the solid residue was triturated with water. This slurry was filtered and the solid was washed with H_2O. The solid was washed with CH_2Cl_2 through the filter paper and the organic filtrate was concentrated. This trituration process was repeated. The organic filtrate was washed with H_2O well, dried over Na_2SO_4 and concentrated, resulting crude product was purified by chromatography over silica gel, eluting with hexane/ethyl acetate (4:1), affording product as a yellow solid (7.81g, 68%). ^{1}H NMR (300 MHz, $CDCl_3$): δ = 8.42 (d, J = 2.0 Hz, 1H), 8.30 (m, 2H), 8.17 (d, J = 8.3 Hz, 1H), 7.91 (dd, J = 8.3, 2.1 Hz, 1H), 7.82 (m, 2H). Spectroscopic data is in agreement with reference.[15]

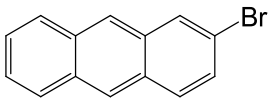

8a

Compound 8a 2-Bromoanthraquinone (**12**) (3.12 g, 10.87 mmol) and isopropanol (60 mL) were added to a 250 mL flask at 25 ^{o}C and stirred to create a suspension. The reaction mixture was treated with $NaBH_4$ (2.06 g, 54.35 mmol, 5.0 equiv.) and was stirred, as the yellow suspension turned brown and then green. After 15 h at 25 ^{o}C, the suspension was poured onto an ice-water mixture and filtered to give a light yellow brown solid that was used without purification. The solid was placed in a 250 mL flask, treated with aqueous HCl (3 M, 64.43 mL), and heated at 75 ^{o}C for 8 h. The suspension was cooled and filtered (H_2O wash) to give a brownish-yellow solid that was used without further purification. The solid was placed in a 250 mL flask with and dissolved in isopropanol (60 mL). The reaction mixture was treated with $NaBH_4$ (2.47 g, 65.22 mmol, 6 equiv.) at 25 ^{o}C and the mixture was warmed at reflux for 20 h. Aqueous 3 M HCl was added until bubbling ceased and the mixture was filtered to provide an off-yellow residue that was washed through the filter paper with CH_2Cl_2.

The filtrate was concentrated to provide a yellowish solid that was purified by chromatography over silica gel, eluting with hexane/dichloromethane (9:1), affording compound **8a** as a light yellow solid (1.51 g, 54%) that was contaminated with 20 mol% anthracene. ^{1}H NMR (300 MHz, $CDCl_3$): δ = 8.40 (s, 1H), 8.32 (s, 1H), 8.19 (m, 1H), 8.00 (m, 2H), 7.89 (d, J = 9.0 Hz, 1H), 7.50 (m, 3H). Spectroscopic data is in agreement with reference.[15]

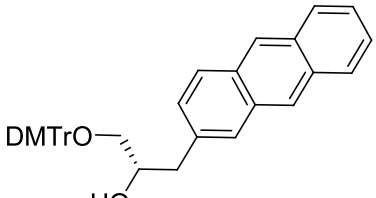

9a

Compound 9a To a solution of 2-bromoanthracene (**8a**) (314 mg, 1.04 mmol) in THF (16 mL) at -78 ^{o}C was added dropwise *n*-BuLi in hexane (0.8 mL, 1.28 mmol) over 20 min. After stirring for 30 min, a suspension of freshly prepared $MgBr_2$ [made as follows: to a suspension of magnesium turnings (50 mg, 2.08 mmol) in THF (5 mL) was added dropwise 1,2-dibromoethane (0.18 mL, 2.12 mmol)] was added dropwise over 20 min. The resulting solution was first kept at -78 ^{o}C with stirring for 30 min and then warmed to 0 ^{o}C and stirring was continued for another 30 min. The solution was then cooled to -40 ^{o}C and stirred for 1 hour. To the resulting solution was added a slurry of CuI (26.3 mg, 0.14 mmol) in THF (1 mL). Then, the epoxide **3** (260 mg, 0.69 mmol) in THF (1 mL) was added and stirring was continued at the same temperature for 2 hours. The solution was warmed to room temperature, stirred for another 1 hour, and the reaction mixture was poured into saturated $NaHCO_3$ and extracted with CH_2Cl_2 (3 × 50 mL). The combined organic extracts were dried over anhydrous Na_2SO_4, concentrated *in vacuo*, and the resulting oil was purified by chromatography over silica gel, eluting with hexanes/ethyl acetate/triethylamine (5:1:0.01), affording compound **9a** as a light yellow foam (200 mg, 53%). ^{1}H NMR (300 MHz, $CDCl_3$): δ = 8.34 (d, J = 21.3 Hz, 2 H), 7.98 (m, 2H), 7.89 (d, J = 8.8 Hz, 1H), 7.71 (s, 1H), 7.45 (m, 4H), 7.34-7.18 (m, 8H), 6.80 (d, J = 9.1 Hz, 4H), 4.11 (m, 1H), 3.74 (s, 6H), 3.26 (dd, J = 9.4, 4.1 Hz, 1H), 3.19 (dd, J = 9.4, 6.2 Hz, 1H), 3.00

(m, 2H), 2.32 (d, J = 4.4 Hz, 1H). ^{13}C NMR (75 MHz, $CDCl_3$): δ = 158.53, 144.88, 136.00, 135.97, 135.10, 131.83, 131.74, 131.45, 130.67, 130.09, 128.25, 128.16, 128.15, 128.11, 127.87, 127.68, 127.50, 126.84, 125.93, 125.65, 125.32, 125.11, 113.15, 86.23, 71.69, 66.50, 55.18, 40.53. IR (thin film): 3051, 2999, 2929, 2834, 1606, 1580, 1507, 1461, 1444, 1410, 1350, 1299, 1246, 1174, 1156, 1068, 1031, 1011, 978, 934, 903, 884, 868, 826, 788, 754, 731, 701, 635, 617, 582 and 539 cm^{-1}. HRMS: m/z [M + H$^+$] calcd for $C_{38}H_{34}O_4$: 554.2452; found: 554.24549.

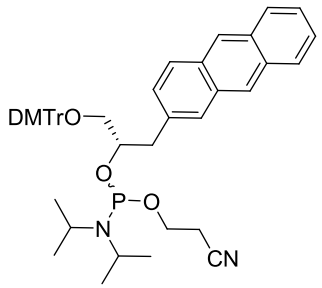

10a

Compound 10a To a solution of **9a** (307 mg, 0.55 mmol) and *N*,*N*-diisopropylethylamine (0.55 mL, 2.94 mmol) in CH_2Cl_2 (9 mL) was added compound **6** (0.25 mL, 1.11 mmol). After 2 h, the reaction mixture was poured into sat. aq. $NaHCO_3$ (40 mL) and extracted with CH_2Cl_2 (3 × 40 mL). The combined organic extracts were dried over anhydrous Na_2SO_4, concentrated *in vacuo*, and the resulting oil was purified by chromatography over silica gel eluting with hexanes/ethyl acetate/triethylamine (5:1:0.01), affording compound **10a** as a colorless foam (283 mg, 69%). ^{31}P NMR (121.5 MHz, $CDCl_3$): δ = 148.98, 148.76. IR (thin film): 2964, 2931, 1607, 1508, 1461, 1445, 1363, 1300, 1248, 1201, 1176, 1156, 1125, 1073, 1032, 1005, 977, 944, 879, 827, 790, 755, 731, 701, 643, 582, 541 and 520 cm^{-1}. HRMS: m/z [M + H$^+$] calcd for $C_{47}H_{52}N_2O_5P_1$: 755.3608; found: 755.3601.

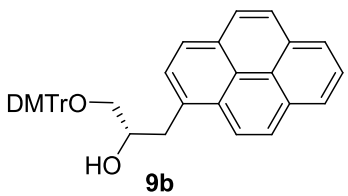

9b

Compound 9b To a solution of 1-bromopyrene (**8b**) (2.56 g, 9.14 mmol) in THF (20

mL) at -78 ^{o}C was added dropwise *n*-BuLi in hexane (7.2mL, 11.5 mmol) over 20 min. After stirring for 30 min, a suspension of freshly prepared $MgBr_2$ [made as follows: to a suspension of magnesium turnings (0.44 g, 18.3 mmol) in THF (37 mL) was added dropwise 1,2-dibromoethane (1.62 mL, 18.7 mmol)] was added dropwise over 20 min. The resulting solution was first kept at -78 ^{o}C with stirring for 30 min and then warmed to 0 ^{o}C and stirring was continued for another 30 min. The solution was then cooled to -40 ^{o}C and stirred for 1 hour. To the resulting solution was added a slurry of CuI (0.23 g, 1.22 mmol) in THF (2.44 mL). Then, the epoxide **3** (2.37 g, 6.1 mmol) in THF (12 mL) was added and stirring was continued at the same temperature for 2 hours. The solution was warmed to room temperature, stirred for another 1 hour, and the reaction mixture was poured into saturated $NaHCO_3$ and extracted with CH_2Cl_2 (3 × 50 mL). The combined organic extracts were dried over anhydrous Na_2SO4, concentrated *in vacuo*, and the resulting oil was purified by chromatography over silica gel, first eluting with hexanes/ethyl acetate/triethylamine (5:1:0.01), then with hexanes/ethyl acetate/triethylamine (3:1:0.01), affording compound **9b** as a light yellow foam (1.79 g, 50%). ^{1}H NMR (300 MHz, $CDCl_3$): δ = 8.26 (d, J = 9.3 Hz, 1H), 8.18 (d, J = 7.8 Hz, 2H), 7.98–8.09 (m, 5H), 7.79 (d, J = 7.8 Hz, 1H), 7.48 (m, 2H), 7.27–7.35 (m, 6H), 7.22 (m, 1H), 6.79 (dd, J = 9.0, 2.3 Hz, 4H), 4.20 (m, 1H), 3.74 (d, J = 2.0 Hz, 6H), 3.58 (dd, J = 13.9, 6.0 Hz, 1H), 3.47 (dd, J =13.7, 7.3 Hz, 1H), 3.28 (m, 2H), 2.37 (d, J = 4.3 Hz, 1H). ^{13}C NMR (75MHz, $CDCl_3$): δ = 158.65, 145.02, 136.13, 132.46, 131.51, 130.99, 130.31, 130.22, 130.20, 129.35, 128.41, 128.30, 127.97, 127.60, 127.51, 126.96, 125.97, 125.18, 125.09, 125.04, 124.94, 124.81, 123.58, 113.26, 86.52, 72.31, 67.00, 55.29, 37.86. IR (thin film): 3037, 2929, 2834, 1605, 1583, 1507, 1461, 1444, 1299, 1175, 1154, 1069, 1031, 980, 907, 840, 827, 791, 754, 726, 703, 682, 647 and 582 cm^{-1}. HRMS: m/z [M^{+}] calcd for $C_{40}H_{34}O_4$: 578.2452; found: 578.2449.

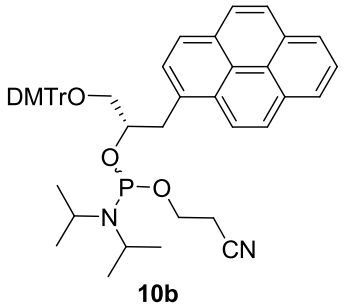

10b

Compound 10b To a solution of **9b** (1.79 g, 3.09 mmol) and *N*,*N*-diisopropylethylamine (3.09 mL, 16.4 mmol) in CH_2Cl_2 (52 mL) was added compound **6** (1.37mL, 6.18 mmol). After 2 h, the reaction mixture was poured into sat. aq. $NaHCO_3$ (40 mL) and extracted with CH_2Cl_2 (3 × 40 mL). The combined organic extracts were dried over anhydrous Na_2SO_4, concentrated *in vacuo*, and the resulting oil was purified by chromatography over silica gel eluting with hexanes/ethyl acetate/triethylamine (5:1:0.01), affording compound **10b** as a light yellow foam (2.02 g, 84%). ^{31}P NMR (121.5 MHz, $CDCl_3$): δ = 147.53, 147.16. IR (thin film): 3038, 2964, 2929, 2872, 2835, 1606, 1583, 1507, 1461, 1445, 1415, 1395,1379, 1363, 1300, 1176, 1155, 1123, 1073, 1029, 975, 951, 894, 878, 843, 826, 790, 754, 725, 700, 682, 640, 616, 582, 552, 517 and 465 cm^{-1}. HRMS: *m*/*z* [M + H^+] calcd for $C_{49}H_{52}N_2O_5P_1$: 779.3608; found: 779.3602.

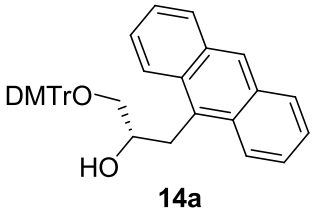

14a

Compound 14a To a solution of 9-bromoanthrancene (**13a**) (0.78 g, 3.05 mmol) in Et_2O (25 mL) at -40 ^oC was added slowly *n*-BuLi in hexane (2.35 mL, 3.75 mmol). After stirring for 30 min at -40 ^oC, the resulting yellow-orange colored suspension was warmed to 0 ^oC and stirred for another 30 min. The solution was then cooled to -40 ^oC and stirred for 1 hour. The solution of compound **3** (1.15 mg, 3.05 mmol) in THF (5 mL) was then added slowly at -40 ^oC. The resulting solution was first kept at -40 ^oC with stirring for 30 min and then warmed to 0 ^oC and stirring was continued

for another 30 min. Then the reaction was quenched with saturated $NaHCO_3$ (50 mL) at 0 ^oC. The mixture was extracted with CH_2Cl_2 (3 × 60 mL). The combined organic layers were dried over anhydrous Na_2SO_4, concentrated *in vacuo*, and the resulting red oil was purified by chromatography over silica gel eluting with hexanes/ethyl acetate/triethylamine (5:1:0.01), affording compound **14a** as a colorless foam (1.02 g, 61%). ^1H NMR (300 MHz, $CDCl_3$): δ = 8.36 (s, 1H), 8.28 (m, 2H), 7.98 (m, 2H), 7.45 (m, 6H), 7.32-7.18 (m, 7 H), 6.79 (dd, J = 9.1, 2.7 Hz, 2H), 4.23 (m, 1H), 3.83 (m, 1H), 3.78 (d, J =1.4 Hz, 6H), 3.48 (dd, J = 14.2, 7.1 Hz, 1H), 3.36 (dd, J = 9.5, 6.2 Hz, 2H), 3.29 (dd, J = 9.5, 4.7 Hz, 2H), 2.19 (s, 1H). ^{13}C NMR (75 MHz, $CDCl_3$): δ = 158.56, 145.02, 136.16, 136.10, 131.60, 130.72, 130.58, 130.16, 129.17, 128.24, 127.86, 126.86, 126.48, 125.64, 124.85, 113.17, 86.56, 72.71, 67.67, 55.22, 32.21. IR (thin film): 3463 (br), 2929, 1606, 1506, 1444, 1246, 1174, 1155, 1068, 1031, 1010, 826, 731, 701, 582 cm^{-1}. HRMS: m/z [M + H^+] calcd for $C_{38}H_{34}O_4$: 554.2452; found: 554.2449.

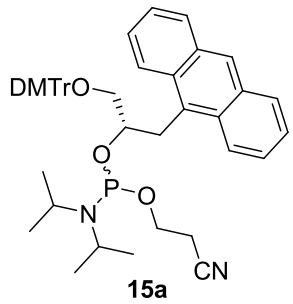

15a

Compound 15a To a solution of **14a** (0.33 g, 0.59 mmol) and *N*,*N*-diisopropylethylamine (0.59 mL, 3.12 mmol) in CH_2Cl_2 (9.6 mL) was added compound **6** (0.26mL, 1.18 mmol). After 2 h, the reaction mixture was poured into sat. aq. $NaHCO_3$ (40 mL) and extracted with CH_2Cl_2 (3 × 40 mL). The combined organic extracts were dried over anhydrous Na_2SO_4, concentrated *in vacuo*, and the resulting oil was purified by chromatography over silica gel eluting with hexanes/ethyl acetate/triethylamine (5:1:0.01), affording compound **15a** as a colorless foam (0.32 g, 74%). ^{31}P NMR (121 MHz, $CDCl_3$): δ = 148.88, 138.30. IR (thin film): 2962, 1606, 1461, 1445, 1363, 1247, 1175, 1155, 1031, 1004, 976, 878, 731, 701, 582, 541 cm^{-1}.

HRMS: *m*/*z* [M + H^+] calcd for $C_{47}H_{52}N_2O_5P_1$: 755.3608; found: 755.3601.

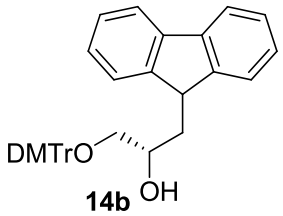

14b

Compound 14b To a solution of 9H-fluorene (**13b**) (0.87 g, 4.24 mmol) in Et_2O (7.5 mL) at -78 ^oC was added slowly *n*-BuLi in hexane (3.34 mL, 5.35 mmol). After stirring for 1 hour at -78 ^oC, the resulting mixture was warm to room temperature slowly and the stirring was continued for overnight. The solution was then cooled to -78 ^oC and stirred for 1 hour. The solution of compound **3** (1.19 g, 3.17 mmol) in THF (3 mL) was then added slowly at -78 ^oC. After stirring for another 1 hour at -78 ^oC, the reaction mixture was warm to room temperature slowly and stirred for another 3 hours. Then the reaction was quenched with saturated $NaHCO_3$ (50 mL). The mixture was extracted with CH_2Cl_2 (3 × 40 mL). The combined organic layers were dried over anhydrous Na_2SO_4, concentrated *in vacuo*, and the resulting red oil was purified by chromatography over silica gel eluting with hexanes/ethyl acetate/triethylamine (5:1:0.01), affording compound **14b** as a light colorless foam (1.30 g, 75%). ^1H NMR (300 MHz, $CDCl_3$): δ = 7.75 (d, *J* = 7.8 Hz, 1H), 7.69 (d, *J* = 7.3 Hz, 1H), 7.61 (d, *J* = 7.3 Hz, 1H), 7.43-7.27 (m, 8H), 7.26-7.18 (m, 7H), 6.80 (d, *J* = 9.0 Hz, 4H), 4.00 (m, 1H), 3.79 (s, 6H), 2.96 (m, 2H), 2.44 (d, *J* = 2.9 Hz, 1H), 2.26 (m, 1H). ^{13}C NMR (75MHz, $CDCl_3$): δ = 158.54, 147.66, 146.86, 144.81, 141.01, 140.72, 135.97, 130.03, 128.12, 127.86, 127.12, 126.98, 126.94, 126.88,126.82, 125.20, 124.29, 120.03, 119.85, 113.18, 86.24, 68.87, 68.09, 55.23, 44.08, 37.11. IR (thin film): 2931, 2808, 1606, 1507, 1445, 1299, 1246, 1174, 1067, 1031, 975, 906, 827, 739, 583 and 529 cm^{-1}. HRMS: *m*/*z* [M^+] calcd for $C_{37}H_{34}O_4$: 542.2452; found: 5422452.

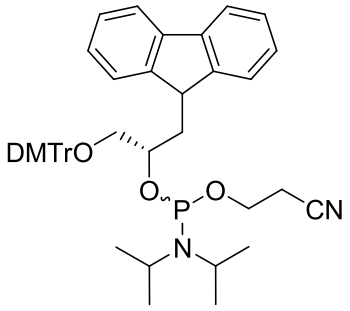

15b

Compound 15b To a solution of 1**4b** (0.39 g, 0.73 mmol) and *N*,*N*-diisopropylethylamine (0.73 mL, 3.87 mmol) in CH_2Cl_2 (12 mL) was added compound **6** (0.32 mL, 1.44 mmol). After 2 h, the reaction mixture was poured into sat. aq. $NaHCO_3$ (40 mL) and extracted with CH_2Cl_2 (3 × 40 mL). The combined organic layers were evaporated and the residue was purified by chromatography over silica gel eluting with hexanes/ethyl acetate/triethylamine (5:1:0.01), affording **15b** as a colorless foam (0.42 g, 79%). ^{31}P NMR (161.9 MHz, $CDCl_3$): δ = 149.98, 148.63. IR (thin film): 2930, 2872, 2809, 1580, 1508, 1462, 1364, 1299, 1248, 1176, 1154, 1076, 1032, 976, 878, 828, 740, 583 and 523 cm^{-1}. HRMS: *m*/*z* [M^+] calcd for $C_{46}H_{52}N_2O_5P_1$: 743.3608; found: 743.3602.

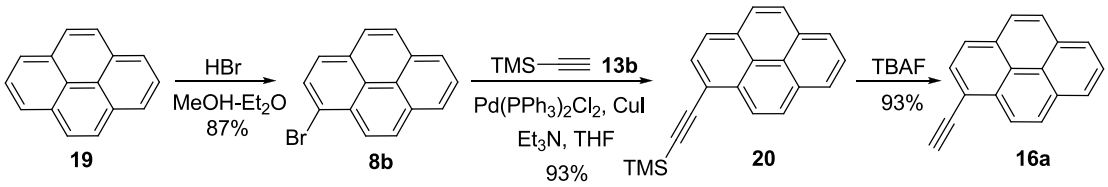

Scheme 2.7 The synthesis of 1-ethynylpyrene (**16a**).

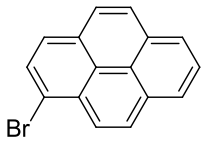

8b

Compound 8b To a stirred solution of pyrene (**19**) (2.02 g, 10 mmol) and hydrobromic acid (1.24 mL of a 48% aqueous solution, 11 mmol) in methyl alcohol-ether (20 mL, 1:1) was slowly added hydrogen peroxide (0.34 g, 0.86 mL of a 35% aqueous solution, 10 mL) over a period of 15 min at 10-15 ^{o}C. The reaction was

left at room temperature for 12 h while its progress was monitored by TLC. After the completion of monobromination, the solvent was removed under reduced pressure and the crude product was taken in ethyl acetate and washed with water and brine and dried over anhydrous Na_2SO_4. The pure product was isolated by careful column chromatography on silica gel to get pure 1-bromopyrene as a light yellow solid (2.44g, 87%). Spectroscopic data is in agreement with reference.[16]

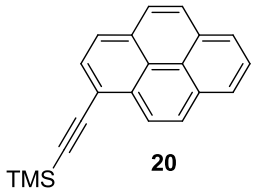

20

Compound 20 1-Bromopyrene (**8b**) (1.68 g, 6.0 mmol), $Pd(PPh_3)_2Cl_2$ (421.2 mg, 0.6 mmol) and CuI (228.6 mg, 1.2 mmol) were placed in a Schlenk flask and the flask was evacuated and recharged with N_2 gas. Piperidine (30 mL) was added and the resulting mixture was degassed for 10 min. Then trimethylsilylacetylene (**16d**) (1.71 mL, 12.0 mmol) was added and the mixture was stirred for 12 hours at 80 °C. After cooling to room temperature, the slovent was removed under vacum, the resulting residue was purified by chromatography over silica gel eluting with hexanes/dichloromethane (100:1), affording compound **20** as a light yellow solid (1.67 g, 93%). ^{1}H NMR (300 MHz, $CDCl_3$): δ = 8.57 (d, J = 9.15 Hz, 1H), 8.24-8.00 (m, 8H), 0.40 (s, 9H). Spectroscopic data is in agreement with reference.[19]

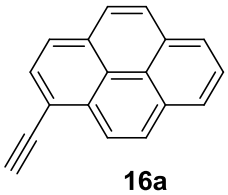

16a

Compound 16a To a solution of compound **20** (1.58 g, 5.31 mmol) in THF (34 mL) was added tetrabutylammonium fluoride (1 M, 15.93 mL) dropwise. The reaction mixture was stirred at room temperature for 4 hours. Then the reaction was quenched by H_2O (50 mL), and stirred for another 30 min at room temperature. After that, the reaction mixture was extracted by CH_2Cl_2 (3 × 40 mL) and the combined organic

layer was washed with brine for 3 times (3 × 40 mL). Then the organic layer was dried over anhydrous Na_2SO4, concentrated *in vacuo*, and the resulting crude product was purified by chromatography over silica gel with hexanes/dichloromethane (100:1), affording compound **16a** as a dark red solid (1.12 g, 93%). ^{1}H NMR (300 MHz, $CDCl_3$): δ = 8.60 (d, J = 9.18 Hz, 1H), 8.24-8.00 (m, 8H), 3.63 (s, 1H). Spectroscopic data is in agreement with reference.[19]

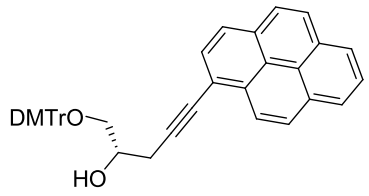

17a

Compound 17a To a solution of 1-ethynylpyrene (**16a**) (300 mg, 1.33 mmol) in THF (8 mL) at -78 ^{o}C was added slowly *n*-BuLi in hexane (0.84 mL, 1.34 mmol). After stirring for 10 min at -78 ^{o}C, $BF_3{\cdot}Et_2O$ (0.17 mL, 1.33 mmol) was added dropwise and the stirring continued for another 5 min. The solution of compound **3** (498.6 mg, 1.33 mmol) in THF (5 mL) was then added slowly at -78 ^{o}C. Stirring was continued for another 15 min at -78 ^{o}C, then the reaction was quenched with saturated $NaHCO_3$ (50 mL) at -78 ^{o}C. The mixture was extracted with CH_2Cl_2 (3 × 40 mL). The combined organic layers were dried over anhydrous Na_2SO_4, concentrated *in vacuo*, and the resulting red oil was purified by chromatography over silica gel eluting with hexanes/ethyl acetate/triethylamine (3:1:0.01), affording compound **17a** as a light yellow foam (0.55 g, 68%). ^{1}H NMR (300 MHz, $CDCl_3$): δ = 8.44 (d, J = 9.1 Hz, 1H), 8.20 (m, 2H), 7.96–8.10 (m, 6H), 7.52 (m, 2H), 7.40 (m, 4H), 7.31 (m, 2H), 7.21 (m, 1H), 6.81 (d, J = 8.9 Hz, 4H), 4.19 (m, 1H), 3.67 (s, 6H), 3.48 (m, 2H), 2.98 (d, J = 6.3Hz, 2H), 2.60 (d, J = 5.3Hz, 1H). ^{13}C NMR (75MHz, $CDCl_3$): δ = 158.46, 144.85, 135.84, 135.83, 131.78, 131.11, 130.95, 130.77, 130.05, 129.66, 128.08, 127.84, 127.78, 127.09, 126.79, 126.05, 125.42, 125.33, 125.29, 124.29, 124.26, 124.18, 118.05, 113.14, 91.53, 86.29, 81.76, 69.74, 66.15, 54.98, 25.34. IR (thin film): 3037, 2929, 2834, 1605, 1581, 1507, 1461, 1442, 1299, 1246, 1174, 1072, 1031, 905, 845, 826, 790, 754, 717, 701, 681, 613, 582 and 543 cm^{-1}. HRMS: m/z [M^+] calcd for

$C_{42}H_{34}O_4$: 602.2452; found: 602.2429.

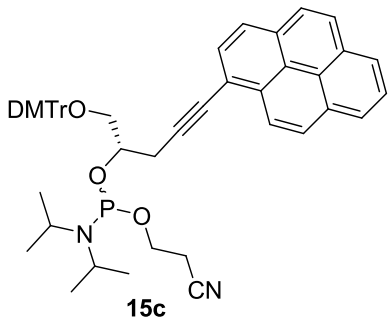

15c

Compound 18a To a solution of 1**7a** (1.0 g, 1.66 mmol) and *N*,*N*-diisopropylethylamine (1.66 mL, 8.83 mmol) in CH_2Cl_2 (27 mL) was added compound **6** (0.55 mL, 2.49 mmol). After 2 h, the reaction mixture was poured into sat. aq. $NaHCO_3$ (30 mL) and extracted with CH_2Cl_2 (3 × 30 mL). The combined organic layers were evaporated and the residue was purified by chromatography over silica gel eluting with hexanes/ethyl acetate/triethylamine (3:1:0.01), affording **18a** as a light yellow foam (1.03 g, 77%). ^{31}P NMR (161.9 MHz, $CDCl_3$): δ = 147.85, 147.80. IR (thin film): 3038, 2964, 2930, 2872, 2835, 1606, 1582, 1507, 1461, 1445, 1414, 1395, 1379, 1363, 1300, 1247, 1201, 1176, 1155, 1123, 1077, 1030, 977, 952, 898, 878, 847, 827, 790, 754, 718, 700, 682, 642, 613, 582, 561, 521, 484 and 465 cm^{-1}. HRMS: *m*/*z* [M + H$^+$] calcd for $C_{51}H_{51}N_2O_5P_1$: 803.3608; found: 803.3570.

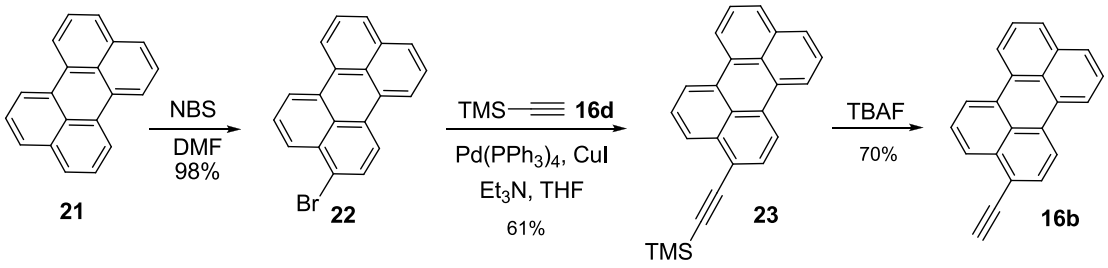

21 **22** **23** **16b**

Scheme 2.8 The synthesis of 3-ethynylperylene (**16b**).

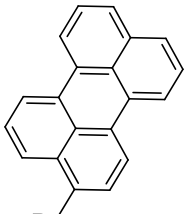

22

Compound 22 To a mixture of perylene (22) (300 mg, 1.20 mmol) and DMF (10 mL) was added NBS (214 mg, 1.20 mmol), and the reaction mixture was stirred at room temperature for 24 hour. Then, the mixture was poured into water (60 mL) and extracted by dichloromethane (2 × 500 mL). The combined organic layer was dried over Na_2SO_4, and evaporated under reduced pressure to offer a yellow solid. The crude product was purified by chromatography over silica gel eluting first with hexane/dichloromethane (10:1), last with dichloromethane, affording compound **22** as a bright yellow solid (388 mg, 98%).[20a]

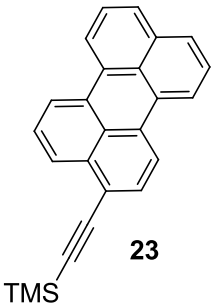

23

Compound 23 3-Bromoperylene (**22**) (200 mg, 0.61 mmol), $Pd(PPh_3)_2Cl_2$ (282 mg, 0.25 mmol) and CuI (70 mg, 0.31 mmol) were placed in a Schlenk flask and the flask was evacuated and recharged with N_2 gas. Piperidine (13 mL) and THF (13 mL) were added and the resulting mixture was degassed for 10 min. Then trimethylsilylacetylene (**16d**) (0.26 mL, 1.82 mmol) was added and the mixture was stirred for 12 hours at 80 °C. After cooling to room temperature, the slovent was removed under vacum, the resulting residue was purified by chromatography over silica gel eluting with hexanes/dichloromethane (100:1), affording compound **23** as a yellow solid (128 mg, 61%). ^{1}H NMR (300 MHz, $CDCl_3$): δ = 8.25-8.16 (m, 4H), 8.11 (d, J = 8.02 Hz, 1H), 7.70 (m, 3H), 7.58 (t, J = 7.9 Hz, 1H), 7.49 (td, J = 7.5, 1.7 Hz, 2H), 0.35 (s, 9H). Spectroscopic data is in agreement with reference.[20]

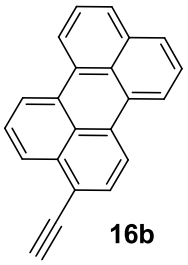

16b

Compound 16b To a solution of compound **23** (243 mg, 0.70 mmol) in THF (15 mL) was added tetrabutylammonium fluoride (1 M, 2.1 mL) dropwise. The reaction mixture was stirred at room temperature for 4 hours. Then the reaction was quenched by H_2O (50 mL), and stirred for another 30 min at room temperature. After that, the reaction mixture was extracted by CH_2Cl_2 (3 × 40 mL) and the combined organic layer was washed with brine for 3 times (3 × 40 mL). Then the organic layer was dried over anhydrous Na_2SO_4, concentrated *in vacuo*, and the resulting crude product was purified by chromatography over silica gel with hexanes/dichloromethane (100:1), affording compound **16b** as a yellow solid (135 mg, 70%). ^{1}H NMR (300 MHz, $CDCl_3$): δ = 8.25-8.16 (m, 4H), 8.11 (d, J = 7.9 Hz, 1H), 7.70 (m, 3H), 7.58 (dd, J = 1.7, 0.8 Hz, 1H), 7.49 (td, J = 7.8, 1.4 Hz, 2H), 3.55 (s, 1H). Spectroscopic data is in agreement with reference.[20]

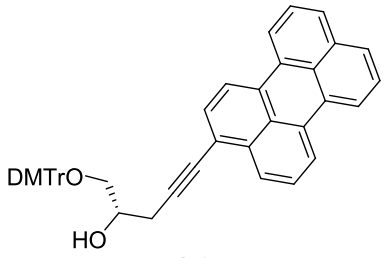

17b

Compound 17b To a solution of 3-ethynylperylene (**16b**) (58 mg, 0.21 mmol) in THF (4 mL) at -78 ^{o}C was added slowly *n*-BuLi in hexane (0.14 mL, 0.21 mmol). After stirring for 10 min at -78 ^{o}C, $BF_3{\cdot}Et_2O$ (0.03 mL, 0.21 mmol) was added dropwise and the stirring continued for another 5 min. The solution of compound **3** (83 mg, 0.21 mmol) in THF (0.5 mL) was then added slowly at -78 ^{o}C. Stirring was continued for another 15 min at -78 ^{o}C, then the reaction was quenched with saturated $NaHCO_3$ (50 mL) at -78 ^{o}C. The mixture was extracted with CH_2Cl_2 (3 × 40 mL). The

combined organic layers were dried over anhydrous Na_2SO_4, concentrated *in vacuo*, and the resulting dark yellow solid was purified by chromatography over silica gel eluting fist with hexanes/ethyl acetate/triethylamine (2:1:0.01) and last with hexanes/ethyl acetate/triethylamine (1:3:0.01), affording compound **14d** as a dark yellow foam (107 mg, 78%). ^{1}H NMR (300 MHz, $CDCl_3$): δ = 8.19 (m, 3H), 8.07 (m, 2H), 7.69 (d, J = 9.0 Hz, 2H), 7.48 (m, 6H), 7.38-7.26 (m, 7H), 7.21 (m, 1H), 6.81 (d, J = 9.0 Hz, 4H), 4.08 (m, 1H), 3.72 (s, 6H), 3.42 (m, 2H), 2.90 (d, J = 6.4 Hz, 2H). ^{13}C NMR (75MHz, $CDCl_3$): δ = 158.57, 144.91, 135.95, 134.70, 134.61, 131.34, 131.26, 130.97, 130.74, 130.13, 128.41, 128.17, 127.92, 127.07, 126.88, 126.59, 126.52, 126.12, 120.65, 120.56, 120.46, 119.49, 113.23, 91.86, 86.36, 81.26, 69.78, 66.20, 63.71, 55.15, 25.38. IR (thin film): 3051, 2927, 2834, 1731, 1605, 1583, 1507, 1461, 1443, 1389, 1299, 1246, 1175, 1155, 1070, 1032, 984, 827, 810, 767, 701 and 582 cm^{-1}. HRMS: m/z [M$^+$] calcd for $C_{42}H_{34}O_4$: 602.2452; found: 602.2429.

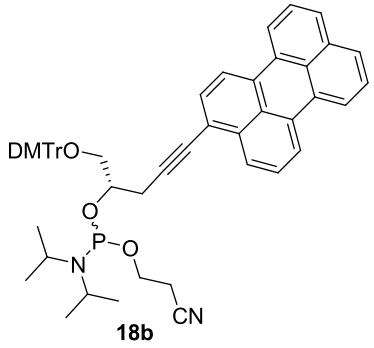

18b

Compound 18b To a solution of **17b** (395 mg, 0.61 mmol) and *N*,*N*-diisopropylethylamine (0.61 mL, 3.22 mmol) in CH_2Cl_2 (10 mL) was added compound **6** (0.27mL, 1.21 mmol). After 2 h, the reaction mixture was poured into sat. aq. $NaHCO_3$ (40 mL) and extracted with CH_2Cl_2 (3 × 40 mL). The combined organic extracts were dried over anhydrous Na_2SO_4, concentrated *in vacuo*, and the resulting oil was purified by chromatography over silica gel eluting with hexanes/ethyl acetate/triethylamine (3:1:0.01), affording compound **18b** as a dark yellow foam (446 mg, 86%). ^{31}P NMR (121.5 MHz, $CDCl_3$): δ = 149.27, 149.00. IR (thin film): 2963, 1507, 1460, 1444, 1389, 1362, 1259, 1175, 1079, 1022, 976, 798, 769, 702, 581 and 519 cm^{-1}. HRMS: m/z [M + H$^+$] calcd for $C_{49}H_{52}N_2O_5P_1$: 779.3608; found: 779.3602.

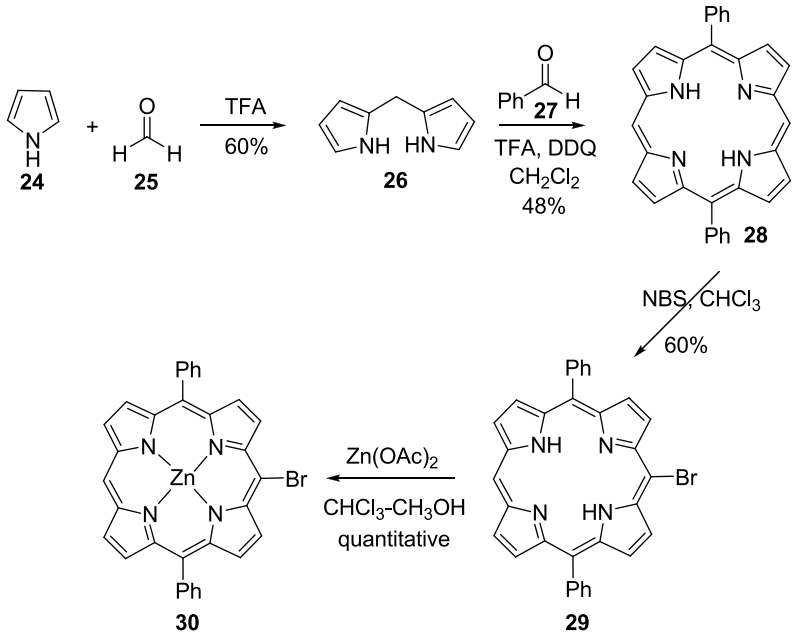

Scheme 2.9 The synthesis of 5-bromo-10,20-diphenylporphinatozinc (**30**).

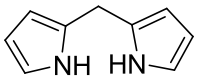

26

Compound 26 A suspension of parahormaldehyde (**25**) (1.21 g, 40.31 mmol) in pyrrole (**24**) (70 mL, 1.01 mmol) was placed in a 250 mL three necked round bottomed flask equipped with an internal thermal meter and a water condenser in the reflex position. The solution was heated to 50 ^{o}C, and then the heat source was removed and TFA (4.03 mmol, 0.3 mL) was added immediately. A sharp increase in the temperature of the solution was observed (to 70 ^{o}C), and the solution rapiddly became clear and dark. After 5 min, the reaction was quenched with 0.1 M NaOH. Ethyl acetate was then added. The organic layer was washed with water and dried over anhydrouse Na_2SO_4, concentrated by rotary evaporation, the redulting residue was distilled with Rugelrohr (condition: 230 ^{o}C, full vaccum). The collected colorless solid was recrystallated with EtOH-H_2O and that offtered compund **26** as a colorless crystal (5.89 g, 60%). ^{1}H NMR (300 MHz, $CDCl_3$): δ = 6.65 (m, 2H), 6.15 (dd, J = 5.9, 2.8 Hz, 2H), 5.90 (m, 2H), 3.98 (s, 2H). Spectroscopic data is in agreement with reference.[21a]

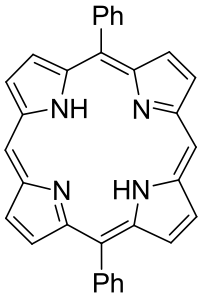

28

Compound 28 A flame dried 1 L flask equipped with a magnetic stirring bar was charged with 2,2′-dipyrrolmethane (**26**) (458 mg, 3.1 mmol), benzaldehyde (**27**) (315 μL, 3.1 mmol), and 600 mL of fleshly distilled methylene chloride. The solution was degased with a stream of dry nitrogen for 15 min. Trifluoroacetic acid (150 μL, 1.95 mmol) was added via syringe, the flask was shield from light with aluminumfoil, and the solution was stirred for 3 h at room temperature. The reaction was quenched by the addition of 900 mg (3.96 mmol) of 2,3-dichloro-3,6-dicyanobenzoquinone (DDQ), and the solution was stirred for an additional 30 min. pyridine (3 mL) was then added, which serves two purpose: 1, it neutralizes exvess acid and 1,4-dihydroxy-2,3-dichloro-5,6-dicyanobenzone, and 2, it reacts with excess DDQ to form an insoluble preciptate which can be filtered from the solution prior to chromatographic work up. The solvent was evaporated leaving purple crystals **28** that were washed with hexane, filtered and dried (680 mg, 48%). ^{1}H NMR (300 MHz, $CDCl_3$): δ = 10.33 (s, 2H), 9.41 (d, J = 4.7 Hz, 4H), 9.10 (d, 4H), 8.29 (m, 4H), 7.82 (m, 6H), -3.12 (S, 2H). Spectroscopic data is in agreement with reference.[21b]

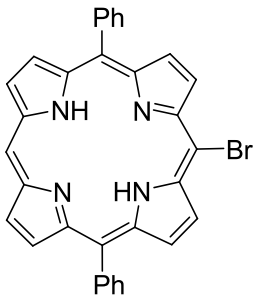

29

Compound 29 To a solution of compound **28** (76.1 mg, 0.16 mmol) and pyridine (67 μL) in $CHCl_3$ (53 mL) was added NBS (29 mg, 0.16 mmol) at 0 ^{o}C and was

stirred for 15 min, then acetone (2.6 mL) was added in. After that, the organic layer was washed with water and dried over anhydrouse Na_2SO_4, concentrated by rotary evaporation, the redulting residue was purified by chromatography over silica gel eluting with hexanes/dichloromethane (5:1), finaly with hexanes/dichloromethane (2:1), affording compound **29** as a purple solid (50 mg, 60%). ^{1}H NMR (300 MHz, $CDCl_3$): δ = 10.18 (s, 1H), 9.75 (d, J = 5.0 Hz, 2H), 9.29 (d, J = 4.6 Hz, 2H), 8.96 (dd, J = 4.6, 3.0 Hz, 4H), 8.22 (m, 4H), 7.79 (m, 6H), -3.01 (s, 1H). Spectroscopic data is in agreement with reference.[21c]

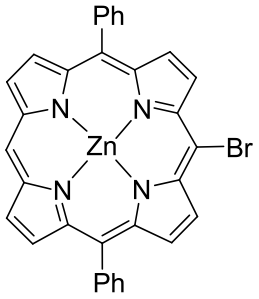

30

Compound 30 To a solution of compound **29** (57.3mg, 1.06 mmol) in mixed solvents $CHCl_3$ (30 mL)-MeOH (3 mL) was added $Zn(OAc)_2$ (192 mg, 10.6 mmol), and the reaction mixture was stirred at 70 ^{o}C for overnight. After cooling to room temperature, the reaction mixture was dilluted to 60 mL and washed well with aqueous $NaHCO_3$ and water. The organic layer was dried over anhydrous Na_2SO_4, concentrated by rotary evaporation, offering product **30** as a purple red solid (64.1 mg, quantitative) that was used in next step without further purification. ^{1}H NMR (300 MHz, $CDCl_3$): δ = 10.23 (s, 1H), 9.81 (d, J = 4.7 Hz, 2H), 9.37 (d, J = 4.6 Hz, 2H), 9.05 (dd, J = 4.6, 2.6 Hz, 4H), 8.22 (m, 4H), 7.80 (m, 6H). Spectroscopic data is in agreement with reference.[21d]

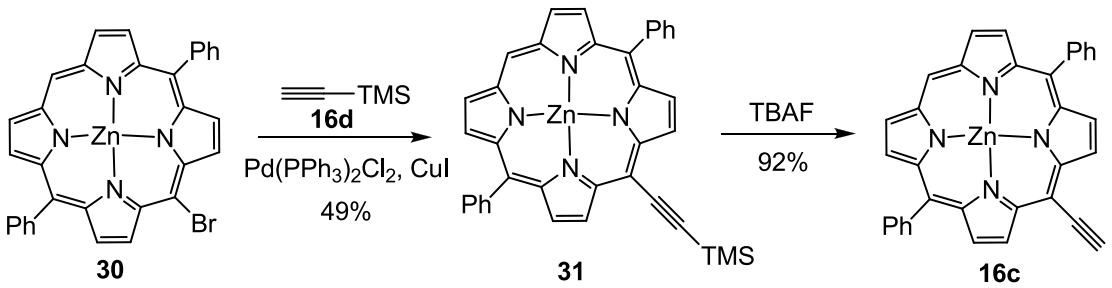

Scheme 2.10 Synthesis of 5-ethynyl-10,20-diphenylporphinatozinc (**16c**).

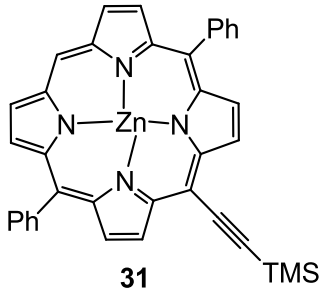

Compound 31 Compound **30** (116 mg, 0.19 mmol), $Pd(PPh_3)_4$ (23.1 mg, 0.02 mmol) and CuI (7.3 mg, 0.04 mmol) were placed in a Schlenk flask and the flask was evacuated and recharged with N_2 gas. Dry THF (6 mL) and dry Et_3N (4 mL) were added and the resulting mixture was degassed for 10 min. Then a solution of ethynyltrimethylsilane **16d** (0.06 mL, 0.39 mmol) in dry THF (1 mL) was added and the mixture was stirred for 12 hours at 65 °C. After cooling to room temperature, the mixture was poured into saturated aqueous $NaHCO_3$, extracted with CH_2Cl_2 (3 × 40 mL), dried over Na_2SO_4, filtered, and evaporated. The resulting residue was purified by chromatography over silica gel eluting with hexanes/dichloromethane (2:1), affording compound **31** as a purple solide (58 mg, 49%). ^{1}H NMR (300 MHz, $CDCl_3$): δ = 9.85 (s, 1H), 9.78 (d, J = 4.7 Hz, 2H), 9.10 (d, J = 4.6 Hz, 2H), 9.0 (d, J = 4.6 Hz, 2H), 8.89 (d, J = 4.5 Hz, 2H), 8.17 (dd, J = 1.6, 7.2 Hz, 4H), 7.78 (m, 6H), 0.65 (s, 9H). Spectroscopic data is in agreement with reference.[21b]

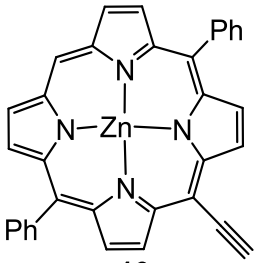

16c

Compound 16c To a solution of compound **31** (94 mg, 0.15 mmol) in THF (10 mL) was added 1.0 M THF solution of tetrabutylammonium fluoride (0.45 mL) and then stirred for 1 hour at room temperature. The reaction was quenched with H_2O and extracted with CH_2Cl_2 (3 × 30 mL). The combined organic extracts were dried over anhydrous Na_2SO_4 and concentrated using rotary evaporation. The resulting oil was purified by chromatography over silica gel eluting with hexanes/THF (8:1), affording compound **16c** as a purple solid (75 mg, 92%). ^{1}H NMR (300 MHz, DMSO): δ = 10.35 (s, 1H), 9.67 (d, J = 4.6 Hz, 2H), 9.46 (d, J = 4.5 Hz, 2H), 8.89 (d, J = 4.6 Hz, 2H), 8.84 (d, J = 4.5 Hz, 2H), 8.20 (m, 4H), 7.84 (m, 6H), 5.76 (s, 1H). Spectroscopic data is in agreement with reference.[21b]

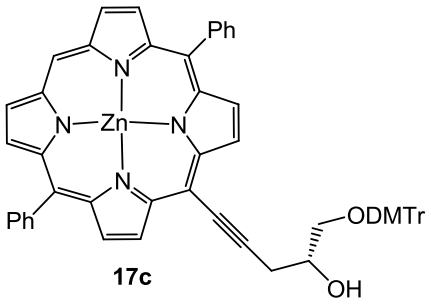

17c

Compound 17c Compound **21** (198 mg, 0.328 mmol), $Pd(PPh_3)_4$ (75.8 mg, 0.066 mmol) and CuI (25 mg, 0.131 mmol) were placed in a Schlenk flask and the flask was evacuated and recharged with N_2 gas. Dry THF (7 mL) and dry Et_3N (6 mL) were added and the resulting mixture was degassed for 10 min. Then compound **17d** (263.8 mg, 0.656 mmol) in anhydrous THF (3 mL) was added and the mixture was stirred for 12 hours at 65 °C. After cooling to room temperature, the mixture was poured into saturated aqueous $NaHCO_3$, extracted with CH_2Cl_2 (3 × 40 mL), dried over Na_2SO_4, filtered, and evaporated. The resulting residue was purified by chromatography over

silica gel eluting with hexanes/dichloromethane/triethylamine (1:1:0.01), affording compound **17c** as a purple foam (289 mg, 95%). ^{1}H NMR (300 MHz, $CDCl_3$): δ = 10.05 (s, 1H), 9.41 (d, J = 4.6 Hz, 2H), 9.25 (d, J = 4.5 Hz, 2H), 8.96 (d, J = 4.5 Hz, 2H), 8.91 (d, J = 4.6 Hz, 2H), 8.19 (dd, J = 7.5, 1.6 Hz, 4H), 7.78 (m, 6H), 7.36 (m, 2H), 7.18-7.26 (m, 6H), 7.10-7.15 (m, 1H), 6.57 (dd, J = 8.9, 1.3 Hz, 4H), 3.74 (m, 1H), 3.38 (m, 1H), 3.33 (d, J = 2.0 Hz, 6H), 3.25 (m, 1H), 2.75 (m, 2H). ^{13}C NMR (125 MHz, $CDCl_3$): δ = 158.42, 152.08, 150.42, 149.77, 149.61, 144.99, 142.94, 135.89, 134.90, 132.54, 132.34, 131.78, 130.97, 130.11, 128.18, 128.00, 127.52, 126.93, 126.69, 120.97, 113.29, 107.06, 86.41, 69.92, 66.35, 55.07, 53.55, 29.85, 25.42. IR (thin film): 3052, 2933, 2831, 1597, 1506, 1489, 1459, 1439, 1382, 1298, 1245, 1219, 1173, 1153, 1058, 1031, 989, 904, 825, 790, 749, 727, 716, 619 and 580 cm^{-1}. HRMS: m/z [M + H^+] calcd for $C_{58}H_{45}N_4O_4Zn_1$: 925.2727; found: 925.2726.

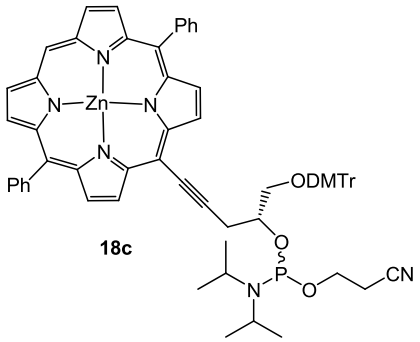

18c

Compound 18c To a solution of compound **17c** (93.6 mg, 0.101 mmol) and *N*,*N*-diisopropylethylamine (0.1 mL, 0.538 mmol) in anhydrous CH_2Cl_2 (4 mL) was added phoramidite reagent **6** (0.034 mL, 0.152 mmol). After 2 h, the reaction mixture was poured into saturated aqueous $NaHCO_3$ and extracted by CH_2Cl_2 (3 × 40 mL). The organic layer was evaporated to dryness and the resulting residue was purified by chromatography over silica gel eluting with hexanes/dichloromethane/triethylamine (2:1:0.01), affording compound **18c** as a purple foam (85 mg, 74%). (compound **18c** is a mixture of two diastermers, the ratio of major and minor isomers is around 2:1 according to ^{1}H NMR) ^{1}H NMR (500 MHz, $CDCl_3$): δ = 10.04 (s, 2H), 9.64 (d, J = 4.5 Hz, 2H), 9.59 (d, J = 4.6 Hz, 2H), 9.23 (d, J = 4.5 Hz, 4H), 8.93-3.98 (m, 8H), 8.23 (d, J = 7.3 Hz, 8H), 7.77-7.83 (m, 12H), 7.51-7.56 (m, 4H), 7.30-7.38(m, 8H),

7.19-7.25 (m, 4H), 7.09-7.14 (m, 2H), 6.50 (d, *J* = 8.9 Hz, 2H), 6.47 (d, *J* = 8.9 Hz, 2H), 6.40 (d, *J* = 8.9 Hz, 2H) (minor isomer), 6.32 (d, *J* = 8.8 Hz, 2H) (minor isomer), 4.57-4.69 (m, 2H), 3.63-3.98 (m, 12H), 3.55-3.60 (m, 2H), 3.38-3.46 (m, 2H), 3.23 (s, 3H), 3.18 (s, 3H), 3.08 (s, 3H) (minor isomer), 2.97 (s, 3H) (minor isomer), 2.41-2.60 (m, 2H), 2.31-2.37 (m, 2H) (minor isomer), 1.32 (d, *J* = 6.8 Hz, 6H) (minor isomer), 1.25 (d, *J* = 6.8 Hz, 6H) (minor isomer), 1.20 (d, *J* = 6.8Hz, 6H), 1.17 (d, *J* = 6.8 Hz, 6H). ^{13}C NMR (125 MHz, $CDCl_3$): δ = 158.22, 158.13, 158.10, 157.94, 152.20, 152.15, 150.43, 150.41, 149.83, 149.70, 149.67, 145.35, 145.32, 142.76, 136.38, 136.29, 136.04, 136.00, 134.72, 132.55, 132.50, 131.85, 131.30, 130.32, 130.13, 130.06, 128.32, 128.28, 127.90, 127.85, 127.62, 126.77, 121.10, 117.80, 117.63, 113.20, 113.17, 113.14, 113.11, 106.98, 86.35, 86.30, 73.12, 72.97, 72.33, 72.20, 65.95, 65.94, 65.79, 65.78, 58.78, 58.74, 58.64, 58.60, 55.10, 54.96, 54.92, 54.84, 43.64, 43.54, 43.49, 25.89, 25.84, 25.81, 24.91, 24.56, 24.81, 24.76, 20.48, 20.42, 20.41, 20.36. ^{31}P NMR (121 MHz, $CDCl_3$): δ = 148.05, 147.85. IR (thin film): 2962, 2930, 2866, 2834, 2253, 2227, 2022, 1507, 1490, 1460, 1440, 1382, 1363, 1297, 1248, 1176, 1154, 1124, 1060, 1032, 1002, 992, 908, 827, 792, 780, 751, 728, 717, 700, 658 and 582 cm^{-1}. HRMS: *m*/*z* [M + H$^+$] calcd for $C_{67}H_{62}N_6O_5P_1Zn_1$: 1125.3805; found: 1125.3807.

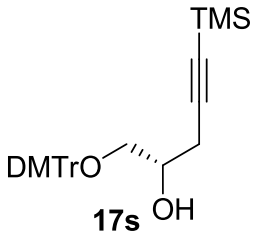

17s

Compound 17s To a solution of ethynyltrimethylsilane (**16d**) (0.47 mL, 3.32 mmol) in dry THF (8 mL) at -78 °C was added slowly a 1.6 M hexane solution of *n*-BuLi (2.1 mL, 3.36 mmol). After stirring for 10 min, boron trifluoride diethyl etherate ($BF_3 \cdot Et_2O$) (0.42 mL, 3.32 mmol) was added dropwise. After an additional 5 min at -78 °C, a solution of compound **3** (1.25 g, 3.32 mmol) in anhydrous THF (4 mL) was added slowly. The resulting solution was stirred for 15 min at -78 °C. The reaction

was then quenched with saturated aqueous $NaHCO_3$ (80 mL) at -78 °C and extracted with CH_2Cl_2 (3 × 60 mL). The combined organic layers were dried over anhydrous Na_2SO_4, concentrated by rotary evaporation, and purified by flash chromatography over silica gel eluting with hexanes/ethyl acetate/triethylamine (10:1:0.01), affording compound **17s** as a colorless oil (1.11 g, 70%). ^{1}H NMR (300 MHz, $CDCl_3$): δ = 7.45 (m, 2H), 7.16-7.38 (m, 7H), 6.84 (d, J = 8.9 Hz, 4H), 3.92 (m, 1H), 3.79 (s, 6H), 3.24 (m, 2H), 2.52 (d, J = 6.4 Hz, 2H), 0.115 (s, 9H). ^{13}C NMR (75 MHz, $CDCl_3$): δ = 158.65, 144.92, 136.08, 130.18, 128.26, 127.96, 126.95, 113.30, 102.79, 87.34, 86.32, 69.49, 66.10, 55.30, 25.46, 0.14. IR (thin film): 2956, 2933, 2175, 1607, 1580, 1508, 1462, 1445, 1414, 1335, 1298, 1246, 1174, 1155,1075, 1032, 826, 790, 756, 726, 701, 645 and 583 cm^{-1}. HRMS: m/z [M + Na$^+$] calcd for $C_{29}H_{34}O_4Si_1Na_1$: 497.2119; found: 497.2120.

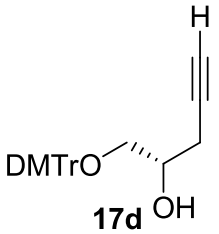

17d

Compound 17d To a solution of compound **17s** (1.73 g, 3.65 mmol) in THF (36.5 mL) was added 1.0 M THF solution of tetrabutylammonium fluoride (11 mL) and then stirred for 1 hour at room temperature. The reaction was quenched with H_2O and extracted with CH_2Cl_2 (3 × 50 mL). The combined organic extracts were dried over anhydrous Na_2SO_4 and concentrated using rotary evaporation. The resulting oil was purified by chromatography over silica gel eluting with hexanes/ethyl acetate/triethylamine (5:1:0.01), affording compound **17d** as a colourless oil (1.45 g, 98%).^{1}H NMR (300 MHz, $CDCl_3$): δ = 7.43 (m, 2H), 7.26-7.34 (m, 6H), 7.19-7.24 (m, 1H), 6.83 (d, J = 8.9 Hz, 4H), 3.91 (m, 1H), 3.79 (s, 6H), 3.24 (m, 2H), 2.47 (ddd, J = 6.2, 2.6, 0.8 Hz, 2H), 2.37 (d, J = 5.0 Hz, 1H), 1.98 (t, J = 2.7 Hz, 1H). ^{13}C NMR (75 MHz, $CDCl_3$): δ = 158.71, 144.88, 136.06, 130.20, 128.28, 128.00, 127.01, 113.32, 86.43, 80.52, 70.67, 69.45, 66.06, 55.37, 24.07. IR (thin film): 3287, 3000, 2836, 2045, 1734, 1607, 1581, 1507, 1462, 1444, 1299, 1245, 1174, 1154, 1072, 1031, 951,

913, 826, 790, 772, 754, 701, 634, and 582 cm^{-1}. HRMS: *m*/*z* [M + Na^+] calcd for $C_{26}H_{26}O_4Na_1$: 425.1723; found: 425.1723.

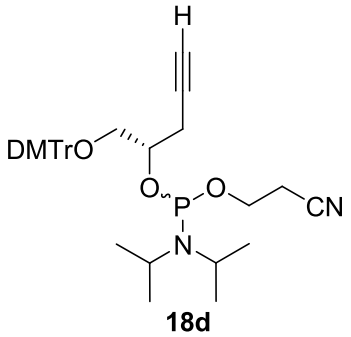

18d

Compound 18d To a solution of compound **17d** (0.40 g, 0.99 mmol) and *N*,*N*-diisopropylethylamine (0.99 mL, 5.24 mmol) in anhydrous CH_2Cl_2 (16 mL) was added phosphoramidite reagent **6** (0.26 mL, 1.18 mmol). After 2 h, the reaction mixture was poured into saturated aqueous $NaHCO_3$ and extracted by CH_2Cl_2 (3 × 40 mL). The organic layer was evaporated to dryness and the resulting residue was purified by chromatography over silica gel eluting with hexanes/ethyl acetate/ triethylamine (3:1:0.01), affording compound **18d** as a colorless oil (0.58 g, 96%).^{31}P NMR (121 MHz, $CDCl_3$): δ = 147.72, 147.64. IR (thin film): 3289, 2965, 2931, 2874, 2836, 1607, 1508, 1462, 1363, 1248, 1176, 1155, 1076, 1031, 976, 828, 727, 700, 640, 583, 524 cm^{-1}. HRMS: *m*/*z* [M + Na^+] calcd for $C_{35}H_{43}N_2O_5P_1Na_1$: 625.2802; found: 625.2801.

Chapter 2.5 References

1. Kolb, H. C.; Finn, M. G.; Sharpless, K. B. *Angewandte Chemie International Edition* **2001**, *40*, 2004.
2. Jacobsen, E. N.; Wu, M. H. In comprehensive Asymmetric Catalysis (Eds.: Jacobsen, E. N.; Pfaltz, A.; Yamamoto, H.), Springer, New York, **1999**; chapter 35.
3. (a) Huynh, D.; Derguini-Boumechal, F.; Linstrumelle, G. *Tetrahedron letter* **1979**, *20,* 1503-1506; (b) Schwartz, P.; Madan, P.; Whitesell, J. K.; Lawrence, R. M. Organic syntheses 1990, 69, 1-9.
4. (a) Eis, M. J.; Wrobel, J. E.; Ganem, B. *Journal of American Chemical Society* **1984**, *106*, 3693-3694; (b) Reich, H. J.; Sanders, A. W.; Fiedler, A. T.; Bevan, M. J. *Journal of American Chemical Society* **2002**, *124*, 13386-13387.
5. Chounan, Y.; Yamamoto, Y. in *Modern Organocopper Chemisty* (Ed.: N. Krause), Wiley-VCH, Weinheim, 2002, chapter 9.
6. Uchiyama, M.; Kameda, M.; Mishima, O.; Yokoyama, N.; Koike, M.; Kondo, Y.; Sakamoto, T. *Journal of American Chemical Society* **1998**, *20*, 4934-4946.
7. Schneider, C.; Brauner, J. *European Journal of Organic Chemistry* **2001**, 4445-4450.
8. Mukeji, I.; Weyda, A. L.; Dabbagh, G.; Bertz, S. H. *Angewandte Chemie International Edition* **1986**, *25*, 734-735.
9. (a) Nugent, W. A. *Journal of the American Chemical Society* **1992**, *14*, 2768–2769; (b) Martinez, L. E.; Leighton, J. L.; Carsten, D. H.; Jacobesen, E. N. *Journal of the American Chemical Society* **1995**, *117*, 5887–5889; (c) Schaus, S. E.; Larrow, J. F.; Jacobsen, E. N. *Journal of Organic Chemistry* **1997**, 62, 4197-4199.
10. (a) Carrée, F.; Gil, R.; Collin, J. *Organic Letters* **2005**, *7*, 1023-1026; (b) Azoulay, S.; Manabe, K.; Kobayashi, S. *Organic Letters* **2005**, *7*, 4593-4595.
11. (a) Iida, T.; Yamamoto, N.; Matsunaga, S.; Woo, H.-G.; Shibasaki, M.

Angewandte Chemie International Edition **1998**, *37*, 2223-2226; (b) Schneider, C.; Sreekanth, A. R.; Mai, E. *Angewandte Chemie International Edition* **2004**, *43*, 5691-5694.

12. (a) Iida, T.; Yamamoto, N. *Journal of the American Chemical Society* **1997**, *119*, 4783–4784; (b) Wu, M. H.; Jacobsen, E. N. *Journal of Organic Chemistry* **1998**, 63, 5252-5254.
13. (a) Denmark, S. E.; Barsanti, P. A.; Wong, K.-T.; Stavenger, R. A. *Journal of Organic Chemistry* **1998**, 63, 2428-2429; (b) Nugent, W. A. *Journal of the American Chemical Society* **1998**, *120*, 7139–7140.
14. (a) Hubbs, J. L.; Heathcock, C. H. *Journal of the American Chemical Society* **2003**, *125*, 12836–12843; (b) Hanessian, S.; Yang, Y.; Giroux, S.; Mascitti, V.; Ma, J.; Raeppel, F. *Journal of the American Chemical Society* **2003**, *125*, 12784–13792; (c) Dakin, L. A.; Panek, J. S. *Organic Letters* **2003**, *5*, 3995-3998; (d) Pichlmair, S.; Marques, M. M. B.; Green, M. P.; Martin, H. J.; Mulzer, J. *Organic Letters* **2003**, *5*, 4657-4659; (e) kim, J. H.; Lim, H. J.; Cheon, S. H. *Tetrahedron* **2003**, *59*, 7501-7507; (f) Schmidt, B.; pohel, M.; Cortisella, B. *Tetrahedron* **2002**, *58*, 7951-7958.
15. Chemla, F.; Vrancken, E.; Patai Series: *The Chemistry of Organolithium Compounds* (Ed.: Z. Rappoport), Wiley, Chichester, 2004, p. 1165-1242.
16. Coleman, R. S.; Mortensen, M. A. *Tetrahedron Letter* **2003**, *44*, 1215-1219.
17. Yang, S.-W.; Elangovan, A.; Hwang, K. -C. And Ho, T.-I. *Journal of Physical chemistry B* **2005**, *109*, 16628-16635.
18. (a) Hodgson, D. M.; Gibbs, A. R.; Lee, G. P. *Tetrahedron* **1996**, *52*, 14361-14384; (b) Satoh, T. Chemical Reviews 1996, 96, 3303-3325; (c) Doris, E.; Dechoux, L.; Mioskowski, C. *Synletter* **1998**, 337-343; (d) O'Brien, P. *Journal of the Chemical Society, Perkin Transactions 1* **1998***, 1439-1458*; (e) Magnus, A.; Bertilsson, S. K.; Andersson, P. G. *Chemical Society Reviews* **2002**, *31*, 223-229; (f) Hodgson, D. M.; Gras, E. *Synthesis 2002*, 1625-1642.
19. Hissler, M.; Harriman, A.; Khatyr, A. and Ziessel, R. *Chemistry - A European Journal* **1999**, *5*, 3366.

20. (a) Burley, G. A.; Avent, A. G.; Gol'dt, I. V.; Hitchcick, P. B.; Al-Matar, H.; Paolucci, D.; Paolucci, F.; Fowler, P. W.; Soncini, A.; Street, J. M.; Taylor, R. *Organic & Biomoleculor Chemistry* **2004**, *2*, 319-329; (b) Andronova, V. L.; Skorobogatyi, M. V.; manasova, E. V.; Berlin, Yu. A.; korshun, V. A.; Galegov, G. A. *Russian Journal of Bioorganic Chemistry* **2003**, *29*, 290-295.

21. (a) Lin, V. S.-Y.; Iovine, P. M.; Dimango, S. G.; Therien, M. J. *Inorganic Syntheses* **2002**, *33*, 55; (b) Fazekas, M.; Pintea, M.; Senge, M. O.; Zawadzka, M. *Tetrahedron Letters* **2008**, *49 (14)*, 2236; (c) Balaban, T. S.; Goddard, R.; Schaetzel, M. L.; Lehn, J.-M. *Journal of American Chemistry Society* **2003**, *125*, 4233; (d) Kai, H.; Nara, S.; Kinbara, K.; Aida, T. *Journal of American Chemistry Society* **2008**, *130*, 6725.

22. Zhang, L.; Peritz, A. E.; Carroll, P. J.; Meggers, E. *Synthesis* **2006**, 645.

23. Zhang, L.; Peritz, A.; Meggers, E. *Journal of the American Chemical Society* **2005**, *127*, 4174 –4175.

Appendix to Chapter 2: ^{1}H, ^{13}C, ^{31}P NMR spectra and IR spectra

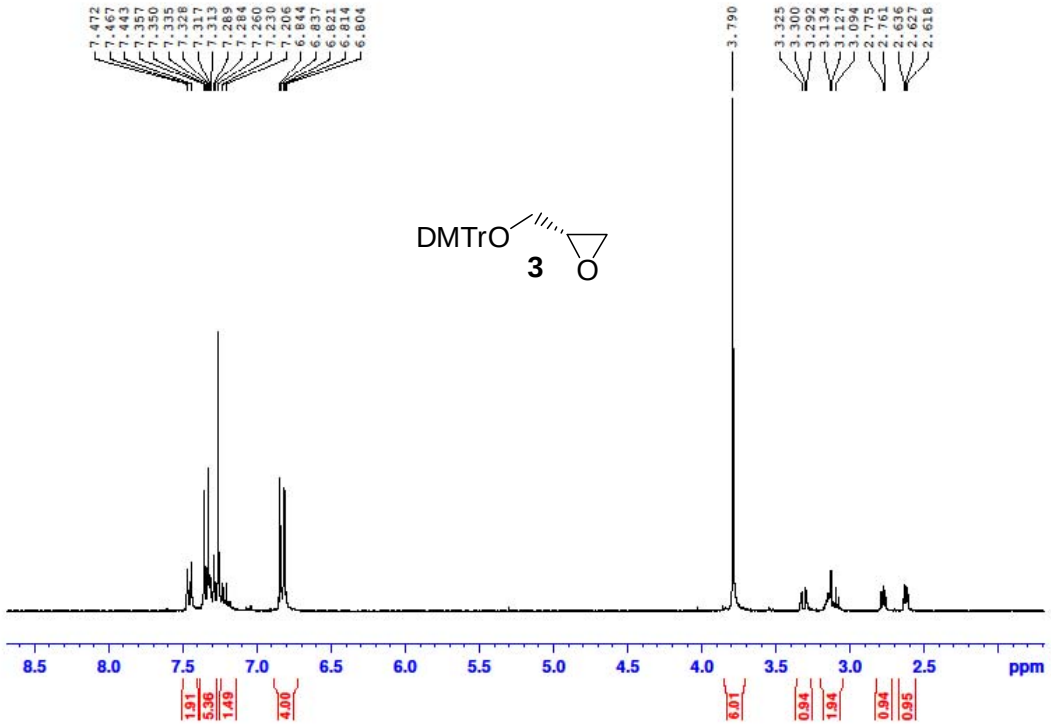

Figure A2.1.1 ^{1}H-NMR spectrum of compound **3** (300 MHz, $CDCl_3$).

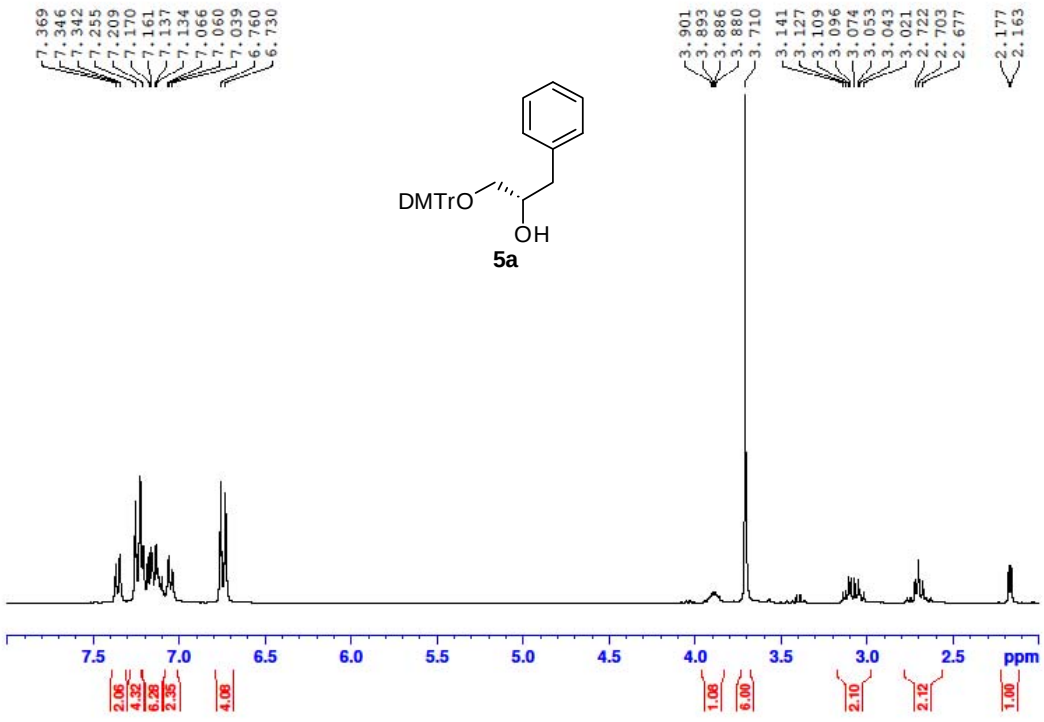

Figure A2.2.1 ^{1}H-NMR spectrum of compound **5a** (300 MHz, $CDCl_3$).

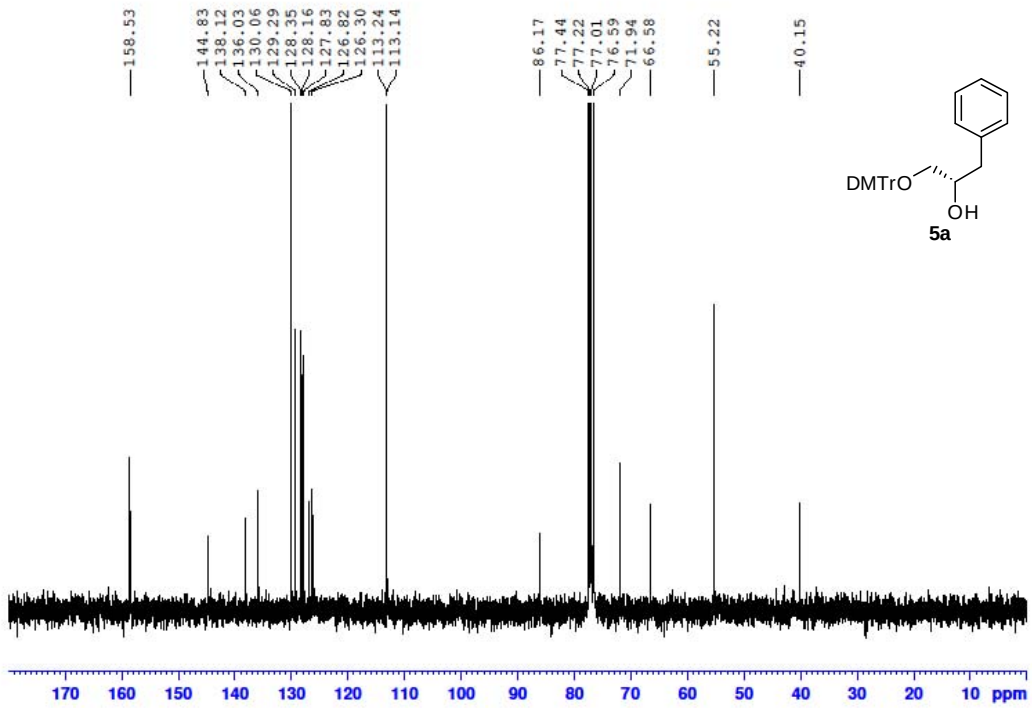

Figure A2.2.2 ^{13}C-NMR spectrum of compound **5a** (75 MHz, $CDCl_3$).

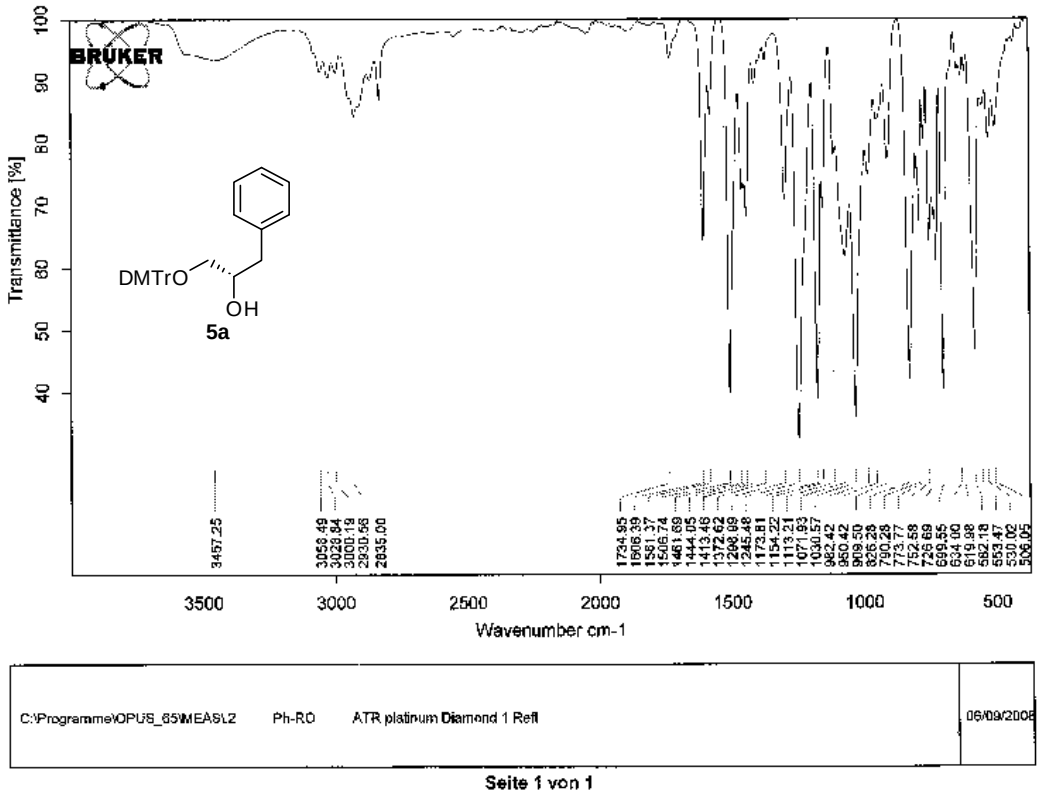

Figure A2.2.3 IR spectrum of compound **5a** (solid).

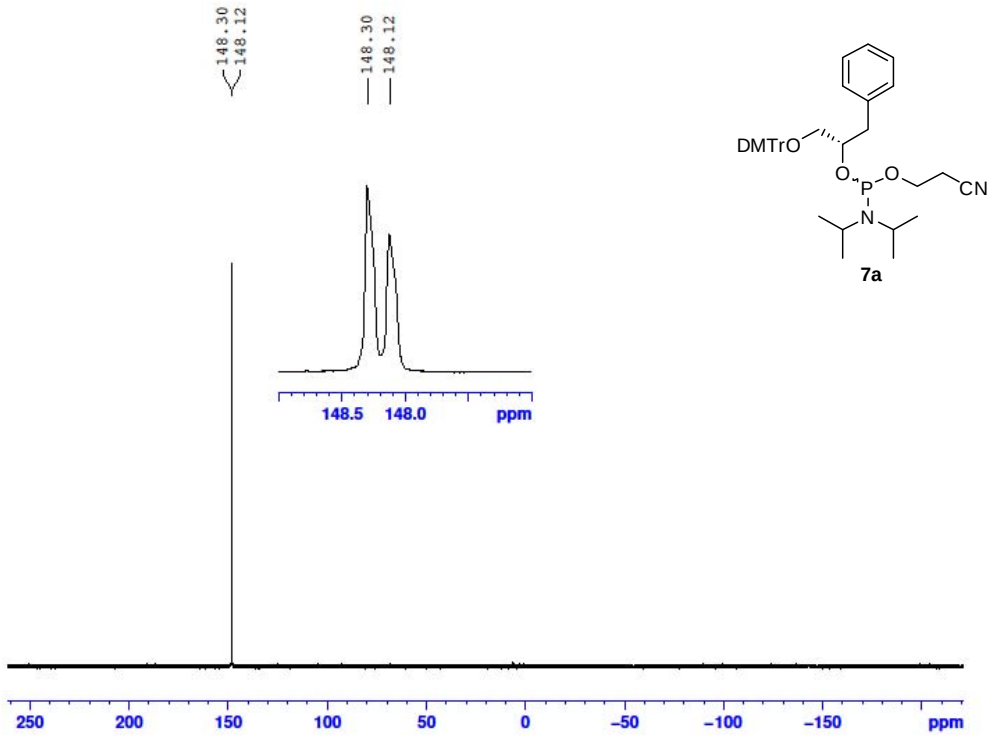

Figure A2.3.1 ^{31}P-NMR spectrum of compound **7a** (121.5 MHz, $CDCl_3$).

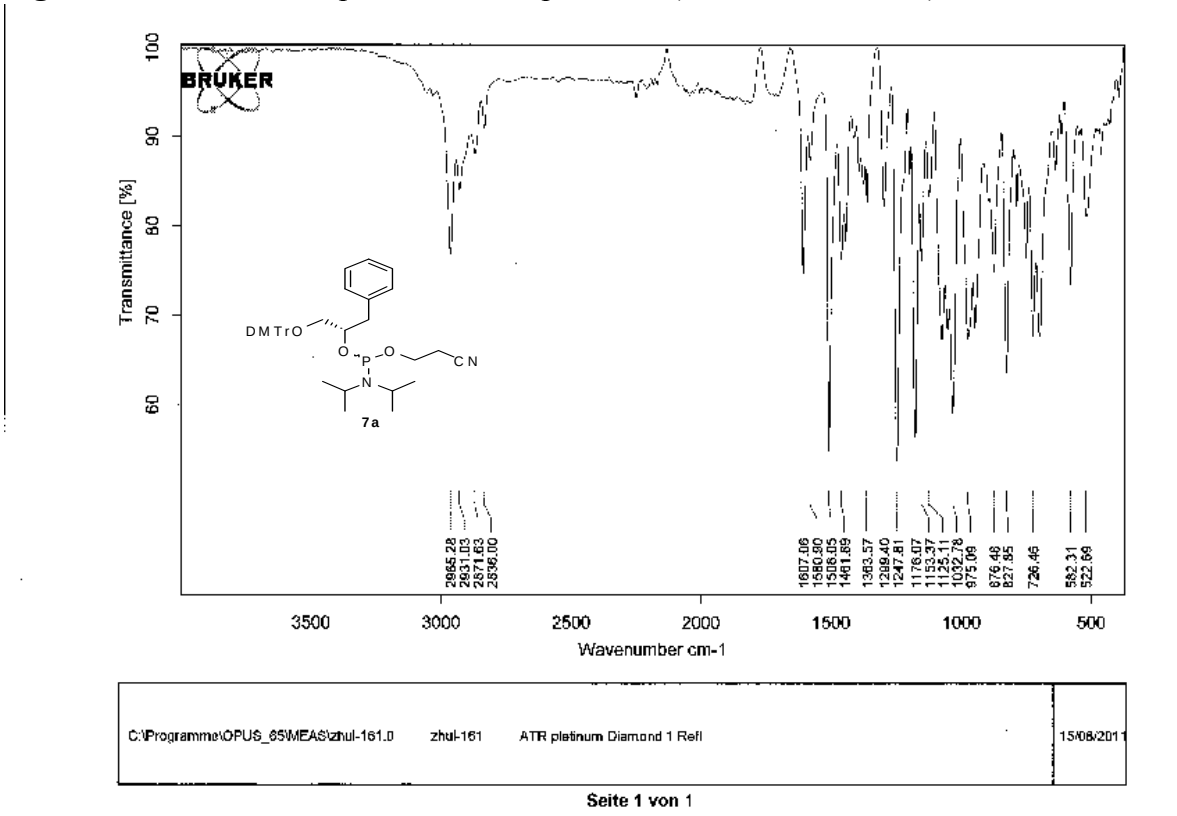

Figure A2.3.2 IR spectrum of compound **7a** (solid).

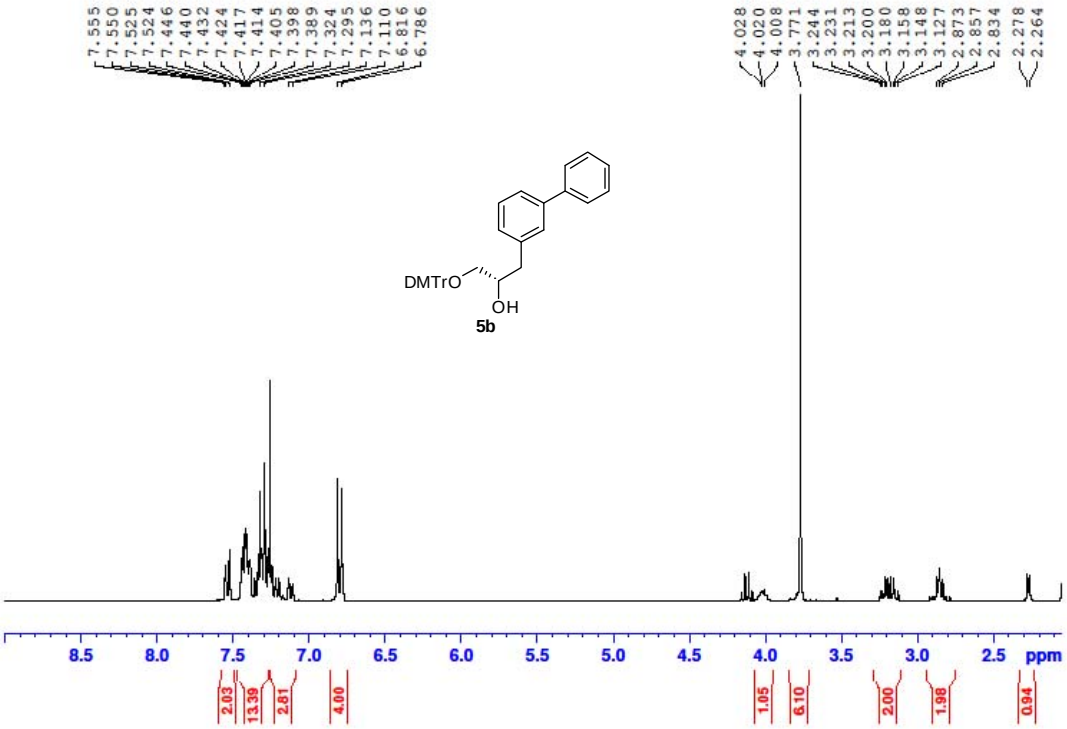

Figure A2.4.1 ^{1}H-NMR spectrum of compound **5b** (300 MHz, $CDCl_3$).

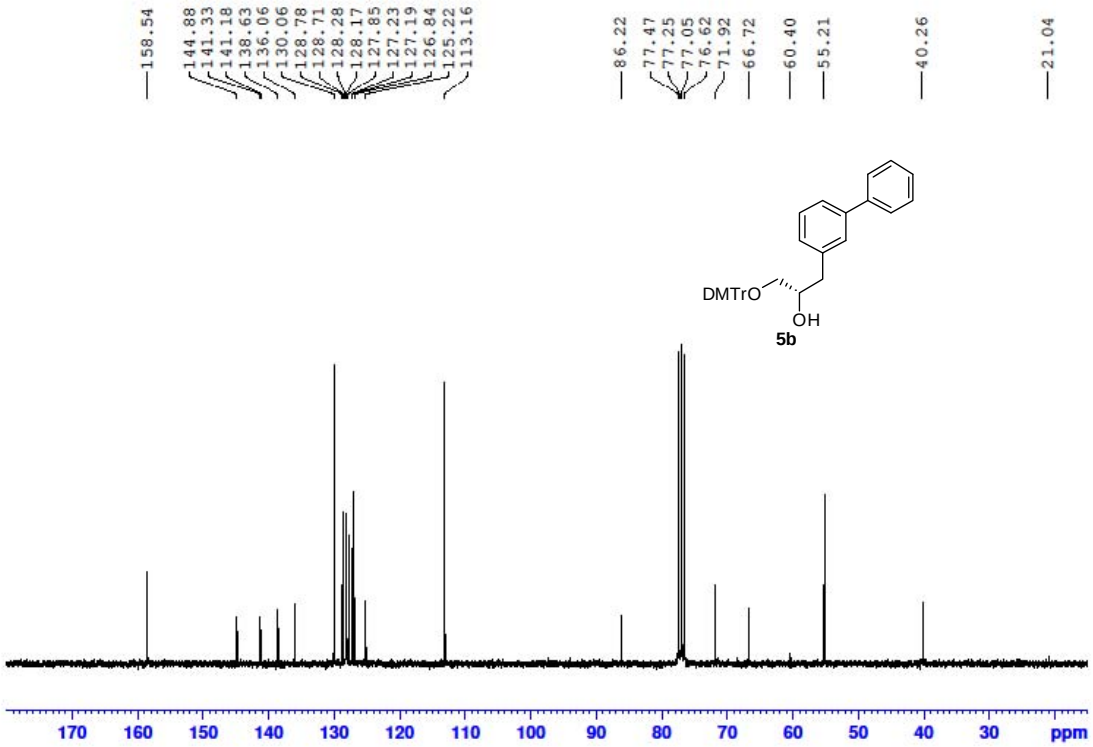

Figure A2.4.2 ^{13}C-NMR spectrum of compound **5b** (75 MHz, $CDCl_3$).

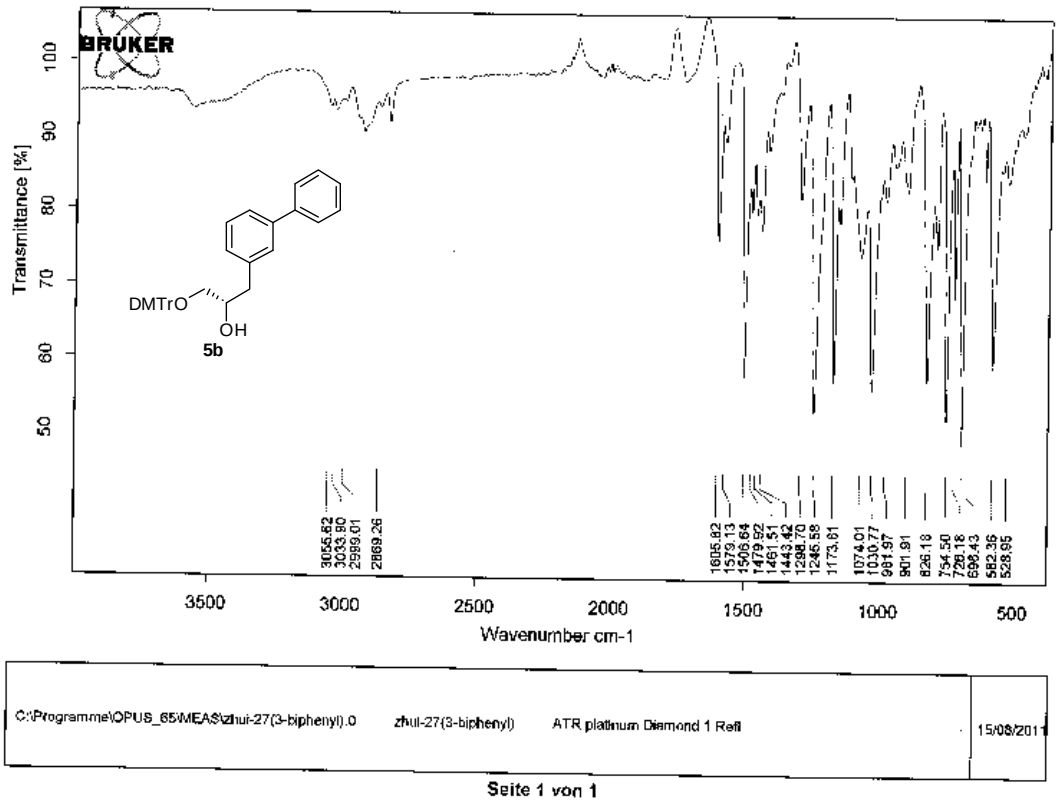

Figure A2.4.3 IR spectrum of compound **5b** (solid).

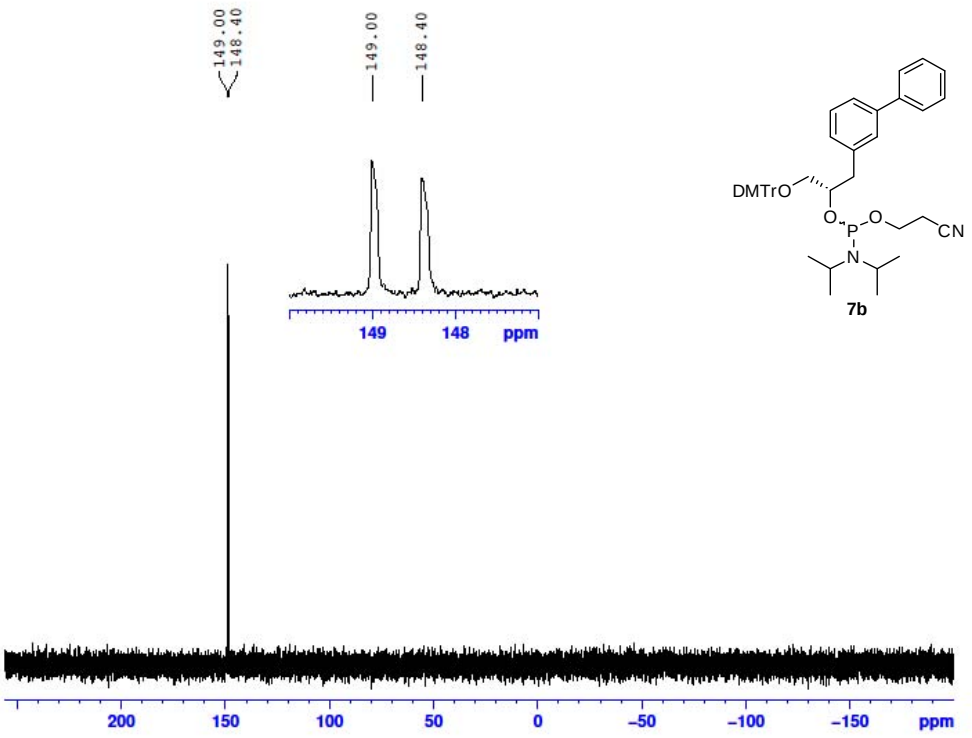

Figure A2.5.1 ^{31}P-NMR spectrum of compound **7b** (121.5 MHz, $CDCl_3$).

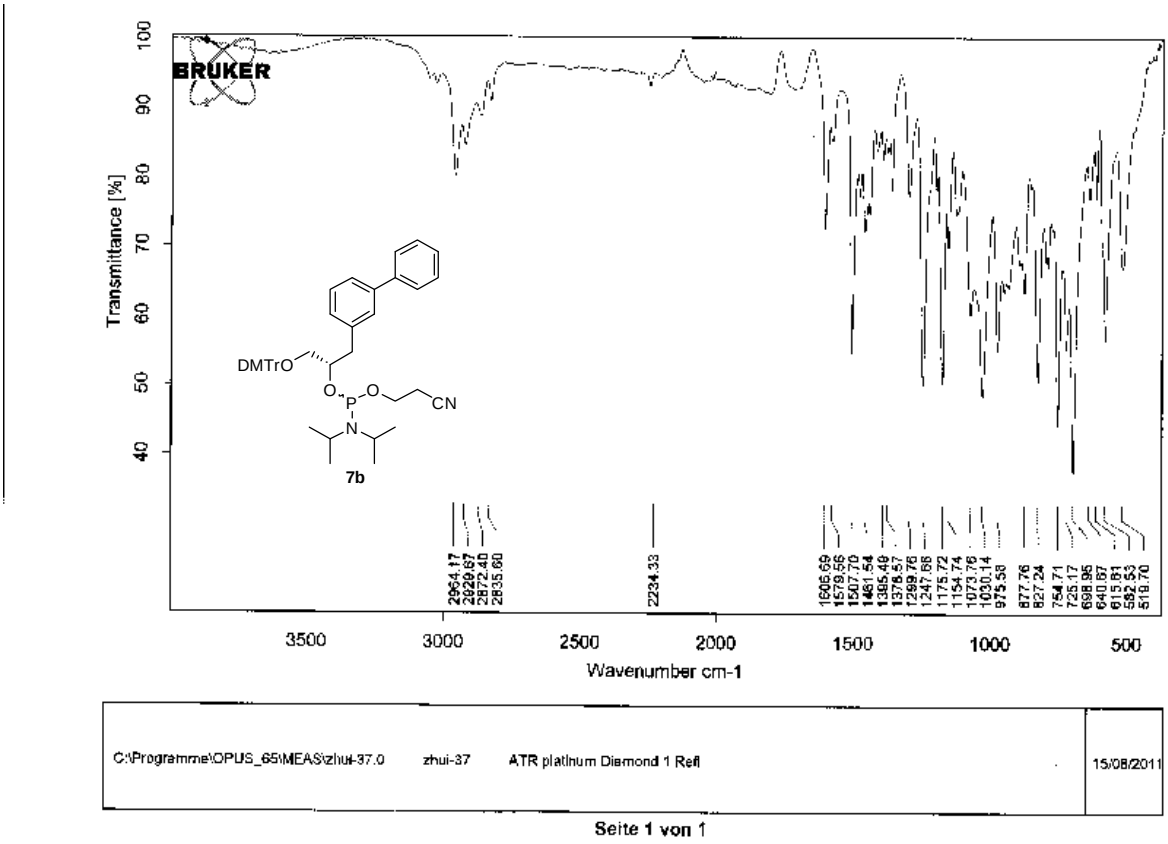

Figure A2.5.2 IR spectrum of compound **7b** (solid).

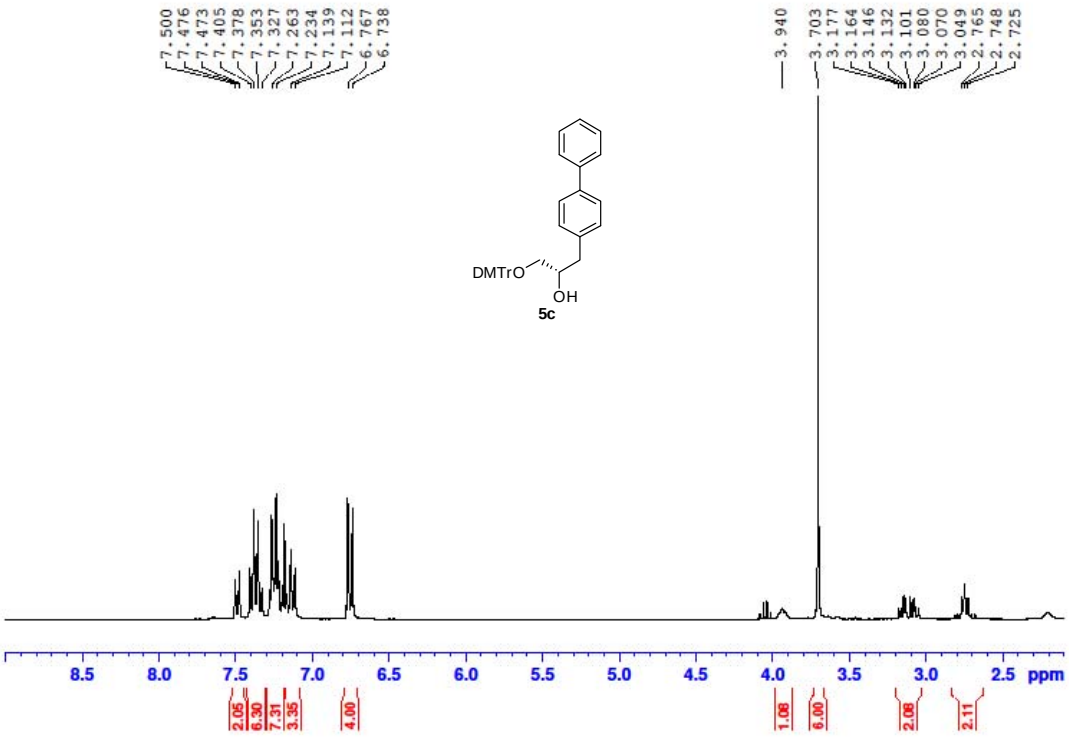

Figure A2.6.1 ^{1}H-NMR spectrum of compound **5c** (300 MHz, $CDCl_3$).

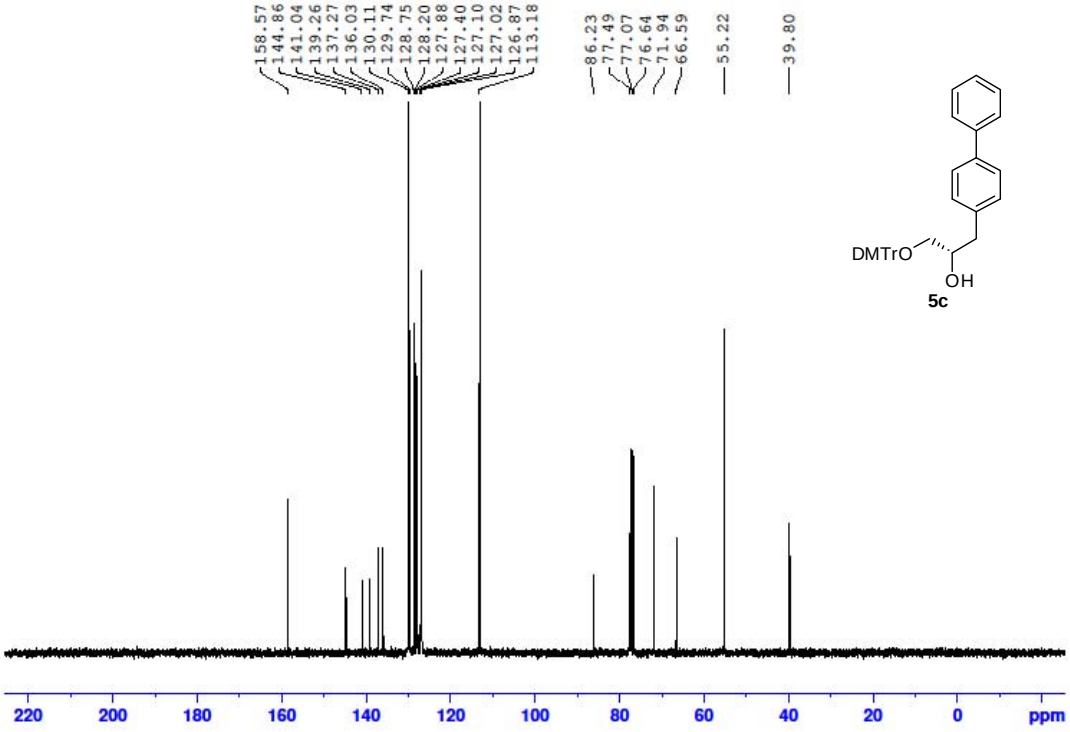

Figure A2.6.2 ^{13}C-NMR spectrum of compound **5c** (75 MHz, $CDCl_3$).

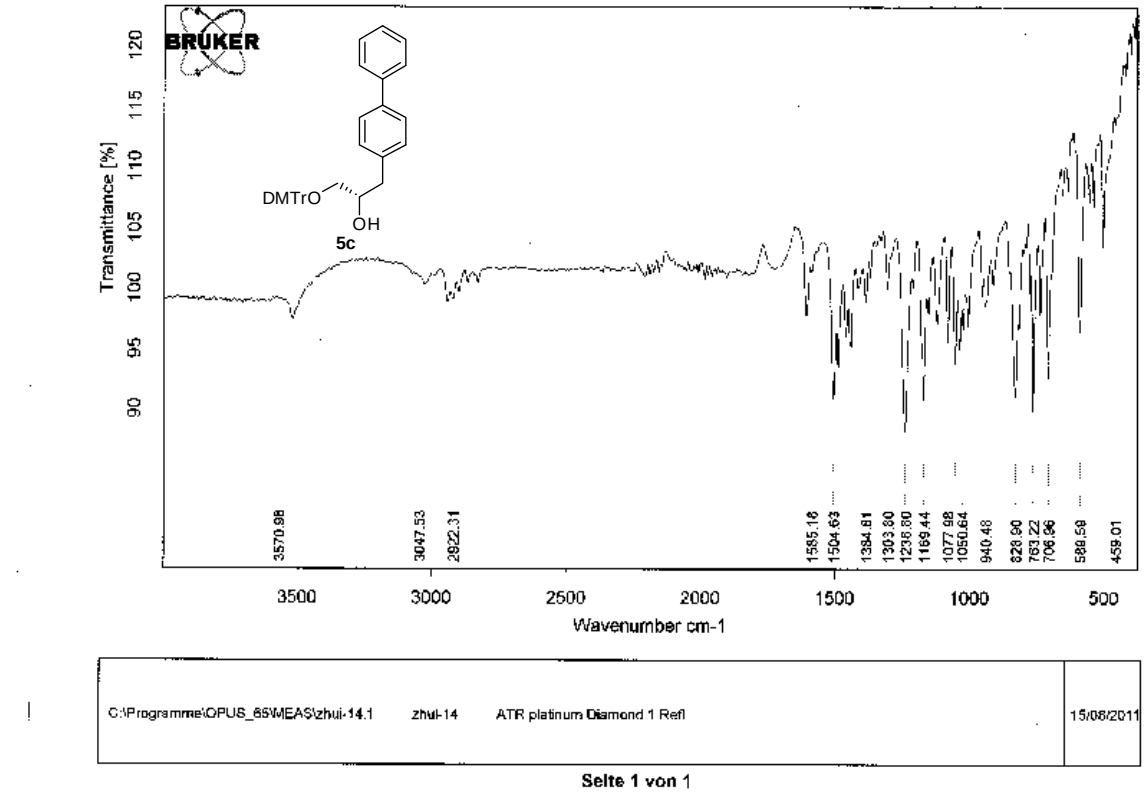

Figure A2.6.3 IR spectrum of compound **5c** (solid).

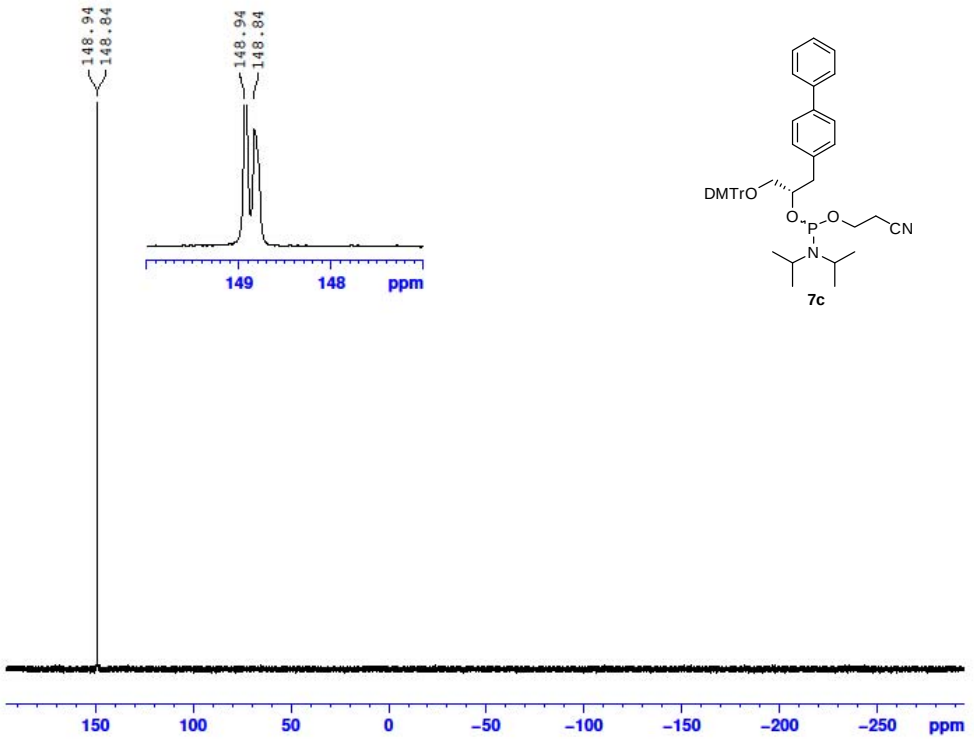

Figure A2.7. 1 ^{31}P-NMR spectrum of compound **7c** (121.5 MHz, $CDCl_3$).

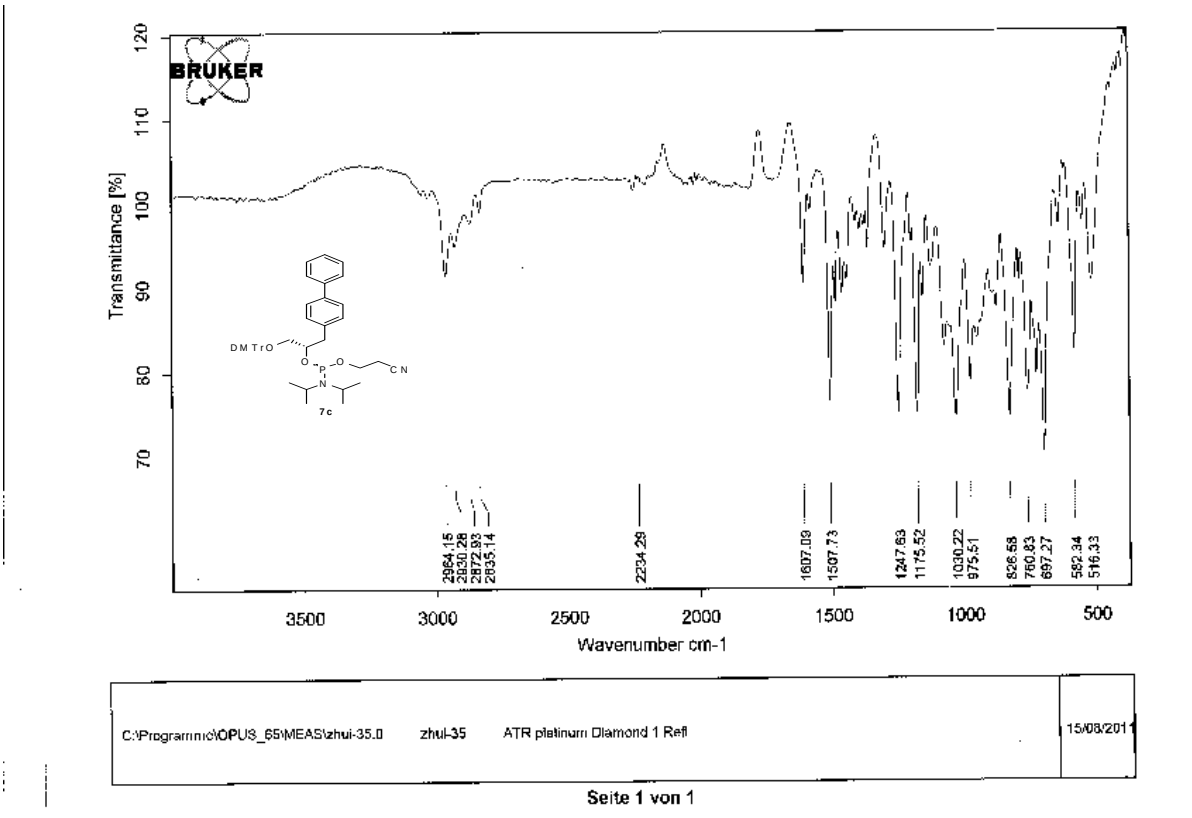

Figure A2.7.2 IR spectrum of compound **7c** (solid).

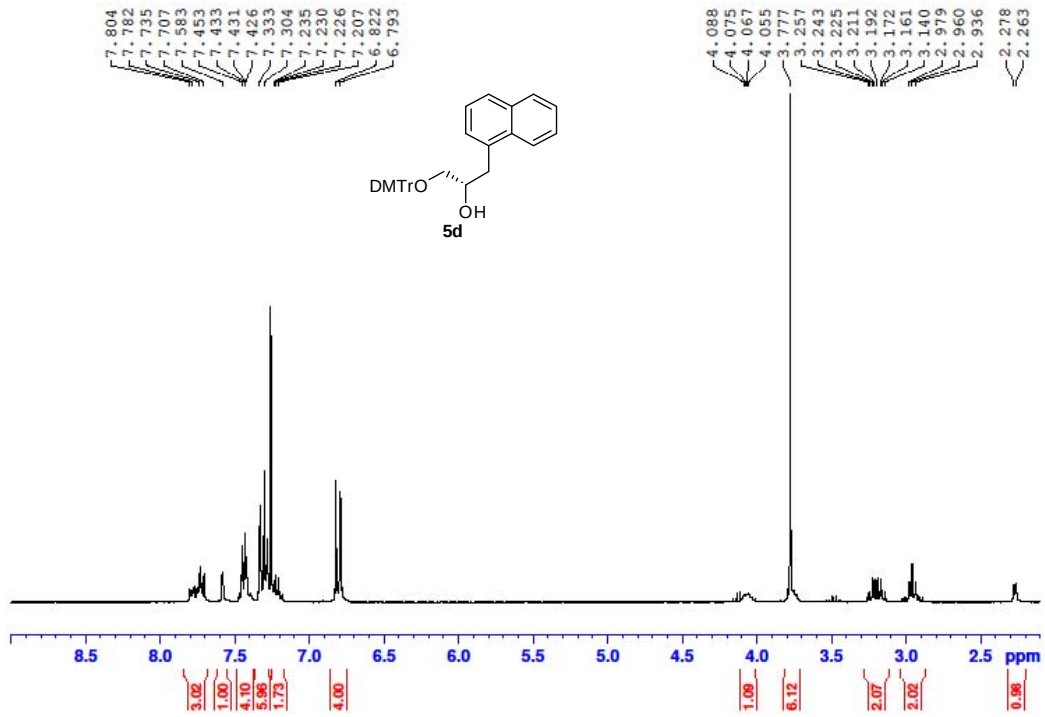

Figure A2.8.1 ^{1}H-NMR spectrum of compound **5d** (300 MHz, $CDCl_3$).

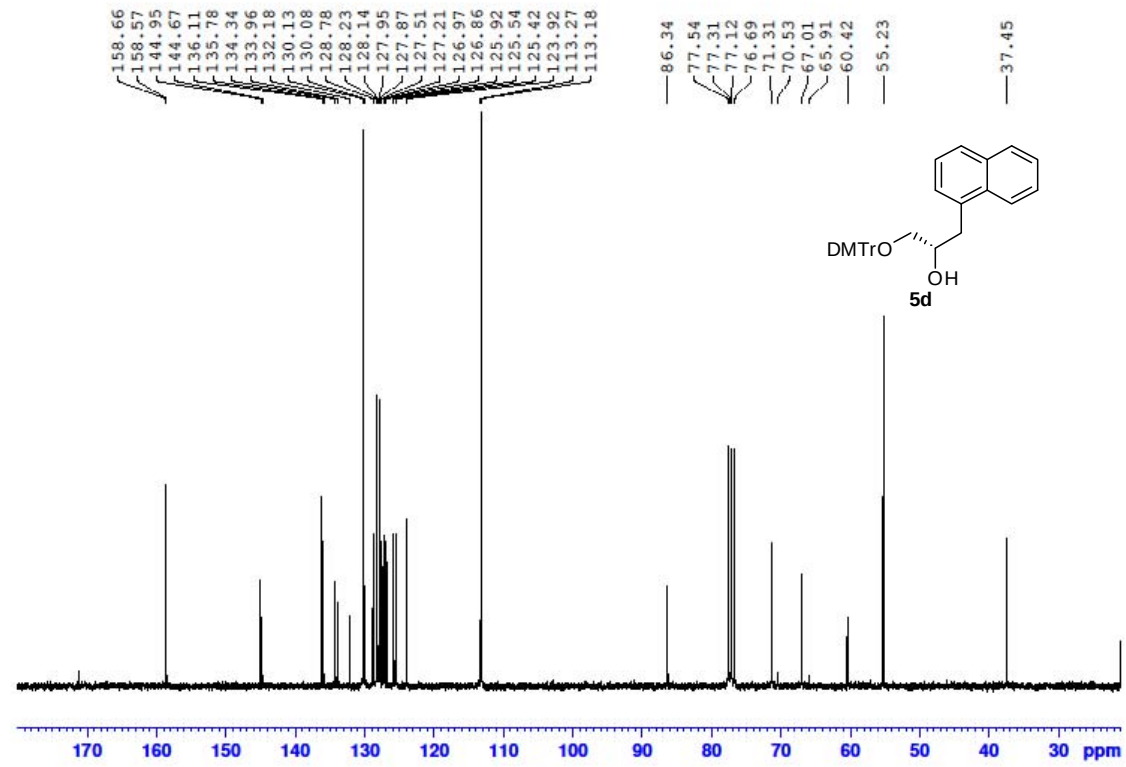

Figure A2.8.2 ^{13}C-NMR spectrum of compound **5d** (75 MHz, $CDCl_3$).

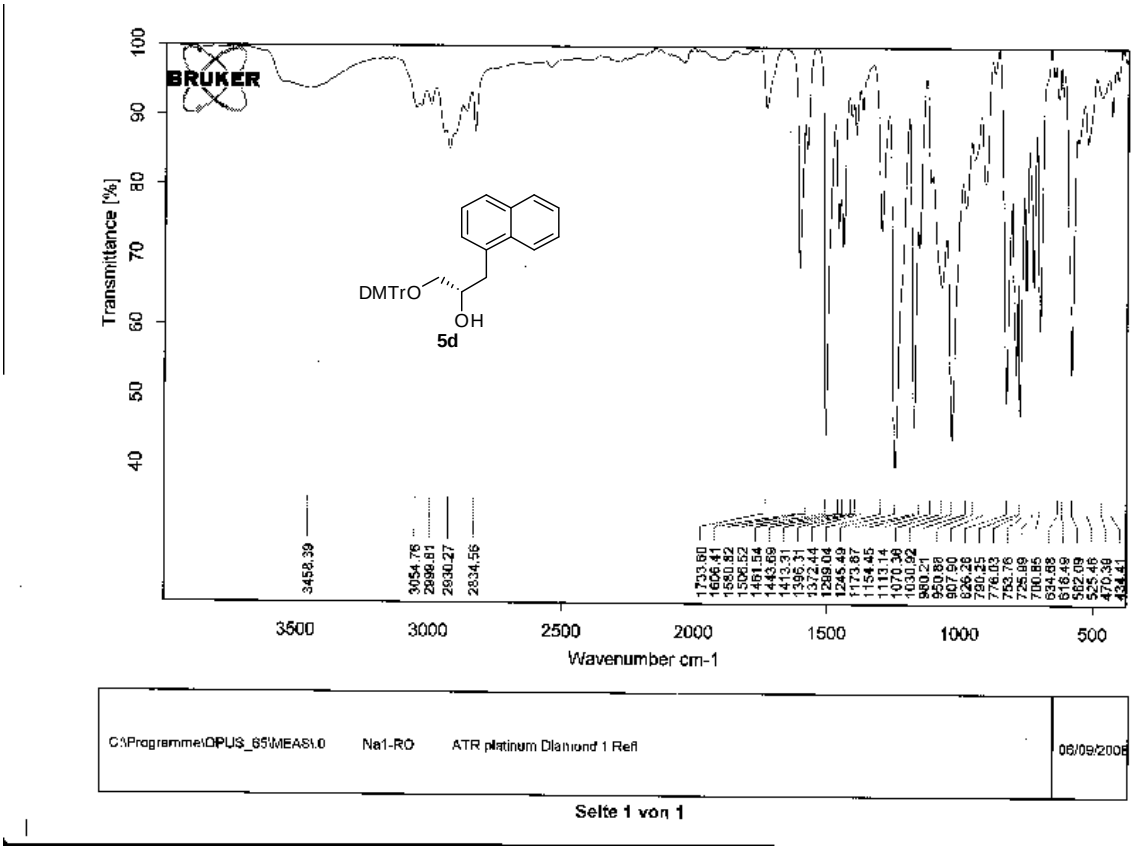

Figure A2.8.3 IR spectrum of compound **5d** (solid).

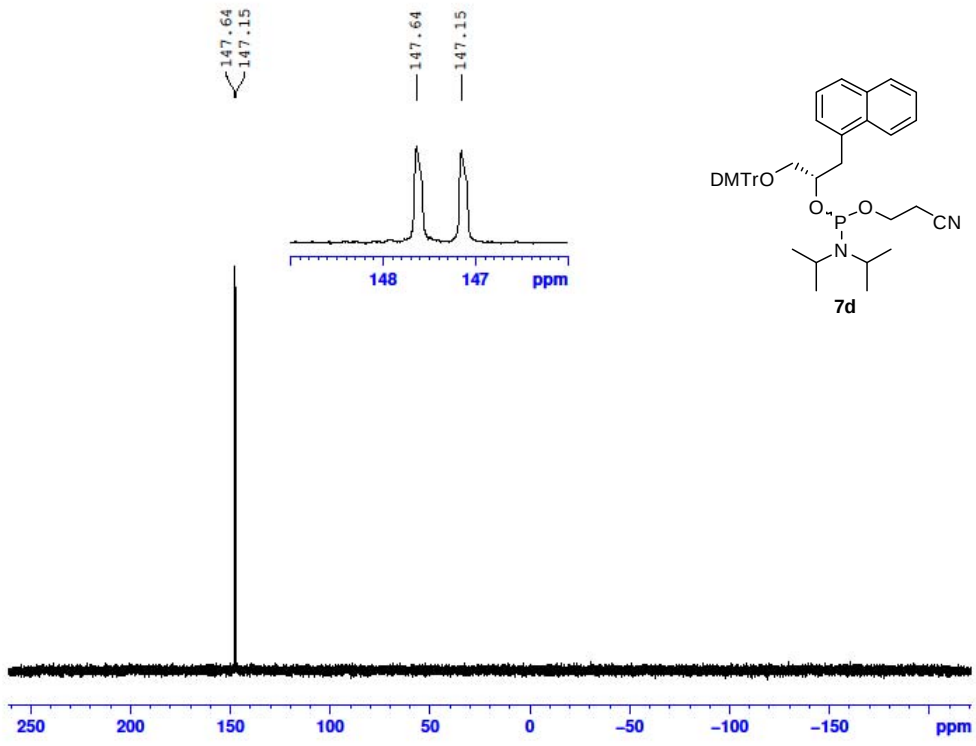

Figure A2.9.1 ^{31}P-NMR spectrum of compound **7d** (121.5 MHz, $CDCl_3$).

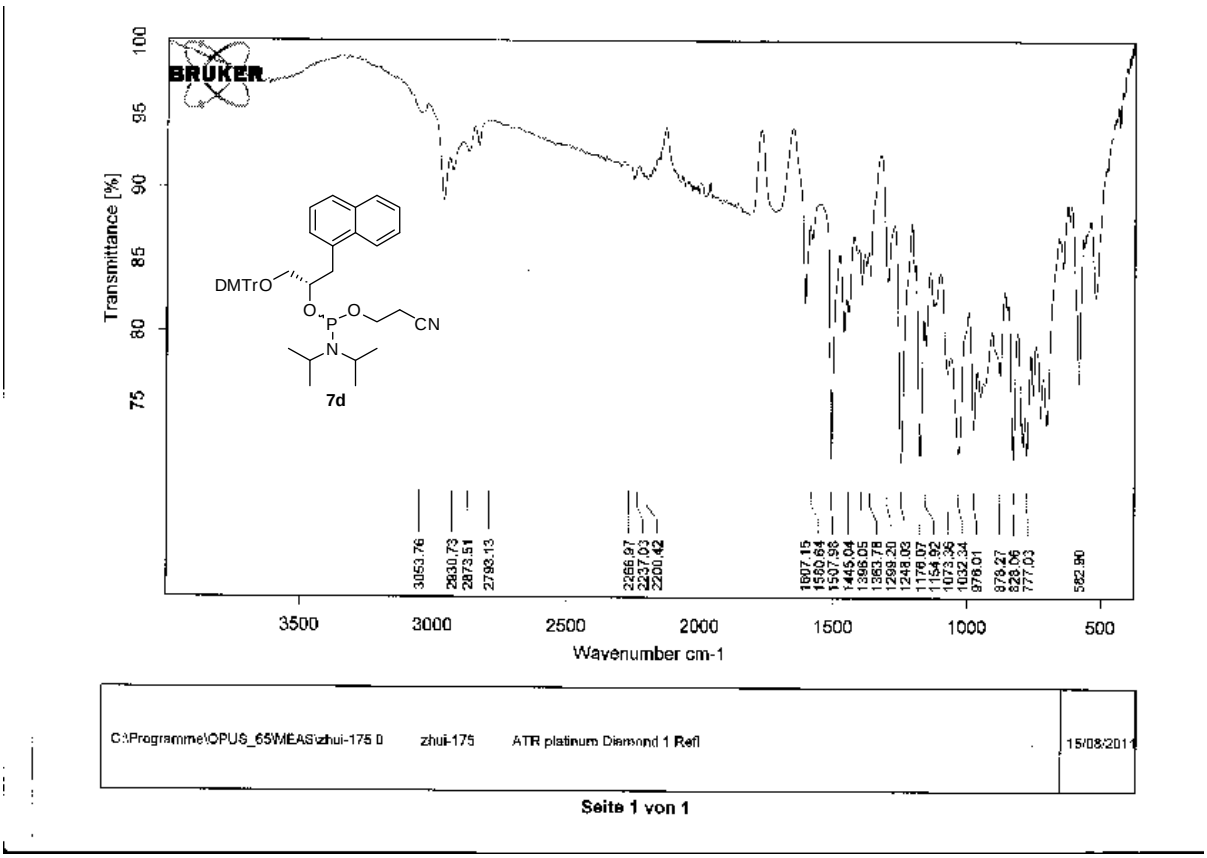

Figure A2.9.2 IR spectrum of compound **7d** (solid).

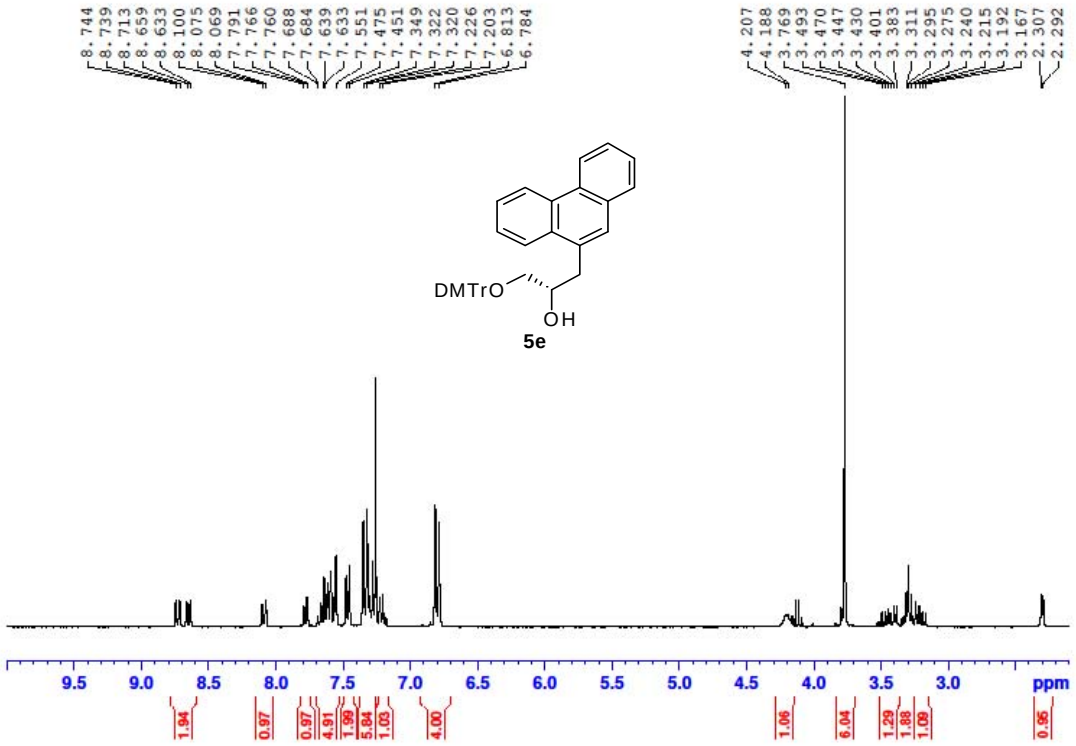

Figure A2.10.1 ^{1}H-NMR spectrum of compound **5e** (300 MHz, $CDCl_3$).

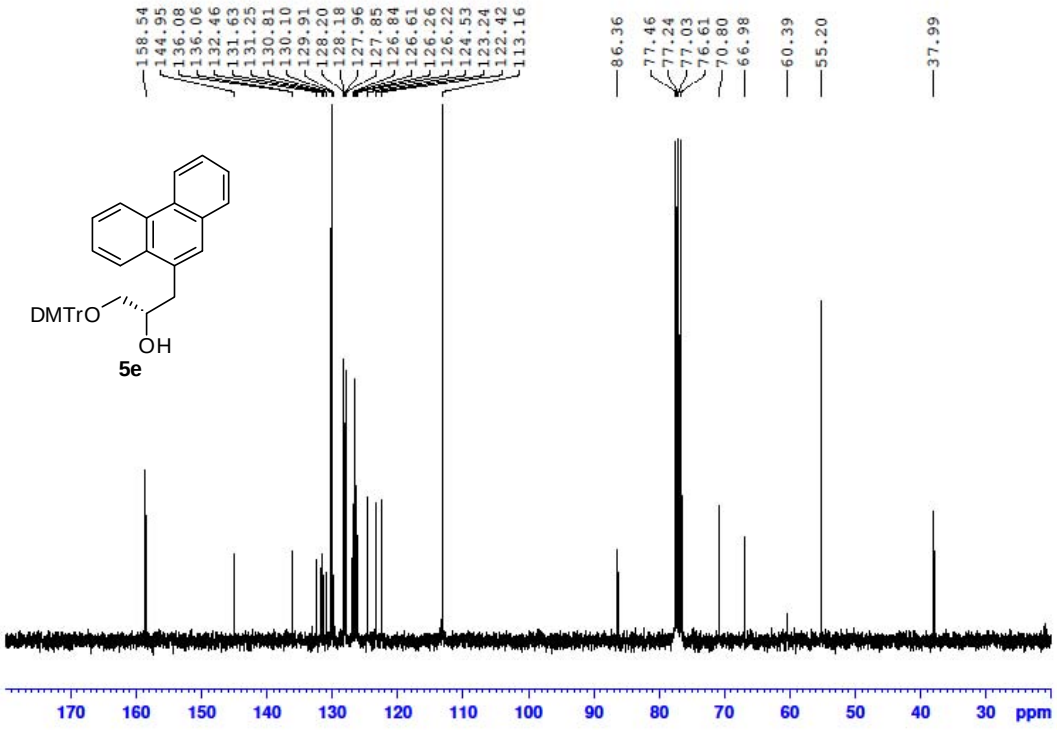

Figure A2.10.2 ^{13}C-NMR spectrum of compound **5e** (75 MHz, $CDCl_3$).

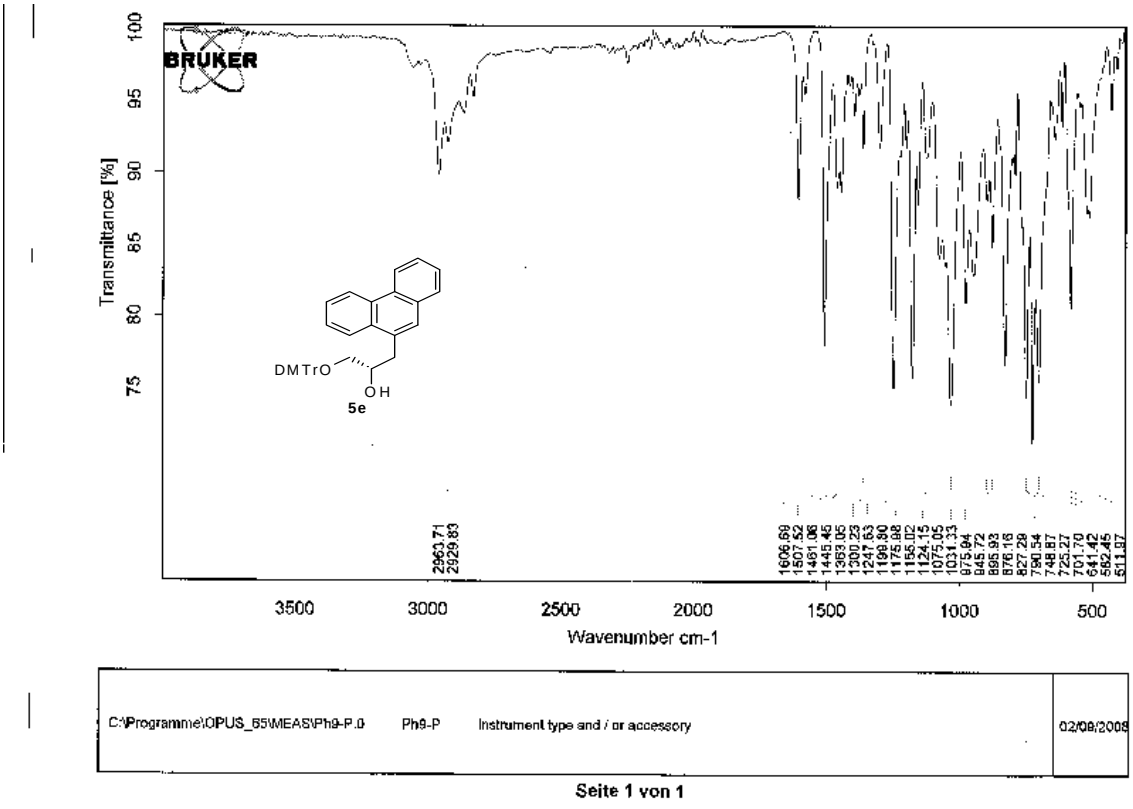

Figure A2.10.3 IR spectrum of compound **5e** (solid).

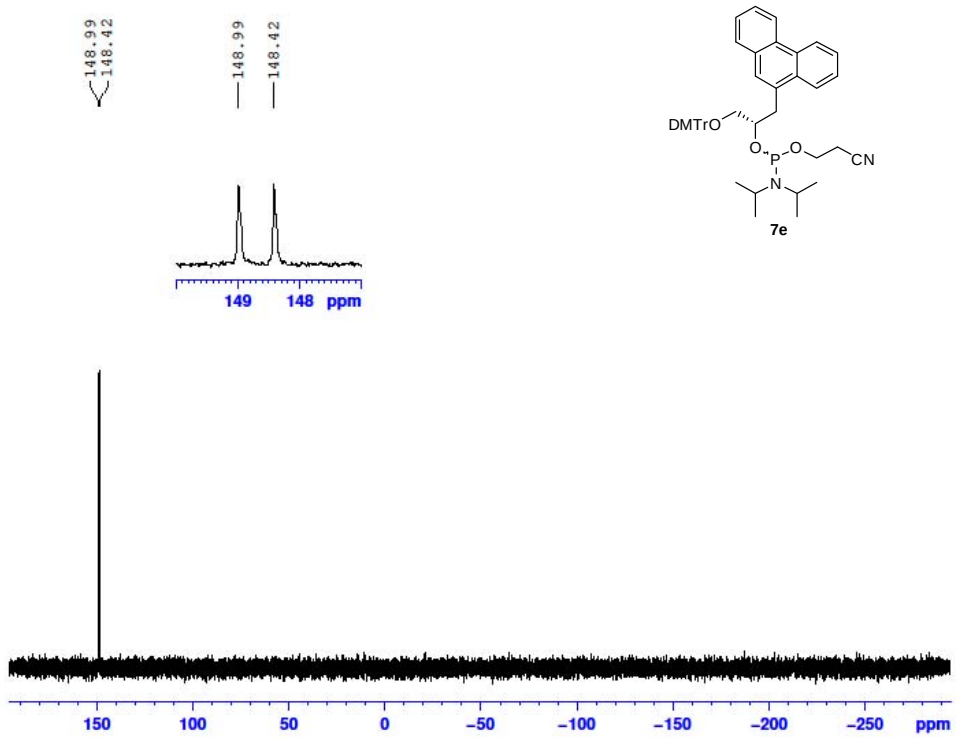

Figure A2.11.1 ^{31}P-NMR spectrum of compound **7e** (121.5 MHz, $CDCl_3$).

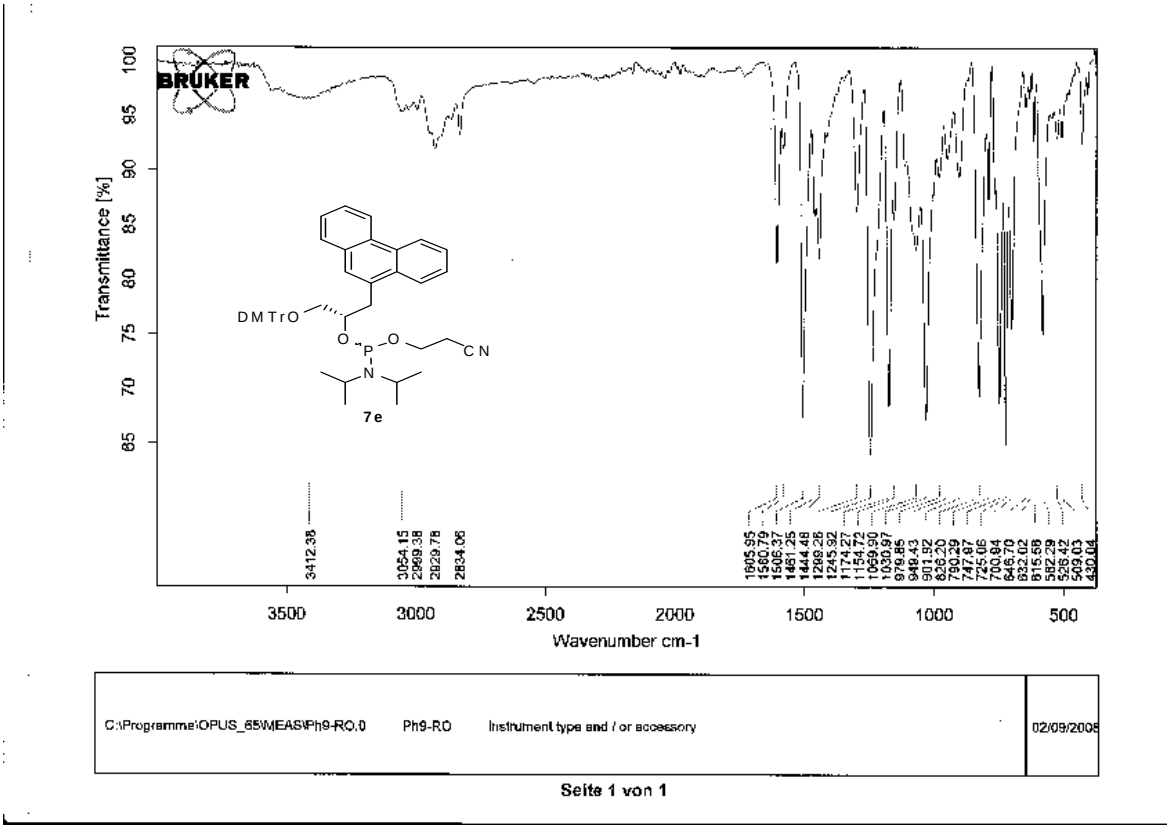

Figure A2.11.2 IR spectrum of compound **7e** (solid).

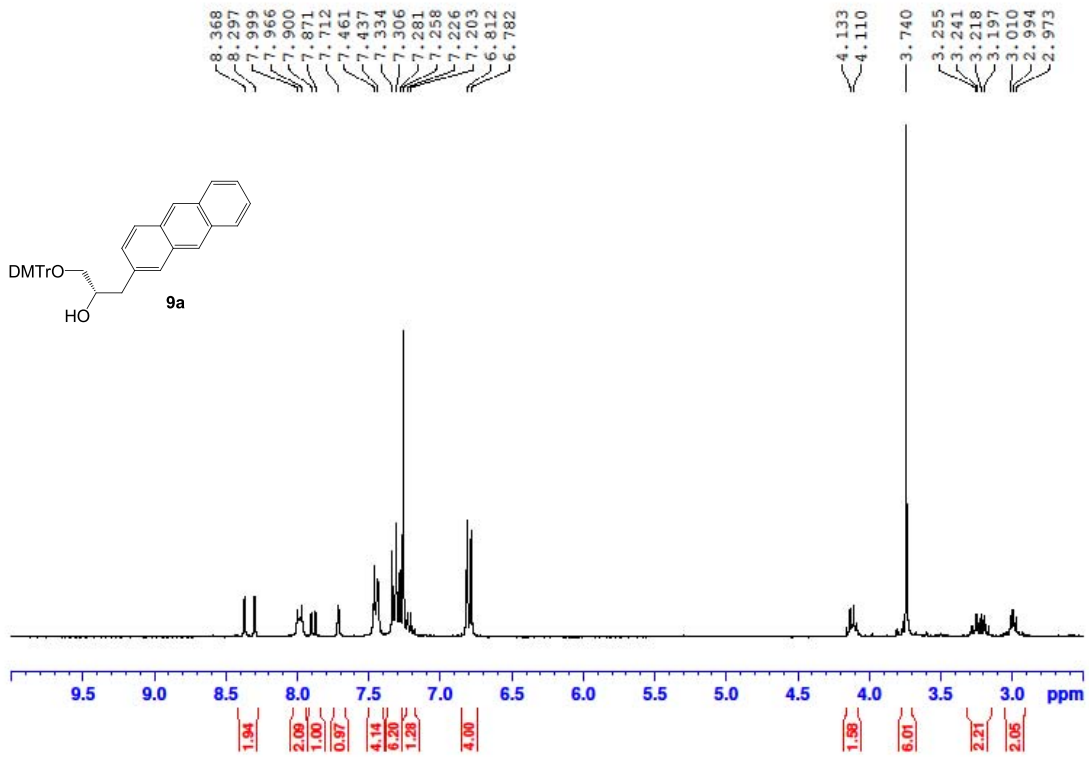

Figure A2.12.1 ^{1}H-NMR spectrum of compound **9a** (300 MHz, $CDCl_3$).

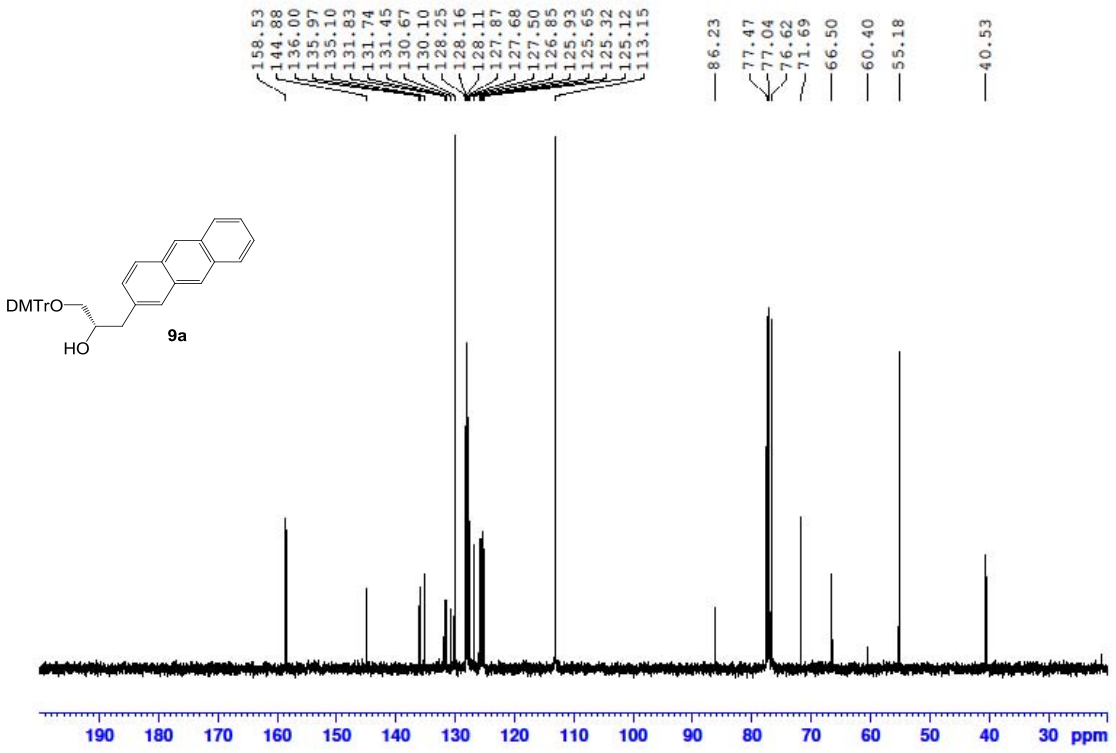

Figure A2.12.2 ^{13}C-NMR spectrum of compound **9a** (75 MHz, $CDCl_3$).

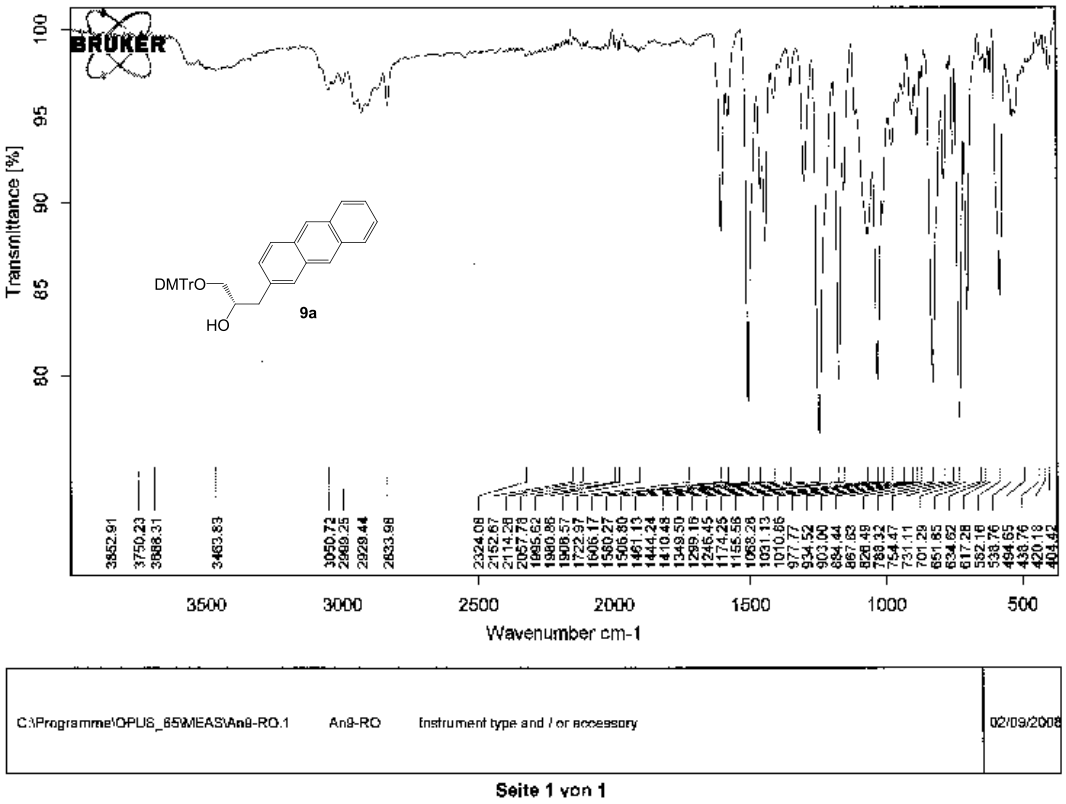

Figure A2.12.3 IR spectrum of compound **9a** (solid).

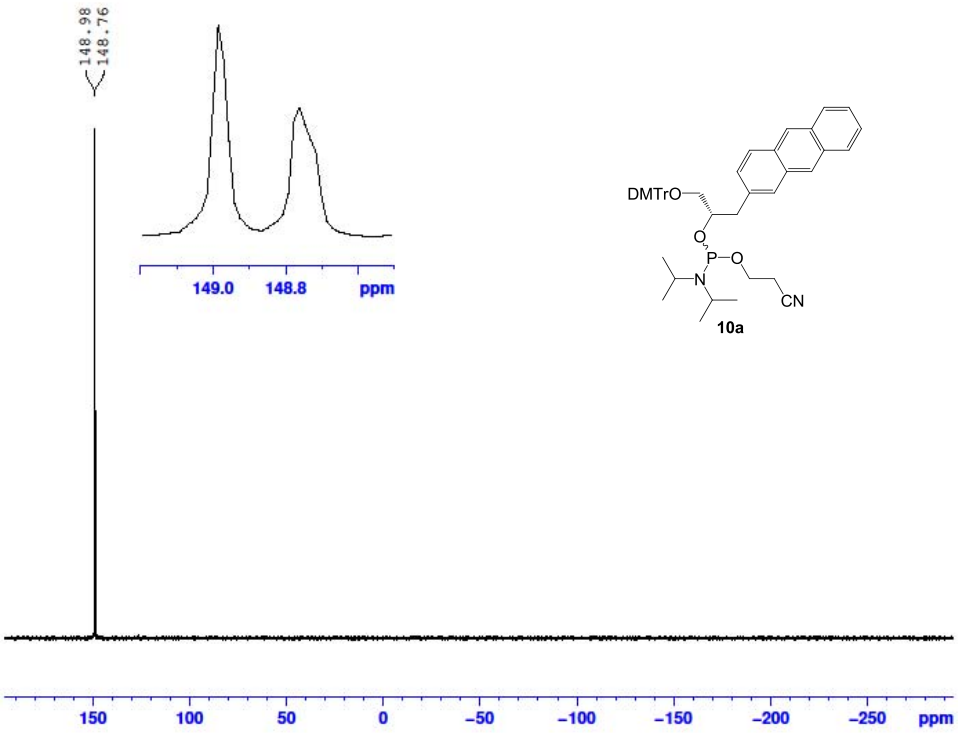

Figure A2.13.1 ^{31}P-NMR spectrum of compound **10a** (121.5 MHz, $CDCl_3$).

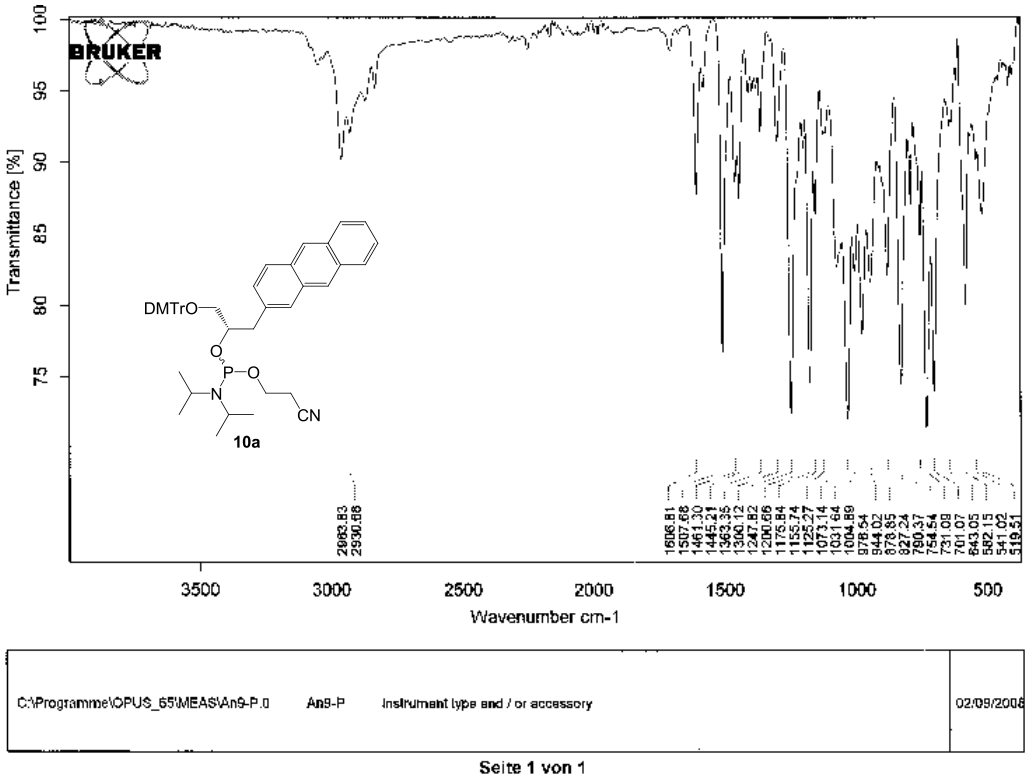

Figure A2.13.2 IR spectrum of compound **10a** (solid).

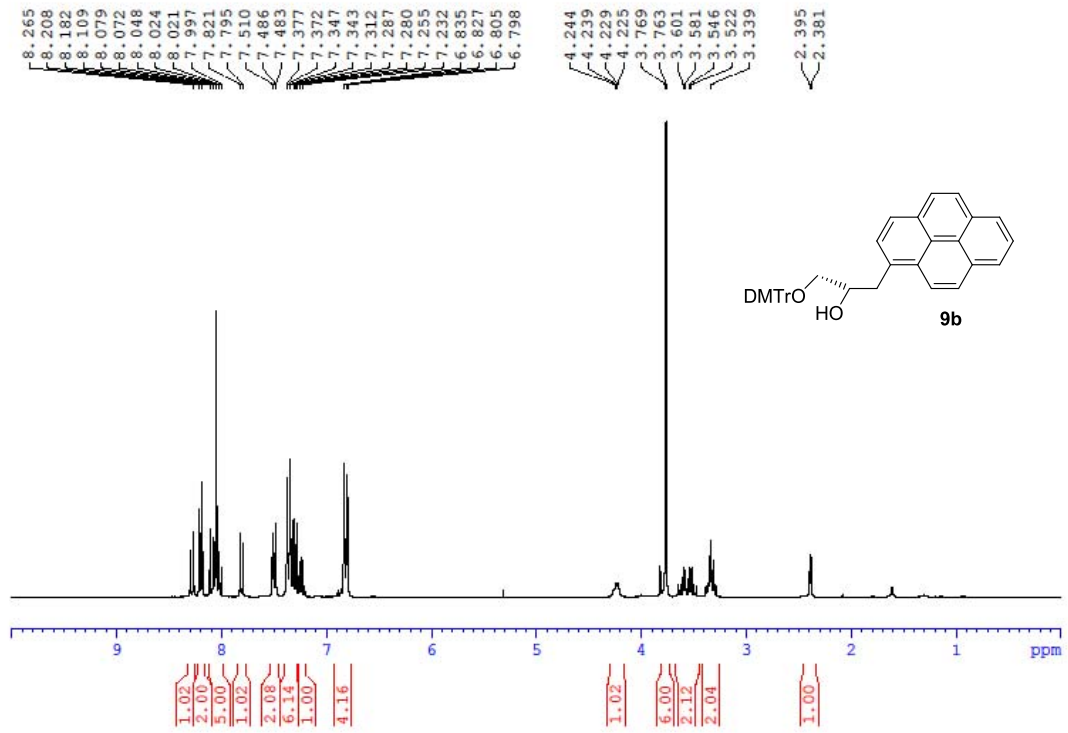

Figure A2.14.1 ^{1}H-NMR spectrum of compound **9b** (300 MHz, $CDCl_3$).

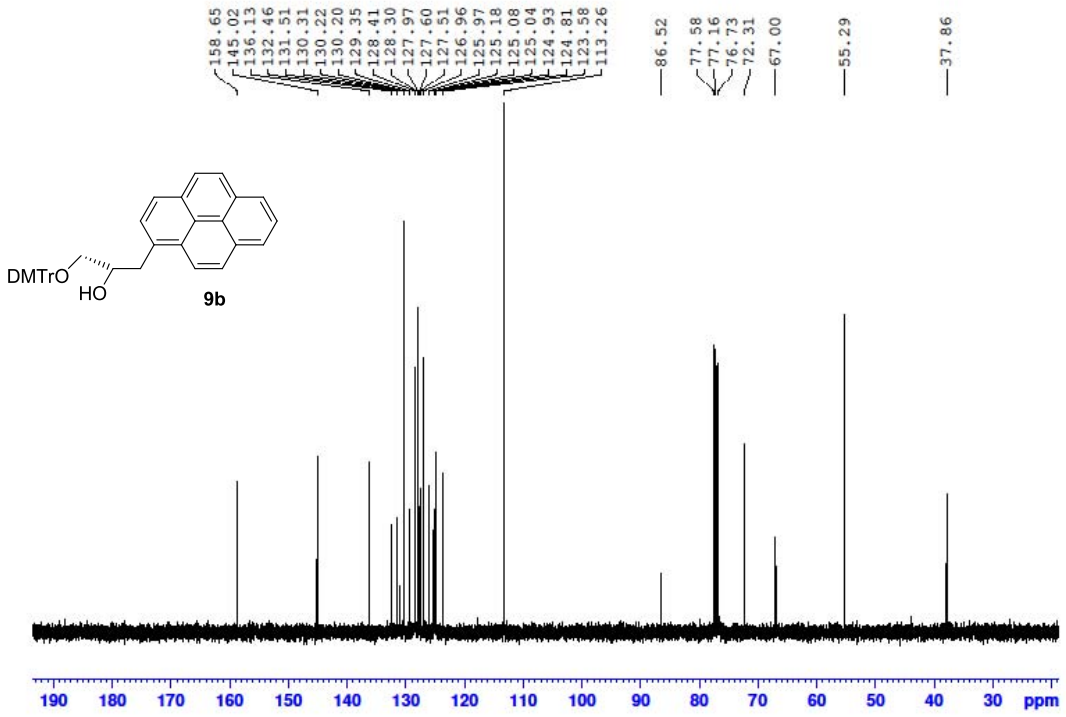

Figure A2.14.2 ^{13}C-NMR spectrum of compound **9b** (75 MHz, $CDCl_3$).

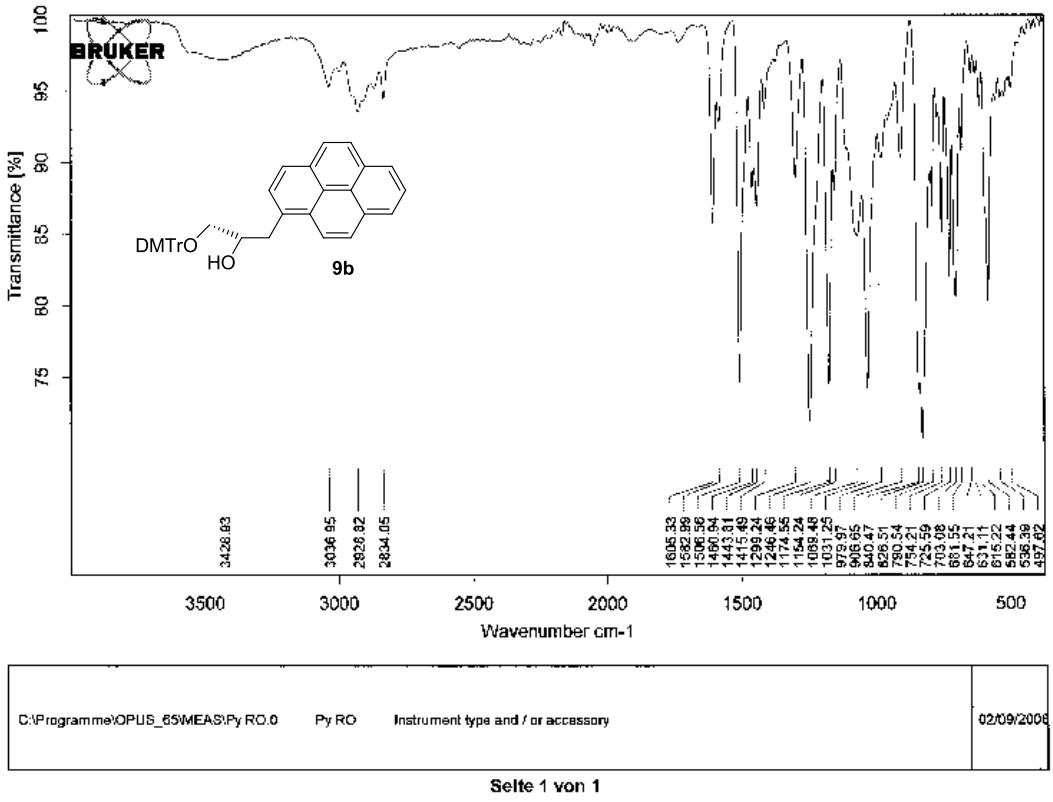

Figure A2.14.3 IR spectrum of compound **9b** (solid).

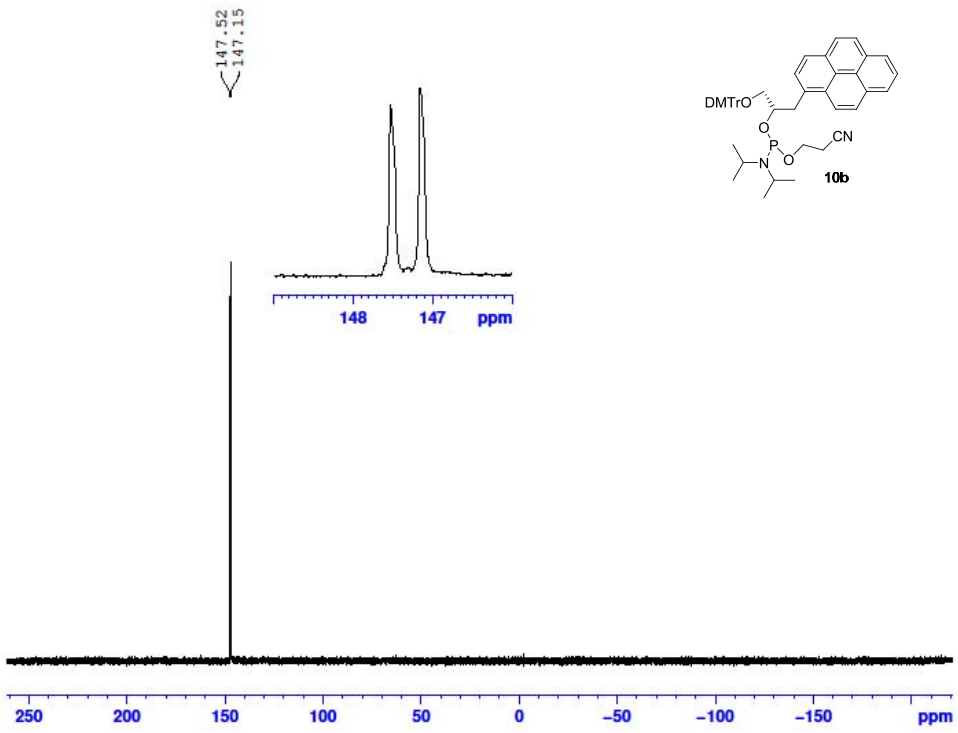

Figure A2.15.1 ^{31}P-NMR spectrum of compound **10b** (121.5 MHz, $CDCl_3$).

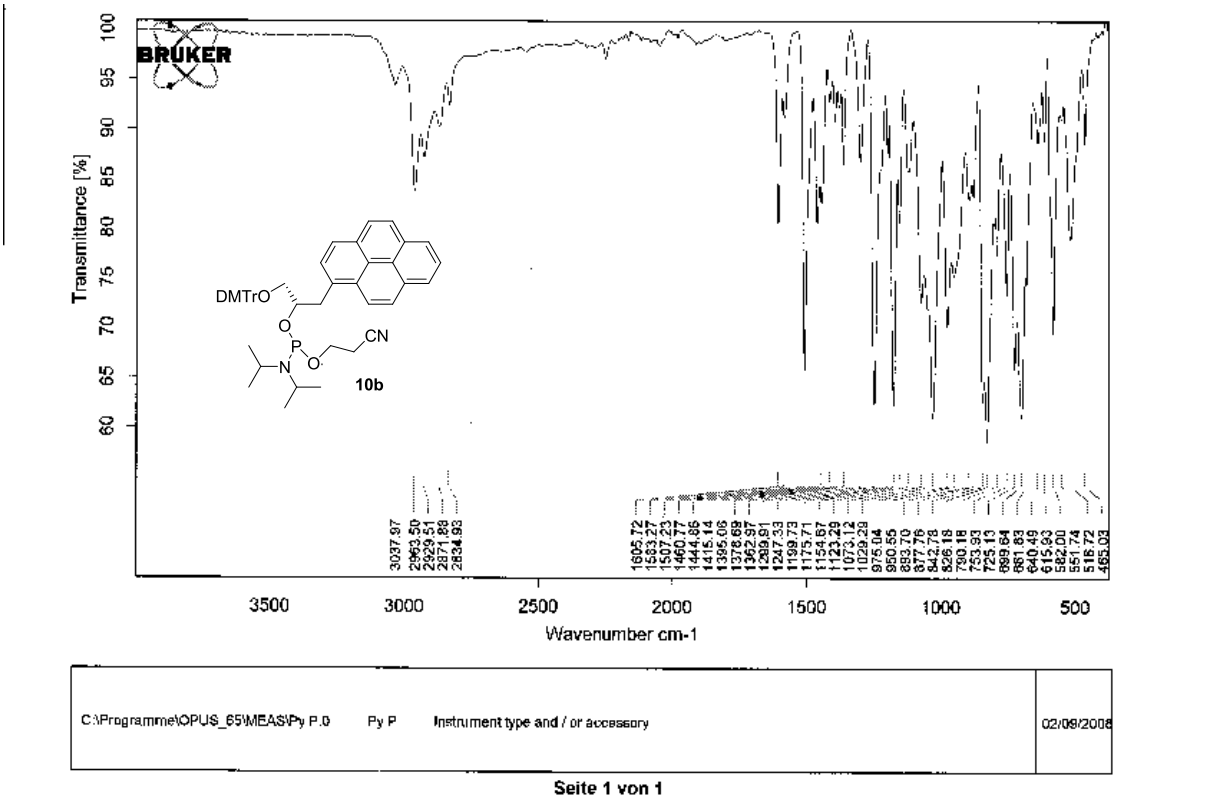

Figure A2.15.2 IR spectrum of compound **10b** (solid).

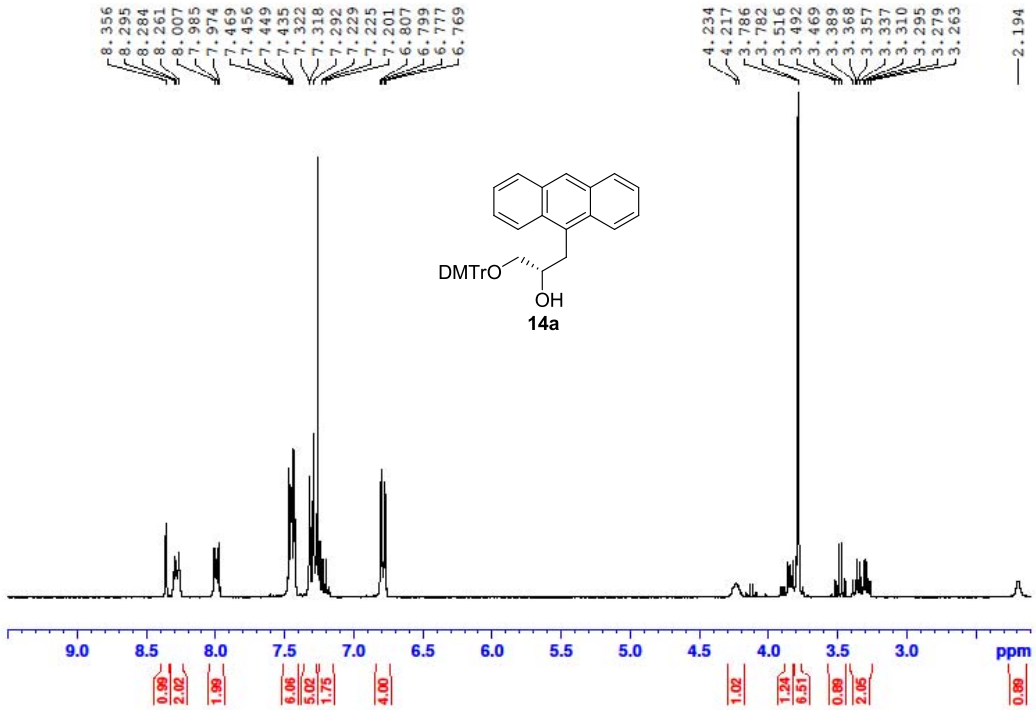

Figure A2.16.1 ^{1}H-NMR spectrum of compound **14a** (300 MHz, $CDCl_3$).

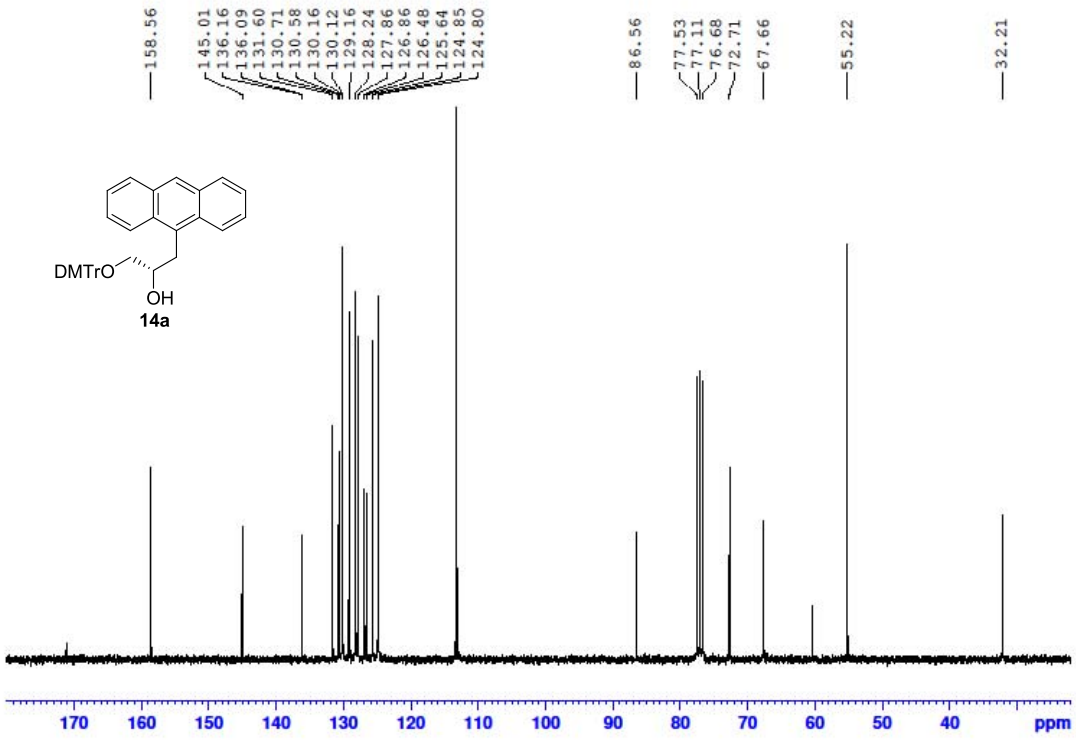

Figure A2.16.2 ^{13}C-NMR spectrum of compound **14a** (75 MHz, $CDCl_3$).

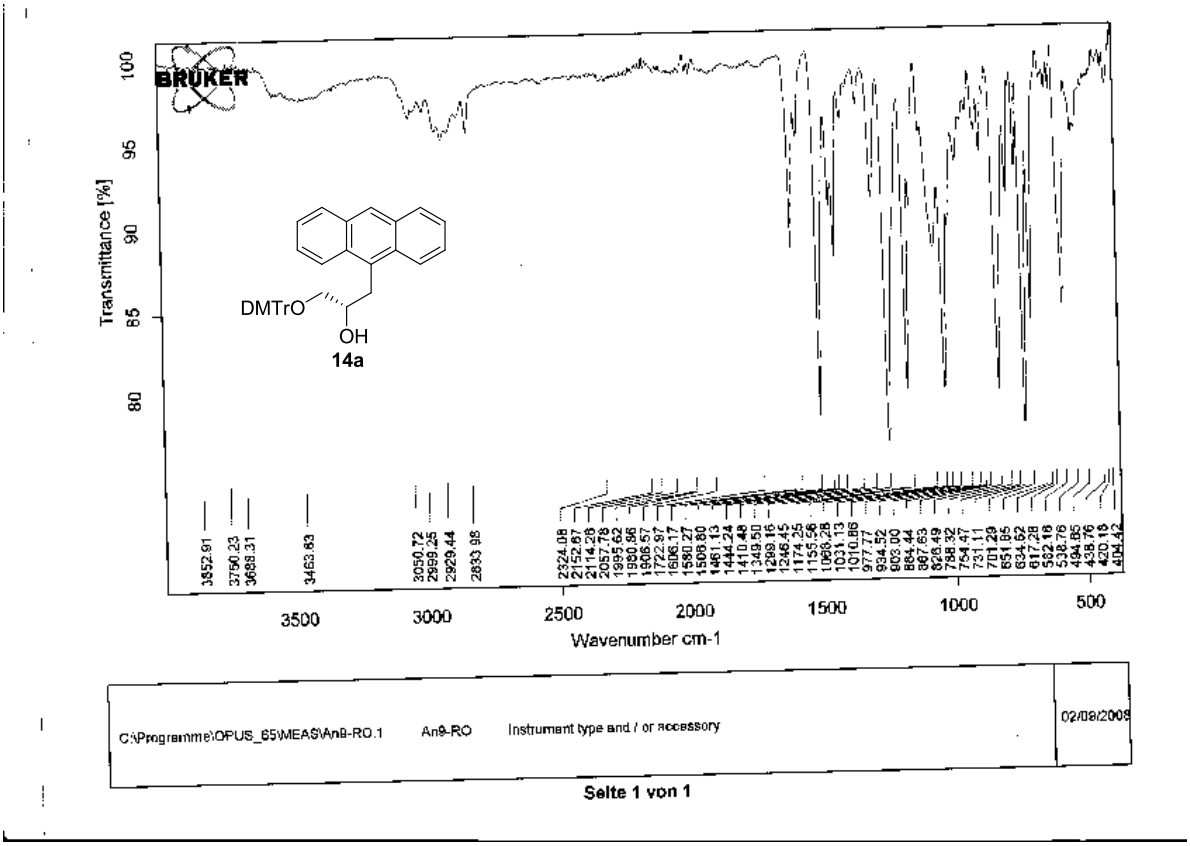

Figure A2.16.3 IR spectrum of compound **14a** (solid).

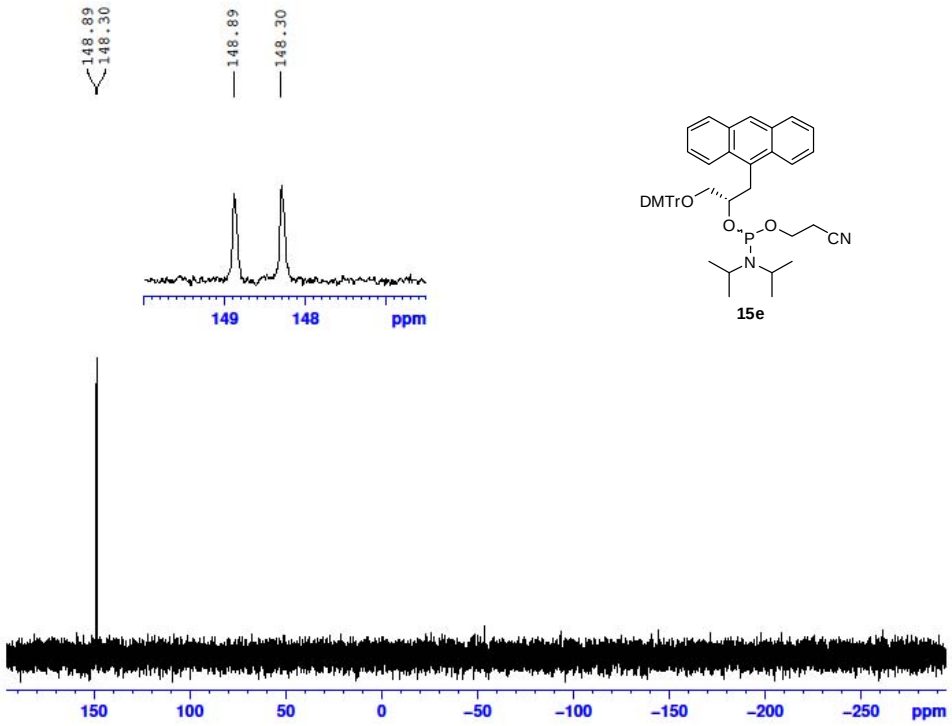

Figure A2.17.1 ^{31}P-NMR spectrum of compound **15a** (121.5 MHz, $CDCl_3$).

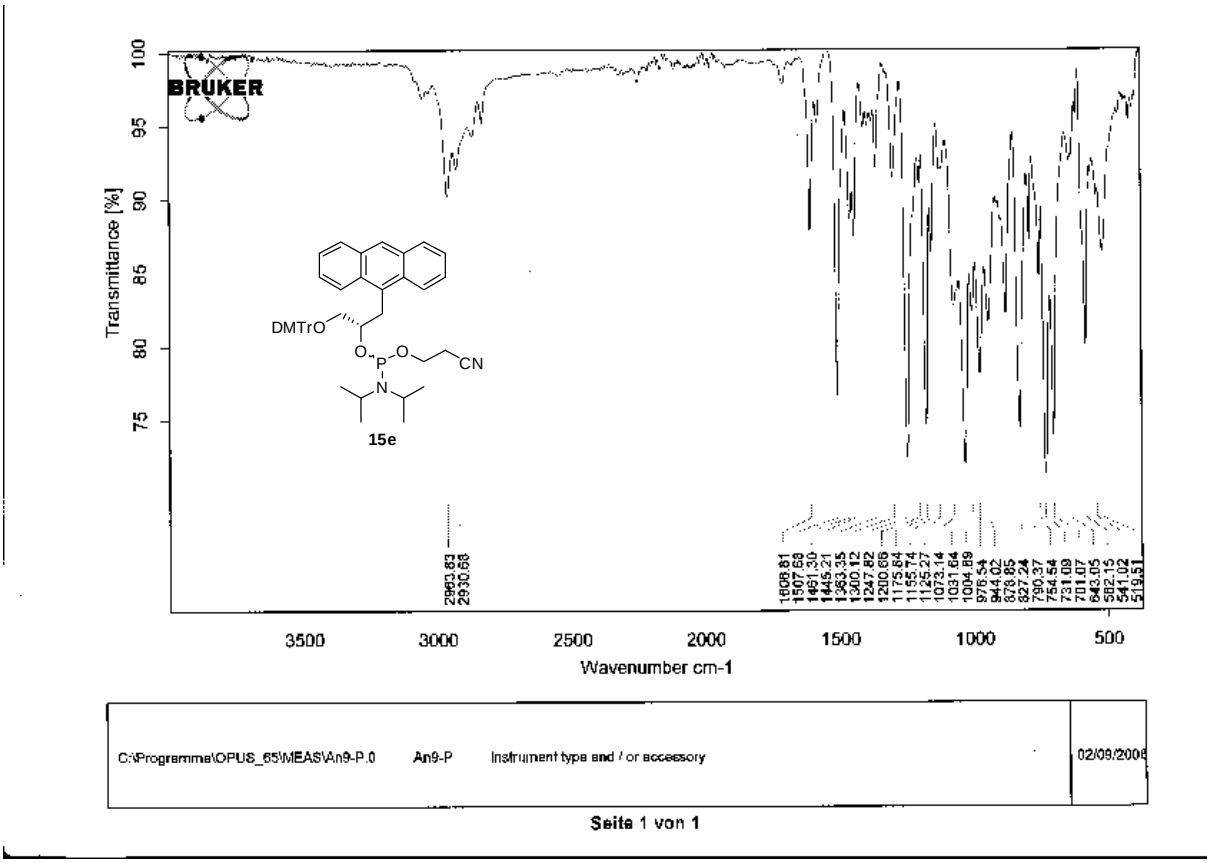

Figure A2.17.2 IR spectrum of compound **15e** (solid).

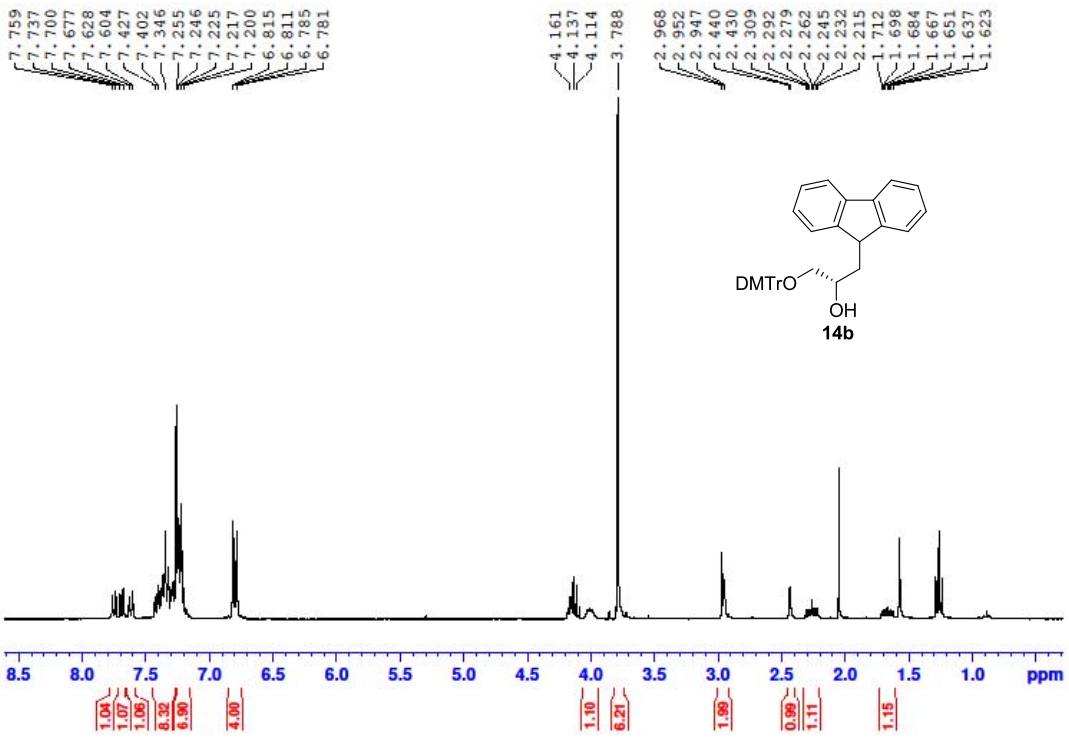

Figure A2.18.1 ^{1}H-NMR spectrum of compound **14b** (300 MHz, $CDCl_3$).

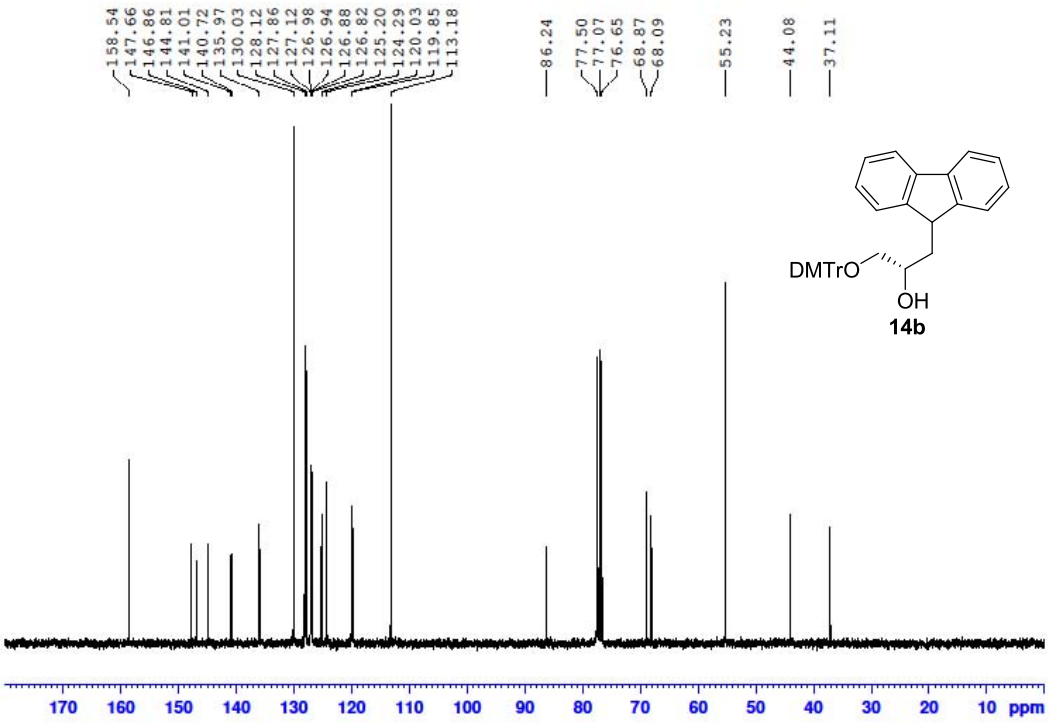

Figure A2.18.2 ^{13}C-NMR spectrum of compound **14b** (75 MHz, $CDCl_3$).

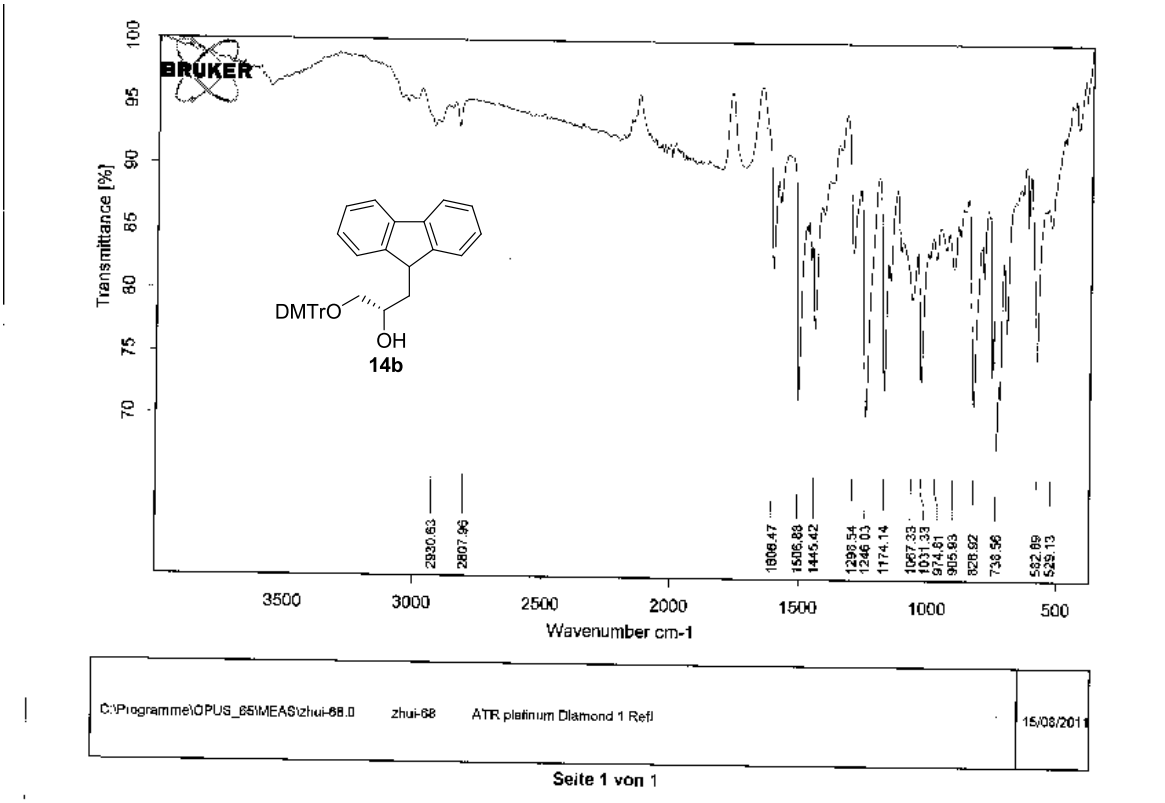

Figure A2.18.3 IR spectrum of compound **14b** (solid).

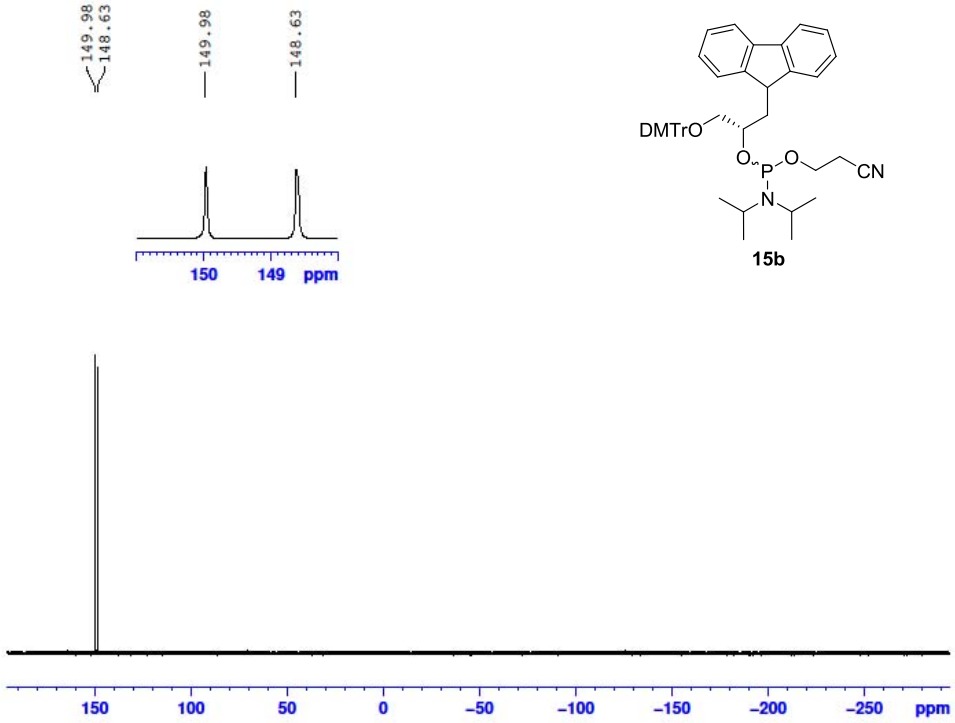

Figure A2.19.1 ^{31}P-NMR spectrum of compound **15b** (121.5 MHz, $CDCl_3$).

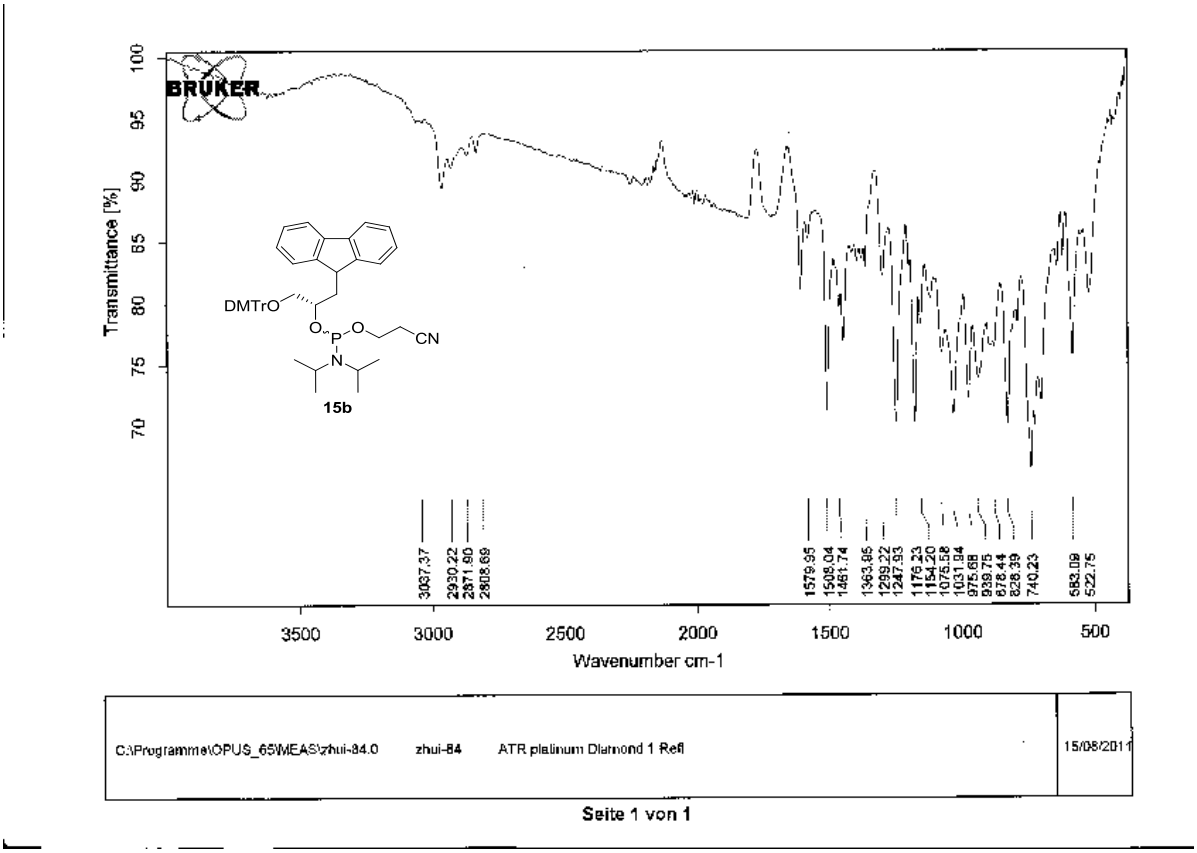

Figure A2.19.2 IR spectrum of compound **15b** (solid).

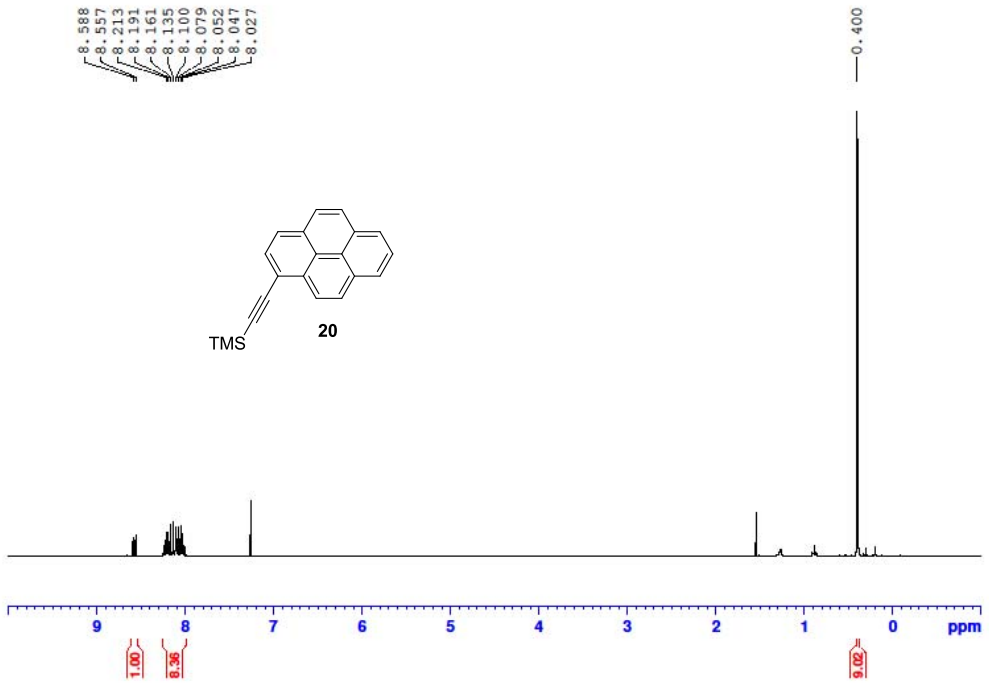

Figure A2.20.1 ^{1}H-NMR spectrum of compound **20** (300 MHz, $CDCl_3$).

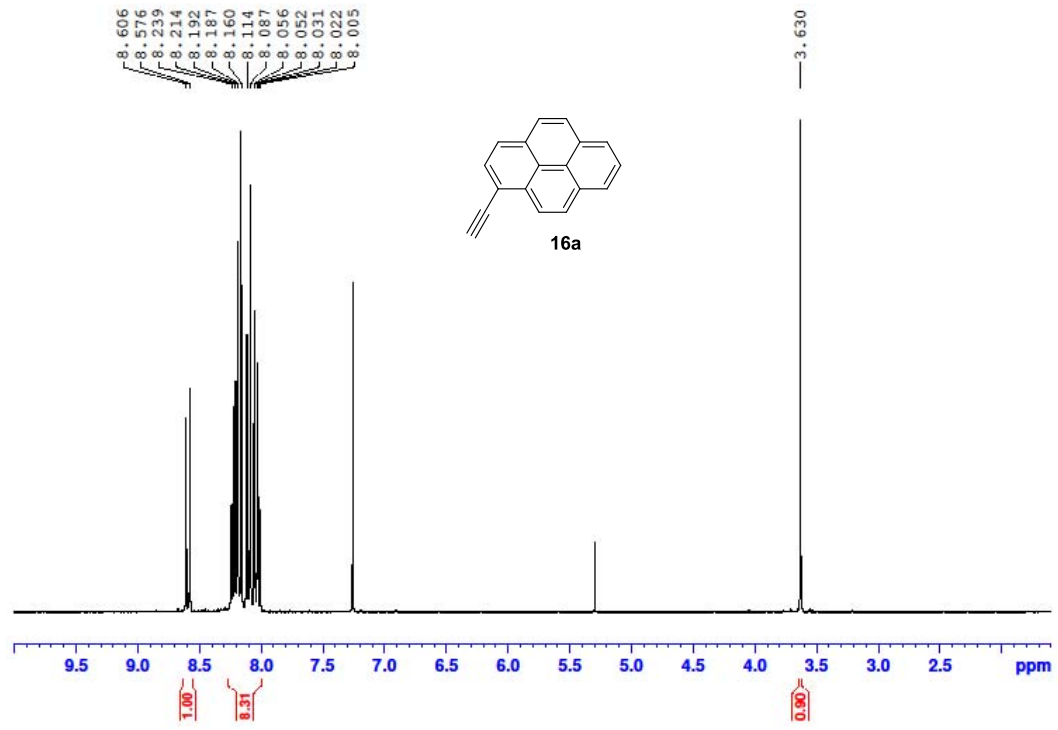

Figure A2.21.1 ^{1}H-NMR spectrum of compound **16a** (300 MHz, $CDCl_3$).

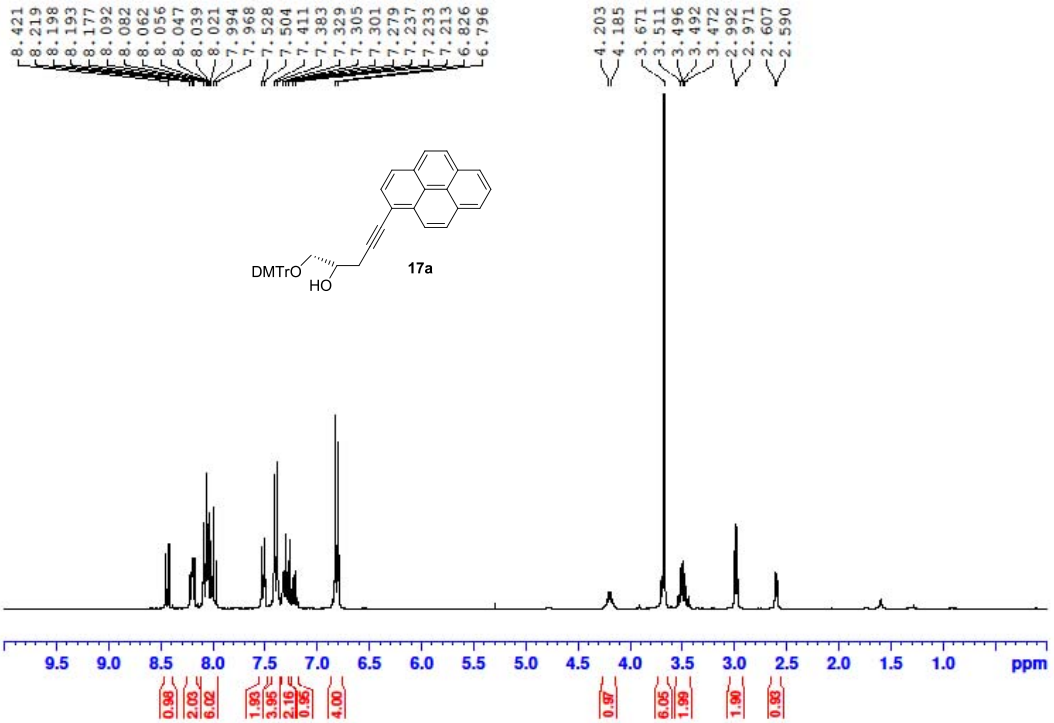

Figure A2.22.1 ^{1}H-NMR spectrum of compound **17a** (300 MHz, $CDCl_3$).

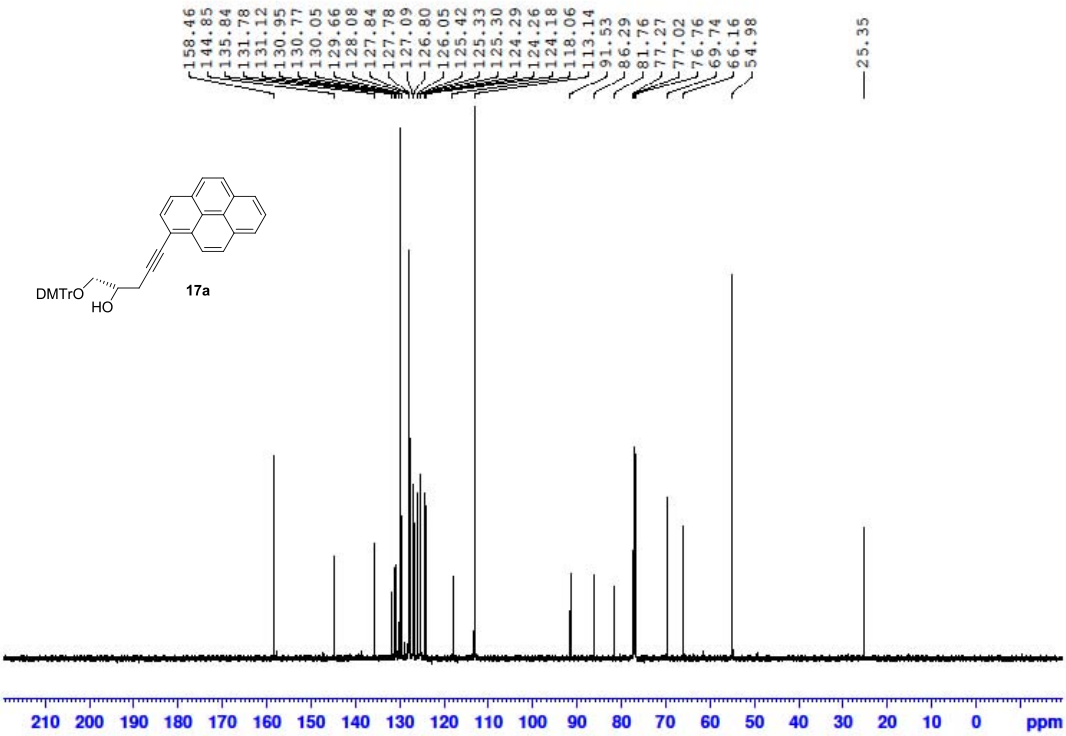

Figure A2.22.2 ^{13}C-NMR spectrum of compound **17a** (75 MHz, $CDCl_3$).

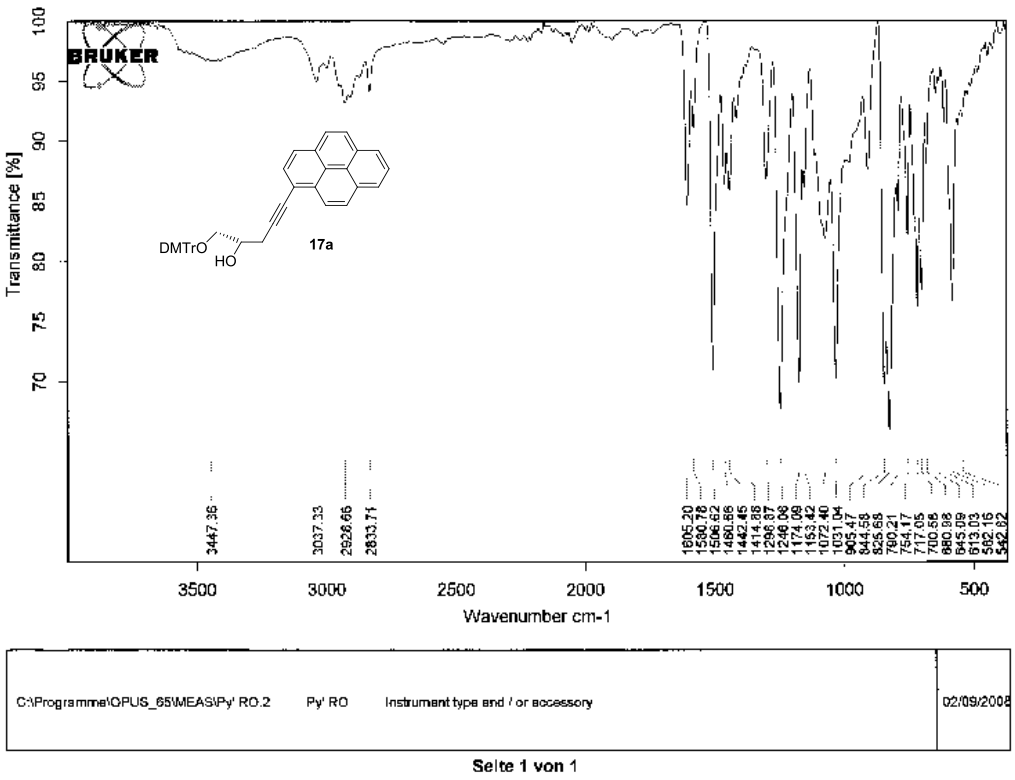

Figure A2.22.3 IR spectrum of compound**17a** (solid).

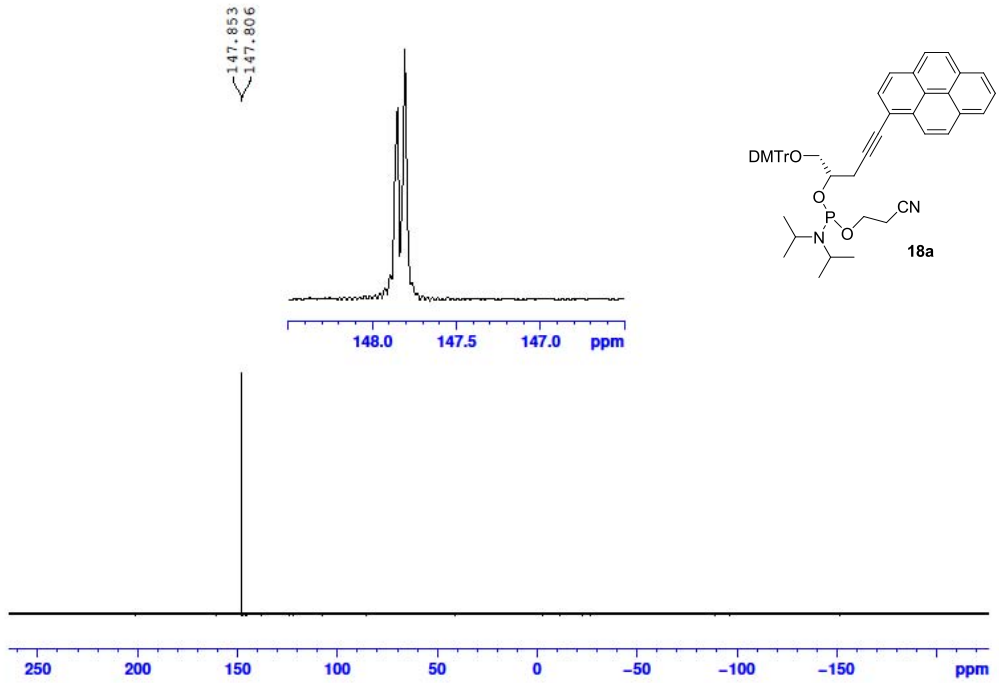

Figure A2.23.1 ^{31}P-NMR spectrum of compound **18a** (121.5 MHz, $CDCl_3$).

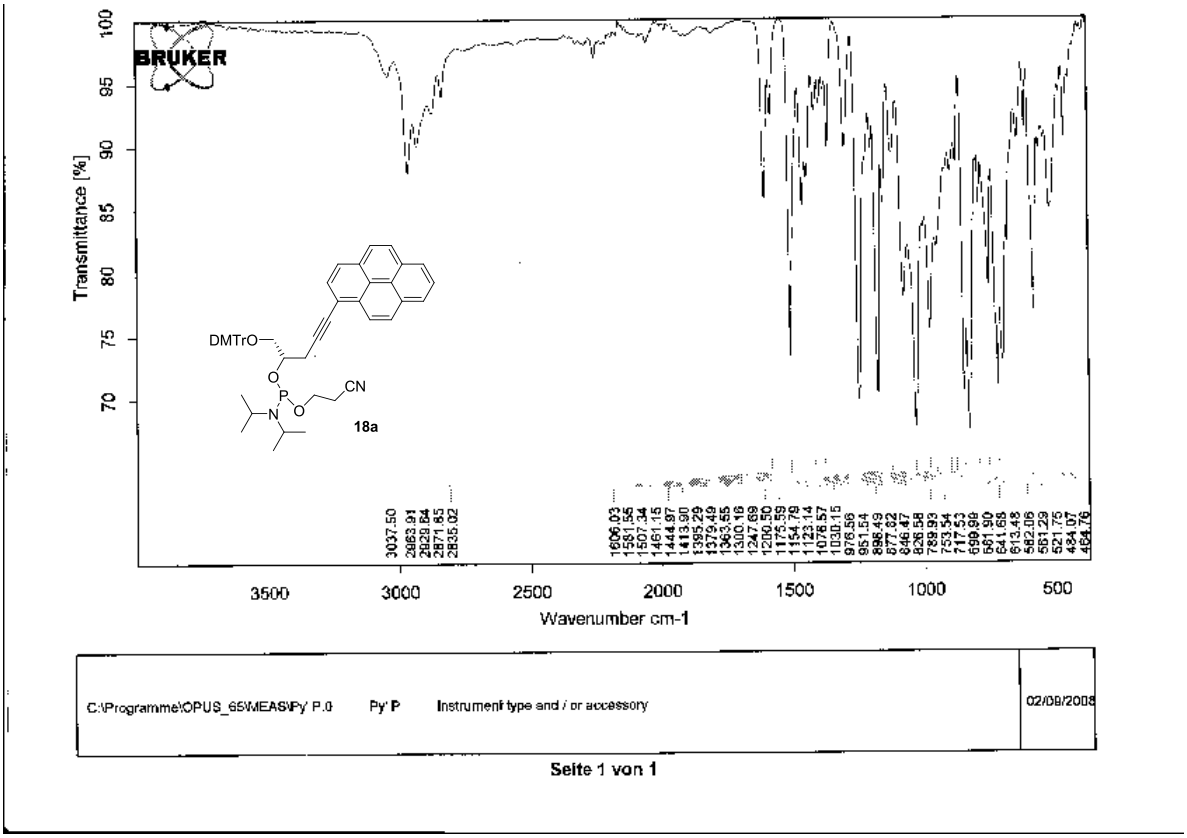

Figure A2.23.2 IR spectrum of compound **18a** (solid).

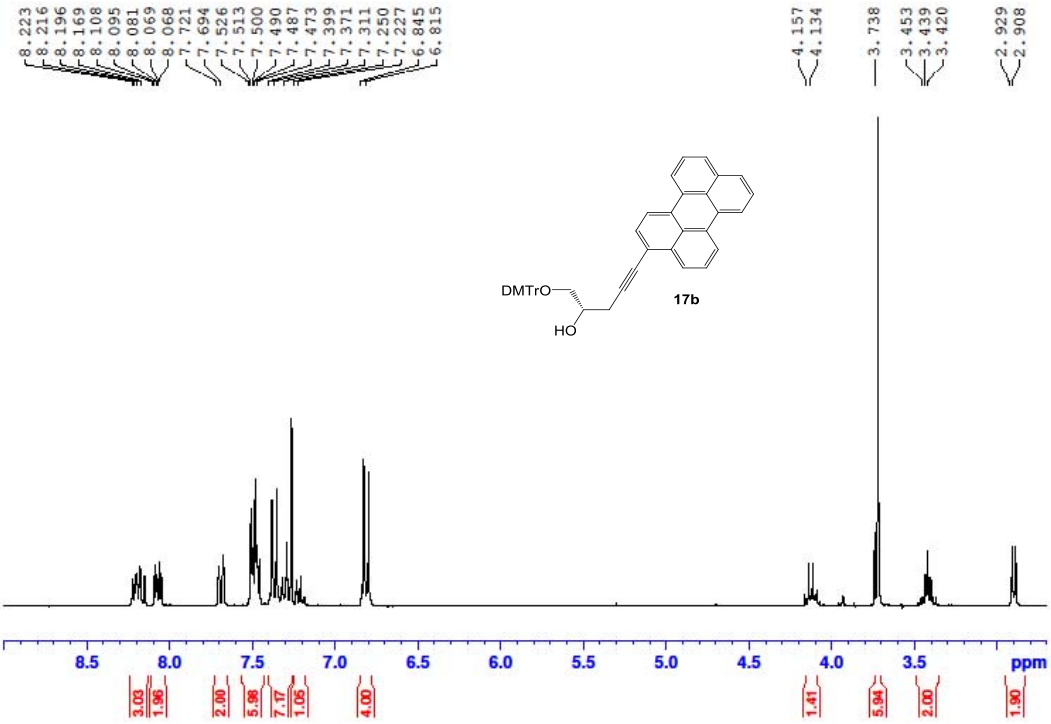

Figure A2.24.1 ^{1}H-NMR spectrum of compound **17b** (300 MHz, $CDCl_3$).

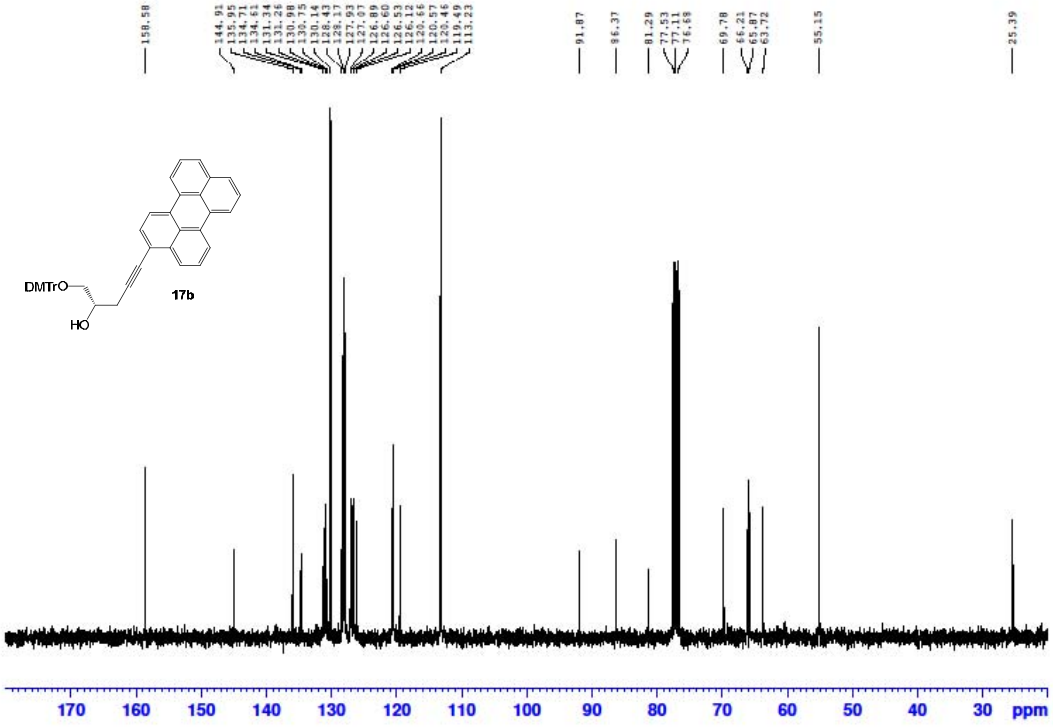

Figure A2.24.2 ^{13}C-NMR spectrum of compound **17b** (75 MHz, $CDCl_3$).

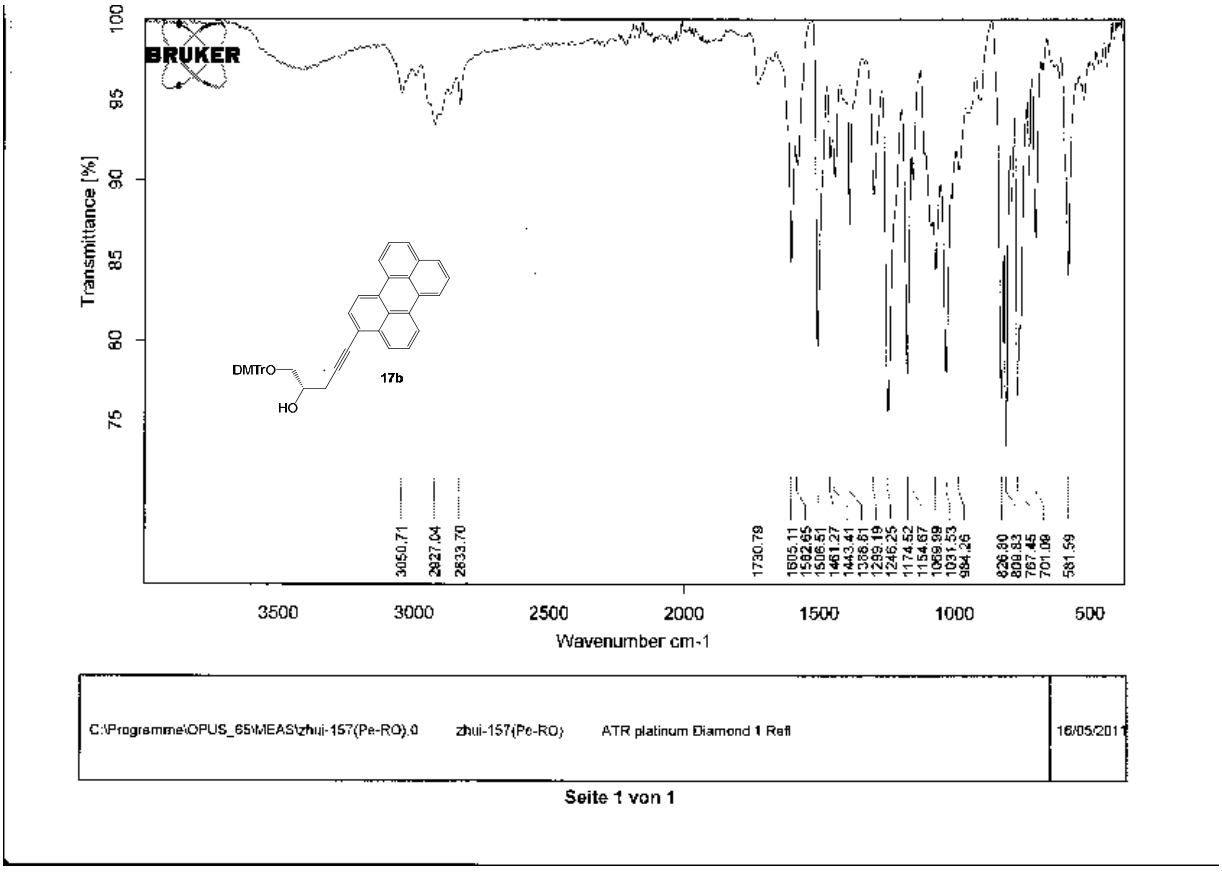

Figure A2.24.3 IR spectrum of compound**17b** (solid).

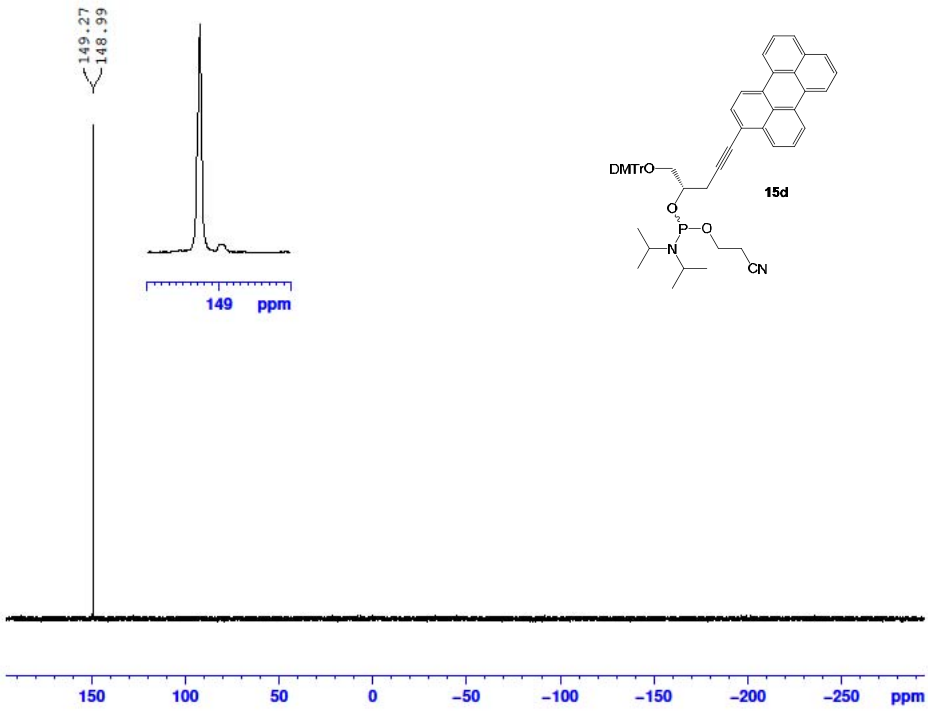

Figure A2.25.1 ^{31}P-NMR spectrum of compound **15d** (121.5 MHz, $CDCl_3$).

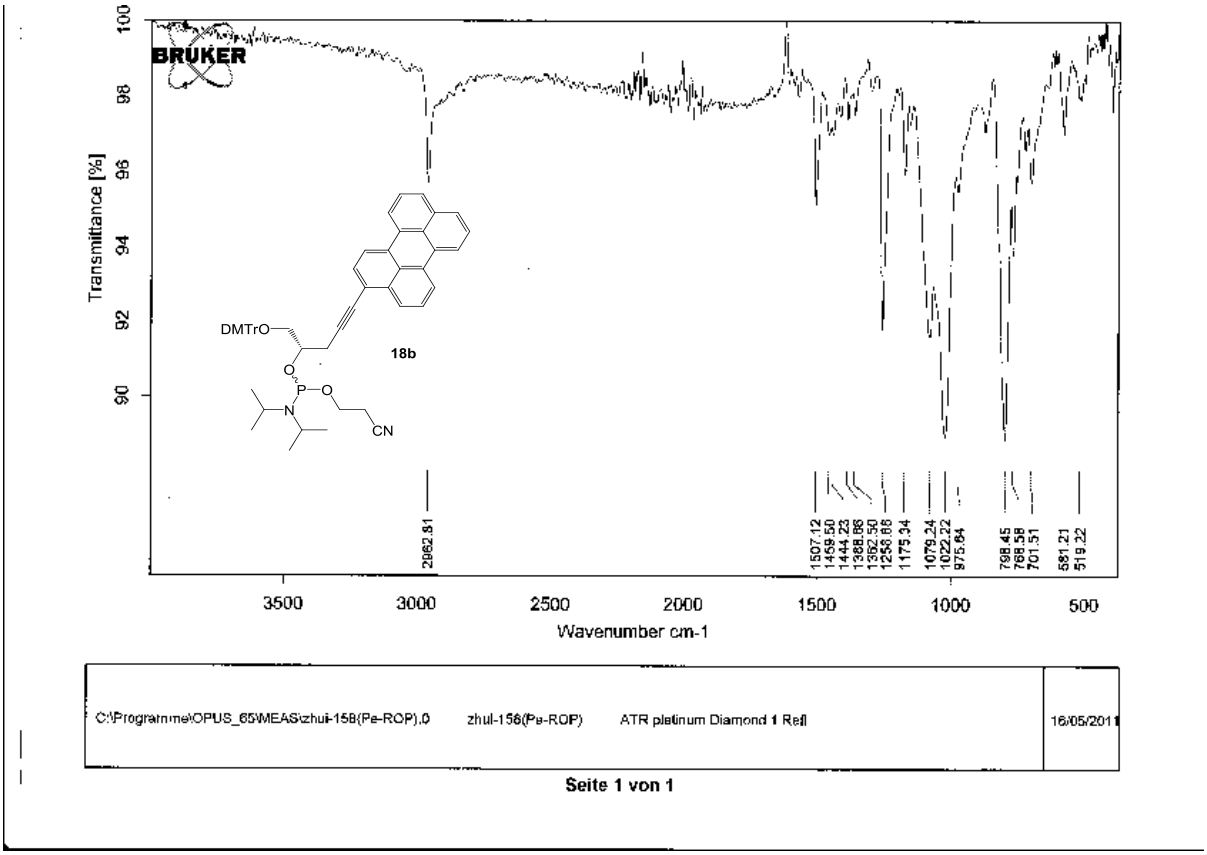

Figure A2.25.2 IR spectrum of compound **18b** (solid).

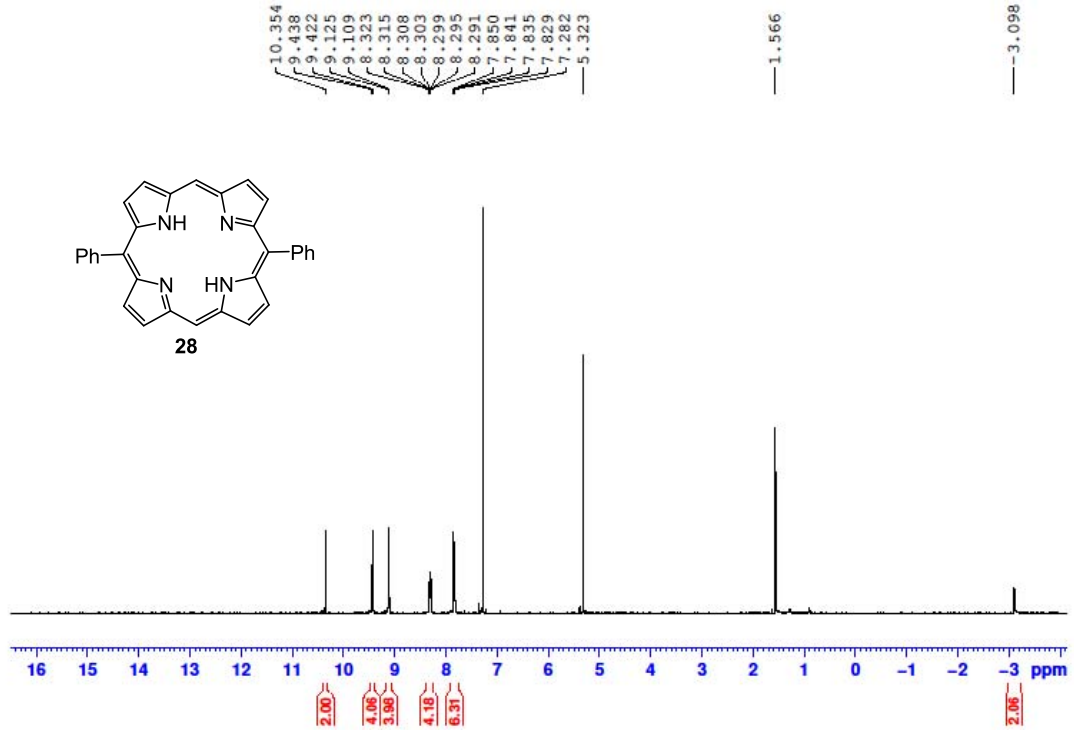

Figure A2.26.1 ^{1}H-NMR spectrum of compound **28** (300 MHz, $CDCl_3$).

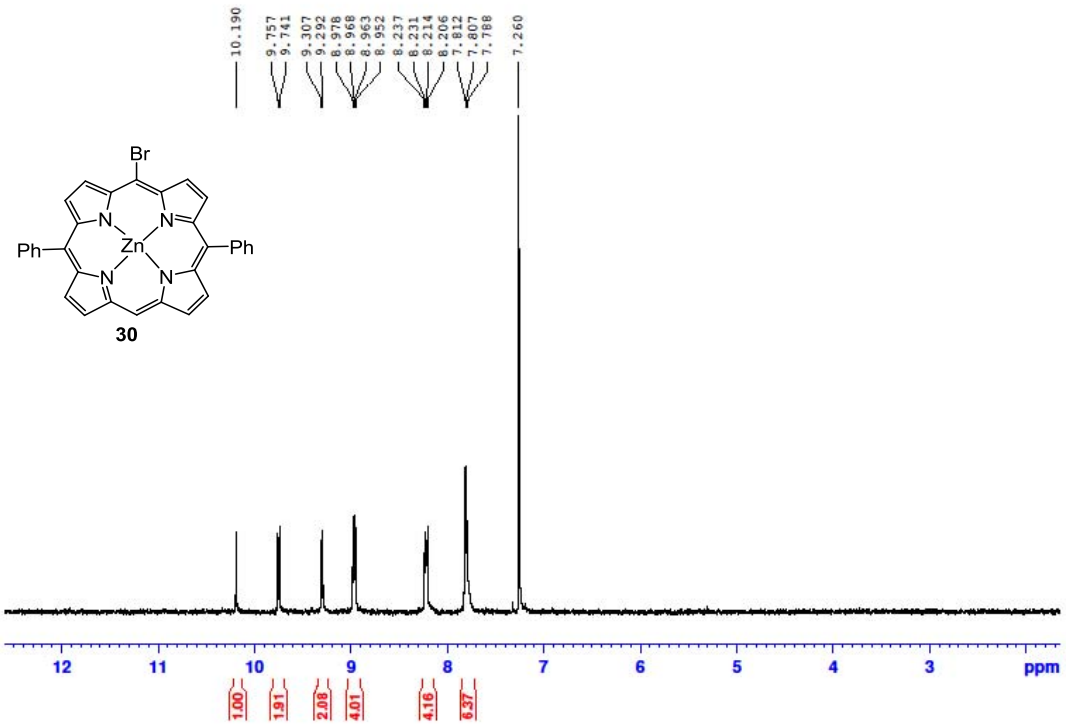

Figure A2.27.1 ^{1}H-NMR spectrum of compound **30** (300 MHz, $CDCl_3$).

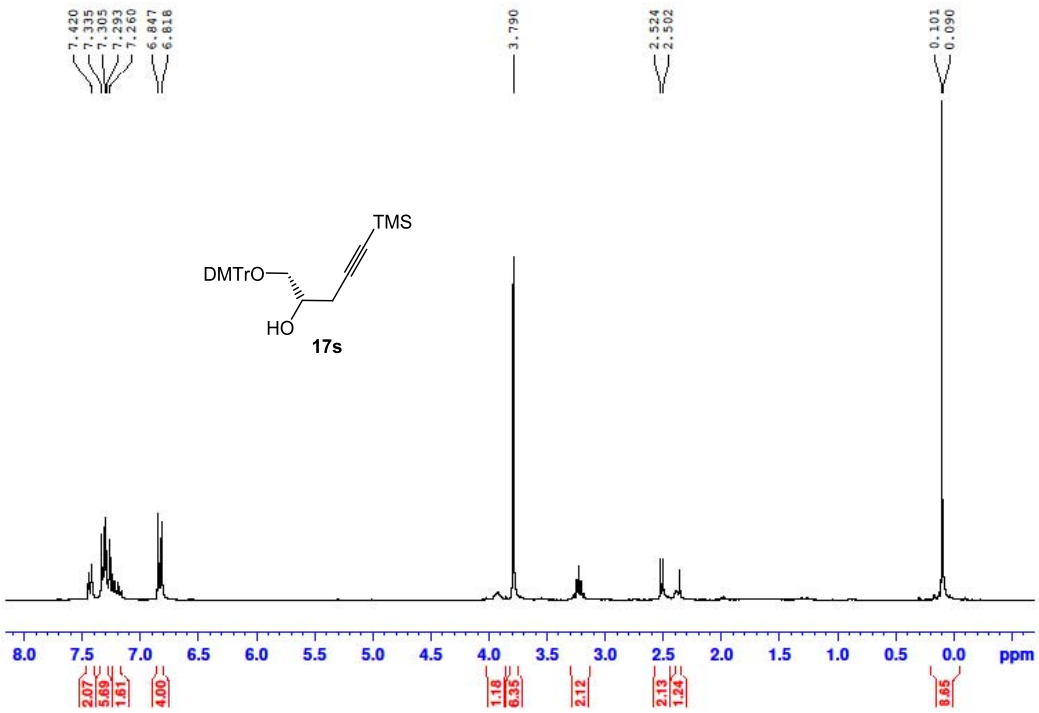

Figure A2.28.1 ^{1}H-NMR spectrum of compound **17s** (300 MHz, $CDCl_3$).

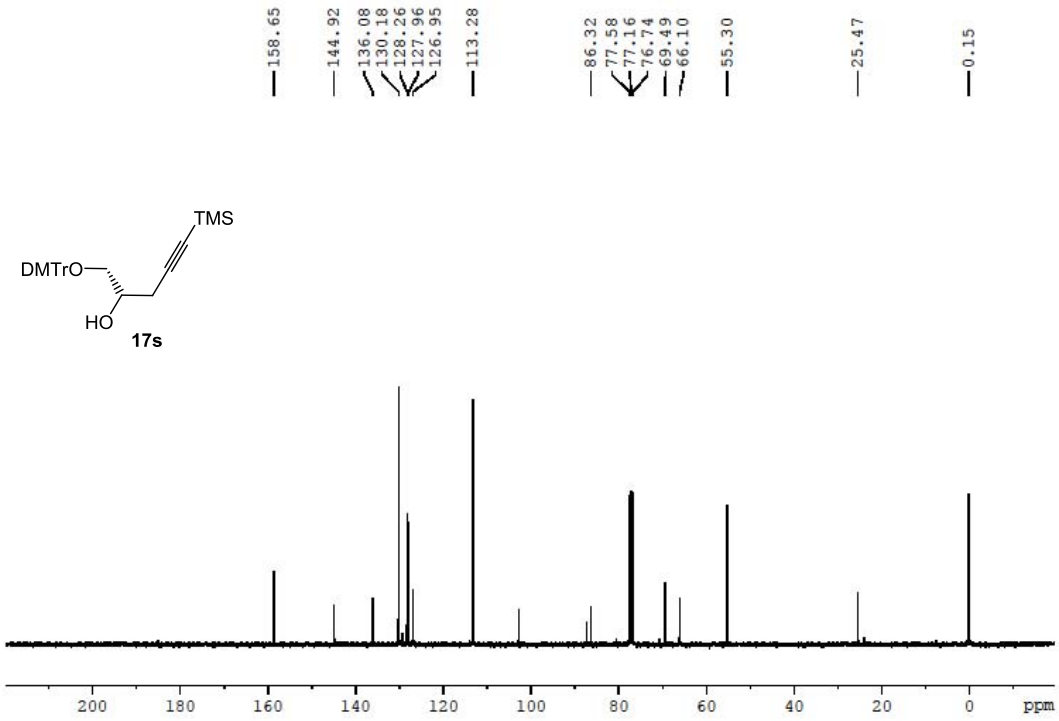

Figure A2.28.2 ^{13}C-NMR spectrum of compound **17s** (75 MHz, $CDCl_3$).

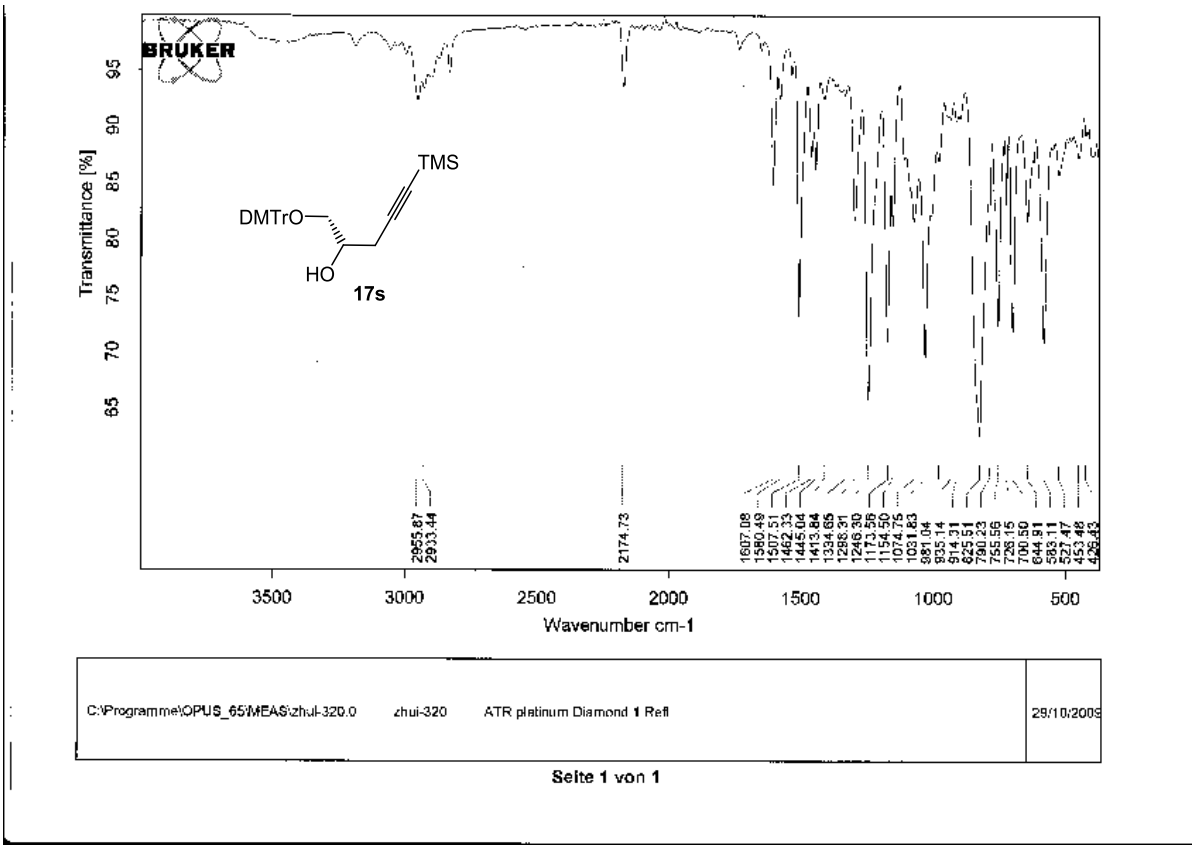

Figure A2.28.3 IR spectrum of compound **17s** (solid).

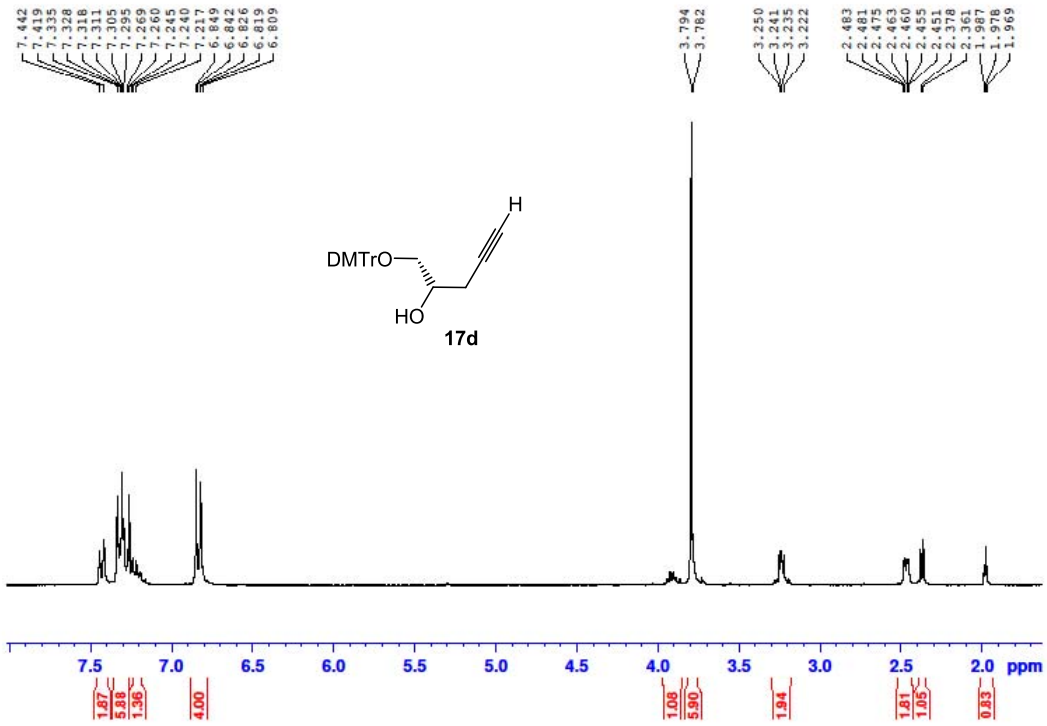

Figure A2.29.1 ^{1}H-NMR spectrum of compound **17d** (300 MHz, $CDCl_3$).

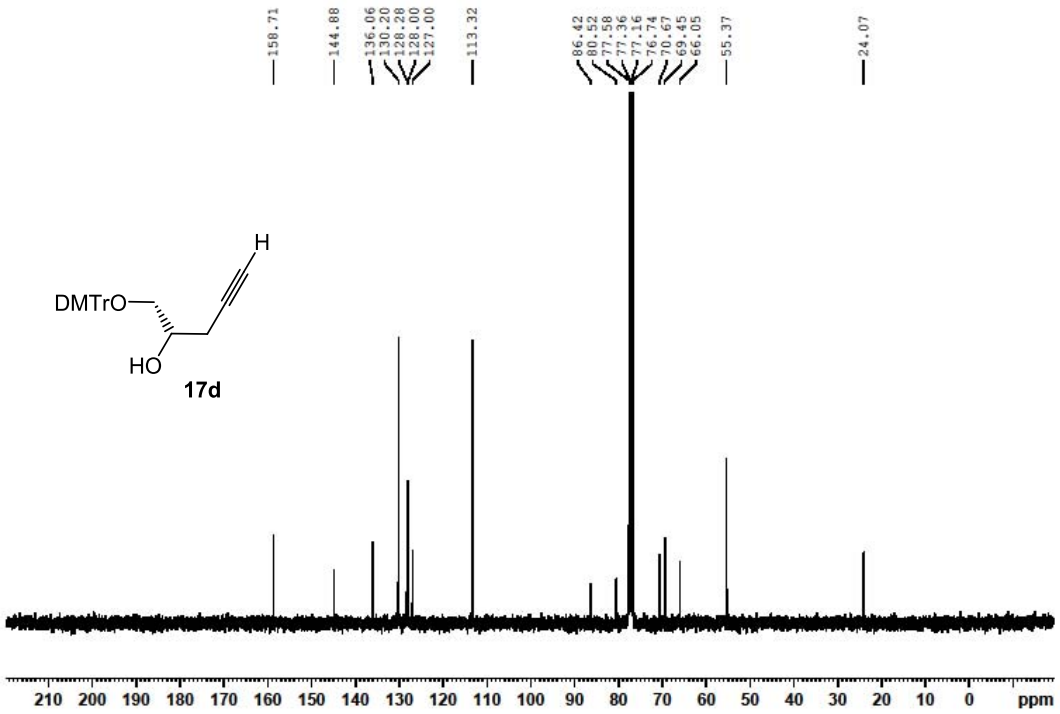

Figure A2.29.2 ^{13}C-NMR spectrum of compound **17d** (75 MHz, $CDCl_3$).

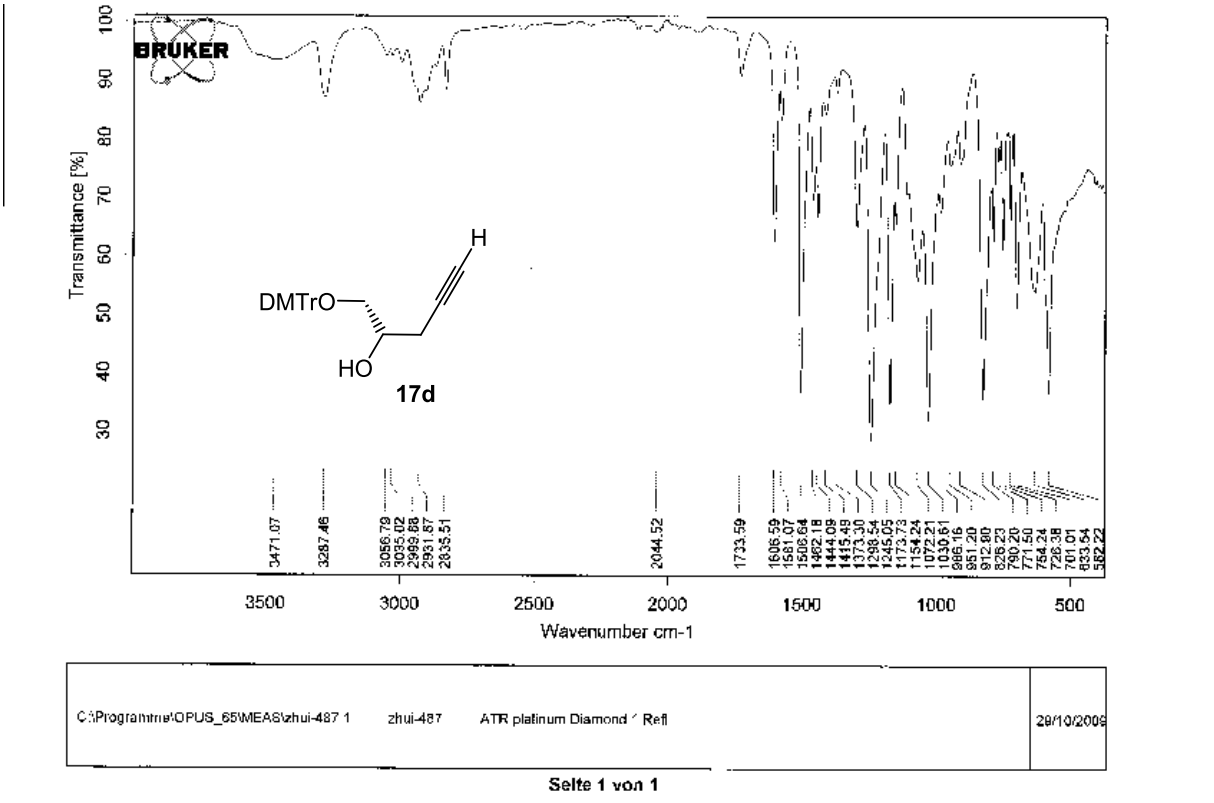

Figure A2.29.3 IR spectrum of compound **17d** (solid).

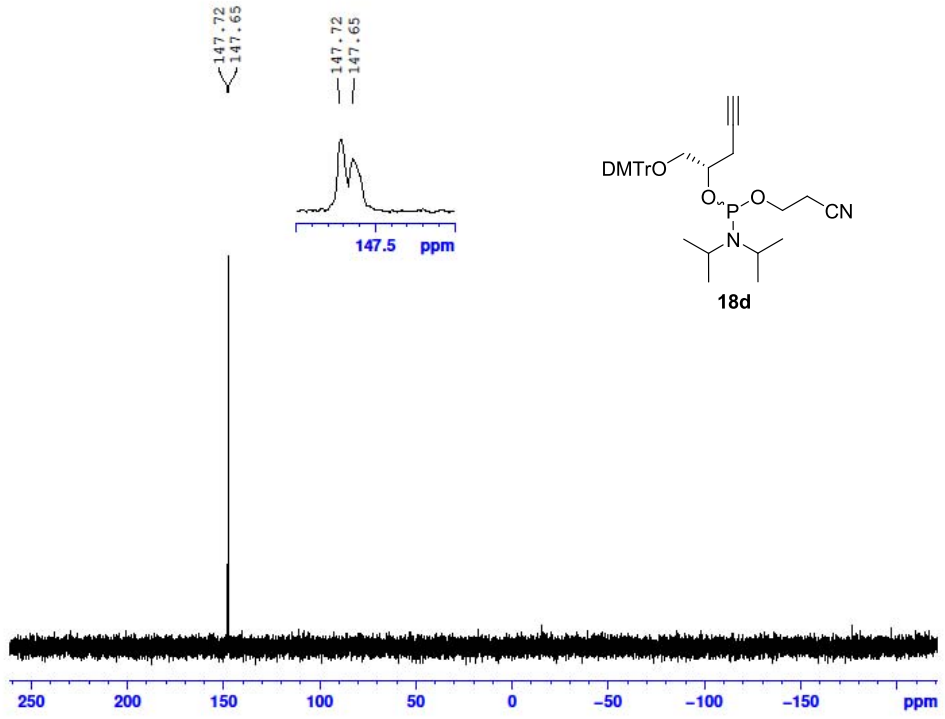

Figure A2.30.1 ^{31}P-NMR spectrum of compound **18d** (121.5 MHz, $CDCl_3$).

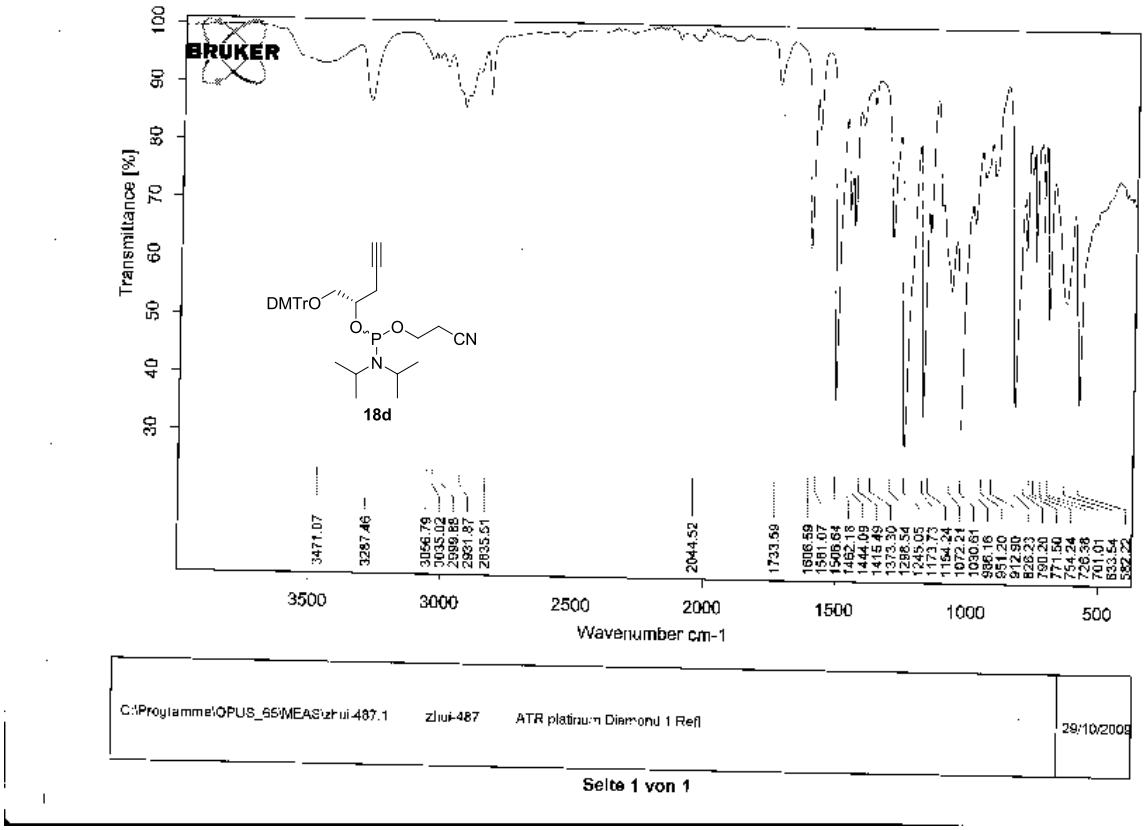

Figure A2.30.2 IR spectrum of compound **18d** (solid).

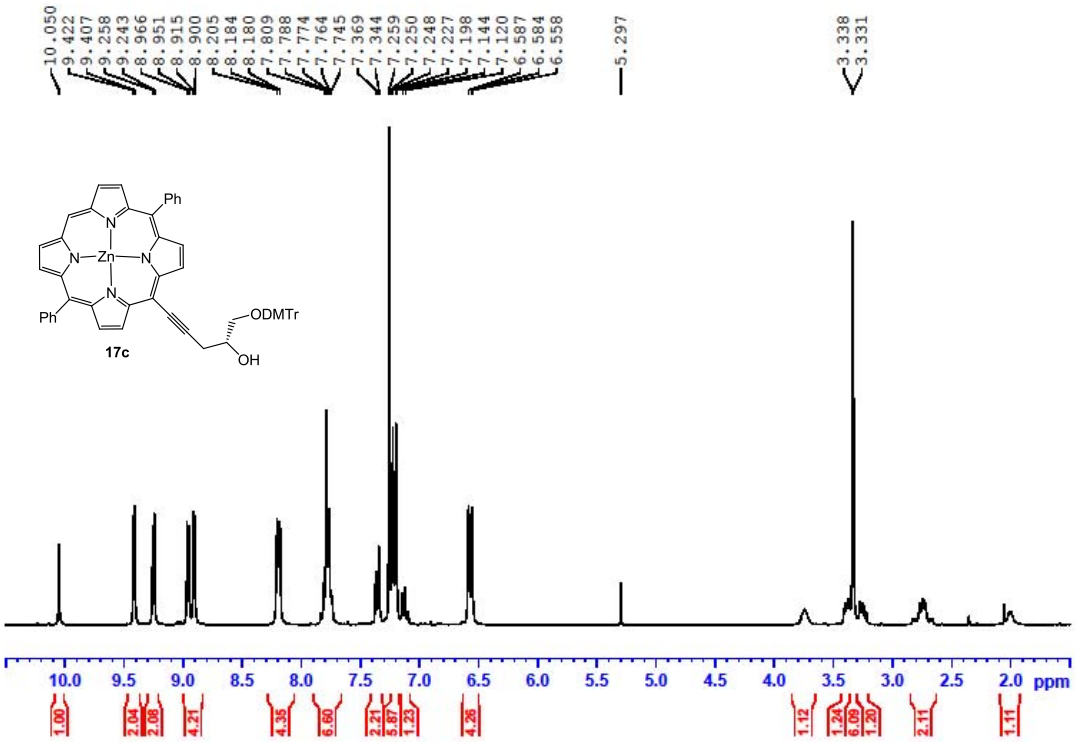

Figure A2.31.1 ^{1}H-NMR spectrum of compound **17c** (300 MHz, $CDCl_3$).

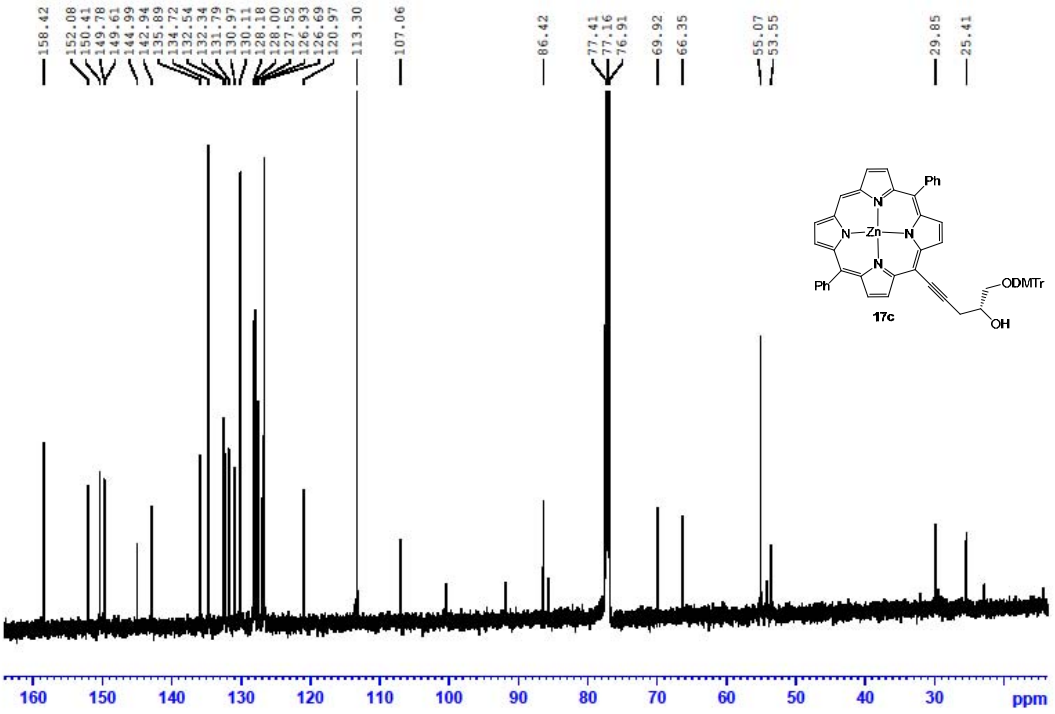

Figure A2.31.2 ^{13}C-NMR spectrum of compound **17c** (125.8 MHz, $CDCl_3$).

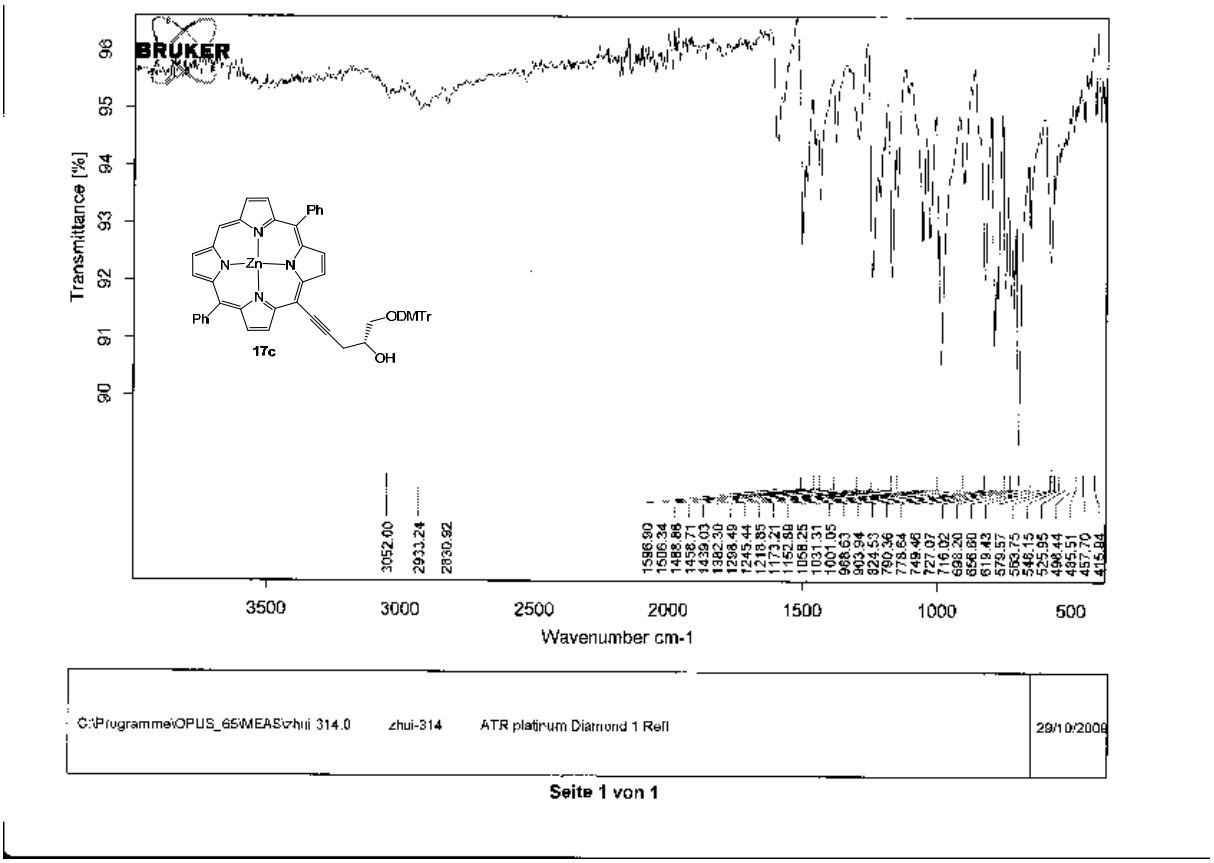

Figure A2.31. 3 IR spectrum of compound **17c** (solid).

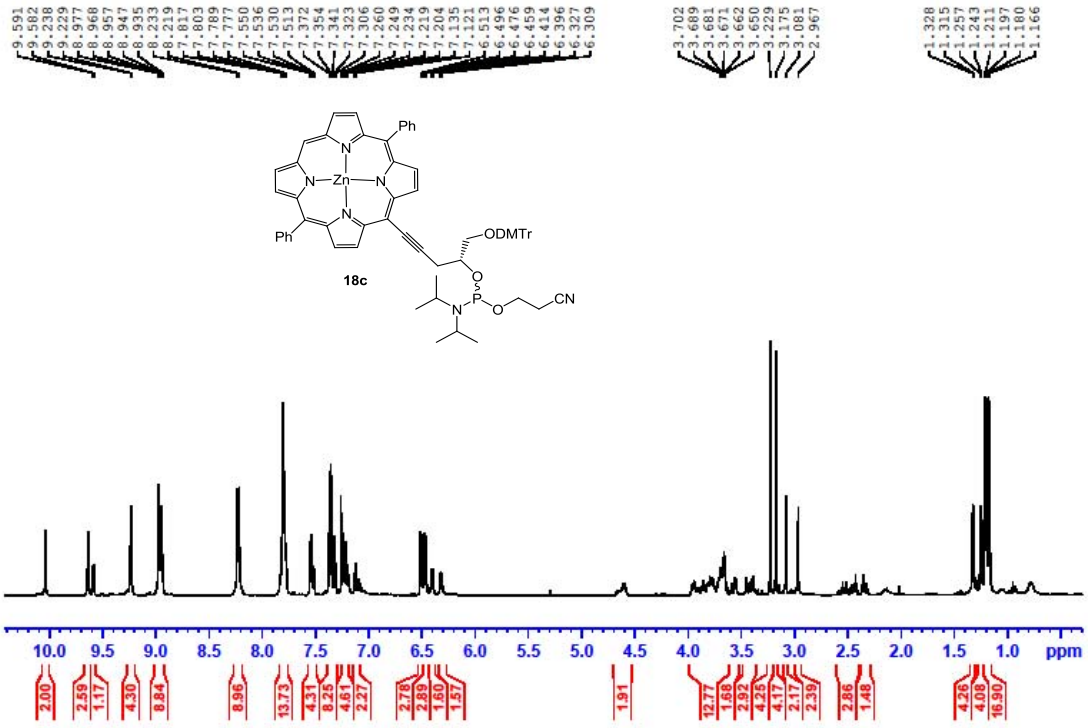

Figure A2.32.1 ^{1}H-NMR spectrum of compound **18c** (500 MHz, $CDCl_3$).

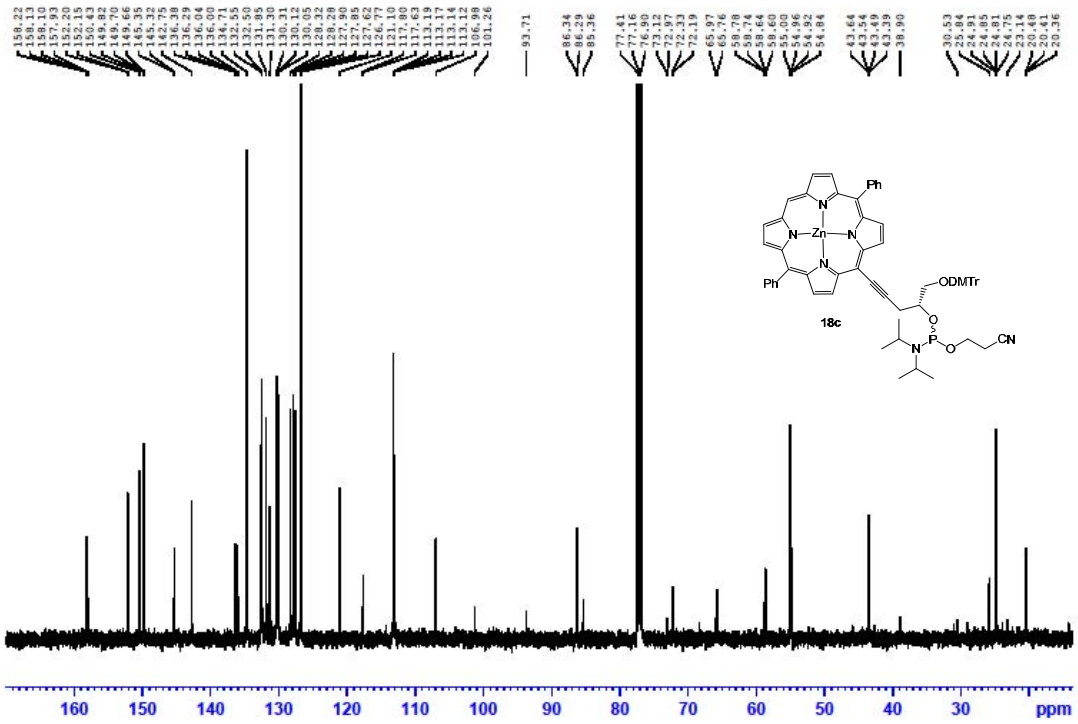

Figure A2.32.2 ^{13}C-NMR spectrum of compound **18c** (125.8 MHz, $CDCl_3$).

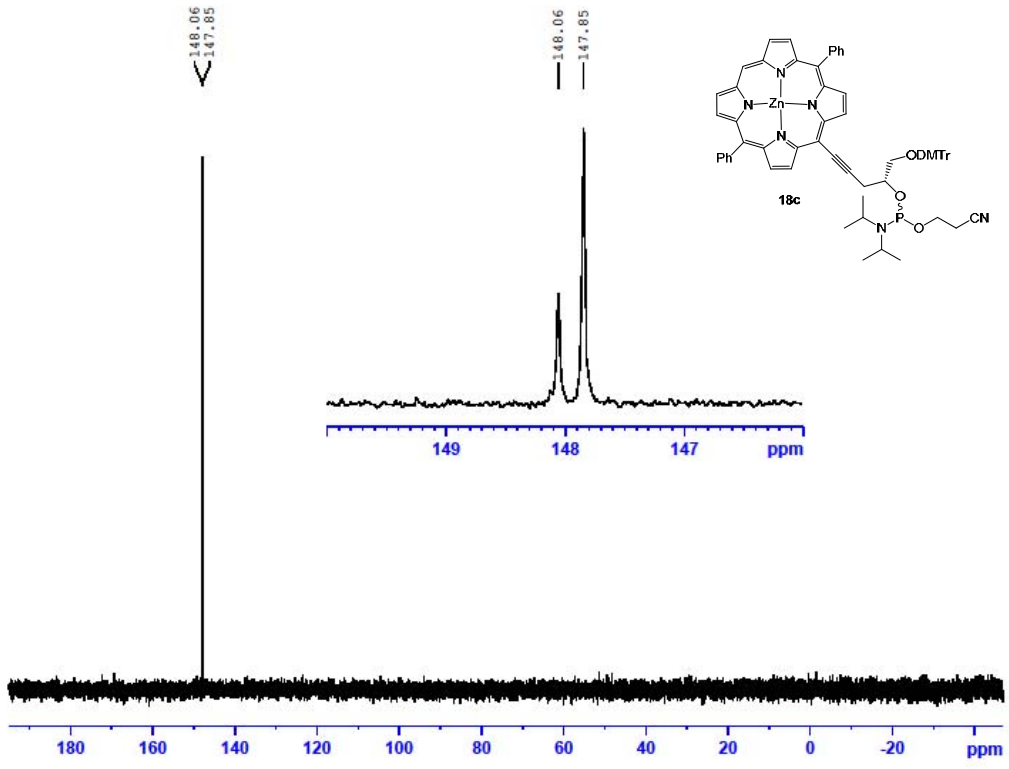

Figure A2.32.3 ^{31}P-NMR spectrum of compound **18c** (121.5 MHz, $CDCl_3$).

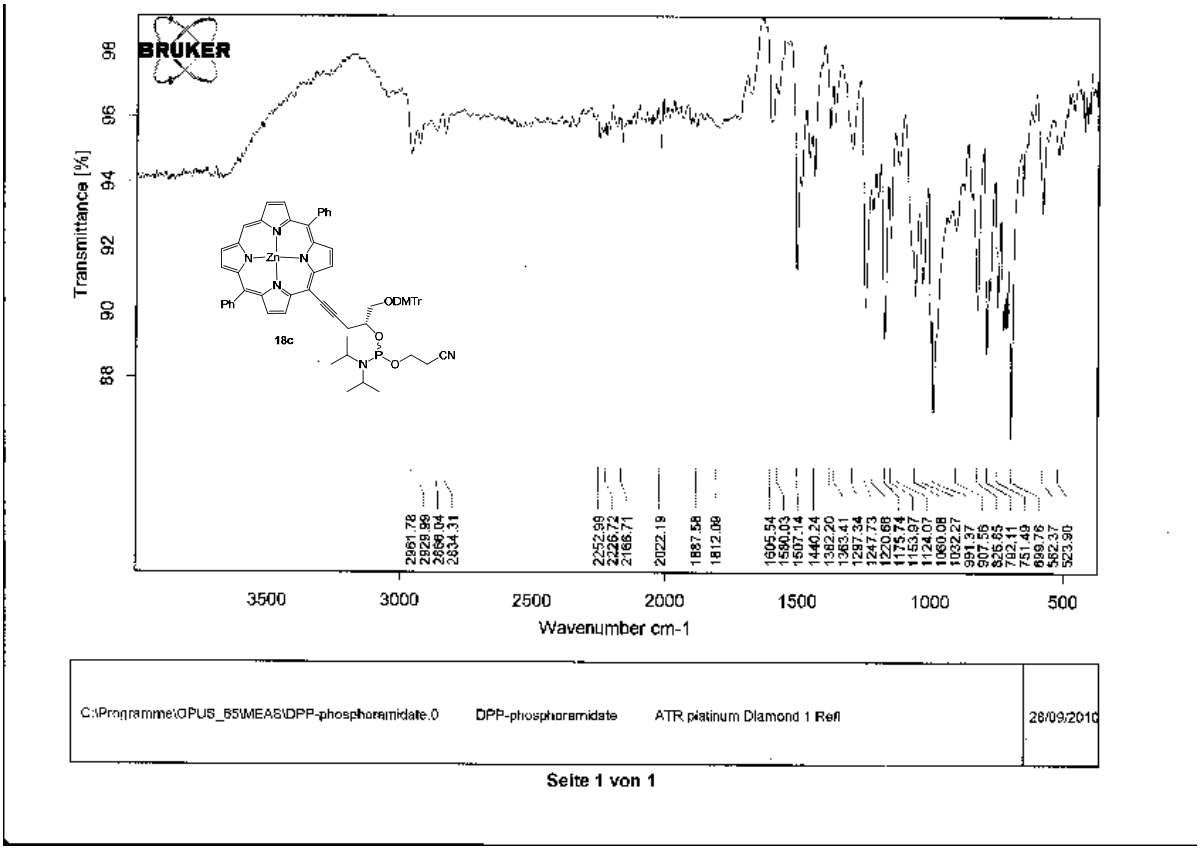

Figure A2.32.4 IR spectrum of compound **18c** (solid).

Chapter 3 Pyrene Acetylide Nucleotides in GNA: Probing Duplex Formation and Sensing of Copper(II) Ions

Chapter 3.1 Introduction

Pyrene is a polycyclic aromatic hydrocarbon consisting of four fused benzenes rings, resulting in a flat aromatic system. Because of efficient planar aromatic stacking, their high quantum yields and their ability to form excimer emission upon stacking, pyrenes have been used extensively in DNA in following three areas:

[1] As a nonpolar artificial base in DNA: Pyrene was introduced into DNA as the nonpolar artificial bases because of its large planar aromatic structure.[1] It was found that dangling pyrene stacks on the duplex extremely strong and pyrene and abasic site could form stable non-hydrogen base pair.[1c] In addition, pyrene c-nucleotides were employed in enzymatic synthesis studies.[2]

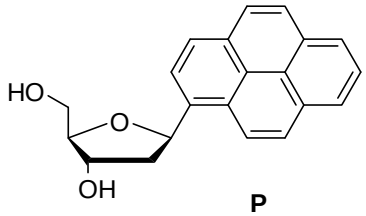

P

Figure 3.1 Pyrene artificial C-nucleoside.

[2] As fluorophores for DNA probes: Fluorescence of pyrene monomer and pyrene excimer has been widely investigated in the development of potential probes for detecting of single nucleotide polymorphisms,[3] single-base mismatches,[4] base-discriminating,[5] DNA or RNA secondary and tertiary structures,[6] and real-time PCR techniques.[7] Pyrene is among the most attractive fluorophores for DNA probes due to the fact that pyrene's long fluorescence lifetimes, sensitivity to microenvironment and its inherent chemical characteristics.[8]

[3] As a building block for constructing a high-ordered nanostructure: π-arrays of pyrene chromophores have been of considerable interest because these kind of close proximity of fluorophores leads to useful changes in fluorescent properties. DNA has been extensively used as a scaffold for assembling

pyrene in a controlled fashion. Up to 14 non-nucleosideic pyrene are embedded in DNA offers an interstrand helical organization.[9] Pyrenes have been covalently attached to nucleobases for using DNA as a scaffold to create helical arrays.[10]

In this chapter, we described the synthesis and evaluation of GNA duplexes containing fluorescent pyrene nucleotides.

Chapter 3.2 Result and Discussion

Chapter 3.2.1 Synthesis of pyrene-GNA

As fluorescent GNA nucleotide building blocks we chose **Pyr** and **Pyr′** in which the natural nucleobases of propylene glycol nucleotides are replaced by pyrene and pyrene-1-acetylide moieties as shown in Figure 3.2B.

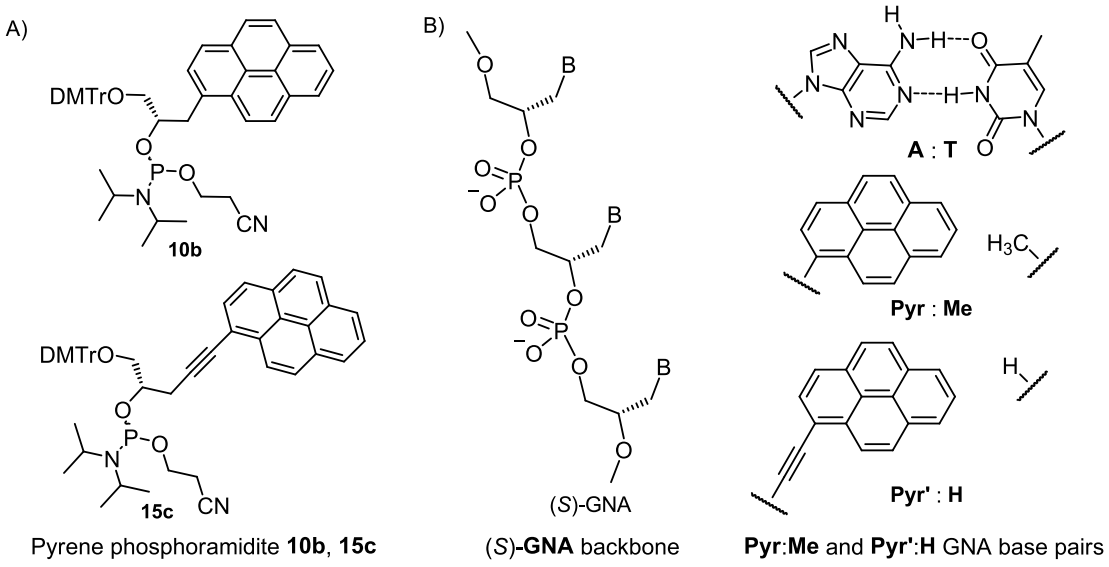

Figure 3.2 (A) Structure of pyrene phosphoramidites **10b** and **15c**. (B) Constitution of (*S*)-GNA. **Pyr**:**Me** and **Pyr′**:**H** base pairs used in this study.

Pyrene phosphoramidites **10b** and **15c** were used to synthesize GNA strands with incorporated pyrene (**Pyr**) and acetylide pyrene (**Pyr′**) nucleotides (Figure 3.2A). Pyrene nucleotides have been demonstrated to fit into the base stacking of nucleic acid duplexes by arranging them opposite abasic sites in order to accommodate for their expanded size.[1c] We therefore chose GNA abasic sites based on ethylene glycol (**H**) and (*S*)-(+)-1,2-propanediol (**Me**) shown in Figure 3.2B. GNA oligonucleotides containing the pyrene nucleotides **Pyr** and **Pyr′**, as well as the abasic sites **Me** and **H**, were synthesized on CPG supports. A standard protocol for 2-cyanoethyl phosphoramidites (0.1 M) was used, except that the coupling was extended to 3 minutes. After the steps of detritylation and purification with a reversed phase HPLC column, the pyrene-containing GNA strands were obtained in high purities.

Chapter 3.2.2 Thermal stability

We first incorporated the pyrene nucleotide **Pyr** into 16mer GNA oligonucleotides. Table 3.1 reveals that **Pyr** was slightly better accommodated opposite a methylated abasic site **Me** (Table 3.1, duplex **D3**) compared to the abasic site **H** (Table 3.1, duplex **D2**), being only by 4 ^{o}C less stable than an **A**:**T** base pair at the same position (Table 3.1, duplex **D1**). Encouraged by these stabilities, we synthesized duplexes **D4**-**D7** (Table 3.1), having incorporated all permutations of adjacent **Pyr**:**Me** base pairs in order to investigate excimer fluorescence formation in GNA duplexes. Table 3.1 demonstrates that all systems form stable duplexes at room temperature.

Table 3.1 Thermal stability of GNA duplexes containing pyrene nucleotides.[a]

3′-TAAAAATNNTAATATT-2′ 2′-ATTTTTANNATTATAA-3′			
Name	Duplexes	T_m(^{o}C)	ΔT_m(^{o}C)
D1	**AA** **TT**	54	2
D2	**HA** **PyrT**	49	-5
D3	**MeA** **PyrT**	50	-4
D4	**MeMe** **PyrPyr**	33	-21
D5	**PyrPyr** **MeMe**	42	-12
D6	**MePyr** **PyrMe**	36	-18
D7	**PyrMe** **MePyr**	43	-11

[a]Conditions: 10 mM sodium phosphate, 100 mM NaCl, 2 μM of each strand.

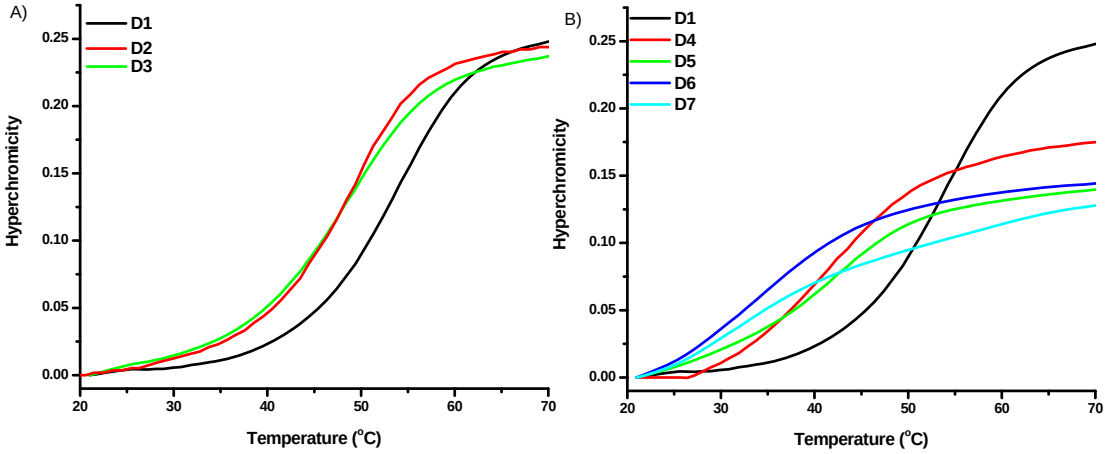

Figure 3.3 UV-melting curves of GNA duplexes containing pyrene nucleotides. Changes in absorbance upon heating as monitored at 260 nm. Conditions: 10 mM sodium phosphate, 100 mM NaCl, pH 7.0, and 2 μM of each strand. (A) Duplexes **D1**, **D2** and **D3**. (B) Duplexes **D1**, **D4**, **D5**, **D6** and **D7** (see Table 3.1 for the sequences).

We then investigated the thermal stability of GNA duplexes contain pyrene acetylide nucleotide **Pyr′**. Interestingly, although significantly larger than **Pyr**, **Pyr′** fits well into GNA duplexes opposite the abasic sites **H** (T_m = 51 °C, Table 3.2, duplex **D9**) and **Me** (T_m = 50 °C, Table 3.2, duplex **D8**), with the base pair **Pyr′**:**H** being only by 3 °C less stable than an **A**:**T** base pair at the same position (Table 3.2, duplex **D1**). Subsequently, duplexes with all permutations of two adjacent **Pyr′**:**H** base pairs were synthesized (Table 3.2, duplexes **D10**-**D13**), all resulting in thermally stable duplexes at room temperature.

Table 3.2 Thermal stability of GNA duplexes containing pyrene acetylide nucleotides.[a]

3′-TAAAAATNNTAATATT-2′ 2′-ATTTTTANNATTATAA-3′			
Name	Duplexes	T_m(°C)	ΔT_m(°C)
D1	**AA** **TT**	54	2
D8	**Pyr′A** **MeT**	50	-4
D9	**Pyr′A** **HT**	51	-3
D10	**HH** **Pyr′Pyr′**	32	-22
D11	**Pyr′Pyr′** **HH**	39	-15
D12	**HPyr′** **Pyr′H**	34	-20
D13	**Pyr′H** **HPyr′**	41	-13

[a]Conditions: 10 mM sodium phosphate, 100 mM NaCl, 2 μM of each strand.

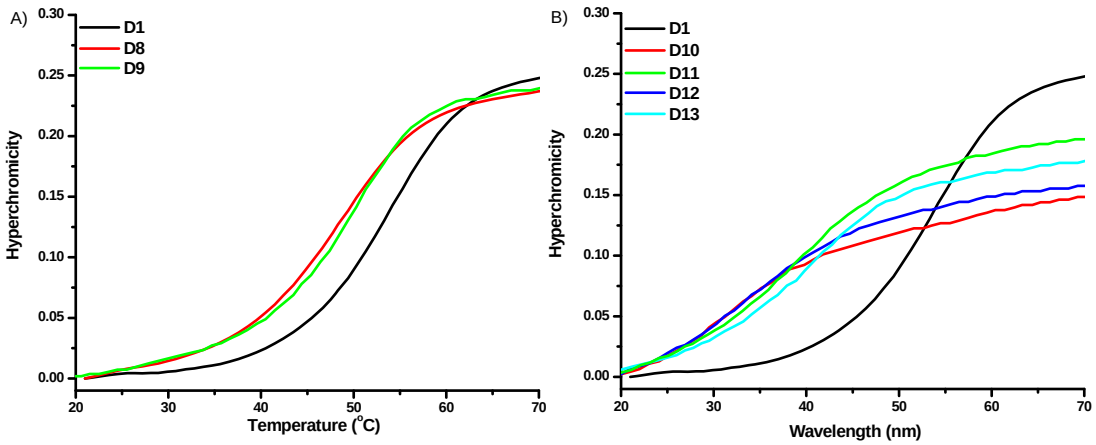

Figure 3.4 UV-melting curves of GNA duplexes containing pyrene acetylide nucleotides. Changes in absorbance upon heating as monitored at 260 nm. Conditions: 10 mM sodium phosphate, 100 mM NaCl, pH 7.0, and 2 μM of each strand. (A) Duplexes **D1**, **D8** and **D9**. (B) Duplexes **D1**, **D10**, **D11**, **D12** and **D13** (see Table 3.2 for the sequences).

Chapter 3.2.3 CD spectroscopy

In order to obtain the information about the secondary structure of GNA duplexes containing pyrene and pyrene acetylide nucleotides, pyrene and pyrene acetylide modified GNA duplexes were investigated by CD spectroscopy.

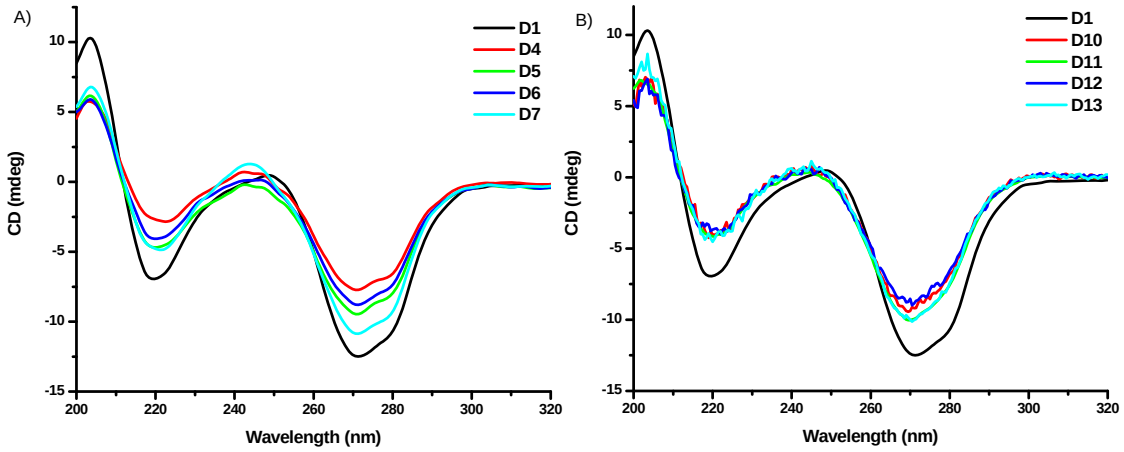

Figure 3.5 CD spectra of GNA duplexes (A) containing pyrene and (B) pyrene acetylide nucleotides (see Table 3.1 and 2.2 for the sequences). Conditions: 10 mM sodium phosphate, 100 mM NaCl, pH 7.0, and 8 μM of each strand, 25 ^{o}C.

The CD signals of modified GNA duplexes are almost identical to native GNA duplex **D1**, except for the lower signal intensities (Figure 3.5). It thus seems that the incorporation of pyrene or pyrene acetylide to GNA duplex does not distort the overall GNA duplex structure.

Chapter 3.2.4 Fluorescence spectroscopy

We then investigated the fluorescence properties of GNA strands which contain pyrene and pyrene acetylide. Excimer emission results of pyrene-containing GNA duplexes turned out to be disappointing.

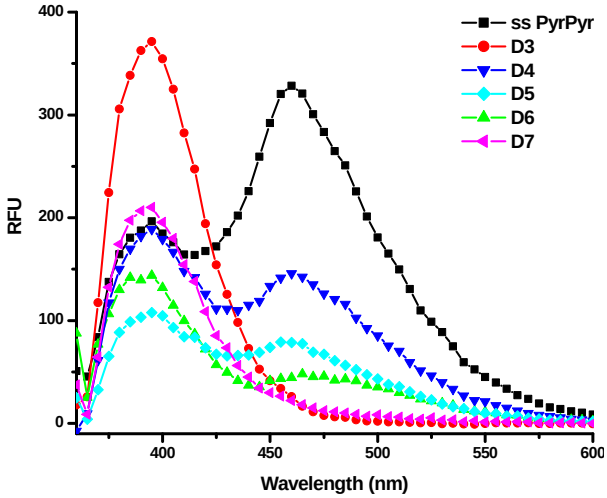

Figure 3.6 Fluorescence properties of pyrene nucleotides in GNA. Conditions: 10 mM sodium phosphate, 100 mM NaCl, pH 7.0, and 2 µM of each strand of a duplex (**D3**-**D7**) or 2 µM for the single strand 3′-TAAAAAT**PyrPyr**TAATATT-2′ (see Table 3.1 for the sequences), excitation at 315 nm with cutoff filter at 325 nm, fluorescence at 460 nm taken as indicator for excimer fluorescence.

Upon excitation at 315 nm, the duplexes **D4**-**D6**, containing each two adjacent pyrene nucleobases, give overall low fluorescence quantum yields with low emissions at 395 nm (regular emission) as well as low emissions at 460 nm (excimer emission) as shown in Figure 3.6, compared to the duplex **D3** harboring a single pyrene (strong regular emission at 395 nm) and a **Pyr**-**Pyr** containing single strand (strong excimer emission at 460 nm). Moreover, duplex **D7** does not yield any excimer emission at all. This latter result can be explained with the strong nucleobase-backbone inclination in GNA duplexes which should result in only a very weak stacking of the two pyrene nucleobase in duplex **D7**. However, the weak excimer emission of duplexes **D4**-**D6**, in combination with the overall low fluorescence quantum yields, remains unclear.

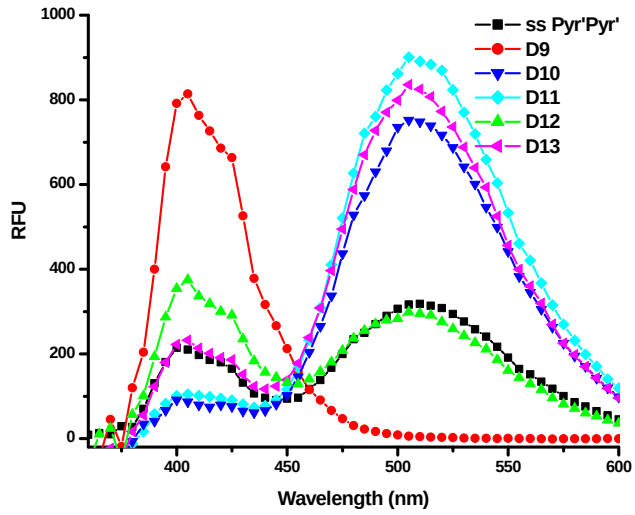

Figure 3.7 Fluorescence properties of pyrene acetylide nucleotides in GNA. Conditions: 10 mM sodium phosphate, 100 mM NaCl, pH 7.0, and 2 µM of each strand of a duplex (**D9-D13**) or 2 µM for the single strand 3′-TAAAAAT**Pyr′Pyr′**TAATATT-2′ (see Table 3.2 for the sequences), excitation at 315 nm with cutoff filter at 325 nm, fluorescence at 500 nm taken as indicator for excimer fluorescence.

Fortunately, replacing pyrene nucleotide **Pyr** by pyrene acetylide **Pyr′**, the fluorescence properties were dramatically improved. Figure 3.7 demonstrates that in particular the duplexes **D10**, **D11**, and **D13** yield very strong excimer emission intensities upon excitation at 315 nm which exceed the excimer emissions of the corresponding pyrene duplexes **D4**, **D5**, and **D7** (Figure 3.6) by around 10-fold. Most interestingly, whereas **D10** and **D11** contain adjacent pyrene acetylides in the same strand, duplex **D13** provides strong excimer fluorescence despite the pyrene acetylide nucleotides **Pyr′** being in opposite strands. The arrangement of **Pyr′** nucleotides in opposite strands in **D13** therefore allows to monitor duplex formation by following the intensity of excimer emission relative to the regular emission of the single strands. Compared to pyrene-containing duplexes (**Pyr**), pyrene acetylide-containing duplexes (**Pyr′**) form much stronger excimers. Most likely, the superior behavior of **Pyr′** in GNA duplexes is due to a combination out of structural effects, influencing the stacking of adjacent **Pyr′** nucleobases, and electronic effects due to the conjugation of the aromatic pyrene with the acetylide π-system.

Chapter 3.2.5 Design of a GNA-based copper ion sensor

As an application of excimer emission upon duplex formation with pyrene acetylide containing GNA strands, we envisioned to develop a metal ion sensor by additionally incorporating a metal-mediated base pair. The hydroxypyridone homo-base pair **M**:**M** is known to increase DNA duplex stability in the presence of Cu^{2+} ions (see Figure 3.8 for the molecular structure).[12] The hydroxypyridone homo-base pair is known to increase DNA and GNA duplex stability in the presence of Cu^{2+} ions. This effect has been demonstrated to be even significant stronger in GNA duplexes compared to DNA with an increase in duplex stability in the presence of Cu^{2+} by around 30 °C.[13]

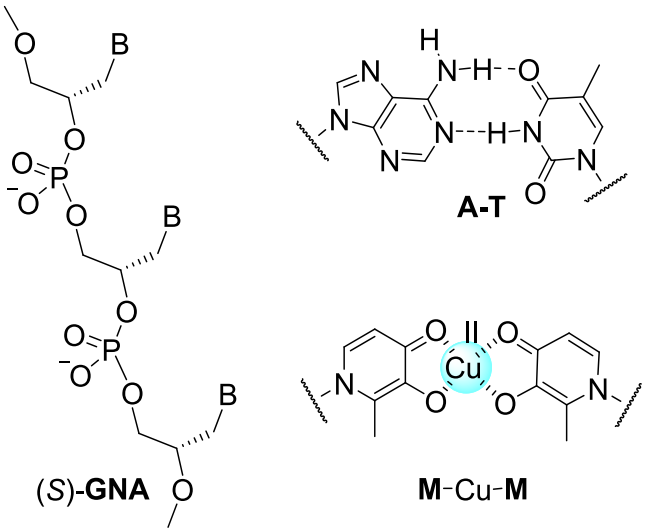

Figure 3.8 Structure of the copper-mediated hydroxypyridone homo-base pairs **M**:**M** (**M** = hydroxypyridone).

Sequence design

We first designed two duplexes **D14** and **D15** (Table 3.3), which include two **Pyr′**:**H** base pairs in analogy to **D13** in addition to a metal-mediated hydroxypyridone homo-base pair **M**:**M**. **D14** is 16 mers, while **D15** is 15 mers. Beside of this, **D14** and

D15 differ in the number of the natural base pairs between two **Pyr′**:**H** base pairs and **M**:**M** base pair, **D14** has 7 and **D15** only has 4 base pairs.

Table 3.3 Comparison of thermal and excimer emission for **D14** and **D15**.

Entry	Sequence	T_m (°C)[a]	Excimer[b] (without Cu^{2+})	Excimer[b] (with Cu^{2+})
D13	3′-TAAAAAT**Pyr′H**TAATATT-2′ 2′-ATTTTTA**HPyr′**ATTATAA-3′	41	strong	strong
D14	3′-TAT**Pyr′H**AAATAAT**M**AAA-2′ 2′-ATA**HPyr′**TTTATTA**M**TTT-3′	no	medium	strong
D15	3′-TATA**Pyr′H**TAAT**M**TAAA-2′ 2′-ATAT**HPyr′**ATTA**M**ATTT-3′	no	weak	strong

[a]Conditions: 10 mM sodium phosphate, 100 mM NaCl, 2 μM each strand of a duplex and without Cu^{2+}.
[b]Excitation at 315 nm with cutoff filter at 325 nm. Fluorescence at 500 nm taken as indicator for excimer fluorescence. 25 °C, 2 μM each strand of a duplex.

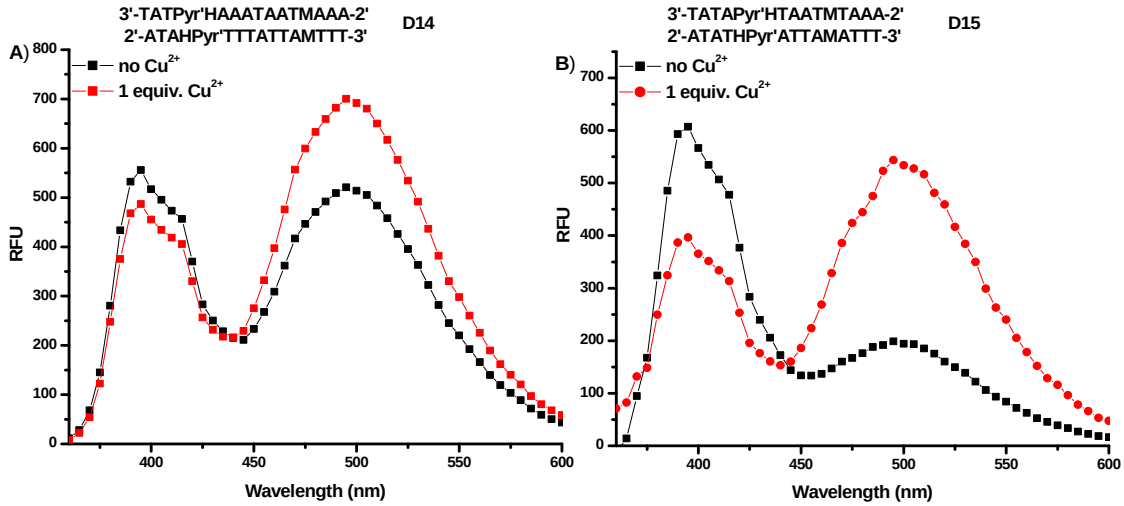

Figure 3.9 Copper(II)-dependent fluorescence properties of duplexes. Conditions: 10 mM sodium phosphate, pH 7.0, 100 mM NaCl, 2 μM of each strand of a duplex, 25 °C, excitation at 315 nm with cutoff filter at 325 nm. (A) **D14**. (B) **D15** (see Table 3.3 for the sequences).

We measured excimer emission of duplex **D14** and **D15** in the presence and absence of $CuCl_2$ (Figure 3.9). In presence of $CuCl_2$, both **D14** and **D15** yielded

strong excimer emission (500 nm). However, **D14** still yielded quite strong excimer emission even in the absence of $CuCl_2$ (Figure3.9A, black line). **D15** only exhibited very weak excimer emission (Figure 3.9B, black line), indicating the two stands of **D15** were mainly dissociated without Cu^{2+}. Therefore, we chose **D15** for further studies.

Optimize the condition

Since the counter-cation concentration has stabilization effect on duplex formation, we measured the melting point and fluorescence of **D15** at varying NaCl concentration in the presence or absence of Cu^{2+}.

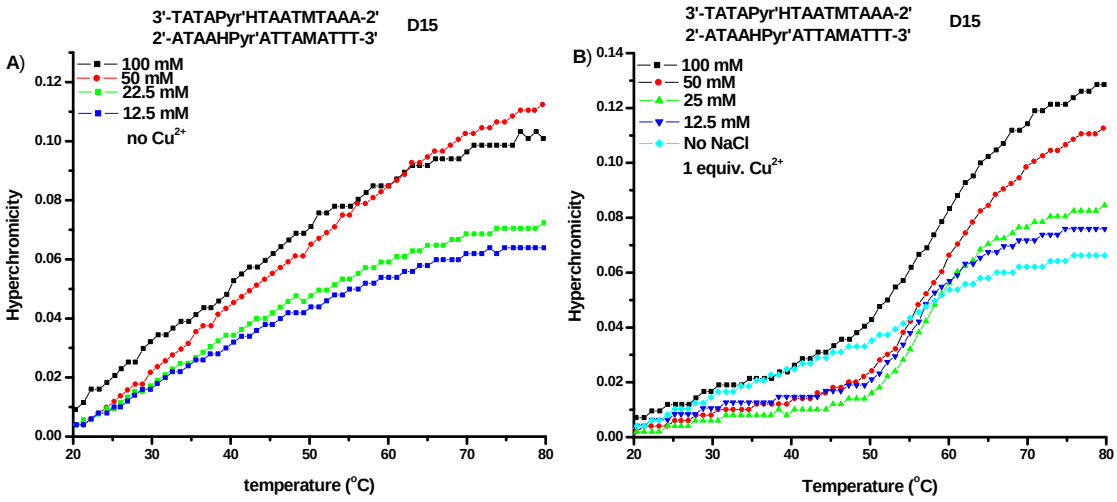

Figure 3.10 NaCl concentration-dependent UV-melting curves of duplex **D15** (see Table 3.3 for the sequences). Conditions: 10 mM sodium phosphate, pH 7.0, and 2 μM of each strand of a duplex. (A) Without Cu^{2+}. (B) With one equivalent Cu^{2+}.

In absence of $CuCl_2$, cooperative melting behavior is not observed at different salt concentrations (Figure 3.10A). However, after the addition of only one equivalent of $CuCl_2$, duplex **D15** was strongly stabilized and cooperative melting behavior could be observed (Figure 3.10B) at NaCl concentration of 12.5 mM or above.

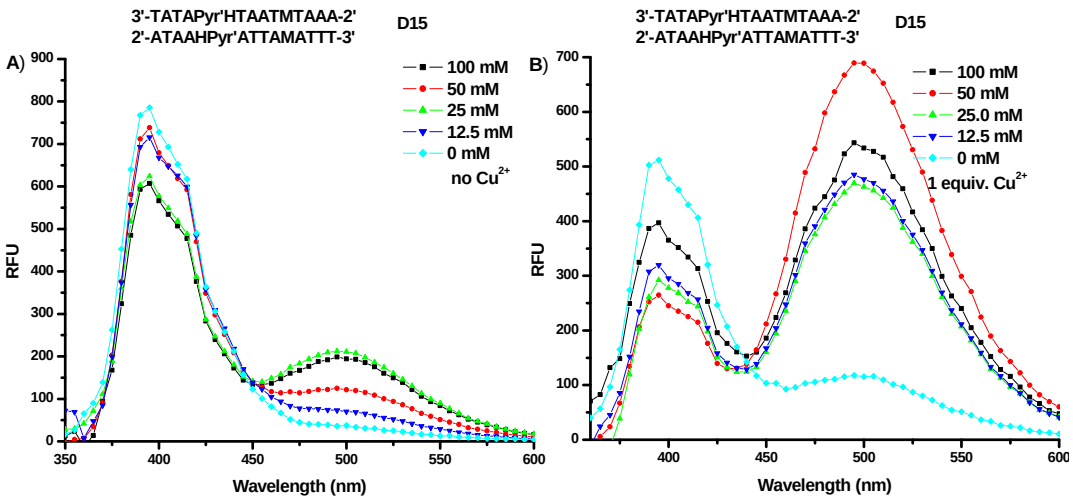

Figure 3.11 NaCl concentration-dependent fluorescence spectrums of duplex **D15** (see Table 3.3 for the sequences). Conditions: 10 mM sodium phosphate, pH 7.0, and 2 μM of each strand of a duplex, 25 ^{o}C, excitation at 315 nm with cutoff filter at 325 nm. (A) Without Cu^{2+}. (B) With one equivalent Cu^{2+}.

We next investigated the effect of salt concentration on the fluorescence property of **D15**. Figure 3.11B reveals that **D15** with one equivalent $CuCl_2$ exhibits the strongest excimer emission at 50 mM NaCl concentration. Together with T_m result, we chose 50 mM NaCl concentration. The optimize condition of sensor **D15** is 40 °C, 50 mL NaCl concentration (Figure 3.12).

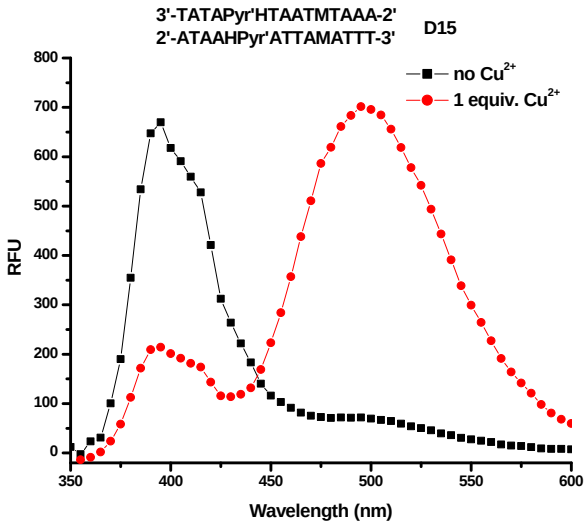

Figure 3.12 Copper(II)-dependent fluorescence properties of duplexes **D15** in optimized condition. Conditions: 10 mM sodium phosphate, 50 mM NaCl, pH 7.0, 2 μM of each strand of a duplex, 40 ^{o}C, excitation at 315 nm with cutoff filter at 325 nm.

Titration Experiment

In order to experimental verify that one equivalent Cu^{2+} is need to stable the hydroxypyridone base pair **M**:**M** in sensor **D15**, titration of Cu^{2+} to a denatured duplex **D15** is carried out under the optimized condition (10 mM sodium phosphate, 50 mM NaCl, pH 7.0, 2 μM each strand of a duplex, 40 °C).

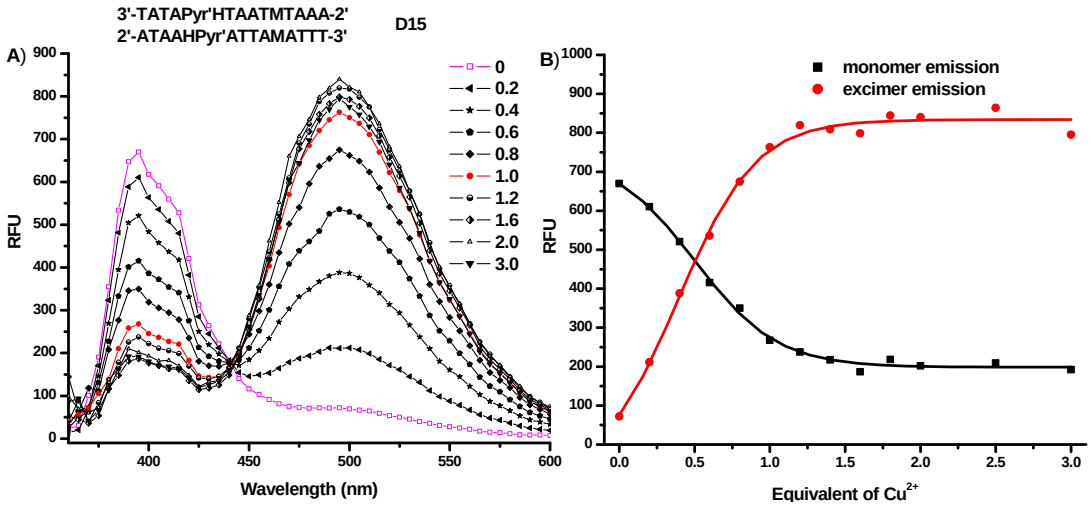

Figure 3.13 Copper(II)-sensing with sensor **D15** (see Table 3.3 for the sequences). Conditions: 10 mM sodium phosphate, 50 mM NaCl, pH 7.0, 2 μM of each strand of a duplex, 40 °C, excitation at 315 nm with cutoff filter at 325 nm. (A) Titration. (B) The trend of monomer emission and excimer emission in titration.

The titration experiment reveals that excimer emission increased with increasing amount of Cu^{2+} until around one equivalent of Cu^{2+} is reached, with only a marginal further increase upon addition of more Cu^{2+} (Figure 3.13). This is in agreement with the notion that one equivalent was needed in order to stabilize the duplex **D15** through a copper(II)-mediated hydroxypyridone base pair.[13]

Metal ion selectivity

Selectivity is the most important characteristic as it determines the extent of utility of any sensor. In order to evaluate whether this sensor exhibits selectivity toward Cu^{2+}, we first measured thermal stabilities of **D15** in presence of different metal ions by UV-monitored thermal melting. Figure 3.14 shows that **D15** is only stabilized by Cu^{2+} ion, other metal ions have no stabilization effect on **D15**.

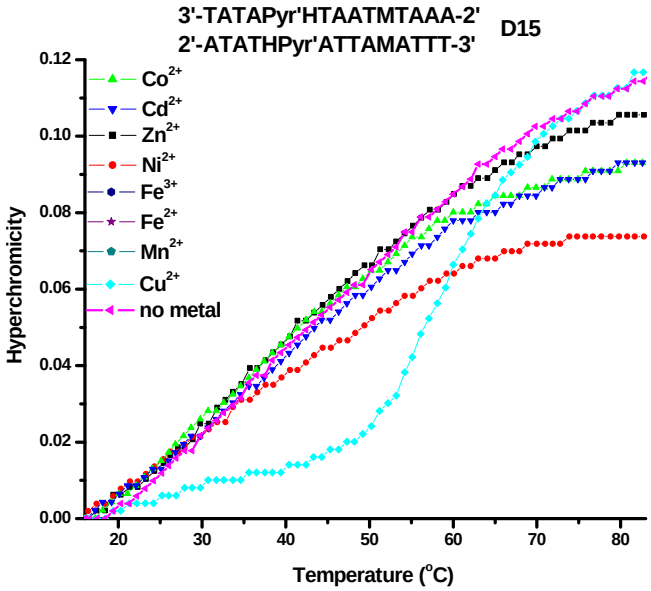

Figure 3.14 Metal ion-dependent UV-melting curves of duplex **D15** (see Table 3.3 for the sequences). Conditions: 10 mM sodium phosphate, 50 mM NaCl, pH 7.0, 1 equivalent metal ion and 2 μM of each strand of a duplex.

We next investigated the fluorescence properties of **D15** with different metal ions at different temperature. Figure 3.14 shows other metal ions such as Ni^{2+}, Co^{2+}, Zn^{2+}, Cd^{2+}, Mn^{2+} or $Fe^{2/3+}$ could not induce any excimer emission at 50 or 60 ^{o}C (Figure 3.15C and D), thus demonstrating **D15** presents excellent selectivity in comparison with other metal ions.

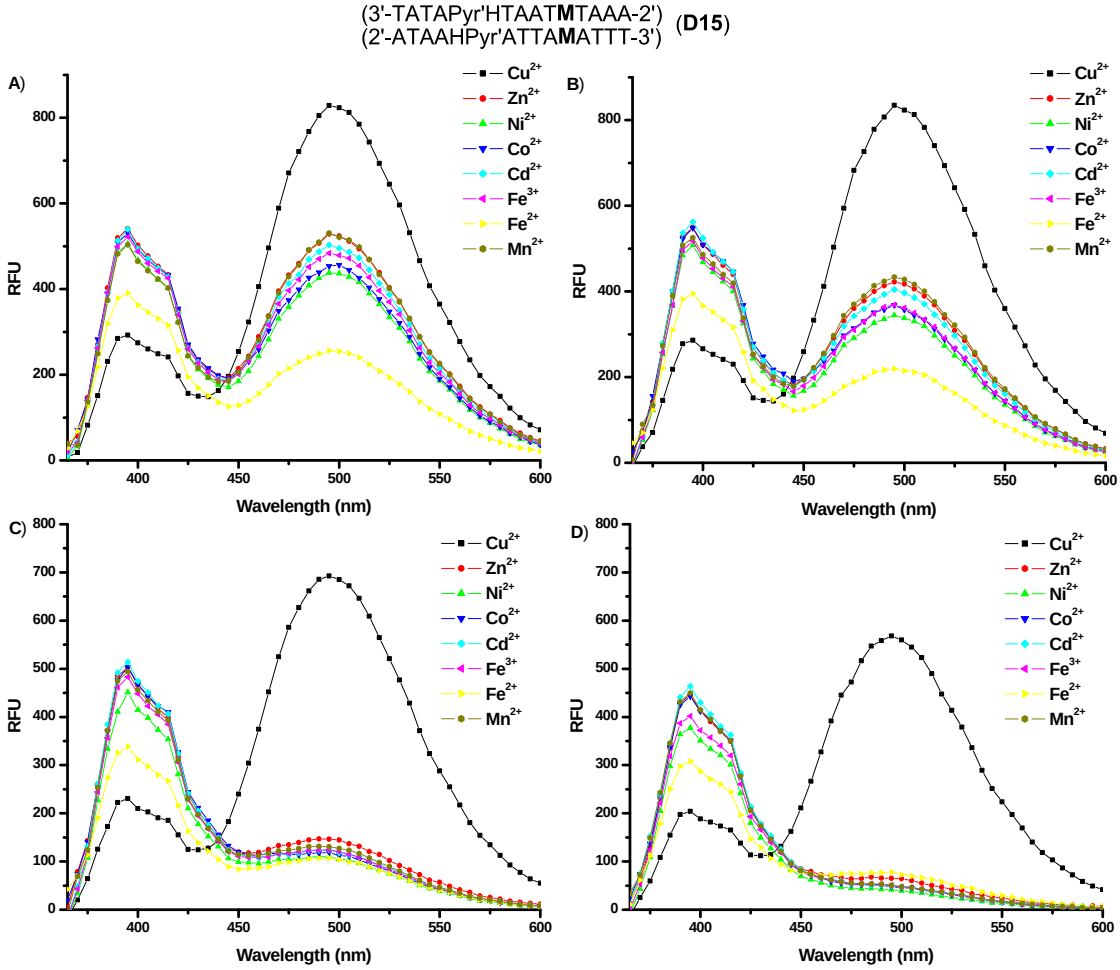

Figure 3.15 Metal ion-selectivity of sensor **D15** at different temperatures (see Table 3.3 for the sequences). Conditions: 10 mM sodium phosphate, 50 mM NaCl, pH 7.0, 1 equivalent metal ion and 2 μM of each strand of duplex, excitation at 315 nm with cutoff filter at 325 nm. A) 25 ^{o}C. B) 40 ^{o}C. C) 50 ^{o}C. D) 60 ^{o}C.

Chapter 3.2.6 Design of a new generation GNA-based copper ion

As reported in chapter 3.2.5, the GNA-based sensor **D15** showed a good selectivity for Cu^{2+} ions in optimized conditions (see Figure 3.15 for more details). Unfortunately, **D15** cannot be used in living cell, since living cell has high salt concentration (0.9% NaCl, nearly 150 mM), and it can not stand the temperature higher than 37 ^{o}C. We tried to modify current sensor for developing a GNA-based copper ion sensor for using in living cell.

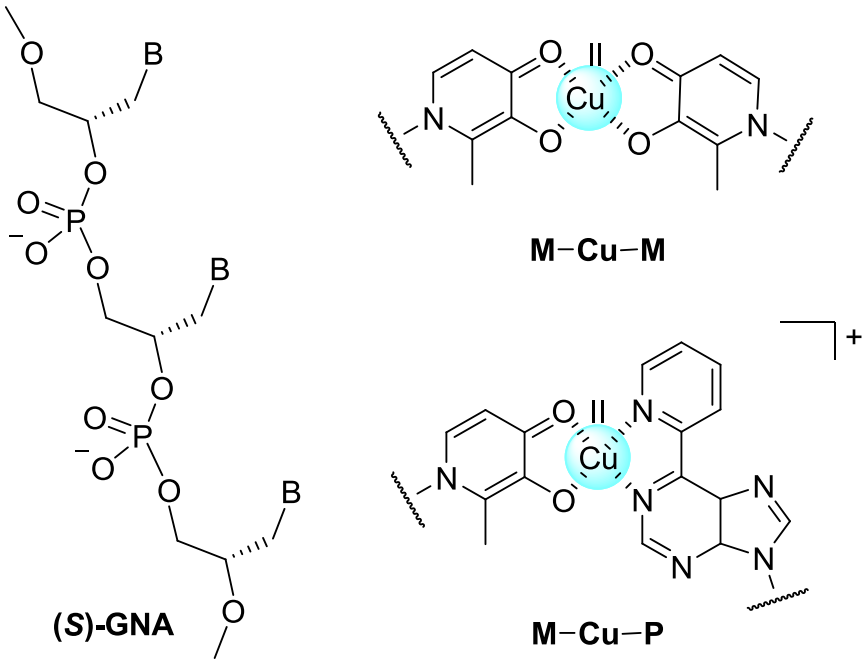

Figure 3.16 Structure of the copper-mediated hydroxypyridone-pyridylpurine hetero-base pairs (**M** = hydroxypyridone, **P** = pyridylpurine).

It has been reported that the hydroxypyridone-pyridylpurine hetero-base pair (**M**:**P**) behaves similarly to the hydroxypyridone homo-base pair in its metal selectivity, but the stabilization of **M**:**P** by Cu^{2+} surpasses the **M**:**M**. We expected that replacing of **M**:**M** base pair with **M**:**P** in sensor duplex may be improve the sensitivity of sensor. Normally, DNA duplexes with dangling ends have increased stability. It has also been reported that a dangling pyrene base at 5′-end of DNA stabilizes the duplex by 23 ^{o}C.[1b] We thus expect that moving pyrene acetylide nucleotide **Pyr′** to the end of

GNA duplex might increase the stability of duplexes. Therefore, we designed the following duplex sequence as a new sensor:

D19

3′-ATT**P**ATTTT**Pyr′**C_3-2′
2′-TAA**M**TAAAA**HPyr′**-3′

We investigated the fluorescence properties of duplex **D19** in the presence or absence of $CuCl_2$ at 37 ^oC (Figure 3.17). In the absence of $CuCl_2$, **D19** exhibits regular emission at around 400 nm (Figure 3.17, black line), indicating the two stands of **D19** were mainly dissociated. Upon the addition of one equivalent of $CuCl_2$, **D19** yields strong excimer emission (500 nm).

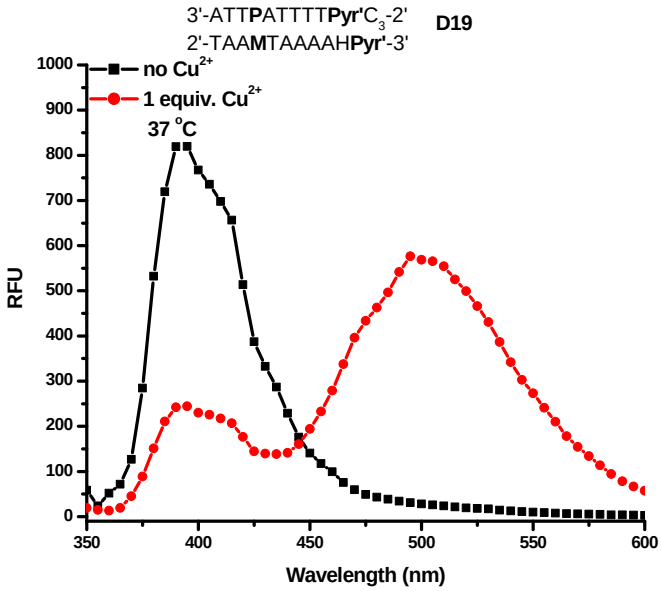

Figure 3.17 Copper(II)-dependent fluorescence properties of duplex **D19**. Conditions: 10 mM sodium phosphate, pH 7.0, 100 mM NaCl, and 2 μM each strand of a duplex, excitation at 315 nm with cutoff filter at 325 nm, 37 ^oC.

Thermal stability and fluorescence studies of **D19** with different metals show that **D19** has good selectivity for Cu^{2+} ion. Figure 3.18A reveals that only Cu^{2+} ion stabilizes D19 strongly, Ni^{2+}, Co^{2+} or Zn^{2+} only stabilizes **D19** very slightly. Figure 3.18B shows that **D19** only exhibits strong excimer emission in the presence of Cu^{2+}, in contrast, other metal ions such as Ni^{2+}, Co^{2+}, Zn^{2+}, Cd^{2+}, Mn^{2+} or $Fe^{2/3+}$ do not show any effect.

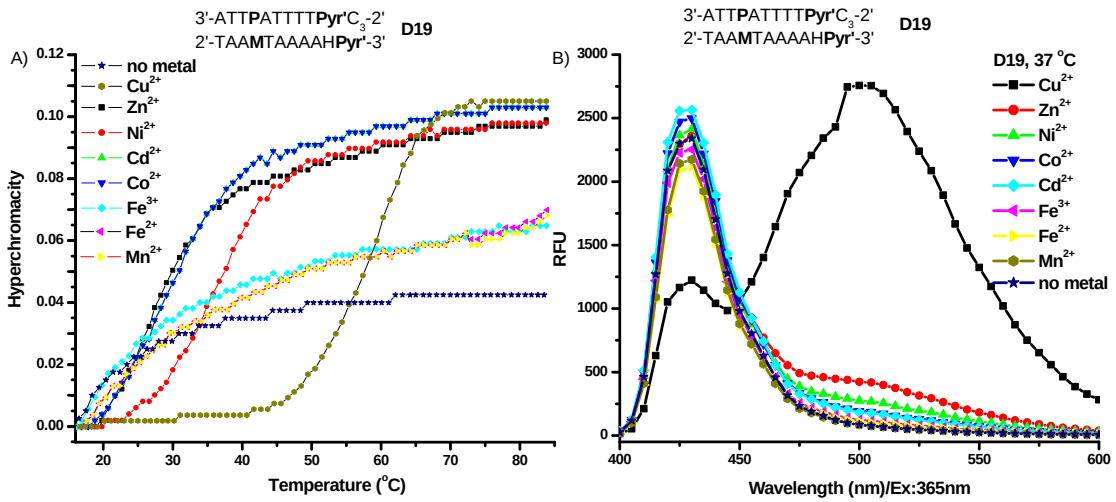

Figure 3.18 (A) Metal-dependent UV-melting curves of duplex **D19**. Conditions: 10 mM sodium phosphate, 100 mM NaCl, pH 7.0, 1 equivalent metal ion and 2 μM each strand of a duplex. (B) Metal ion-selectivity of sensor **D19**. Conditions: 15 mM sodium phosphate, 153 mM NaCl, pH 7.0, 1 equivalent ion and 1 μM each strand of duplex, excitation at 365 nm with cutoff filter at 420 nm, 37 °C.

It is worthy to note that regular emission and excimer emission of pyrene acetylide are strongly increased upon excitation at 365 nm in comparison with that upon excitation at 315 nm.

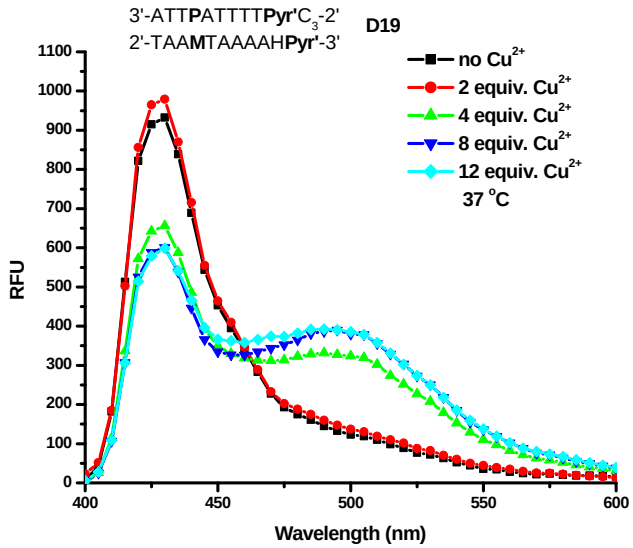

Figure 3.19 Copper(II)-sensing with GNA **D19** in Dulbecco's Modified Eagle's medium. Conditions: in Dulbecco's Modified Eagle's medium, 1 μM each strand of a duplex, excitation at 365 nm with cutoff filter at 420 nm, 37 °C.

For testing the applicability of sensor **D19** in biological system, we first studied fluorescence properties of the **D19** in the presence and absence of $CuCl_2$ in

Dulbecco's Modified Eagle's medium. Dulbecco's Modified Eagle's medium is widely used in cell culture, and is mainly consists of NaCl (6.4 g/L), $NaHCO_3$ (3.7 g/L) and L-glutamine (0.58 g/L). Figure 3.19 shows that only weak excimer emission is observed when four equivalent or above $CuCl_2$ is added. The sensitivity of **D19** is dropped dramatically in Dulbecco's Modified Eagle's medium, based on this disappointed result, we did not proceed the experiment with living cell.

Chapter 3.3 Conclusions

In this chapter, we investigated the properties of GNA duplexes containing fluorescent pyrene nucleotides. Pyrene phosphoramidite building block **10b** and pyrene acetylide phosphoramidite building block **15c** were used to synthesize GNA strands with incorporated pyrene (**Pyr**) and acetylide pyrene (**Pyr′**) nucleotides. Pyrene acetylide GNA nucleotides enable to monitor duplex formation by excimer fluorescence detection, and this was applied to the design of copper(II) ion sensor. Although **D15** is a very sensitive and selective Cu^{2+} "turn-on" fluorescent sensors, our attempt to develop a Cu^{2+} sensor in real biological system was failed.

Chapter 3.4 Experimental

GNA oligonucleotide synthesis and purification (General protocol)

The synthesis and purification of phosphoramidites was followed by repeated coevaporation with toluene to remove trace amounts of water. Then the phosphoramidites was left under high vacuum and repeatedly dissolved and evaporated with methylene chloride to remove traces of toluene. The phosphoramdites were left overnight under high vacuum. The phosphoramidites were dissolved using anhydrous acetonitrile to a final concentration of 100 mM. Solid supports were synthesized from the dimethoxytrityl protected nucleosides as previously reported.[19]

All oligonucleotides were prepared on an ABI 394 DNA/RNA Synthesizer on a 1 micromole scale. A standard protocol for 2-cyanoethyl phosphoramidites (0.1 M) was used, except that the coupling was extended to 3 minutes. After the trityl-on synthesis, the resin was incubated with conc. Aq. NH_3 at 55 ^oC for 12 h and then evaporated. The tritylated oligonucleotides were purified by C18 reverse phase HPLC (Merck LiChroCART 250 × 4.6 mm, Purospher STAR RP-18e) with 0.05 M aq. TEAA and MeCN as the eluent (gradient: 15–80% MeCN in 20 min). The oligonucleotides were then detritylated with 80% AcOH for 20 min, precipitated with *i*-PrOH after addition of NaOAc, and again purified by HPLC. In an alternative protocol, the tritylated oligonucleotides were purified by Water Sep-Pak classic C18 cartridges. The trityl-off oligonucleotides were purified by using a Waters Xterra column (MSC18, 4.6 × 50 mm) at 55 ^oC with 0.05 M aq. TEAA and MeCN as the eluent.

The identities of all oligonucleotides were confirmed by MALDI-TOF MS (Table 3.4). Samples were prepared at a concentration of approximately 10 μM. One microliter of a saturated solution of trihydroxyacetophenone in 50% aqueous acetonitrile was mixed with one microliter of 100 mM ammonium tartrate and then one microliter of the GNA sample. The drided sample was then analyzed in the

negative mode for detection of the sample mass.

Thermal denaturation

The melting studies were carried out in 1 cm path length quartz cells (total volume 325 μL; 200 μL sample solutions were covered by mineral oil) on a Beckman 800 UV-VIS spectrophotometer equipped with a thermo-programmer. Melting curves were monitored at 260 nm with a heating rate of 1 ^{o}C/min. Melting temperatures were calculated from the first derivatives of the heating curves. Experiments were performed in duplicate and mean values were taken.

Fluorescence measurements

The experiments were performed in 96-well plates on a Molecular Devices SpectraMax M5.

CD spectroscopy

CD measurements were performed on a JASCO J-810 spectrometer in a 1 mm path length quartz cuvette. The GNA single strands or duplexes were prepared in 10 mM sodium phosphate, 100 mM NaCl, pH 7.0, and the concentration of each strand was 8 μM. Each measurement was repeated 5 times and the average taken.

Table 3.4 MALDI-TOF MS data of used oligonucleotides.

Name	Oligonucleotides	M_{calcd}	M_{found}
D1	3′-TAAAAATAATAATATT-2′	$C_{128}H_{167}N_{62}O_{74}P_{15}$(4220.7)	4223.3
	2′-ATTTTTATTATTATAA-3′	$C_{128}H_{171}N_{50}O_{82}P_{15}$(4184.7)	4185.5
D2	3′-TAAAAATHATAATATT-2′	$C_{122}H_{162}N_{57}O_{74}P_{15}$(4073.7)	4076.0
	2′-ATTTTTAPyrTATTATAA-3′	$C_{139}H_{175}N_{48}O_{80}P_{15}$(4260.7)	4161.8
D3	3′-TAAAAATMeATAATATT-2′	$C_{123}H_{164}N_{57}O_{74}P_{15}$(4087.7)	4090.3
	2′-ATTTTTAPyrTATTATAA-3′	$C_{139}H_{175}N_{48}O_{80}P_{15}$(4260.7)	4161.8
D4	3′-TAAAAATMeMeTAATATT-2′	$C_{118}H_{161}N_{52}O_{74}P_{15}$(3954.6)	3956.6
	2′-ATTTTTAPyrPyrATTATAA-3′	$C_{150}H_{179}N_{46}O_{78}P_{15}$(4336.8)	4339.1
D5	3′-TAAAAATPyrPyrTAATATT-2′	$C_{150}H_{177}N_{52}O_{74}P_{15}$(4354.8)	4356.0
	2′-ATTTTTAMeMeATTATAA-3′	$C_{118}H_{163}N_{46}O_{78}P_{15}$(3936.6)	3938.1
D6	3′-TAAAAATMePyrTAATATT-2′	$C_{134}H_{169}N_{52}O_{74}P_{15}$(4154.7)	4155.9
	2′-ATTTTTAPyrMeATTATAA-3′	$C_{134}H_{171}N_{46}O_{78}P_{15}$(4136.7)	4137.5
D7	3′-TAAAAATPyrMeTAATATT-2′	$C_{134}H_{169}N_{52}O_{74}P_{15}$(4154.7)	4156.5
	2′-ATTTTTAMePyrATTATAA-3′	$C_{134}H_{171}N_{46}O_{78}P_{15}$(4136.7)	4137.7
D8	3′-TAAAAATPyr′ATAATATT-2′	$C_{141}H_{172}N_{57}O_{74}P_{15}$(4311.7)	4313.9
	2′-ATTTTTAMeTATTATAA-3′	$C_{123}H_{167}N_{48}O_{80}P_{15}$(4060.7)	4062.8
D9	3′-TAAAAATPyr′ATAATATT-2′	$C_{141}H_{172}N_{57}O_{74}P_{15}$(4311.7)	4313.9
	2′-ATTTTTAHTATTATAA-3′	$C_{122}H_{165}N_{48}O_{80}P_{15}$(4046.6)	4048.2
D10	3′-TAAAAATHHTAATATT-2′	$C_{116}H_{157}N_{52}O_{74}P_{15}$(3926.6)	3928.8
	2′-ATTTTTAPyr′Pyr′ATTATAA-3′	$C_{154}H_{179}N_{46}O_{78}P_{15}$(4384.8)	4387.1
D11	3′-TAAAAATPyr′Pyr′TAATATT-2′	$C_{154}H_{177}N_{52}O_{74}P_{15}$(4402.8)	4405.2
	2′-ATTTTTAHHATTATAA-3′	$C_{116}H_{159}N_{46}O_{78}P_{15}$(3908.5)	3910.0
D12	3′-TAAAAATHPyr′TAATATT-2′	$C_{135}H_{167}N_{52}O_{74}P_{15}$(4164.7)	4165.4
	2′-ATTTTTAPyr′HTTATAA-3′	$C_{135}H_{169}N_{46}O_{78}P_{15}$(4146.7)	4147.1
D13	3′-TAAAAATPyr′HTAATATT-2′	$C_{135}H_{167}N_{52}O_{74}P_{15}$(4164.7)	4166.5
	2′-ATTTTTAHPyr′ATTATAA-3′	$C_{135}H_{169}N_{46}O_{78}P_{15}$(4146.7)	4148.6
D14	3′-TATPyr′HAAATAATMAAA-2′	$C_{136}H_{167}N_{54}O_{72}P_{15}$(4174.6)	4174.9
	2′-ATAHPyr′TTATTAMTTT-3′	$C_{136}H_{172}N_{39}O_{82}P_{14}$(4129.5)	4128.7
D15	3′-TATAPyr′HTAATMTAAA-2′	$C_{128}H_{158}N_{46}O_{70}P_{14}$(3892.7)	3893.3
	2′-ATATHPyr′ATTAMATTT-3′	$C_{128}H_{160}N_{40}O_{74}P_{14}$(3874.7)	3875.6
D16	3′-AATATTATTATTTTAPyr′C_3-2′	$C_{144}H_{128}N_{48}O_{84}P_{16}$(4424.8)	4424.7
	2′-TTATAATAATAAAATHPyr′-3′	$C_{143}H_{177}N_{57}O_{78}P_{16}$(4437.9)	4437.3
D17	3′-AATATTATTATTTTAHPyr′C_3-2′	$C_{146}H_{187}N_{48}O_{88}P_{17}$(4548.9)	4545.5
	2′-TTATAATAATAAAATPyr′-3′	$C_{141}H_{172}N_{57}O_{74}P_{15}$(4313.8)	4312.1
D18	3′-ATTATTPATTTTPyr′C_3-2′	$C_{125}H_{153}N_{36}O_{70}P_{13}$(3682.4)	3684.5
	2′-TAATAAMTAAAAHPyr′-3′	$C_{120}H_{146}N_{47}O_{62}P_{13}$(3641.4)	3643.0
D19	3′-ATTPATTTTPyr′C_3-2′	$C_{101}H_{121}N_{27}O_{54}P_{10}$(2886.9)	2886.8
	2′-TAAMTAAAAHPyr′-3′	$C_{96}H_{115}N_{35}O_{48}P_{10}$(2836.9)	2837.1

Chapter 3.5 References

1. (a) Ren, R. X.-F; Chaudhuri, N. C.; Paris, P. L.; Rumney, S. and Kool, E. T. *Journal of American Chemical Society* **1996**, *118*, 7671; (b) Guckian, K. M.; Schweitzer, B. A.; Ren, R. X.-F.; Sheils, C. J.; Paris, P. L.; Tahamassebi, D. C. and Kool, E. T. *Journal of American Chemical Society* **1996**, *118*, 8182; (c) Matray, T. J. and Kool, E. T. *Journal of American Chemical Society* **1998**, *120*, 6191; (d) Guckian, K. M.; Schweitzer, B. A.; Ren, R. X.-F.; Sheils, C. J.; Paris, P. L.; Tahamassebi, D. C. and Kool, E. T. *Journal of American Chemical Society* **2000**, *122*, 2213.
2. Cho, Y. J. and Kool, E. T. *ChemBioChem* **2006**, *7*, 669.
3. (a) Sun, L. P.; Wang, M.; Kool, E. T. and Taylor, J.-S. *Biochemistry* **2000**, *39*, 14603; (b) Sun, L. P.; Zhang, K. J.; Zhou, L. L.; Hohler, P.; Kool, E. T.; Yuan, F. H.; Wang, Z. G. and Taylor, J.-S. *Biochemistry* **2003**, *42*, 9431.
4. Lewis, F. D.; Zhang, Y. F. and Letsinger, R. L. *Journal of American Chemical Society* **1997**, *119*, 5451.
5. Okamoto, A.; Kanatani; K. and Saito, I. *Journal of American Chemical Society* **2004**, *126*, 4820.
6. (a) Kierzek, R.; Li, Y.; Turner, D. H.; Bevilacqua, P. C. *Journal of American Chemical Society* **1993**, *115*, 4985; (b) Bevilacqua, P. C.; Kierzek, R.; Johnson, K. A.; Turner, D. H. *Science* **1992**, *258*, 1355; (c) Yamana, K.; Gokota, T.; Ozaki, H.; Nakano, H.; Sangen, O.; Shimidzu, T. *Nucleosides & Nucleotides* **1992**, *11*, 383; (d) Okamoto, A.; Ochi, Y. and Saito, I. *Chemical Commun*ication **2005**, 1128.
7. (a) Jung, D.; Cho, Y.; Meyer, J. N. and Di Giulio, R. T. *Comparative Biochemistry and Physiology, Part C* **2009**, *149*, 182; (b) Tang, S.-C.; Sheu, G.-T.; Wong, R.-H.; Weng, M.-W.; Lee, L.-W. and Hsu, C.-P. *Toxicology Letters* **2010**, *192*, 316.
8. (a) Saito, Y.; Miyauchi, Y.; Okamoto, A. and Saito, I. *Chemical communication*

2004, 1704; (b) Mahara, A.; Iwase, R.; Sakamoto, Y.; Yamana, K.; Tamaoka, T. and Murakami, A. *Angewandte Chemie International Edition* **2002**, *41*, 3648; (d) Zhang, Y. and Letsinger, R. L. *Journal of American Chemical Society* **1997**, *119*, 5451.

9. Malinovskii, V. L.; Samain, F. and Häner, R. *Angewandte Chemie International Edition* **2007**, *46*, 4464.
10. (a) M-Enthart, E. and Wagenknecht, H.-A. *Angewandte Chemie International Edition* **2006**, *45*, 3372; (b) Barbaric, J. and Wagenknecht, H.-A. *Organic & Biomoleculor Chemistry* **2006**, *4*, 2088.
11. Hissler, M.; Harriman, A.; Khatyr, A. and Ziessel, R. *Chemistry - A European Journal* **1999**, *5*, 3366.
12. Tanaka, K.; Tengeiji, A.; Kato, T.; Toyama, N.; Shiro, M. and Shionoya, M. *Journal of American Chemistry Society* **2002**, *124*, 12494.
13. Schlegel, M. K.; Zhang, L.; Pagano, N. and Meggers, E. *Organic & Biomoleculor Chemistry* **2009**, *7*, 476-482.
14. Zhang, L.; Peritz, A. E.; Carroll, P. J.; Meggers, E. *Synthesis* **2006**,645.
15. (a) Ferreira, F.; Meyer, A.; Vasseur, J.-J. and Morvan, F. *Journal Organic Chemistry* **2005**, *70*, 9198; (b) Mahajan, S.; Kumar, P. and Gupta, K. C. *Bioconjugate Chemistry* **2006**, *17*, 1184.
16. (a) Fathi, R.; Rudolph, M. J.; Gentles, R. G.; Patel, R.; Macmillan, E.W.; Reitman, M. S.; Pelham, D. and Cook, A. F. *Journal of Organic Chemistry* **1996**, *61*, 5600; (b) Fontanel, M.-L.; Bazin, H. and Teoule, R. *Nucleic Acids Research* **1994**, *22*, 2022.
17. Damha, M. J.; Giannaris, P. A.; Zabarylo, S. V. *Nucleic Acids Research* **1990**, *18*, 3813-3821.
18. Yang, S.-W.; Elangovan, A.; Hwang, K. -C. And Ho, T.-I. *Journal of Physical chemistry B* **2005**, *109*, 16628-16635.
19. Damha, M. J.; Giannaris, P. A.; Zabarylo, S. V. *Nucleic Acids Research* **1990**, *18*, 3813-3821.

Chapter 4 Incorporation of Porphyrin Acetylides into Duplexes of the Simplified Nucleic Acid GNA

Chapter 4.1 Introduction

Porphyrins are heterocyclic macrocycles composed of four modified pyrrole subunits interconnected at their *α* carbon atoms *via* methine bridges. Due to the unique and highly tunable chemical and photophysical properties, porphyrins have been introduced extensively into DNA for following four purposes:

[1] As DNA binding agents: Porphyrins are one of the most widely investigated DNA binding agents. Porphyrins have been employed for studies on electron transfer through DNA,[1] nucleic acid-directed porphyrin aggregation[2], potential DNA damage induced by sensitizers for photodynamic therapy of neoplastic tissue[3], and so on.

[2] As sensors of DNA probes: Porphyrins have been attracted widespread attention as chromophores for studies on circular dichroism (CD), owing to their unique electronic and geometric properties. They are capable of serving as versatile and powerful CD reporter groups to detect DNA conformational changes,[4] porphyrin-DNA interaction,[5] and conformation of porphyrins in DNA.[6] Moreover, porphyrins' unique UV-vis absorption and fluorescence spectra enable themselves to be spectroscopic sensors for conformation studies of DNA.[6,7]

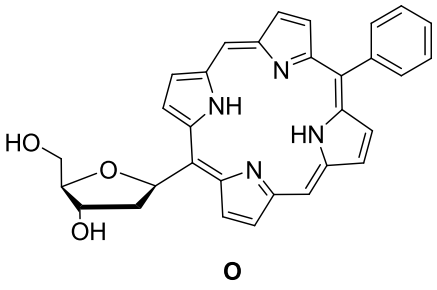

Figure 4.1 Porphyrin artificial C-nucleoside.

[3] As an artificial base in DNA: Porphyrins, which contain flat aromatic heterocycle and entirely hydrophobic core, are incorporated into DNA as the artificial base, and strongly intercalate in the duplex when introduced in the

middle of DNA.[8,9] Although the non-hydrogen base pair of porphyrin and abasic site destabilize duplex significantly, the well-designed structures with porphyrin C-nucleotides as dangling ends could provide substantial stabilization of the helix.[9]

[4] As a building block for constructing a highly ordered nanostructure: Researches on DNA as supramolecular scaffolds to create high ordered structures have achieved impressive progress, such as in producing helical multiporphyrin arrays,[11] which are attractive for the design of artificial light harvesting systems and photoelectrical devices.[10] Up to eleven porphyrines were introduced into DNA through attachment of porphyrins to position 5 of 2′-deoxyuridine *via* a rigid acetylene spacer, offering helical porphyrin arrays in single strand or within the major groove of duplexes.[11a,c]

However, there are only very few reports in which porphyrins are placed in the interior of the DNA as part of the π-stacking, most likely due to the challenging synthesis of the necessary porphyrin nucleotide building blocks.[7,9]

As discussed before, GNA has been employed as a convenient duplex scaffold for the generation of functional architectures recently.[12] Thus, the high duplex stabilities exceeding the stabilities of analogous DNA and RNA duplexes, in combination with an economical and fast synthesis of (modified) phosphoramidite building blocks, render GNA an attractive nucleic acid scaffold for introduction of porphyrin in the interior of the molecule.

In this part, we described the incorporation of a porphyrin-modified GNA nucleotide into GNA, and behavior of such non-metallated and metallated porphyrins in the context of GNA duplexes.

Chapter 4.2 Results and Discussion

Chapter 4.2.1 Synthesis of porphyrin-GNA

We were looking for a propane-1,2-diol-modified porphyrin building block that has a unique combination properties: (i) The building block is capable of stacking in GNA duplexes opposite an ethylene glycol spacer as shown in Figure 4.2; and (ii) the phosphoramidite building block is synthetically easily accessible. Based on these two criteria we selected **18c** as the phosphoramidite building block, which was used to synthesize GNA strands with incorporated diphenylporphyrin acetylide nucleotides (**P**, Figure 4.2).

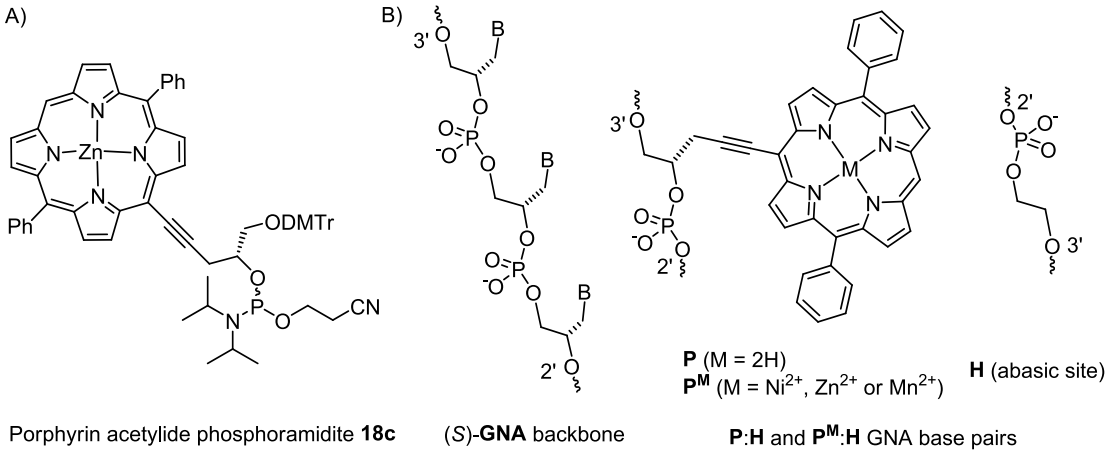

Figure 4.2 (A) Structure of porphyrin acetylide phosphoramidite **18c**. (B) Constitution of the (*S*)-GNA backbone. **P**:**H** and $\mathbf{P^M}$:**H** base pairs used in this study.

The porphyrin-GNA strands were synthesized according to previous method. Due to the low solubility in the standard solvent acetonitrile, porphyrin acetylide phosphoramidite **18c** was dissolved in THF for the use in the DNA synthesizer and the coupling times were extended to 15 minutes. The synthesis and detritylation of GNA strands was followed by an additional purification step with a reversed phase HPLC column, the porphyrin-containing GNA strands were obtained in high purities and devoid of the Zinc ions, most likely due to the acidic conditions during the

individual detritylation steps.[11a]

However, zinc(II), manganese(II) and nickel(II) ions could be readily (re)introduced into the coordination sites of the porphyrin nucleotides in GNA oligunucleotides to give $\mathbf{P^M}$ (Figure 4.2) by mixing the purified single strands with $Zn(OAc)_2$, $Ni(OAc)_2$ and $MnCl_2$ in Tris-HCl buffered solution. Other metal ions we tested which could not be introduced into porphyrin properly, for example, $CdSO_4$, $FeCl_2$ or $FeCl_3$ do not metallate the porphyrin in GNA, while $CuCl_2$ leads to the decomposition of GNA strands during the reaction.

Chapter 4.2.2 Thermal stability of duplex porphyrin-GNA

Measuring the thermal stability of DNA duplex is a main tool for studying the effect of a modification on DNA. In order to study the effect of porphyrin-modification on GNA, the thermal stability of GNA duplexes containing a single non-metallated (**P**) or metallated porphyrin ($\mathbf{P^M}$) were investigated.

Table 4.1 Thermal stabilities of porphyrin-containing 16mer GNA duplexes together with Watson-Crick reference duplexes.

Entry	Sequence		T_m (°C) [a]
1	3′-TAAAAATAATAATATT-2′	(**ON1**)	54
	2′-ATTTTTATTATTATAA-3′	(**ON2**)	
2	3′-TAAAAATATAATATT-2′	(**ON3**)	52
	2′-ATTTTTATATTATAA-3′	(**ON4**)	
3	3′-TAAAAAT**P**ATAATATT-2′	(**ON6**)	48
	2′-ATTTTTA**H**TATTATAA-3′	(**ON7**)	
4	3′-TAAAAAT**P**ATAATATT-2′	(**ON6**)	44
	2′-ATTTTTA**T**TATTATAA-3′	(**ON2**)	
5	3′-TAAAAAT**P**ATAATATT-2′	(**ON6**)	45
	2′-ATTTTTA**A**TATTATAA-3′	(**ON5**)	
6	3′-TAAAAAT$\mathbf{P^{Zn}}$ATAATATT-2′	(**ON6**$^{\mathbf{Zn}}$)	42
	2′-ATTTTTA**H**TATTATAA-3′	(**ON7**)	
7	3′-TAAAAAT$\mathbf{P^{Ni}}$ATAATATT-2′	(**ON6**$^{\mathbf{Ni}}$)	49
	2′-ATTTTTA**H**TATTATAA-3′	(**ON7**)	
8	3′-TAAAAAT$\mathbf{P^{Mn}}$ATAATATT-2′	(**ON6**$^{\mathbf{Mn}}$)	33
	2′-ATTTTTA**H**TATTATAA-3′	(**ON7**)	
9	3′-TAAAAATTAATATT-2′	(**ON8**)	49
	2′-ATTTTTAATTATAA-3′	(**ON9**)	
10	3′-TAAAAAT**PH**TAATATT-2′	(**ON10**)	43
	2′-ATTTTTA**HP**ATTATAA-3′	(**ON11**)	
11	3′-TAAAAAT$\mathbf{P^{Zn}}$**H**TAATATT-2′	(**ON10**$^{\mathbf{Zn}}$)	34
	2′-ATTTTTA**H**$\mathbf{P^{Zn}}$ATTATAA-3′	(**ON11**$^{\mathbf{Zn}}$)	

[a]Conditions: 10 mM sodium phosphate, 100 mM NaCl, and 2 μM individual strands.

Table 4.1 shows the UV-melting data of duplexes with **P** and $\mathbf{P^M}$ incorporated into the position 8 of 16mer duplexes and two reference duplexes. All GNA duplexes investigated in this work do only contain **A** and **T** nucleotides in order to keep the GNA scaffold as simple as possible. Pairing **P** with the ethylene glycol abasic site **H**

afforded a duplex melting point (T_m) of 48 °C (Table 4.1, entry 3), compared to 54 °C for an **A**:**T** base pair at the same position (Table 4.1, entry 1). Removing one **A**:**T** base pair of the Watson-Crick reference duplex as in **ON3**:**ON4** (Table 4.1, entry 2) resulted in a melting point of 52 °C, thus demonstrating that the incorporation of a single **P**:**H** base pair has a net destabilizing effect of ΔT_m = 4 °C. Replacing the abasic site **H** of the **P**:**H** base pair in **ON6**:**ON7** (Table 4.1, entry 3) for the natural nucleobases **T** or **A**, resulting in **P**:**T** and **P**:**A** base pairs, reduces the stability by additional 4 and 3 °C, respectively (Table 4.1, entries 4 and 5). Apparently, these larger natural nucleobases cannot be accommodated well opposite the space consuming diphenylporphyrin acetylide nucleobase **P**, suggesting that the porphyrin nucleobase is accommodated within the π-π stacking of the GNA duplex.

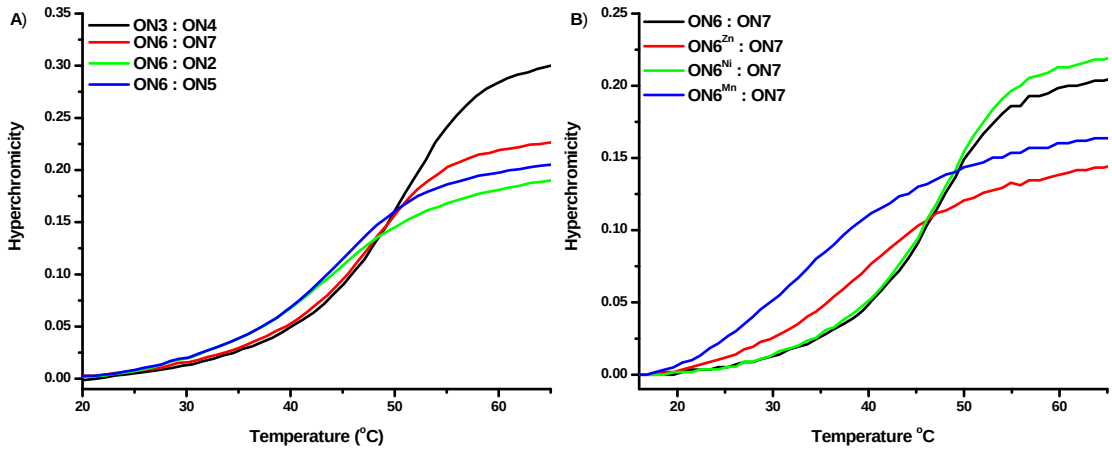

Figure 4.3 UV-melting curves of GNA duplexes. Changes in absorbance upon heating as monitored at 260 nm. Conditions: 10 mM sodium phosphate, 100 mM NaCl, pH 7.0, and 2 μM of each strand. (A) Duplexes **ON3**:**ON4**, **ON6**:**ON7**, **ON6**:**ON2**, and **ON6**:**ON5**. (B) Duplexes **ON6**:**ON7**, **ON6^{Zn}**:**ON7**, **ON6^{Ni}**:**ON7**, and **ON6^{Mn}**:**ON7** (see Tables 4.1 for the sequences).

Interestingly, the incorporation of a Zn^{2+} ion or Mn^{2+} ion into the porphyrin results in a significant further destabilization for duplex containing **P^{Zn}**:**H** base pair (T_m = 42 °C, Table 4.1, entry 6), or **P^{Mn}**:**H** base pair (T_m = 33 °C, Table 4.1, entry 8) respectively. Whereas the incorporation of a Ni^{2+} ion slightly increases the stability compared to **P**:**H** (ΔT_m = + 1 °C), and is only by 3 °C less stable than **ON3:ON4**. These modulations of duplex stabilities by the nature of the metal ion incorporated

into the porphyrin nucleobases can be interpreted by their different coordination behavior. Zn^{2+} and Mn^{2+} prefer to coordinate to axial ligands[13a] when incorporated into a porphyrin in an octahedral fashion, and needs to dissociate these ligands if it wants to stack within GNA between neighboring base pairs. In contrast, Ni^{2+} prefers square planar coordination and can thus be accommodated easily in the base stacking.[13b]

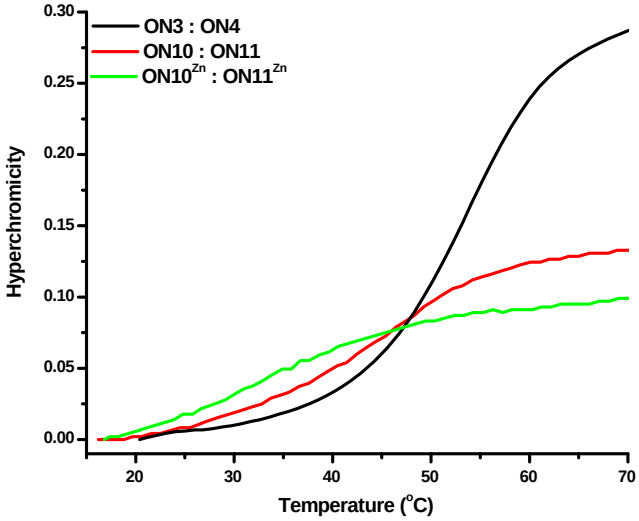

Figure 4.4 UV-melting curves of GNA duplexes **ON3**:**ON4**, **ON10**:**ON11** and **ON10^{Zn}**:**ON11^{Zn}** (see Tables 4.1 for the sequences). Changes in absorbance upon heating as monitored at 260 nm. Conditions: 10 mM sodium phosphate, 100 mM NaCl, pH 7.0, and 2 μM of each strand.

Duplexes containing two adjacent porphyrin acetylide nucleobases were also investigated. Incorporation of a second adjacent **P**:**H** base pair positioning the porphyrins on opposite strands (Table 4.1, entry 10) reduces the duplex melting temperature further (T_m = 43 °C), being 6 °C below the melting temperature of a reference duplex that is devoid of the two **P**:**H** base pairs (Table 4.1, entry 9). Nevertheless, the incorporation of two adjacent **P**:**H** base pairs still affords a duplex that is thermally stable at room temperature. As expected, the introduction of Zn^{2+} ions into the two porphyrins strongly destabilized the duplex to T_m = 34 °C (Table 4.1, entry 11), similar to what was observed in duplex with a single Zn(II)-porphyrin (Table 4.1, entry 6).

Table 4.2 Thermal stabilities of porphyrin-containing 22mer GNA duplexes together with Watson-Crick reference duplexes.

Entry	Sequence		T_m (°C)[a]
1	3′-TTATAAAAATAATAATATTAAT-2′	(**ON12**)	63
	2′-AATATTTTTATTATTATAATTA-3′	(**ON13**)	
2	3′-TTATAAAAATTAATATTAAT-2′	(**ON14**)	61
	2′-AATATTTTTAATTATAATTA-3′	(**ON15**)	
3	3′-TTATAAAAAT**PH**TAATATTAAT-2′	(**ON16**)	56
	2′-AATATTTTTA**HP**ATTATAATTA-3′	(**ON17**)	
4	3′-TTATAAAAAT**HP**TAATATTAAT-2′	(**ON18**)	56
	2′-AATATTTTTA**PH**ATTATAATTA-3′	(**ON19**)	
5	3′-TTATAAAAAT**P^{Zn}H**TAATATTAAT-2′	(**ON16^{Zn}**)	48
	2′-AATATTTTTA**HP^{Zn}**ATTATAATTA-3′	(**ON17^{Zn}**)	
6	3′-TTATAAAAAT**P^{Ni}H**TAATATTAAT-2′	(**ON16^{Ni}**)	59
	2′-AATATTTTTA**HP^{Ni}**ATTATAATTA-3′	(**ON17^{Ni}**)	
7	3′-TTATAAAAAT**P^{Zn}H**TAATATTAAT-2′	(**ON16^{Zn}**)	54
	2′-AATATTTTTA**HP^{Ni}**ATTATAATTA-3′	(**ON17^{Ni}**)	
8	3′-TTATAAAAAT**P^{Ni}H**TAATATTAAT-2′	(**ON16^{Ni}**)	52
	2′-AATATTTTTA**HP^{Zn}**ATTATAATTA-3′	(**ON17^{Zn}**)	
9	3′-TTATAAAAAT**P^{Mn}H**TAATATTAAT-2′	(**ON16^{Mn}**)	51
	2′-AATATTTTTA**HP^{Mn}**ATTATAATTA-3′	(**ON17^{Mn}**)	
10	3′-TTATAAAAAT**HP^{Zn}**TAATATTAAT-2′	(**ON18^{Zn}**)	49
	2′-AATATTTTTA**P^{Zn}H**ATTATAATTA-3′	(**ON19^{Zn}**)	
11	3′-TTATAAAAAT**HP^{Ni}**TAATATTAAT-2′	(**ON18^{Ni}**)	60
	2′-AATATTTTTA**P^{Ni}H**ATTATAATTA-3′	(**ON19^{Ni}**)	
12	3′-TTATAAAAAT**HP^{Mn}**TAATATTAAT-2′	(**ON18^{Mn}**)	52
	2′-AATATTTTTA**P^{Mn}H**ATTATAATTA-3′	(**ON19^{Mn}**)	

[a]Conditions: 10 mM sodium phosphate, 100 mM NaCl, and 2 μM individual strands.

Due to this general destabilization trend, we continued to evaluate duplexes containing two porphyrins in longer (22mer) and thus more stable duplexes as displayed in Table 4.2. These data confirm that two adjacent **P**:**H** base pairs in opposite orientation lead to a destabilization relative to the reference duplexes **ON12:ON13** and **ON14:ON15**, but still provide duplexes with robust stabilities (Table 4.2, entries 1-4). And this stability can be modulated by the incorporation of Zn^{2+} (further destabilization), Mn^{2+} (further destabilization) and Ni^{2+} (stabilization relative to the free porphyrin). Duplex **ON16^{Ni}**:**ON17^{Ni}** containing nickel(II)-porphyrin is only by 1 °C less stable than the reference duplex (Table 4.2, entries 5-12).

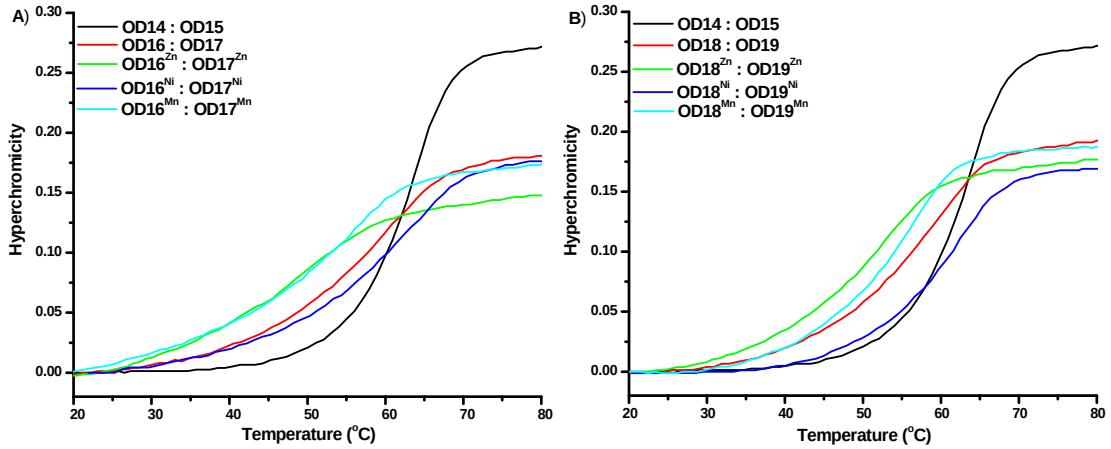

Figure 4.5 UV-melting curves of GNA duplexes. Changes in absorbance upon heating as monitored at 260 nm. Conditions: 10 mM sodium phosphate, 100 mM NaCl, pH 7.0, and 2 μM of each strand. (A) Duplexes **ON14**:**ON15**, **ON16**:**ON17**, **ON16^{Zn}**:**ON17^{Zn}**, **ON16^{Ni}**:**ON17^{Ni}** and **ON16^{Mn}**:**ON17^{Mn}**. (B) Duplexes **ON14**:**ON15**, **ON18**:**ON19**, **ON18^{Zn}**:**ON19^{Zn}**, **ON18^{Ni}**:**ON19^{Ni}** and **ON18^{Mn}**:**ON19^{Mn}** (see Table 4.2 for the sequences).

It is obvious that the slopes of the melting curves of GNA duplexes containing porphyrins are more shallow compared to the related unmodified duplexes, which might be caused by lower cooperativity among the nucleobases due to interference by the porphyrin macrocycle (Figure 4.5).[11] Additionally, the hyperchromicity of the duplexes containing porphyrins is reduced, presumably due to a weaker stacking of base pairs in proximity of **P**:**H** base pairs.

Chapter 4.2.3 Conformation of porphyrins in GNA

UV-Vis and circular dichroism spectroscopy are important tools for understanding the relative conformation of closely located molecules. In addition, the fluorescence of chromophores was also used in aggregation analysis. Here, we investigated porphyrin-modified GNA by UV-vis, fluorescence and CD spectrometry to get the conformation information of porphyrins in GNA.

UV-vis spectroscopy

Due to increased duplex stabilities we investigated the UV-vis absorption properties of porphyrin GNA strands and the corresponding duplexes with the 22mer system. We began by analyzing porphyrin-modified single strands without and with incorporated zinc(II), Mn(II) and nickel(II) ions.

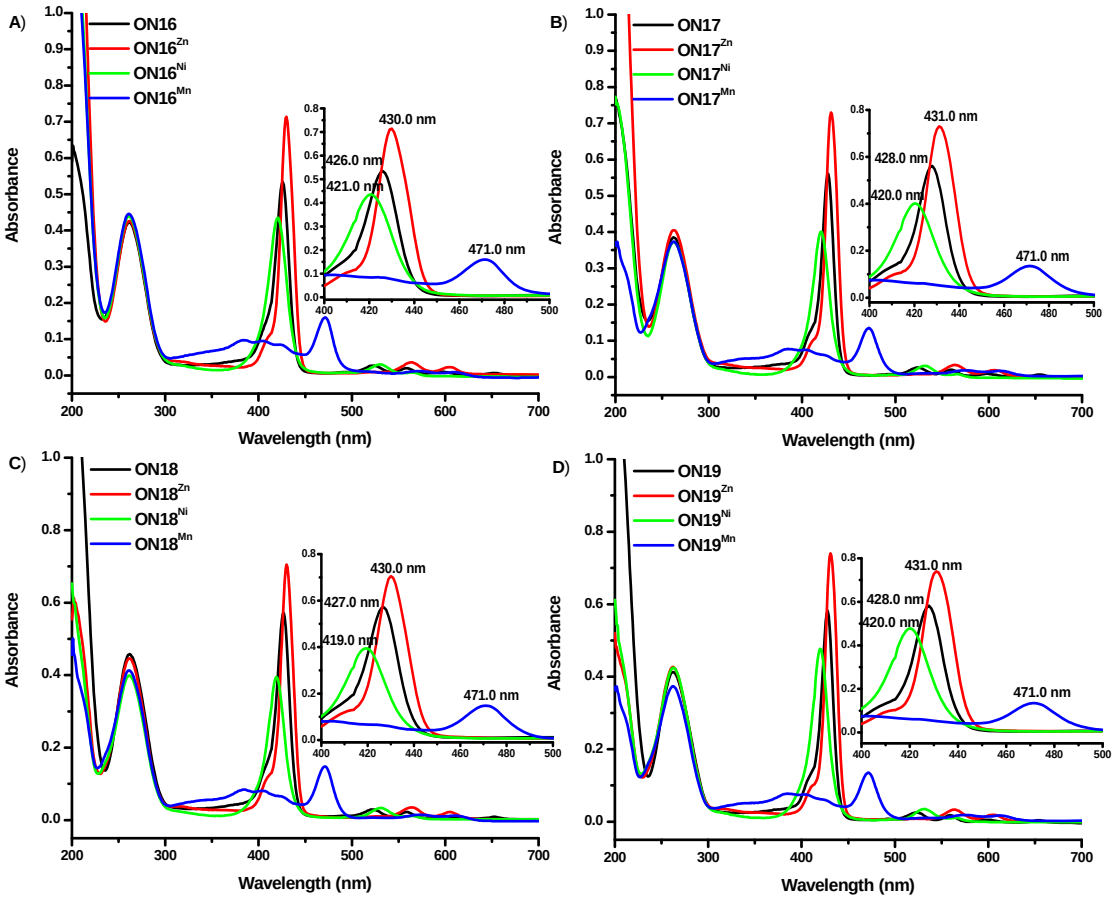

Figure 4.6 UV-vis Absorption spectra of porphyrin-GNA single strands without and with incorporated metal ions. Conditions: 10 mM sodium phosphate, 100 mM NaCl, pH 7.0, and 2 μM of single strands. (A) **ON16**, **ON16^{Zn}**, **ON16^{Ni}** and **ON16^{Mn}**. (B) **ON17**, **ON17^{Zn}**, **ON17^{Ni}** and **ON17^{Mn}**. (C) **ON18**, **ON18^{Zn}**, **ON18^{Ni}** and **ON18^{Mn}**. (D) **ON19**, **ON19^{Zn}**, **ON19^{Ni}** and **ON19^{Mn}** (see Tables 4.2 for the sequences). The insert shows the expanded porphyrin Soret band region.

Taking **ON16** for example to illustrate the changes after metalation of porphyrin in GNA, the UV-vis spectra of the single strands **ON16**, **ON16^{Zn}**, **ON16^{Mn}** and **ON16^{Ni}** are shown in Figure 4.6A and clearly confirm the successful insertion of the metal ions into the porphyrins. The absorption spectrum of **ON16** displays a Soret band at 428 nm and four Q bands, while **ON16^{Zn}**, **ON16^{Mn}** and **ON16^{Ni}** exhibit one Soret band at 431 nm, 471 nm and 420 nm respectively, and just two Q bands. The reduced number of Q bands is typical of metalloporphyrins.[14] In addition, the obvious red shift of the Soret band for **ON16^{Zn}** and **ON16^{Mn}**, and blue shift for **ON16^{Ni}** are consistent with the well-known red shift of porphyrin Soret bands upon Zn(II) or Mn(II) coordination, and blue shift of Soret bands upon Ni(II) coordination.[14] UV-vis

spectra of single strands **ON17**, **ON18**, **ON19** and their metal derivatives are also provided in Figure 4.6 and reveal the successful insertion of the metal ions into the porphyrins.

Next, we compared the UV-vis spectra of duplexes and their corresponding single strands in order to obtain information about the relative orientations of the porphyrin units in the GNA duplexes. Pronounced changes in the absorption spectra were observed upon duplex formation.

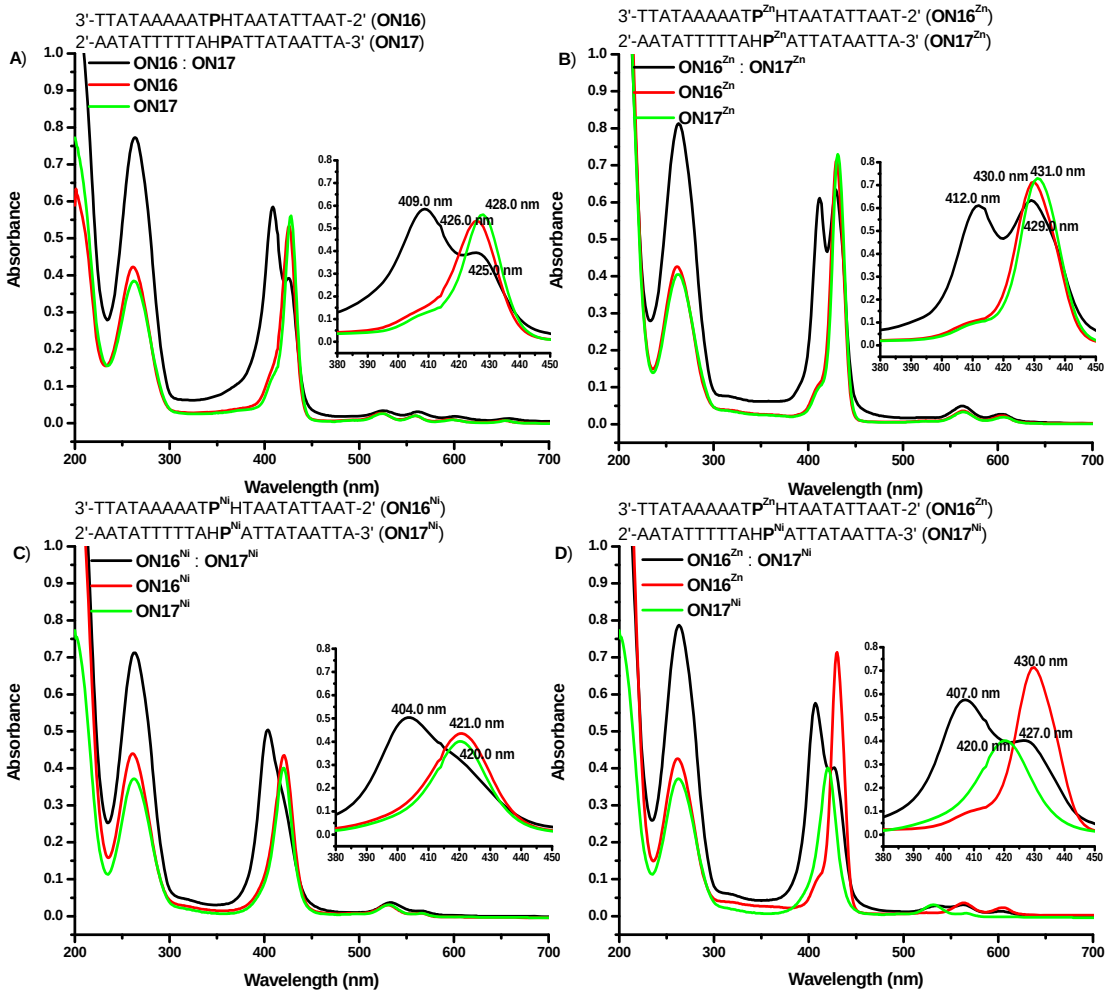

Figure 4.7 UV-vis spectra of GNA duplexes and their corresponding single strands. Conditions: 10 mM sodium phosphate, 100 mM NaCl, pH 7.0, and 2 μM of each strand. (A) **ON16**, **ON17** and **ON16**:**ON17**. (B) **ON16^{Zn}**, **ON17^{Zn}** and **ON16^{Zn}**:**ON17^{Zn}**. (C) **ON16^{Ni}**, **ON17^{Ni}** and **ON16^{Ni}**:**ON17^{Ni}**. (D) **ON16^{Zn}**, **ON17^{Ni}** and **ON16^{Zn}**:**ON17^{Ni}** (see Tables 4.2 for the sequences). The inserts show expanded porphyrin Soret band regions.

As displayed in Figure 4.7, duplexes **ON16**:**ON17**, **ON16^{Zn}**:**ON17^{Zn}**, **ON16^{Ni}**:**ON17^{Ni}** and **ON16^{Zn}**:**ON17^{Ni}** show clear peak splits of the Soret band. The splitting energies between the low- and high-energy Soret bands are 920 cm^{-1} for duplex **ON16**:**ON17**, 962 cm^{-1} for duplex **ON16^{Zn}**:**ON17^{Zn}**, and duplex **ON16^{Zn}**:**ON17^{Ni}** with the mixed metal porphyrins having the highest excition energy (1151 cm^{-1}). The duplex **ON16^{Ni}**:**ON17^{Ni}** exhibits a broadened Soret band instead of two distinct peaks.

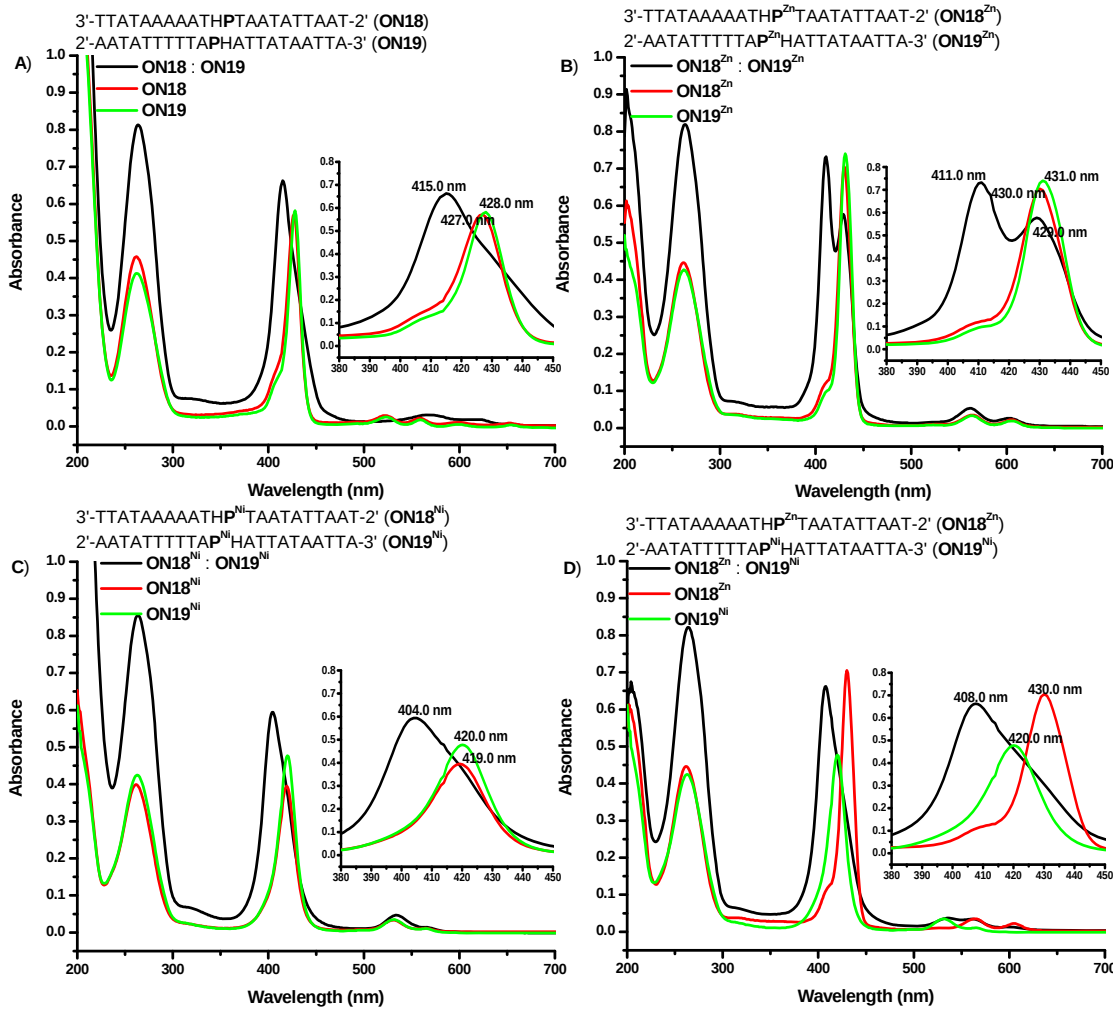

Figure 4.8 UV-vis spectra of GNA duplexes and their corresponding single strands. Conditions: 10 mM sodium phosphate, 100 mM NaCl, pH 7.0, and 2 μM of each strand. (A) **ON18**, **ON19** and **ON18**:**ON19**. (B) **ON18^{Zn}**, **ON19^{Zn}** and **ON18^{Zn}**:**ON19^{Zn}**. (C) **ON18^{Ni}**, **ON19^{Ni}** and **ON18^{Ni}**:**ON19^{Ni}**. (D) **ON18^{Zn}**, **ON19^{Ni}** and **ON18^{Zn}**:**ON19^{Ni}** (see Tables 4.2 for the sequences). The inserts show expanded porphyrin Soret band regions.

Figure 4.8 shows the obvious change of the Soret band of duplexes **ON18**:**ON19**, **ON18^{Zn}**:**ON19^{Zn}**, **ON18^{Ni}**:**ON19^{Ni}** and **ON18^{Zn}**:**ON19^{Ni}**. The splitting energies between the low- and high-energy Soret bands are 1021 cm^{-1} for duplex **ON18^{Zn}**:**ON19^{Zn}**, and duplexes **ON18**:**ON19**, **ON18^{Ni}**:**ON19^{Ni}** and **ON18^{Zn}**:**ON19^{Ni}** all show a blue-shifted and broadened Soret band instead of two distinct peaks.

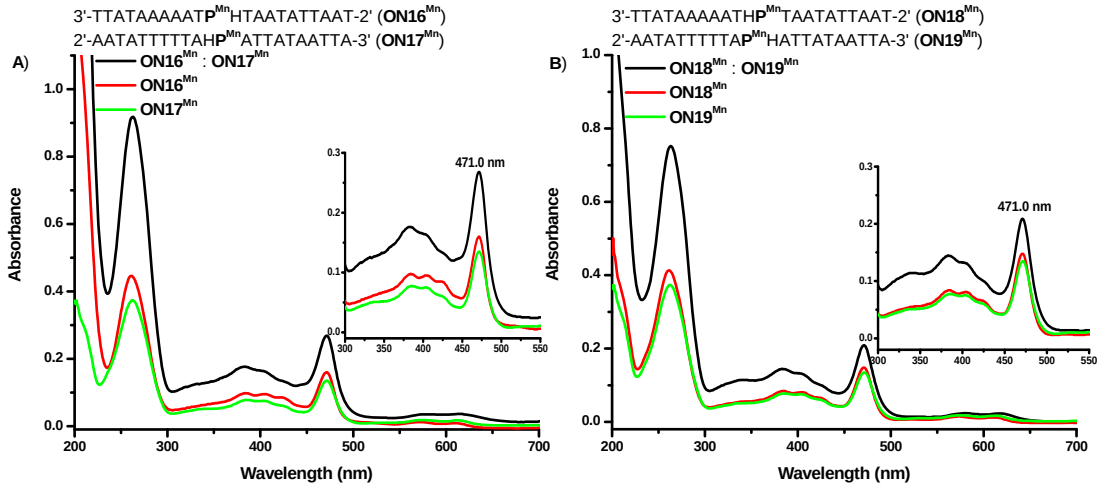

Figure 4.9 UV-vis spectra of GNA duplexes and their corresponding single strands. Conditions: 10 mM sodium phosphate, 100 mM NaCl, pH 7.0, and 2 μM of each strand. (A) **ON16^{Mn}**, **ON17^{Mn}** and **ON16^{Mn}**:**ON17^{Mn}**. (B) **ON18^{Mn}**, **ON19^{Mn}** and **ON18^{Mn}**:**ON19^{Mn}** (see Tables 4.2 for the sequences). The inserts show expanded porphyrin Soret band regions.

However, the duplex **ON16^{Mn}**:**ON17^{Mn}** and **ON18^{Mn}**:**ON19^{Mn}** do not show obvious change of the Soret band (Figure 4.9), which remains unclear.

The obvious change of the Soret bands of the duplex accompanied by a blue shift reveals that a ground state interaction of the two porphyrin moieties occurred in GNA. It has been reported that split Soret bands can be caused by dipole-dipole exciton coupling from slipped-cofacial interactions between two porphyrins.[15]Thus, the two adjacent porphyrin units in the GNA duplex might adopt slipped-cofacial geometry. The Soret band of duplexes shifted to shorter wavelengths, indicating that in each duplex two porphyrin units overlap face-to-face (H-dimer).[16]

Table 4.3 Absorption of porphyrin in GNA strands as single and double strands[a]

Entry	Abs. of Soret band (nm)	Abs. of Q band (nm)
ON 16	426	523, 558, 597, 652
ON 16^{Zn}	430	564, 605
ON 16^{Mn}	471	574, 609
ON 16^{Ni}	421	531, 566
ON 17	428	525, 560, 599, 654
ON 17^{Zn}	431	563, 606
ON 17^{Mn}	471	575, 599
ON 17^{Ni}	420	532, 567
ON 18	427	522, 558, 597, 652
ON 18^{Zn}	430	565, 607
ON 18^{Ni}	419	531, 566
ON 18^{Mn}	471	577, 612
ON 19	428	523, 559, 597, 653
ON 19^{Zn}	431	565, 607
ON 19^{Mn}	471	575, 613
ON 19^{Ni}	420	532, 565
ON16:ON17	409, 425	525, 561, 602,656
ON16^{Zn}:ON17^{Zn}	412, 429	562, 604
ON16^{Mn}:ON17^{Mn}	471	576, 613
ON16^{N}:ON17^{Ni}	404	533, 567
ON18:ON19	415	567, 623
ON18^{Zn}:ON19^{Zn}	411, 429	563, 604
ON18^{Ni}:ON19^{Ni}	404	534, 567
ON18^{Mn}:ON19^{Mn}	471	580, 612

[a]Conditions: 10 mM sodium phosphate, 100 mM NaCl, and 2 μM individual strands.

Subsequently, we analyzed the influence of temperature on the UV-vis spectra for the duplexes. The duplex **ON16^{Mn}**:**ON17^{Mn}** and **ON18^{Mn}**:**ON19^{Mn}** were not investigated, since they do not show obvious change of the Soret band.

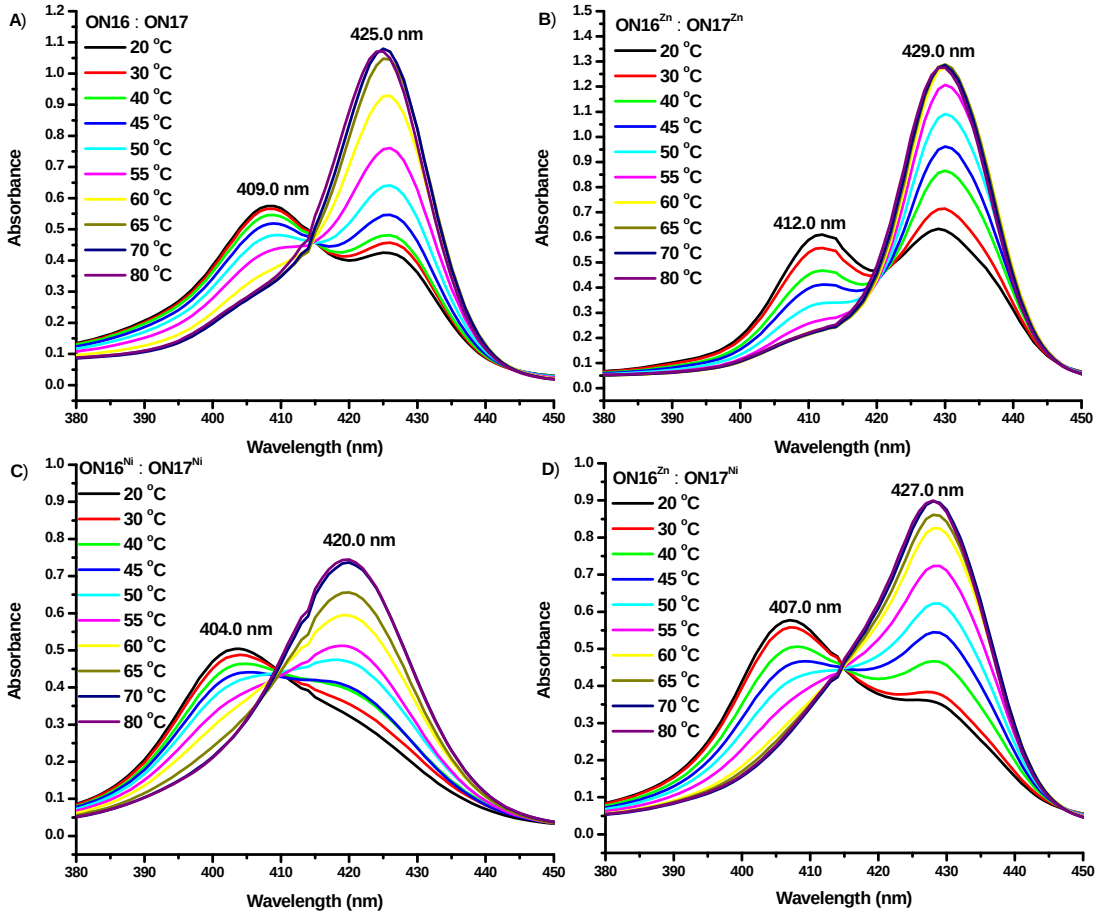

Figure 4.10 Temperature-dependent UV-vis spectra of GNA duplexes at Soret band region. Conditions: 10 mM sodium phosphate, 100 mM NaCl, pH 7.0, and 2 μM of each strand. (A) **ON16**:**ON17**. (B) **ON16^{Zn}**:**ON17^{Zn}**. (C) **ON16^{Ni}**:**ON17^{Ni}**. (D) **ON16^{Zn}**:**ON17^{Ni}** (see Tables 4.2 for the sequences).

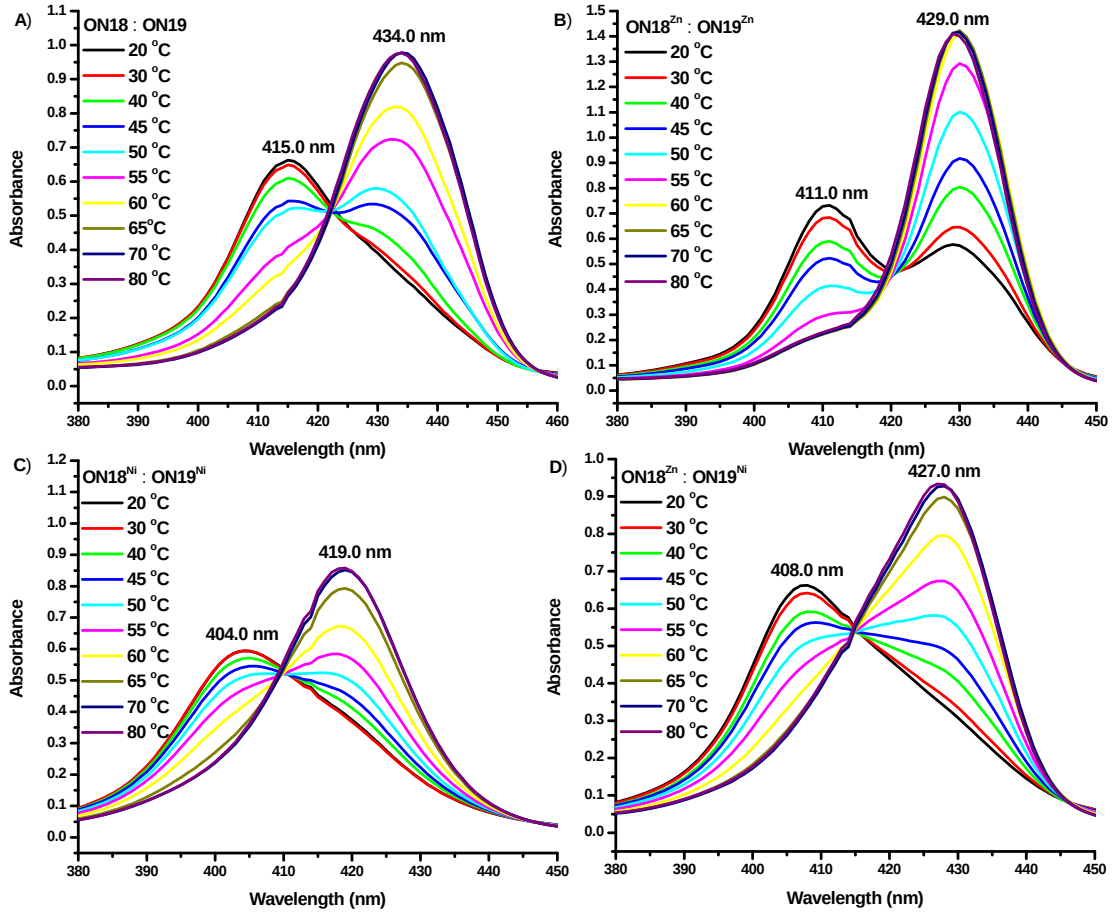

Figure 4.11 Temperature-dependent UV-vis spectra of GNA duplexes at Soret band region. Conditions: 10 mM sodium phosphate, 100 mM NaCl, pH 7.0, and 2 μM of each strand. (A) **ON18**:**ON19**. (B) **ON18^{Zn}**:**ON19^{Zn}**. (C) **ON18^{Ni}**:**ON19^{Ni}**. (D) **ON18^{Zn}**:**ON19^{Ni}** (see Tables 4.2 for the sequences).

The results are shown in Figure 4.10 and 4.11, by increasing the temperature from 20 to 80 ^{o}C, the peaks gradually shifted to a longer wavelength accompanied by disappearance of the splitting of the peaks, and this shift could be interpreted by the dissociation of the duplexes into their single strands: two porphyrin moieties in two strands lost their interaction.

Fluorescence spectroscopy

In order to obtain the fluorescence properties of porphyrins in GNA, the duplexes were investigated by fluorescence spectrometry. Mn(II) and Ni(II) porphyrins could not be investigated because they are not fluorescent.[14]

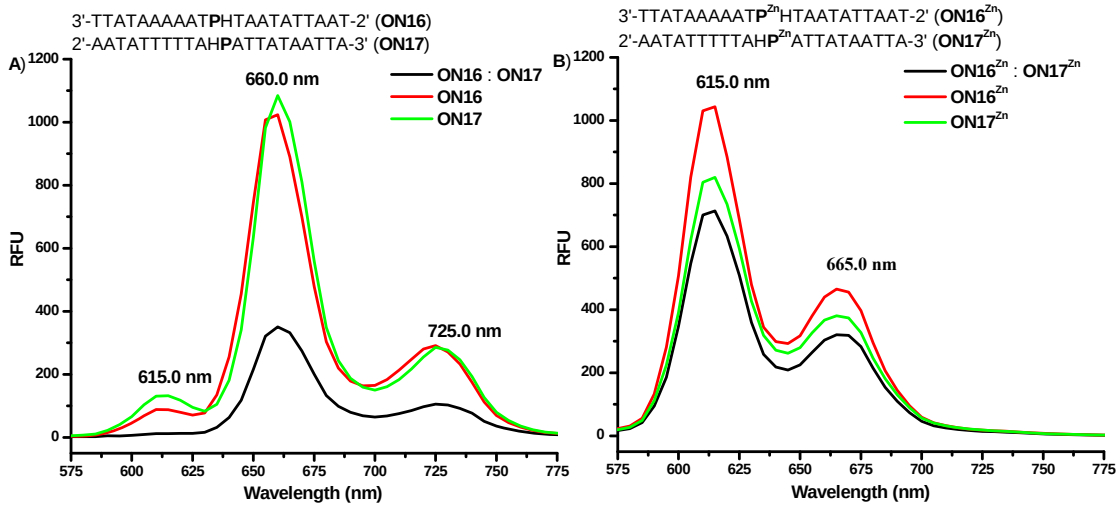

Figure 4.12 Fluorescence spectra of GNA duplexes and their corresponding single strands. Conditions: 10 mM sodium phosphate, 100 mM NaCl, pH 7.0, and 2 μM of each strand. (A) **ON16**, **ON17**, and **ON16**:**ON17**. (B) **ON16**^{Zn}, **ON17**^{Zn}, and **ON16**^{Zn}:**ON17**^{Zn} (see Tables 4.2 for the sequences).

Figure 4.12 shows the fluorescence spectra of **ON16**, **ON17**, **ON16**:**ON17**, and **ON16**^{Zn}, **ON17**^{Zn}, **ON16**^{Zn}:**ON17**^{Zn}. **ON16** and **ON17** which contain free porphyrins displayed the characteristic two emission peaks at 660 nm and 725 nm, while **ON16**^{Zn} and **ON17**^{Zn} showed features of Zn(II)-prophyrin emission spectra: the emission peaks are situated at 615 nm and 665 nm which are 50 nm blue shifted compared to **ON16** and **ON17**.[14] Aside from the change in intensity, the fluorescent spectra of duplexes **ON16**:**ON17** and **ON16**^{Zn}:**ON17**^{Zn} are rather similar. The decrease of fluorescence intensity is consistent with the formation of porphyrin aggregates. In addition, **ON16**:**ON17** shows lower emission quantity compared to **ON16**^{Zn}:**ON17**^{Zn}, which is in agreement with the fact that the free porphyrins can stack better within the GNA duplex.

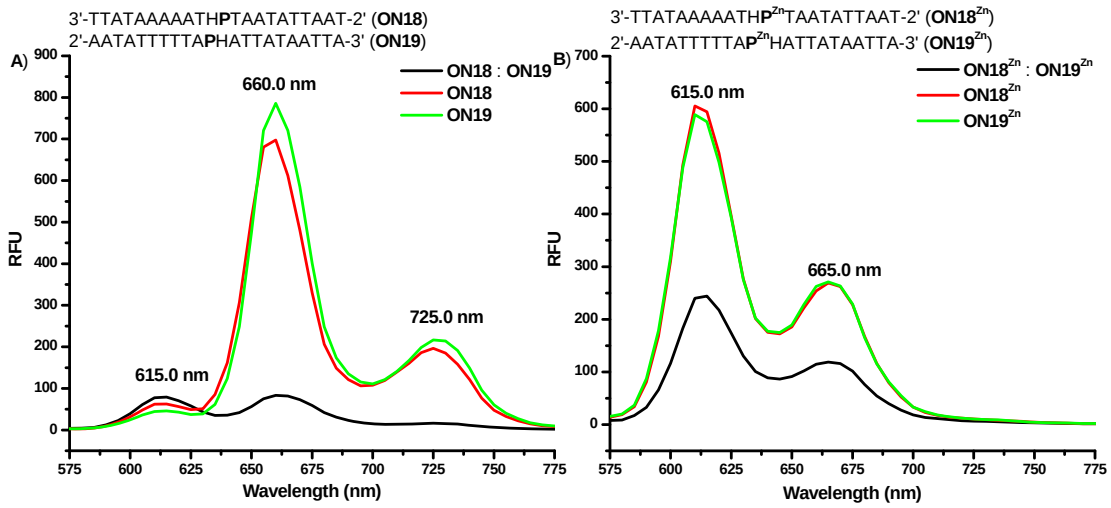

Figure 4.13 Fluorescence spectra of GNA duplexes and their corresponding single strands. Conditions: 10 mM sodium phosphate, 100 mM NaCl, pH 7.0, and 2 μM of each strand. (A) **ON18**, **ON19**, and **ON18**:**ON19**. (B) **ON18**^{Zn}, **ON19**^{Zn} and **ON18**^{Zn}:**ON19**^{Zn} (see Tables 3.2 for the sequences).

The similar phenomenon was observed in the fluorescence spectra of **ON18**, **ON19**, **ON18**:**ON19**, and **ON18**^{Zn}, **ON19**^{Zn}, **ON18**^{Zn}:**ON19**^{Zn} (Figure 4.13), and we will not repeat the details.

Overall, the UV-vis together with the fluorescence data support interactions between the porphyrins within the GNA duplexes.

CD spectroscopy

In order to learn more about the conformation of the porphyrins in GNA duplex, porphyrin-modified GNA duplexes were investigated by CD spectroscopy.

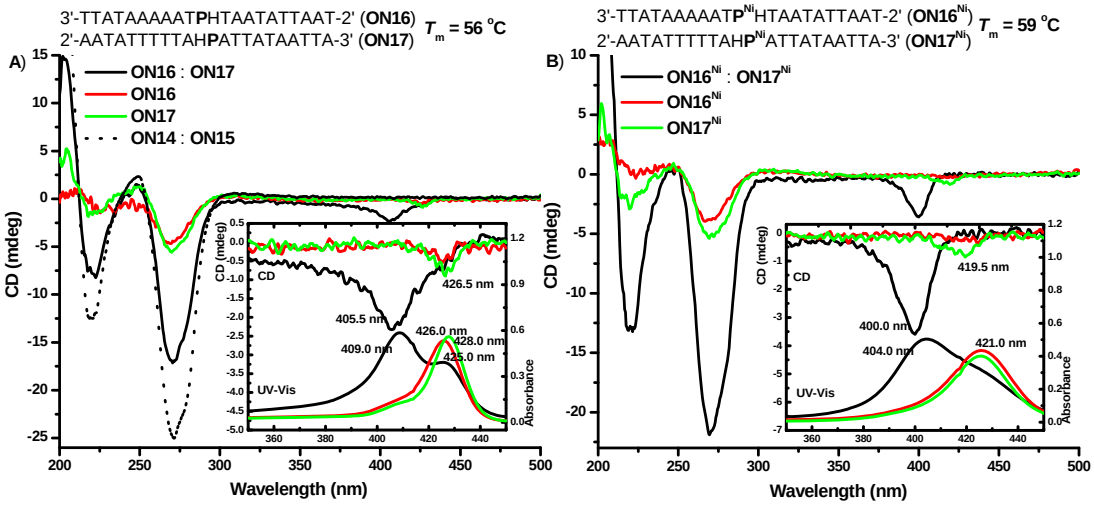

Figure 4.14 CD spectra of GNA duplexes and their corresponding single strands. Conditions: 10 mM sodium phosphate, 100 mM NaCl, pH 7.0, and 12 μM of each strand. (A) **ON16**, **ON17**, **ON16**:**ON17**, and **ON14**:**ON15**. (B) **ON16**^{Ni}, **ON17**^{Ni}, and **ON16**^{Ni}:**ON17**^{Ni} (see Tables 4.2 for the sequences). Inserts: overlap plot of CD and absorption spectra at the Soret region.

As shown in Figure 4.14, the CD signals of porphyrin-GNA duplexes in the GNA absorption region are almost identical to those of the unmodified GNA duplex, except for the lower signal intensities. It thus seems that the porphyrin modifications do not distort the overall GNA duplex conformation to a significant extent. In the porphyrin absorption region, induced negative Cotton effects at 406 nm and 400 nm are observed in the case of **ON16**:**ON17** (Figure 4.14A) and **ON16**^{Ni}:**ON17**^{Ni} (Figure 4.14B), respectively. Typically for porphyrin-modified DNA system, an induced negative Cotton effect in the Soret region is a signature of the intercalation of the porphyrin moiety into the DNA duplex.[17,18] Together with the T_m data, we therefore conclude that the porphyrin rings in duplex **ON16**:**ON17** and **ON16**^{Ni}:**ON17**^{Ni} intercalate into the GNA duplex and stack to neighboring base pairs.

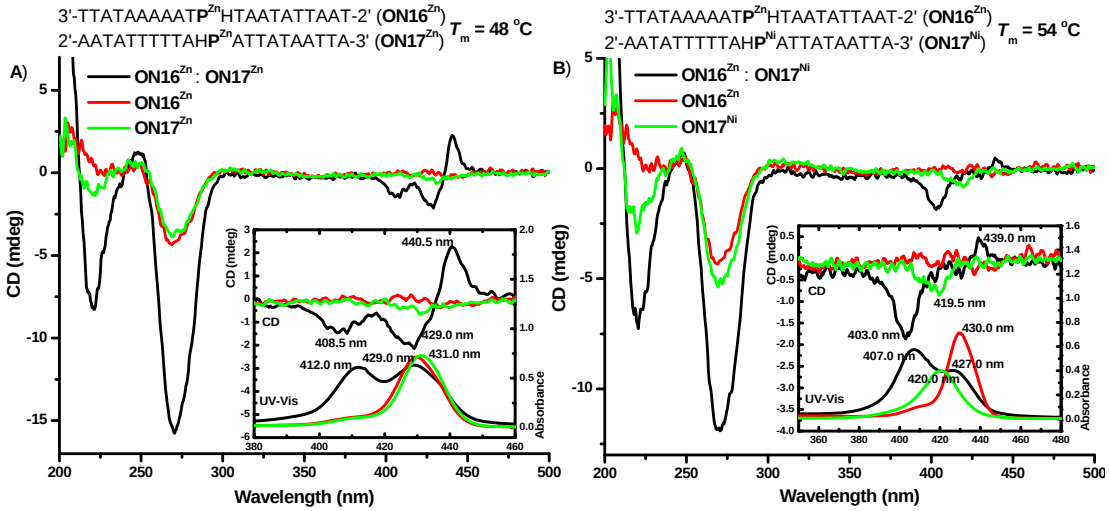

Figure 4.15 CD spectra of GNA duplexes and their corresponding single strands. Conditions: 10 mM sodium phosphate, 100 mM NaCl, pH 7.0, and 12 μM of each strand. (A) **ON16^{Zn}**, **ON17^{Zn}**, and **ON16^{Zn}**:**ON17^{Zn}**. (B) **ON16^{Zn}**, **ON17^{Ni}** and **ON16^{Zn}**:**ON17^{Ni}** (see Tables 4.2 for the sequences). Inserts: overlap plot of CD and absorption spectra at the Soret region.

However, the CD spectra of duplexes containing Zn(II)-porphyrins are different. In the case of **ON16^{Zn}**:**ON17^{Zn}** (Figure 4.15A), a clear multisignate CD spectrum, consisting of two negative bands at 409 and 429 nm and a positive band at 441 nm is observed. The CD spectrum of **ON16^{Zn}**:**ON17^{Ni}** (Figure 4.15B) shows a strong negative band at 403 nm and a weak positive band at 439 nm. Bisignate or multisignate CD spectra were observed in a system with porphyrins covalently attached to the 5′-end of DNA duplexes, and such CD spectra were interpreted for the evidence of through space dipole-dipole electronic interactions between the two porphyrin chromophores.[18] Together with the melting point results (Tables 4.2), we thus assume that the Zn(II)-porphyrins interact with each other although they are not as close in contact as the porphyrins in the analogous systems devoid of any metal or coordinated to nickel ions.

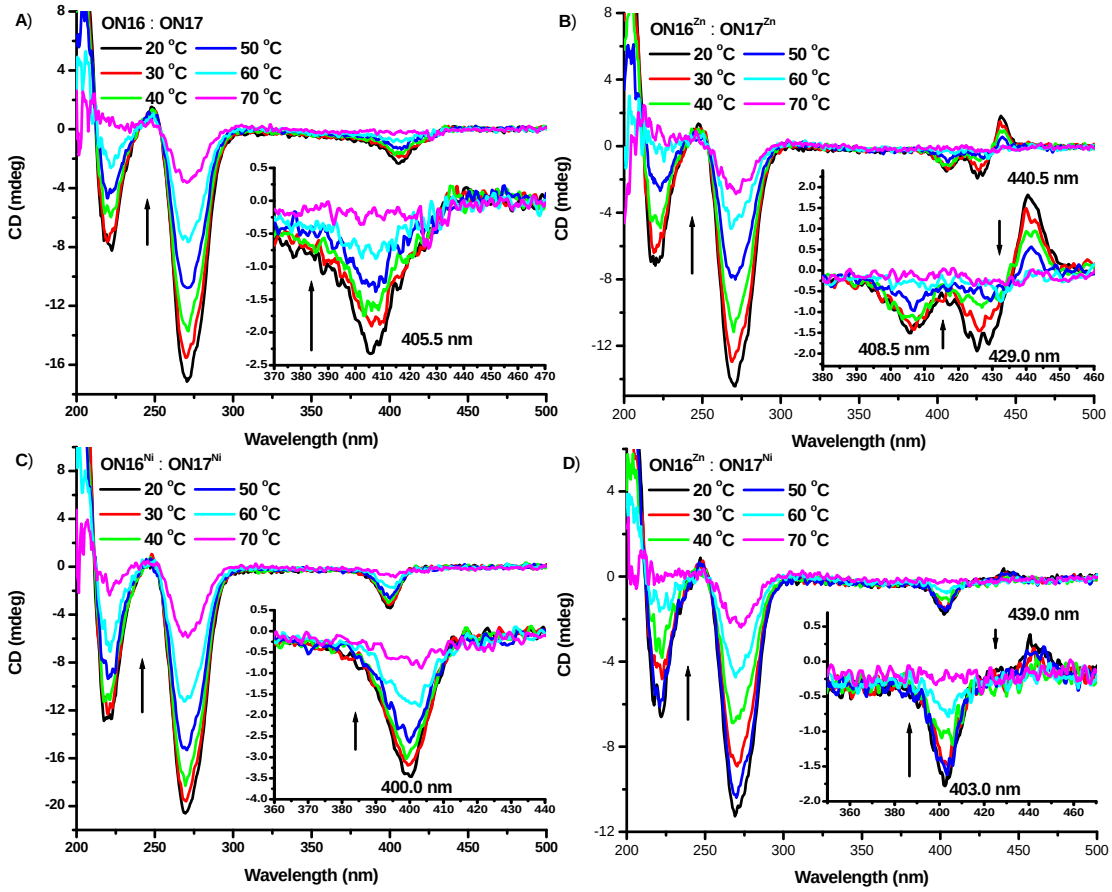

Figure 4.16 Temperture-dependent CD spectra of GNA duplexes. Conditions: 10 mM sodium phosphate, 100 mM NaCl, pH 7.0, and 12 μM of each strand. (A) **ON16**:**ON17**. (B) **ON16^{Zn}**:**ON17^{Zn}**. (C) **ON16^{Ni}**:**ON17^{Ni}**. (D) **ON16^{Zn}**:**ON17^{Ni}** (see Tables 4.2 for the sequences). The inserts show expanded porphyrin Soret band regions.

Next, we studied the influence of temperature on the CD spectra for the duplexes **ON16**:**ON17**, **ON16^{Zn}**:**ON17^{Zn}**, **ON16^{Ni}**:**ON17^{Ni}** and **ON16^{Zn}**:**ON17^{Ni}**. Upon increasing the temperature, the CD singal in the 200-300 nm region gradually disappeared, indicating the loss of helicity due to the denaturation. While in the Soret band of the porphyrin moieties, the peaks gradually disappeared which could be attributed to the dissociation of the duplexes into their single strands: two porphyrin moieties lost their electronic interaction or intercalation with GNA.

Chapter 4.3 Conclusions

In this chapter, we described a straightforward synthetic strategy to use GNA as a scaffold to organize porphyrins chromophores. A diphenylporphyrin acetylide phosphoramidite GNA building block **18c** was used to synthesize GNA strands with incorporated diphenylporphyrin acetylide nucleotides (**P**). Incorporated opposite an ethylene glycol abasic site (**H**), such porphyrin acetylides (**P**) did not significantly perturb the overall GNA duplex structures.

Interestingly, the thermal stabilities of duplex contaiing **P**:**H** base pairs can be modulated by the incorporation of zinc(II) and nickel(II) ion which lead to a decrease or increase in duplex stability, respectively. This can be rationalized with a flipped-out conformation of the zinc-porphyrin in contrast to a stacking of the nickel-porpyhrin within the base stacking of the GNA duplex. Thus, the conformation of porphyrins in GNA can be modulated by the bound metal ions. Furthermore, we demonstrated that GNA duplexes are a suitable scaffold to bring two porphyrins into close contact and to allow the interaction of porphyrins with different coordinated metal ions.

Future work will be focused on applications of such porphyrin-GNA conjugates as well as modified GNA containing porphyrin and other chromophores for light harvesting and charge transport.

Chapter 4.4 Experimental

Synthesis of metalloporphyrin-GNA oligonucleotide and purification

Zinc metallation of porphyrin in GNA. To a solution of porphyrin-GNA single strands (12.0 nmol GNA single strands in 140 μL of 10 mM Tris-HCl buffer solution, pH 7.6) was added a solution of $Zn(OAc)_2$ in H_2O (10 mM, 12 μL,10 eq.). The solution was shaken at 25 ^oC and the reaction was followed by absorption spectroscopy. After around 2 hours, the reaction mixture was diluted to 1000 μL with 3% ammonia solution. Excess Zn^{2+} was removed by treating the reaction mixture with ion-exchange resins (Chelex 100 sodium form). The strands were purified by HPLC using a Water XTerra colume at 55 °C with aqueous TEAA and acetonitrile as the eluent. The identities of the oligonucleotides were confirmed by MALDI-TOF MS (Table 4.4).

Nickel metallation of porphyrin in GNA. Nickel metallation was carried out by heating (80 ºC) under nitrogen atomosphere a solution of porphyrin-GNA single strands (2.5 nmol GNA in 325 μL of 10 mM Tris-HCl buffer solution, pH 7.6, and 60 equiv. $Ni(OAc)_2$ (10 mM)). The reaction was followed by absorption spectroscopy and found to be completed after heating for 16 hours. Workup was performed in analogy to the zinc(II) complexation.

Manganese metallation of porphyrin in GNA. Manganese metallation was carried out by heating (80 ºC) under nitrogen atomosphere a solution of porphyrin-GNA single strands (2.5 nmol GNA in 300 μL of 10 mM Tris-HCl buffer solution, pH 7.6, and 60 equiv. $MnCl_2$ (10 mM)). The reaction was followed by absorption spectroscopy and found to be completed after heating for 1 hour. Workup was performed in analogy to the zinc(II) complexation.

Other metallatons of porphyrin in GNA. Other metallations were carried out accoring to the nickel metallation. Unfortunately, the GNA strand was decomposed duiring the copper metallation that was confirmed by MALDI-TOF

MS. Other metal complexes such as $CdSO_4$, $AgPF_6$, $FeCl_2$ and $FeCl_3$ do not metallate the porphyrin in GNA.

Thermal denaturation

The melting studies were carried out in 1 cm path length quartz cells (total volumn 325 μL; 200 μL sample solutions were covered by mineral oil) on a Beckman 800 UV-Vis spectrophotometer equipped with a thermo-programmer. Melting curves were monitored at 260 nm with a heating rate of 1 °C/min. Melting temperatures were calculated from the first derivatives of the heating curves. Experiments were performed in duplicate and mean values were taken.

UV-vis spectroscopy

The absorptions of oligonucleotide solutions were measured in a quartz cuvette with a path length of 1 cm at 260 nm on Beckman 800 UV-Vis spectrophotometer. Temperature-dependent absorption spectra were obtained on Beckman 800 UV-Vis spectrophotometer equipped with a temperature controller. Spectra were obtained every 10 °C by heating from 20 to 80 °C. Both single strands and duplexes (2 μM of each strand) were prepared in 10 mM sodium phosphate, 100 mM NaCl, pH 7.0.

Fluorescence spectroscopy

The experiments were performed in 96-well plates on a Molecular Devices SpectraMax M5 with excitation at 427 nm and a cutoff filter at 435 nm. The experiments with single strands or duplexes were performed in 10 mM sodium phosphate, 100 mM NaCl, pH 7.0, and the concentration of each strand was 2 μM.

CD spectroscopy

CD measurements were performed on a JASCO J-810 spectrometer in a 1 mm

path length quartz cuvette. The GNA single strands or duplexes were prepared in 10 mM sodium phosphate, 100 mM NaCl, pH 7.0, and the concentration of each strand was 12 μM. Each measurement was repeated 5 times and the average taken.

Table 4.4 MALDI-TOF MS data of used oligonucleotides.

Name	Oligonucleotides	M_{calcd}	M_{found}
ON 1	3′-TAAAAATAATAATATT-2′	4222.7($C_{128}H_{167}N_{62}O_{74}P_{15}$)	4223.3
ON 2	3′-AATATTATTATTTTTA-2′	4186.6($C_{128}H_{171}N_{50}O_{82}P_{15}$)	4185.5
ON 3	3′-TAAAAATATAATATT-2′	3951.5($C_{120}H_{157}N_{57}O_{70}P_{14}$)	3949.3
ON 4	3′-AATATTATATTTTTA-2′	3924.5($C_{120}H_{160}N_{48}O_{76}P_{14}$)	3923.2
ON 5	3′-AATATTATAATTTTTA-2′	4195.7($C_{128}H_{170}N_{53}O_{80}P_{15}$)	4195.0
ON 6	3′-TAAAAATPATAATATT-2′	4574.1($C_{157}H_{184}N_{61}O_{74}P_{15}$)	4574.3
ON 6^{Zn}	3′-TAAAAATP^{Zn}ATAATATT-2′	4637.5($C_{157}H_{182}N_{61}O_{74}P_{15}Zn_1$)	4638.3
ON 6^{Ni}	3′-TAAAAATP^{Ni}ATAATATT-2′	4630.8($C_{157}H_{182}N_{61}Ni_1O_{74}P_{15}$)	4630.5
ON 6^{Mn}	3′-TAAAAATP^{Mn}ATAATATT-2′	4627.0($C_{157}H_{182}N_{61}Mn_1O_{74}P_{15}$)	4626.4
ON 7	3′-AATATTATHATTTTTA-2′	4048.5($C_{122}H_{165}N_{48}O_{80}P_{15}$)	4048.2
ON 8	3′-TAAAAATTAATATT-2′	3680.3($C_{112}H_{147}N_{52}O_{66}P_{13}$)	3678.2
ON 9	3′-AATATTAATTTTTA-2′	3662.3($C_{112}H_{149}N_{46}O_{70}P_{13}$)	3661.2
ON 10	3′-TAAAAATPHTAATATT-2′	4427.0($C_{151}H_{179}N_{56}O_{74}P_{15}$)	4434.2
ON 10^{Zn}	3′-TAAAAATP^{Zn}HTAATATT-2′	4490.4($C_{151}H_{177}N_{56}O_{74}P_{15}Zn_1$)	4498.1
ON 11	3′-AATATTA PHATTTTTA-2′	4408.9($C_{151}H_{181}N_{50}O_{78}P_{15}$)	4416.9
ON 11^{Zn}	3′-AATATTA P^{Zn} ATTTTTA-2′	4472.3($C_{151}H_{179}N_{50}O_{78}P_{15}Zn_1$)	4479.6
ON 12	3′-TTATAAAAATAATAATATTAAT-2′	5822.7($C_{176}H_{230}N_{83}O_{104}P_{21}$)	5821.5
ON 13	3′-ATTAATATTATTATTTTTATAA-2′	5786.6($C_{176}H_{234}N_{71}O_{112}P_{21}$)	5784.0
ON 14	3′-TTATAAAAATTAATATTAAT-2′	5280.3($C_{160}H_{210}N_{73}O_{96}P_{19}$)	5277.6
ON 15	3′-ATTAATATTAATTTTTATAA-2′	5262.3($C_{160}H_{212}N_{67}O_{100}P_{19}$)	5260.5
ON 16	3′-TTATAAAAATPHTAATATTAAT-2′	6027.0($C_{199}H_{242}N_{77}O_{104}P_{21}$)	6025.8
ON 16^{Zn}	3′-TTATAAAAATP^{Zn}HTAATATTAAT-2′	6090.3($C_{199}H_{240}N_{77}O_{104}P_{21}Zn_1$)	6088.3
ON 16^{Ni}	3′-TTATAAAAATP^{Ni}HTAATATTAAT-2′	6083.6($C_{199}H_{240}N_{77}Ni_1O_{104}P_{21}$)	6082.2
ON 16^{Mn}	3′-TTATAAAAATP^{Mn}HTAATATTAAT-2′	6079.9($C_{199}H_{240}N_{77}Mn_1O_{104}P_{21}$)	6085.0
ON 17	3′-ATTAATATTAPHATTTTTATAA-2′	6008.9($C_{199}H_{244}N_{71}O_{108}P_{21}$)	6006.6
ON 17^{Zn}	3′-ATTAATATTAP^{Zn}HATTTTTATAA-2′	6072.3($C_{199}H_{242}N_{71}O_{108}P_{21}Zn_1$)	6072.4
ON 17^{Ni}	3′-ATTAATATTAP^{Ni}HATTTTTATAA-2′	6065.6($C_{199}H_{242}N_{71}Ni_1O_{108}P_{21}$)	6068.0
ON 17^{Mn}	3′-ATTAATATTAP^{Mn}HATTTTTATAA-2′	6061.8($C_{199}H_{242}N_{71}Mn_1O_{108}P_{21}$)	6063.8
ON 18	3′-TTATAAAAATHPTAATATTAAT-2′	6027.0($C_{199}H_{242}N_{77}O_{104}P_{21}$)	6027.1
ON 18^{Zn}	3′-TTATAAAAATHP^{Zn}TAATATTAAT-2′	6090.3($C_{199}H_{240}N_{77}O_{104}P_{21}Zn_1$)	6089.2
ON 18^{Ni}	3′-TTATAAAAATHP^{Ni}TAATATTAAT-2′	6083.6($C_{199}H_{240}N_{77}Ni_1O_{104}P_{21}$)	6082.4
ON 18^{Mn}	3′-TTATAAAAATHP^{Mn}TAATATTAAT-2′	6079.9($C_{199}H_{240}N_{77}Mn_1O_{104}P_{21}$)	6081.2
ON 19	3′-ATTAATATTAHPATTTTTATAA-2′	6008.9($C_{199}H_{244}N_{71}O_{108}P_{21}$)	6006.7
ON 19^{Zn}	3′-ATTAATATTAHP^{Zn}ATTTTTATAA-2′	6072.3($C_{199}H_{242}N_{71}O_{108}P_{21}Zn_1$)	6072.4
ON 19^{Ni}	3′-ATTAATATTAHP^{Ni}ATTTTTATAA-2′	6065.6($C_{199}H_{242}N_{71}Ni_1O_{108}P_{21}$)	6064.8
ON 19^{Mn}	3′-ATTAATATTAHP^{Mn}ATTTTTATAA-2′	6061.8($C_{199}H_{242}N_{71}Mn_1O_{108}P_{21}$)	6059.9

Chapter 4.5 References

1. Brun, A. M.; Harriman, A. *Journal of American Chemical Society* **1994**, *116*, 10383-10393.
2. Pasternack, R. F.; Collings, P. J. *Science* **1995**, *269*, 935-939.
3. (a) Meunier, B. *Chemical Review* **1992**, *92*, 1411-1456; (b) Marzilli, L. G. *New Journal of Chemistry* **1990**, *14*, 409-420; (c) Pass, H. I. *Journal of the National Cancer Institute* **1993**, *85*, 443-456; (d) O'Connor, A. E.; Gallagher, W. M.; Byrne, A. T. Photochemistry and Photobiology **2009**, *85*, 1053.
4. (a) Balaz, M.; Holmes, A. E.; Benedetti, M.; Rodriguez, P. C.; Berova, N.; Nakanishi, K.; Proni, G. *Journal of American Chemical Society* **2005**, *127*, 4172; (b) Balaz, M.; Li, B. C.; Steinkruger, J. D.; Ellestad, G.A.; Nakanishi, K.; Berova, N. *Organic & Biomoleculor Chemistry* **2006**, *4*, 1865-1867; (c) Balaz, M.; Bitsch-Jensen, K.; Mammana, A.; Ellestad, G. A.; Nakanishi, K. and Berova, N. *Pure Apply Chemistry* **2007**, *79*, 801.
5. (a) Pasternack, R. F.; Gibbs, E. J. Metal Ions in Biological Systems. In *Probing of Nucleic Acids by Metal Ions Complexes of Small Molecules*; Sigel, A., Sigel, H., Eds.; Marcel Dekker: New York, 1996; Vol. 33, pp 367-397; (b) Wall, R. K.; Shelton, A. H.; Bonaccorsi, L. C.; Bejune, S. A.; Dube, D.; McMillin, D. R. *Journal of American Chemical Society* **2001**, *123*, 11480.
6. (a) Endo, M.; Fujitsuka, M.; Majima, T. *Journal of Organic Chem*istry **2008**, *73*, 1106-1112; (b) Mammana, A.; Pescitelli, G.; Asakawa, T.; Jockusch, S.; Petrovic, A. G.; Monaco, R. R.; Purrello, R.; Turro, N. J.; Nakanishi, K; Ellestad, G. A.; Balaz, M.; Berova, N. *Chemistry-A European Journal* **2009**, *15*,11853.
7. (a) Murashima, T.; Hayata, K.; Saiki, Y.; Matsui, J.; Miyoshi, D.; Yamada, T.; Miyazawa, T. and Sugimoto, N. *Tetrahedron Letter* **2007**, *48*, 8514; (b) Berlin, K.; Jain, R. K.; Simon, M. D.; Richert, C. *Journal of Organic Chemistry* **1998**, *63*, 1527.
8. *The Porphyrin Handbook*; Kadish, K. M, Smith, K. M, Guilard, R., Eds.;

Academic Press: Boston, MA, 2000; Vols. 1-10.

9. Morales-Rojas, H.; Kool, E. T. *Organic Letters* **2002**, *4*, 4377.
10. (a) Choi, M.-S.; Yamazaki, T.; Yamazaki, I. and Aida, T. *Angewandte Chemie International Edition* **2004**, *43*, 150; (b) Kim, D. and Osuka, A. *Accounts of Chemical Research* **2004**, *37*, 735; (c) Balaban, T. S. *Accounts of Chemical Research* **2005**, *38*, 612; (d) Endo, M., Fujitsuka, M. and Majima, T. *Chemistry-A European Journal* **2007**, *13*,8660.
11. (a) Fendt, L.-A.; Bouamaied, I.; Thöni, S.; Amiot, N.; Stulz, E. *Journal of the American Chemical Society* **2007**, *129*, 15319; (b) Bouamaied, I.; Nguyen, T. N.; Rühl, T.; Stulz, E. *Organic & Biomoleculor Chemistry* **2008**, *6*, 3888; (c) Nguyen, T. N.; Brewer, A.; Stulz, E. *Angewandte Chemie International Edition* **2009**, *48*, 1974; (d) Endo, M.; Fujitsuka, M.; Majima, T.; *Tetrahedron* **2008**, *64*, 1839; (e) Bouamaied, I.; Fendt, L.-A.; Haeussinger, D.; Wiesner, M.; Thoeni, S.; Amiot, N.; Stulz, E. *Nucleotides Nucleic Acids* **2007**, ***26***, 1533.
12. Zhou, H.; Ma, X.; Wang, J.; Zhang, L. *Organic & Biomoleculor Chemistry* **2009**, *7*, 2297.
13. (a) Elemans, J. A. A. W.; Bijsterveld, E. J. A.; Rowan, A., E.; Nolte, R. J. M. *Eropean Journal of Organic Chemistry* **2007**, 751; (b) Pasternack, R. F.; Francescon, L.; Raff, D.; Spiro, E. *Inorganic Chemistry* **1973**, *12*, 2606.
14. Zhen, W.; Shan, N.; Yu, L.; Wang, X. *Dyes and Pigments* **2007**, *77*, 153.
15. (a) Kobuke, Y.; Miyaji, H. *Journal of American Chemistry Society* **1994**, *116*, 4111; (b) Hajjaj, F.; Yoon, Z. S.; Yoon, M.-C.; Park, J.; Satake, A.; Kim, D.; Kobuke, Y. *Journal of American Chemistry Society* **2006**, *128*, 4612; (c) Ogawa, K.; Zhang, T.; Yoshihara, K.; Kobuke, Y. *Journal of American Chemistry Society* **2002**, *124*, 22.
16. (a) Shirakawa, M.; Kawano, S.-I.; Fujita, N.; Sada, K.; Shinkai, S. *Journal of Organic Chemistry* **2003**, *68*, 5037; (b) Maiti, N. C.; Mazumdar, S.; Periasamy, N. *J. Porphyrins Phthalocyanines* **1998**, *2*, 369.
17. McMillin, D. R.; Shelton, A. H.; Bejune, S. A.; Fanwick, P. E.; Wall, R. K. *Coordination Chemistry Review* **2005**, *249(13-14)*, 1451.

18. Nitta, Y.; Kuroda, R. *Biopolymers* **2006**, *81*, 376.

19. (a) Mammana, A.; Asakawa, T.; Jensen, K. B.; Wolfe, A.; Chaturantabut, S.; Otani, Y.; Li, X.; Li, Z.; Nakanishi, K.; Balaz, M.; Ellestad, G. A.; Berova, N. *Bioorganic & Medical Chemistry* **2008**, *16*, 6544; (b) Balaz, M.; Jensen, K. B.; Mammana, A.; Ellestad, G. A.; Nakanishi, K.; Berova, N. *Pure and Apply Chemistry* **2007**, *79*, 801.

20. Meggers, E. and Zhang, L. *Accounts of Chemical Research* **2010,** *43*, 1092.

21. Synthesis of the 5-ethynyl-10,20-diphenylporphinatozinc **3.3**: (a) Lin, V. S.-Y.; Iovine, P. M.; Dimango, S. G.; Therien, M. J. *Inorganic Syntheses* **2002**, *33*, 55; (b) Fazekas, M.; Pintea, M.; Senge, M. O.; Zawadzka, M. *Tetrahedron Letters* **2008**, *49 (14)*, 2236; (c) Balaban, T. S.; Goddard, R.; Schaetzel, M. L.; Lehn, J.-M. *Journal of American Chemistry Society* **2003**, *125*, 4233; (d) Kai, H.; Nara, S.; Kinbara, K.; Aida, T. *Journal of American Chemistry Society* **2008**, *130*, 6725.

22. Zhang, L.; Peritz, A. E.; Carroll, P. J.; Meggers, E. *Synthesis* **2006**, 645.

Chapter 5 GNA as a Supramolecular Scaffold for the Zipper-like Arrangement of Perylene Bisimide and Porphyrin Units

Chapter 5.1 Introduction

Over the past decades, DNA emerged as one of the most appealing scaffolds for the precise arrangement of chromophores. The π-π stacking chromophore arrays can be organized in the DNA-like single strand, and the interior or grooves of duplex DNA.

Although studies on DNA as a scaffold for the arrangement of chromophores have achieved remarkable success, few studies have reported on electron donor-acceptor systems composed of interstrand-stacked chromophores in DNA.[1] With all the nucleotides in hand, we try to organize them in zipper-like fashion to examine the properties of resulting systems. Here we described the organization of donor-acceptor chromophore systems in duplex GNA, which was mainly composed of perylene bisimide (**PBI**) and acetylide porphyrin (**P**).

Chapter 5.2 Results and Discussion

Chapter 5.2.1 Electron donor-acceptor pair in duplex GNA

In this study, perylene bisimide (**PBI**) was chosen as electron acceptor chromophore, and the electron donor chromophores were pyrene (**Pyr**), acetylide pyrene (**Pyr′**), acetylide perylene (**Pe′**) and acetylide porphyrin (**P**). To study the effect of incorporating electron donor-acceptor chromophores on GNA, the thermal stability of duplexes GNA containing two adjacent chromophores was investigated. The adjacency of chromophores increases the potential of forming interstrand-stacked pairs.

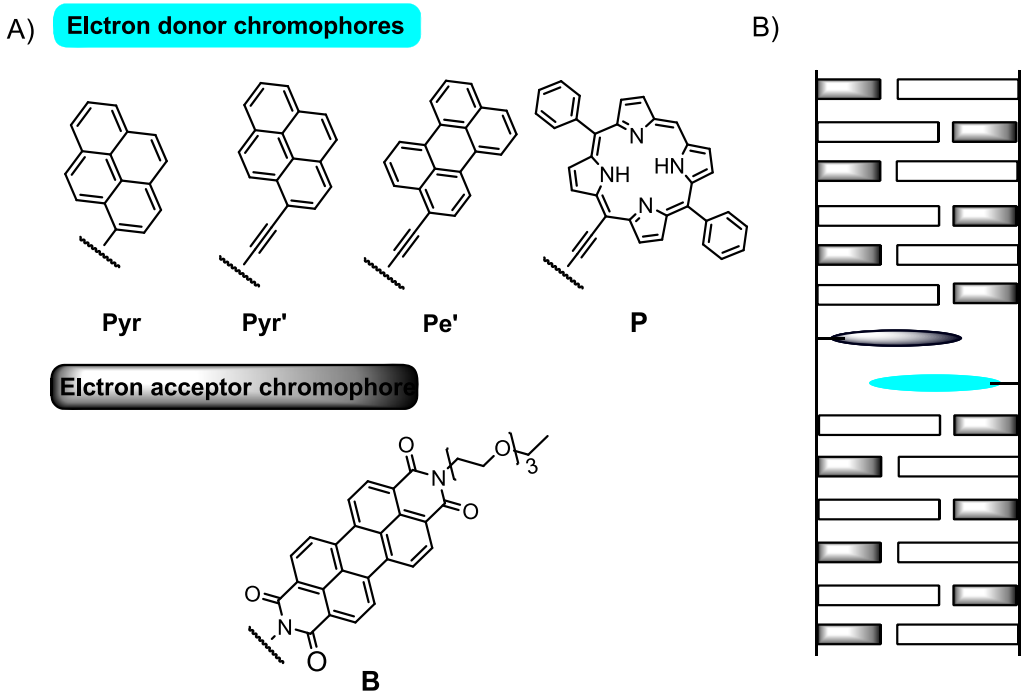

Figure 5.1 (A) Structure of chromophores used in the present study. (B) Position of electron donor-acceptor stacking chromophores in the middle of duplex GNA.

Table 5.1 lists the electron donor-acceptor chromophore pairs that were incorporated into the middle of a 16mer duplex GNA. The combination includes **B-Pyr**, **B-Pyr′**, **B-Pe′**, and **B-P**. The resulting contribution of the π-π stacking between electron donor-acceptor chromophores in the GNA interior to the duplex

stability was measured by thermal denaturation experiments. A duplex without the artificial nucleotide was used for comparison.

Table 5.1 Thermal stabilities of GNA duplexes containing chromophore pair together with Watson-Crick reference duplexes.[a]

Entry	GNA duplex		T_m [°C][a]
1	3′-TAAAAATTAATATT-2′ 2′-ATTTTTAATTATAA-3′	(**ON1**) (**ON2**)	49
2	3′-TAAAAAT**AA**TAATATT-2′ 2′-ATTTTTA**TT**ATTATAA-3′	(**ON3**) (**ON4**)	54
3	3′-TAAAAAT**BH**TAATATT-2′ 2′-ATTTTTA**HPyr**ATTATAA-3′	(**ON8**) (**ON6**)	50
4	3′-TAAAAAT**BH**TAATATT-2′ 2′-ATTTTTA**HPyr′**ATTATAA-3′	(**ON8**) (**ON7**)	57
5	3′-TAAAAAT**BH**TAATATT-2′ 2′-ATTTTTA**HPe′**ATTATAA-3′	(**ON8**) (**ON9**)	57
6	3′-TAAAAAT**BH**TAATATT2′ 2′-ATTTTTA**HP**ATTATAA-3′	(**ON8**) (**ON10**)	64
7	3′-TAAAAAT**PH**TAATATT-2′ 2′-ATTTTTA**HB**ATTATAA-3′	(**ON11**) (**ON12**)	63

[a]Conditions: 10 mM sodium phosphate, 100 mM NaCl, and 2 μM of each strand.

As described in Table 5.1, **B-Pyr** pair afforded a duplex melting point (T_m) of 50 °C (entry 3), compared with 54 °C for two **A**:**T** base pairs at the same position (entry 2). Removing two **A**:**T** base pairs of the Watson-Crick reference duplex as in **ON1**:**ON2** (entry 1) resulted in a melting point of 49 °C, demonstrating that the incorporation of a **B-Pyr** pair had a very slight stabilizing effect (ΔT_m = 1 °C). However, replacing **Pyr** of the **B-Pyr** pair in **ON8**:**ON6** (entry 3) by **Pyr′**, **Pe′**, or **P** resulted in **B-Pyr′**, **B-Pe′** or **B-P**, and increased stability by additional 8, 8, and 15 °C, respectively (entries 4-6). The **B-P** pair evidently stabilized the duplex more strongly than the other electron donor-acceptor pair shown in Table 5.1. This finding indicates a stronger π-π stacking between porphyrin and **PBI** in the duplex.

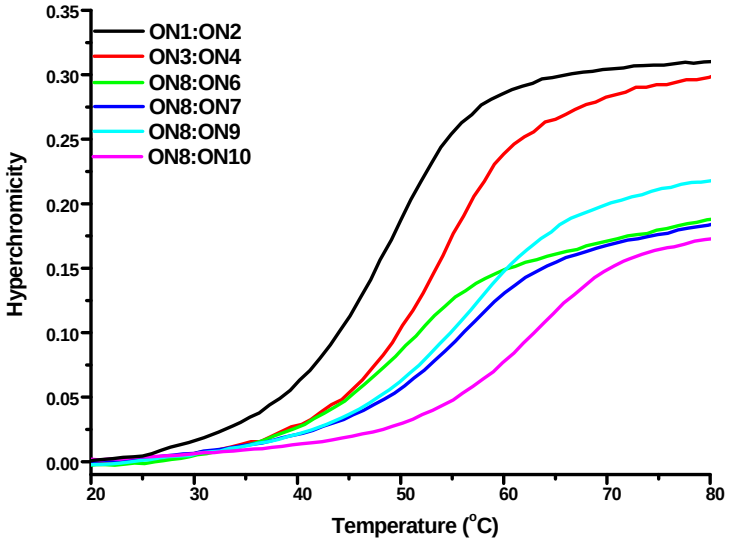

Figure 5.2 UV-melting curves of the GNA duplexes **ON1**:**ON2**, **ON3**:**ON4**, **ON8**:**ON6**, **ON8**:**ON7**, **ON8**:**ON9**, and **ON8**:**ON10** (see Table 5.1 for the sequences). Changes in absorbance upon heating were monitored at 260 nm. Conditions: 10 mM sodium phosphate, 100 mM NaCl, pH 7.0, and 2 μM of each strand.

Chapter 5.2.2 Zipper-like arrangement of chromophores in GNA

Both photo-induced electron transfer and energy transfer between porphyrin and **PBI** have been theoretically predicted.[2] Hence, porphyrin and **PBI** have been frequently employed in building photoactive systems recently. Porphyrins are normally electron donors and energy acceptors, whereas **PBI**s are electron acceptors and energy donors in porphyrin-**PBI** systems.[3] π-π stacking array composed of porphyrin and **PBI** was seldom investigated in DNA.

Chromophores in DNA have been reported to recognize each other based on interstrand aromatic stacking to form zipper-like aggregates.[4] As discussed in chapter 5.2.1, the interstrand-stacking **P**-**B** pair significantly stabilized the duplex. This exciting result stimulated us to introduce additional **B** and **P** into the duplex for creating a π-π stacking array of **B** and **P**. The corresponding modified GNA duplexes are shown in Table 5.2. The porphyrin and **PBI** nucleotides were organized in the middle of a 16mer duplex GNA. The number of stacking chromophores ranged from two to five.

Thermal stability

The influence of porphyrin and **PBI** nucleotides on the stability of the duplexes was evaluated by thermal denaturation studies. Table 5.2 shows the experimental T_m values of the corresponding duplexes as well as of the reference duplex.

Table 5.2 Thermal stabilities of 16mer modified duplexes together with Watson-Crick reference duplexes.[a]

Entry	GNA duplex		T_m [°C]	ΔT_m [°C]
1	3′-TAAAAAT**AA**TAATATT-2′ 2′-ATTTTTA**TT**ATTATAA-3′	(**ON3**) (**ON4**)	54	
2	3′-TAAAAAT**BH**TAATATT-2′ 2′-ATTTTTA**HP**ATTATAA-3′	(**ON8**) (**ON10**)	64	+10
3	3′-TAAAAAT**PH**TAATATT-2′ 2′-ATTTTTA**HB**ATTATAA-3′	(**ON11**) (**ON12**)	63	+9
4	3′-TAAAAA**HPH**TAATATT-2′ 2′-ATTTTT**BHB**ATTATAA-3′	(**ON13**) (**ON14**)	57	+3
5	3′-TAAAAA**HBH**TAATATT-2′ 2′-ATTTTT**PHP**ATTATAA-3′	(**ON15**) (**ON16**)	78	+23
6	3′-TAAAAA**HPHP**AATATT-2′ 2′-ATTTTT**BHBH**TTATAA-3′	(**ON17**) (**ON18**)	70	+16
7	3′-TAAAAA**HBHB**AATATT-2′ 2′-ATTTTT**PHPH**TTATAA-3′	(**ON19**) (**ON20**)	66	+12
8	3′-TAAAAA**HBHBH**ATATT-2′ 2′-ATTTTT**PHPHP**TATAA-3′	(**ON23**) (**ON24**)	79	+25

[a]Conditions: 10 mM sodium phosphate, 100 mM NaCl, and 2 μM individual strand.

As shown in Table 5.2, the GNA duplex containing sandwich-type **P-B-P** exhibited a melting point (T_m) of 78 °C, it improved the duplex stability by an additional 23 °C (entry 5). When the **B-P-B-P** and **P-B-P-B** were incorporated into the GNA duplex, the corresponding duplexes showed melting points of 70 and 66 °C, respectively (entries 6 and 7). The duplex modified by **P-B-P-B-P** had the highest melting point (T_m = 79 °C; entry 8). Overall, Table 5.2 reveals that porphyrin-**PBI** aggregates have remarkably positive effects on the stabilization of the duplex.

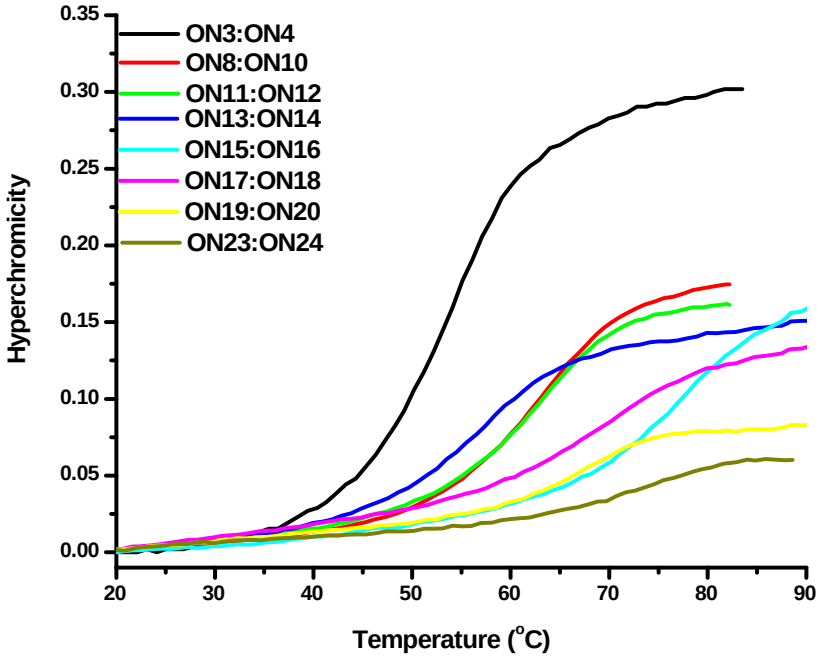

Figure 5.3 UV-melting curves of the GNA duplexes **ON3**:**ON4**, **ON8**:**ON10**, **ON11**:**ON12**, **ON13**:**ON14**, **ON15**:**ON16**, **ON17**:**ON18**, **ON19**:**ON20**, and **ON23**:**ON24** (see Table 5.2 for the sequences). Changes in absorbance upon heating were monitored at 260 nm. Conditions: 10 mM sodium phosphate, 100 mM NaCl, pH 7.0, and 2 μM of each strand.

Interactions of chromophores in heteroaggregates

The J-aggregation of identical dyes is known to show a red shift of the absorption band because of the strong exciton coupling. In contrast, H-aggregation shows a blue shift of the absorption for the same reason.[5] However, little experimental and theoretical investigations on such heteroaggregations have been performed. As far as we know, only several heteroaggregates of chromophores in DNA were reported by Asanuma et al.[6] and Haner et al.[1,7] The heteroaggregate of porphyrin and **PBI** in DNA is not reported.

To acquire information about the interaction between porphyrin and **PBI** in the GNA duplexes in the present study, the modified duplexes and their corresponding single strands were investigated by UV-vis and circular dichroism (CD) spectrometry.

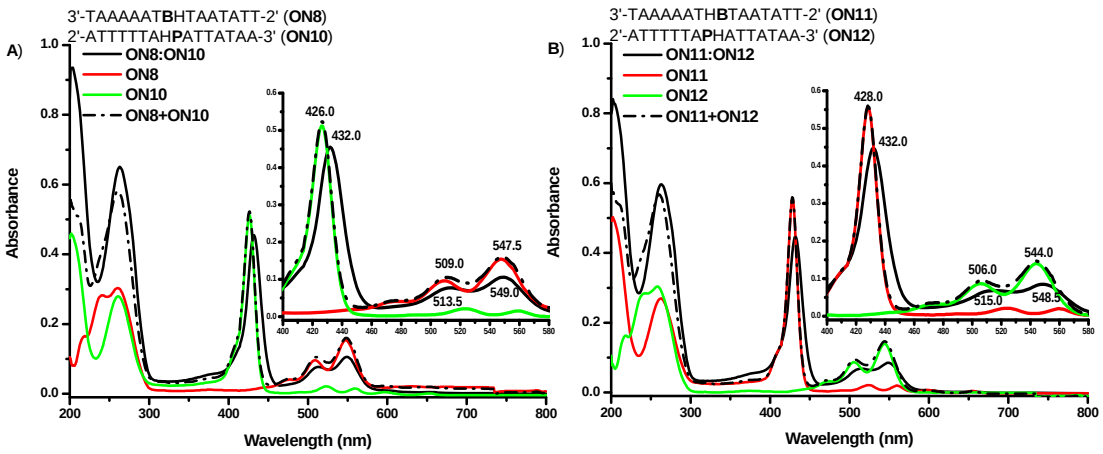

Figure 5.4 UV-vis spectra of modified GNA duplexes and their corresponding single strands. Conditions: 10 mM sodium phosphate, 100 mM NaCl, pH 7.0, and 2 μM of each strand. (A) **ON8**, **ON10,** and **ON8**:**ON10**. (B) **ON11**, **ON12,** and **ON11**:**ON12**. The inset shows the expanded porphyrin Soret band and the **PBI** absorption band.

The UV-vis spectra of duplexes containing **B**-**P** and their corresponding single strands were first analyzed. Figure 5.4 shows the changes in the absorption band of the chromophores upon duplex formation. For **ON8**:**ON10**, the Soret band shifted from 426 to 432 nm, whereas the **PBI** absorption band shifted from 509 to 514 nm. Similar red shifts were also observed for **ON11**:**ON12**. The UV-vis spectra of **ON8**:**ON10** and **ON11**:**ON12** did not coincide with the simple sum of the spectra of each strand.

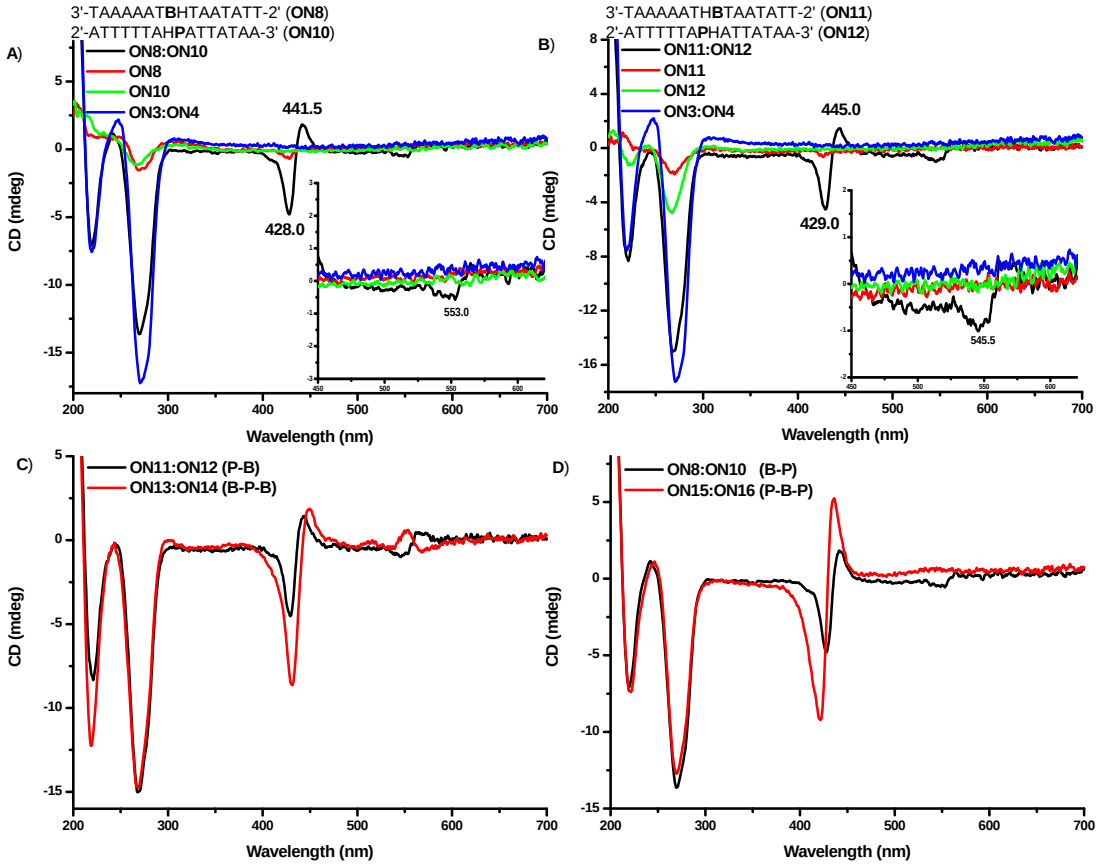

Figure 5.5 CD spectra of modified GNA duplexes and their corresponding single strands. (A) **ON8**, **ON10**, **ON8**:**ON10**, and **ON3**:**ON4**. (B) **ON11**, **ON12**, **ON11**:**ON12**, and **ON3**:**ON4**. (C) **ON11**:**ON12** and **ON13**:**ON14**. (D) **ON8**:**ON10** and **ON15**:**ON16**. The inset shows the expanded **PBI** absorption region. Conditions: 10 mM sodium phosphate, 100 mM NaCl, pH 7.0, and 12 μM of each strand.

Aside from the red-shifted absorption band, both **ON8**:**ON10** and **ON11**:**ON12** containing **B-P** showed bisignate CD spectra with a major negative peak in the porphyrin Soret band and a weak signal in the **PBI** region (Figure 5.5A and B). Typical for a porphyrin-modified DNA system, an induced negative Cotton effect in the Soret region is a signature of the intercalation of the porphyrin moiety into the DNA duplex.[8] Together with the T_m data, we therefore believe the porphyrin rings intercalate into the GNA duplex and stack to neighboring base pairs due to the π-π stacking interaction of **B** and **P**.

These spectroscopic behaviors demonstrate that **B** and **P** in the heteroaggregates interacted with each other and had different spectroscopic properties from those in the monomeric states. This statement was further supported by the increased intensities of

the bisignate CD spectra in the Soret bands of **ON13**:**ON14** and **ON15**:**ON16**, resulting from the π-π stacking interaction in sandwich-like aggregates **B**-**P**-**B** or **P**-**B**-**P** (Figure 5.5C and D).

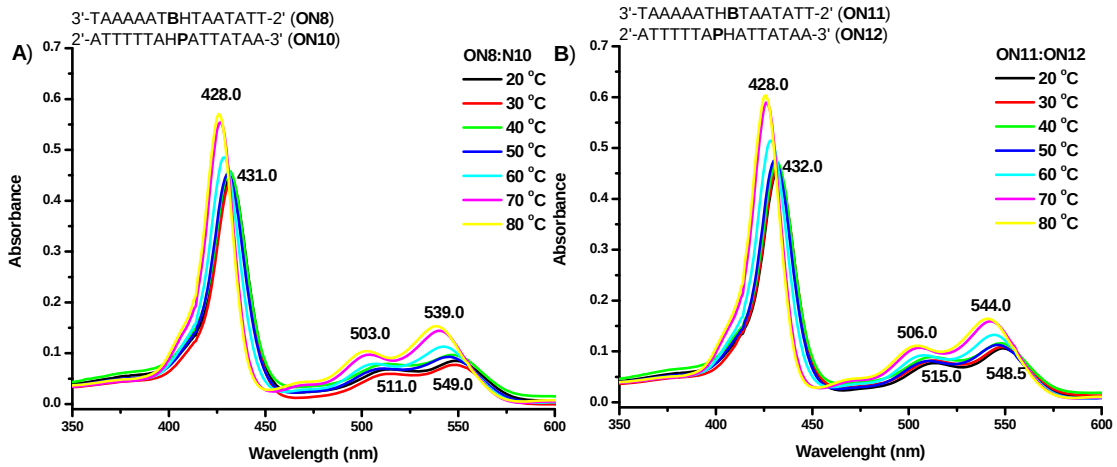

Figure 5.6 Temperature-dependent UV-vis spectra of GNA duplexes at the porphyrin Soret band and the **PBI** absorption band region. (A) **ON8**:**ON10**. (B) **ON11**:**ON12**. Conditions: 10 mM sodium phosphate, 100 mM NaCl, pH 7.0, and 2 μM of each strand.

The influence of temperature on the UV-vis spectra of the duplexes was analyzed next. As shown in Figure 5.6, heating from 20 to 80 °C resulted in the gradual shift of the absorption band to a shorter wavelength. At 70 °C, which is higher than the melting temperature T_m of **ON8**:**ON10** and **ON11**:**ON12**, the spectra almost coincided with the simple sum of the two individual spectra of their corresponding single strands. This shift could be explained by the dissociation of the duplexes into their single strands (porphyrin and **PBI** moieties), leading to no interaction.

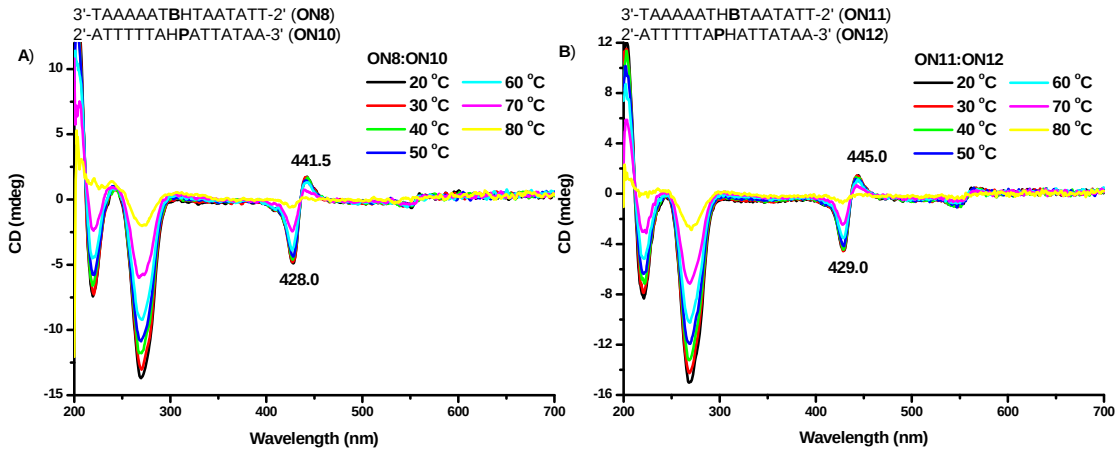

Figure 5.7 Temperature-dependent CD spectra of GNA duplexes. (A) **ON8**:**ON10**. (B) **ON11**:**ON12**. Conditions: 10 mM sodium phosphate, 100 mM NaCl, pH 7.0, and 12 μM of each strand.

Concurrently, in the CD spectra of **ON8**:**ON10** and **ON11**:**ON12**, the peaks gradually disappeared (Figure 5.7). This disappearance was illustrated by the loss of helicity due to denaturation, whereas the **PBI** and porphyrin moieties, as in two separate strands, lost their interaction.

Overall, these spectroscopic behaviors combined with the melting temperature data demonstrated the π-π stacking interaction of porphyrin and **PBI** in GNA.

Conformation of heteroaggregates

Subsequently, the absorption spectra of the duplexes containing more than two chromophores and their corresponding single strands were investigated. Figure 5.8 demonstrates similar red shifts in the absorption bands of the chromophores upon duplex formation. Table 5.3 reveals that **ON25**:**ON26** containing **P**-**B**-**P**-**B**-**P** had the largest red shift of 19 nm in the porphyrin Soret band and 12 nm red shift in the **PBI** absorption, which could be associated with an increase in the aggregation number.

Table 5.3 Absorption data of porphyrin Soret and **PBI** absorption bands in modified GNA as single and double strands.[a]

Entry	Absorbance of Soret band (nm)	Red-shift (**P**) (nm)	Absorbance of **B** band (nm)	Red-shift (**B**) (nm)
ON8			509.0, 547.5	
ON10	426.0			
ON8:**ON10**	432.0	6.0	513.5, 549.0	4.5
ON11	428.0			
ON12			506.0, 544.0	
ON11:**ON12**	432.0	4.0	515.0, 548.5	9.0
ON13	424.0			
ON14			505.5, 546.0	
ON13:**ON14**	432.0	8.0	509.0, 547.0	3.5
ON15			504.5, 542.0	
ON16	409.0			
ON15:**ON16**	424.0	15.0	544.0	2.0
ON17	408.0			
ON18			505.0, 545.0	
ON17:**ON18**	424.0	16.0	509.0, 548.0	4.0
ON19			505.0, 547.0	
ON20	409.0			
ON19:**ON20**	424.0	15.0	509.0, 548.0	4.0
ON23			505.0, 546.0	
ON24	404.0			
ON23:**ON24**	423.0	19.0	517.0, 553.0	12.0

[a]Conditions: 10 mM sodium phosphate, 100 mM NaCl, and 2 μM individual strand.

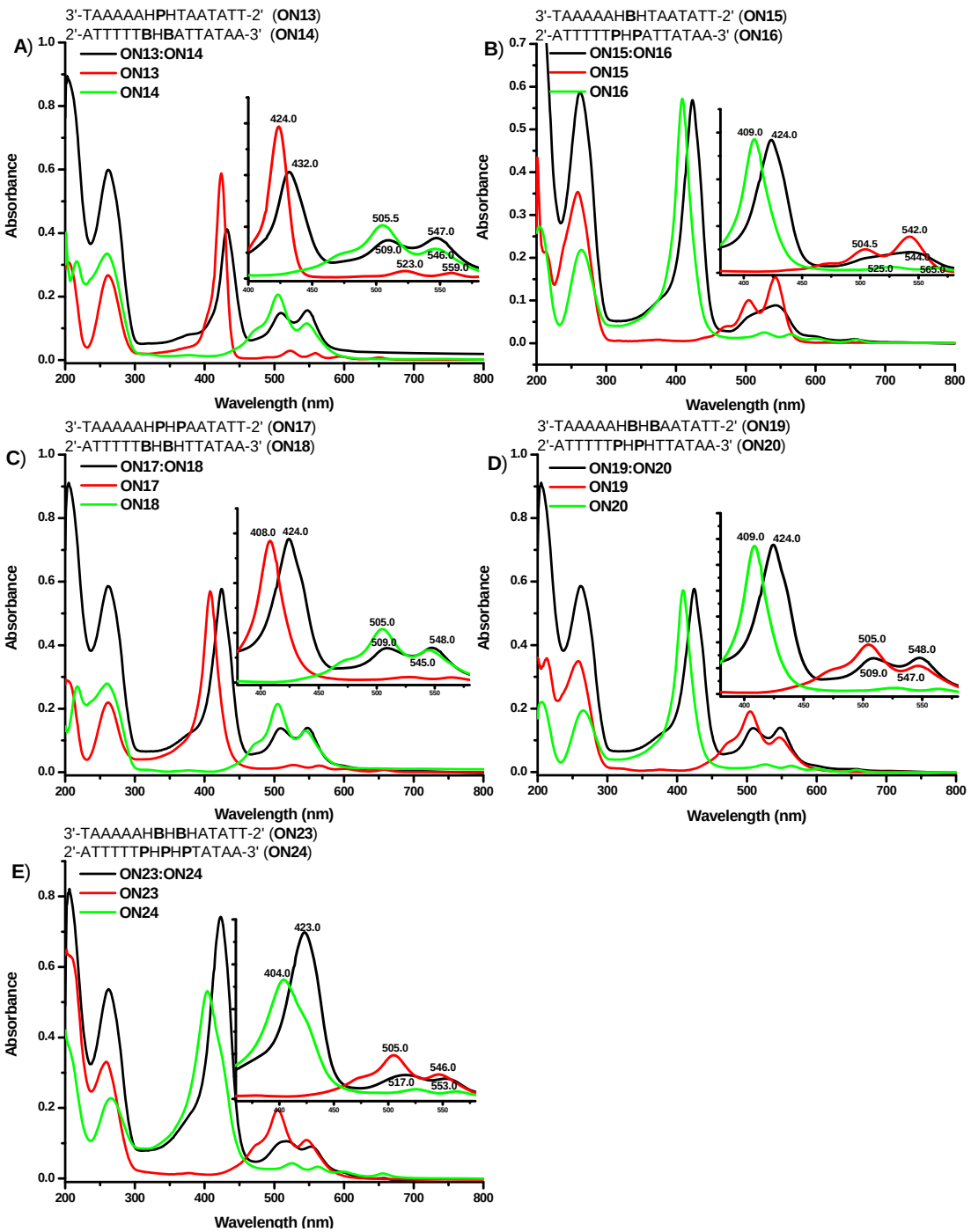

Figure 5.8 UV-vis spectra of GNA duplexes and their corresponding single strands. (A) **ON13**, **ON14,** and **ON13**:**ON14**. (B) **ON15**, **ON16,** and **ON15**:**ON16**. (C) **ON17**, **ON18,** and **ON17**:**ON18**. (D) **ON19**, **ON20,** and **ON19**:**ON20**. (E) **ON23**, **ON24,** and **ON23**:**ON24**. The inset shows the expanded porphyrin Soret and **PBI** absorption bands. Conditions: 10 mM sodium phosphate, 100 mM NaCl, pH 7.0, and 2 μM of each strand.

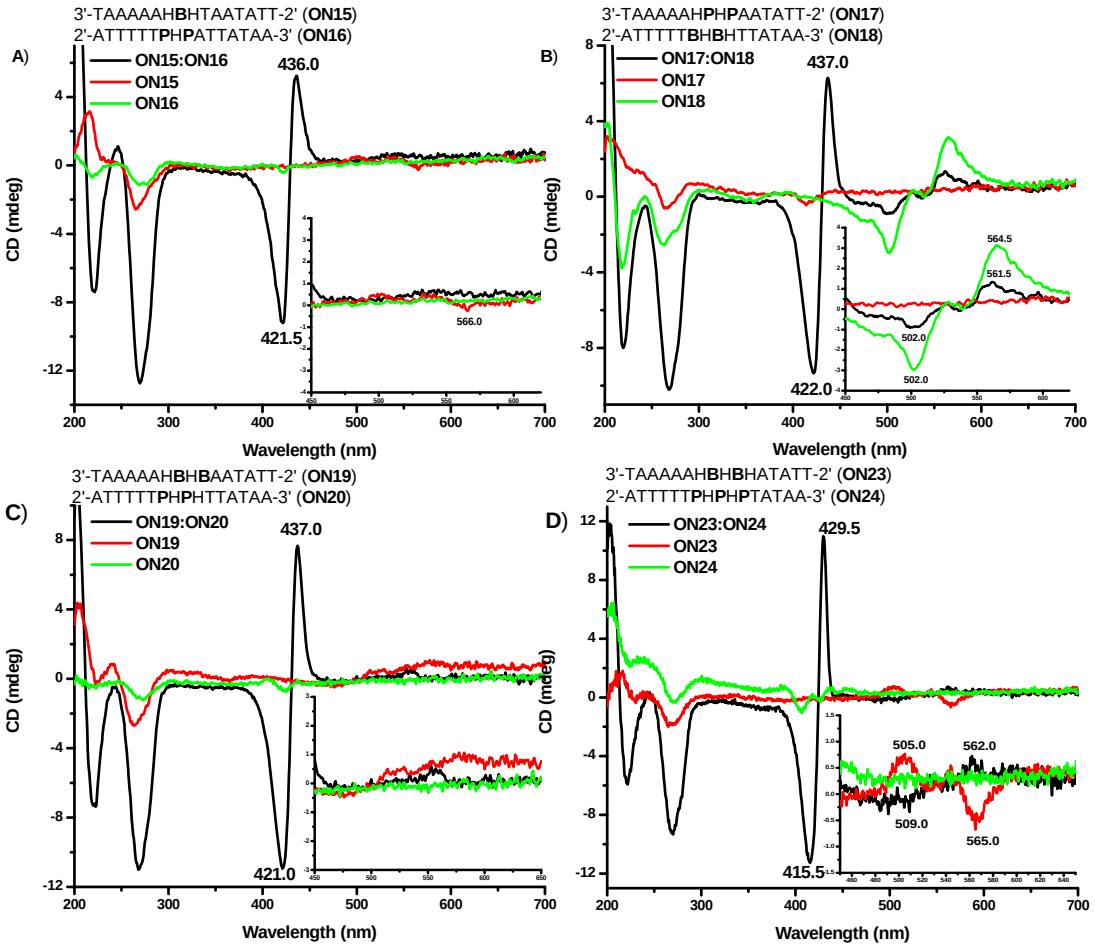

Figure 5.9 CD spectra of GNA duplexes and their corresponding single strands. (A) **ON15**, **ON16**, and **ON15**:**ON16**. (B) **ON17**, **ON8**, and **ON17**:**ON18**. (C) **ON19**, **ON20**, and **ON19**:**ON20**. (D) **ON23**, **ON24**, and **ON23**:**ON24**. The inset shows the expanded **PBI** absorption region. Conditions: 10 mM sodium phosphate, 100 mM NaCl, pH 7.0, and 12 μM of each strand.

The CD spectra of the modified duplexes containing more than two chromophores were next investigated. Figure 5.9 shows the obvious bisignate CD spectra in the Soret band of porphyrin upon duplex formation. The peak intensity of the bisignate CD signal gradually increased with the increased amount of porphyrin nucleobases in the duplex. Figure 5.9D illustrates that **ON23**:**ON24**, which contains **P**-**B**-**P**-**B**-**P**, had a very classic bisignate CD signal. The intensity of the positive peak was almost equal to the negative peak.

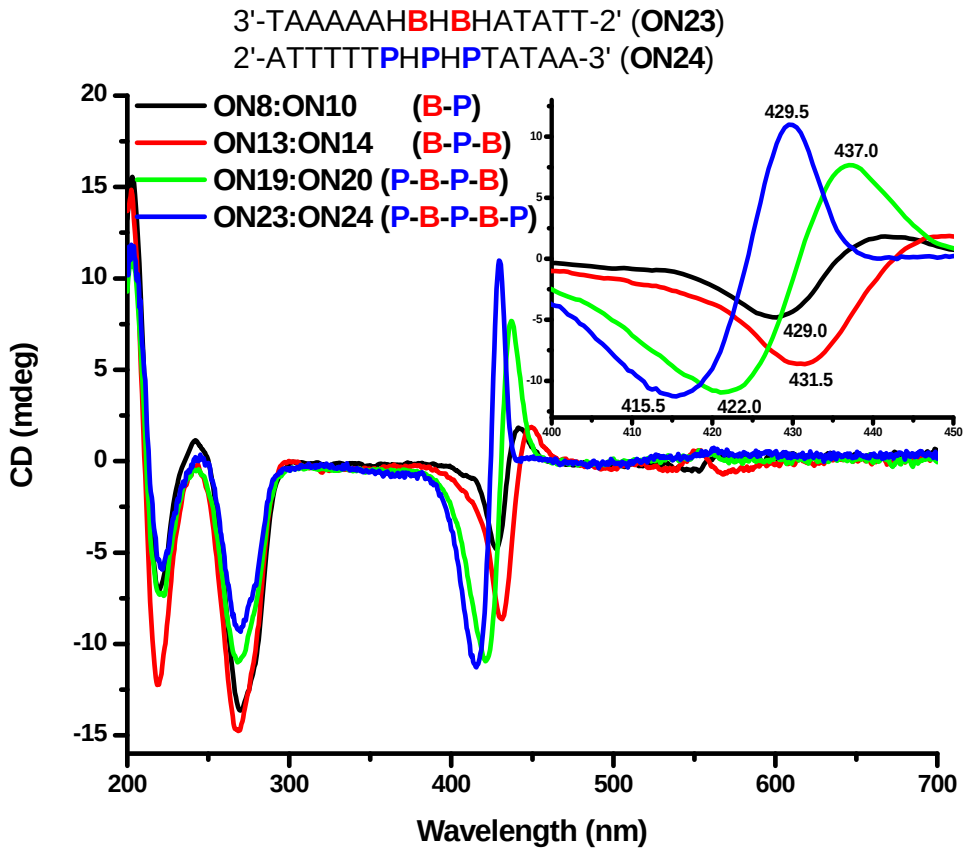

Figure 5.10 CD spectra of GNA duplexes the **ON8**:**ON10**, **ON13**:**ON14**, **ON19**:**ON20**, and **ON23**:**ON24**. Conditions: 10 mM sodium phosphate, 100 mM NaCl, pH 7.0, and 12 μM of each strand. The insets show the expanded porphyrin Soret band region.

The intensity of the CD signal accompanying the blue-shift of the bisignate CD spectra in the Soret band increased with the increased amount of chromophore moieties (Figure 5.10). Generally, a continuous shift in a CD spectrum with increased amounts of chromophores (without a sudden major change in shape) indicates highly ordered helical structures.[9] Therefore, together with the melting temperature and the UV-vis data, we propose that the aggregate **P-B-P-B-P** in **ON23**:**ON24** was highly organized in a zipper-like arrangement.

Chapter 5.2.3 Effect of natural bases on arrangement

As described in chapter 5.2.2, a zipper-like **P-B-P-B-P** interstrand stacking array stabilized the duplex by an additional 25 °C, which prompted us to construct hecial array composed of **B** and **P** with less natural base pairs. At the initial stage, to test the recognition ability of **P** and **B** based on interstrand π-π stacking in short duplex, the amount of natural base pairs in the modified duplexes was decreased to four. A 7mer duplex **ON21**:**ON22** and a 9mer duplex **ON29**:**ON30** were synthesized based on **ON15**:**ON16** and **ON23**:**ON24** (Table 5.4), respectively.

Table 5.4 Presentation of functionalized GNA strands used in this chapter.

Entry	GNA duplex	
1	3′-TAAAAA**HBH**TAATATT-2′	(**ON15**)
	2′-ATTTTT**PHP**ATTATAA-3′	(**ON16**)
2	3′-AA**HBH**TA-2′	(**ON21**)
	2′-TT**PHP**AT-3′	(**ON22**)
3	3′-TAAAAA**HBHBH**ATATT-2′	(**ON23**)
	2′-ATTTTT**PHPHP**TATAA-3′	(**ON24**)
4	3′-AA**HBHBH**AT-2′	(**ON29**)
	2′-TT**PHPHP**TA-3′	(**ON30**)

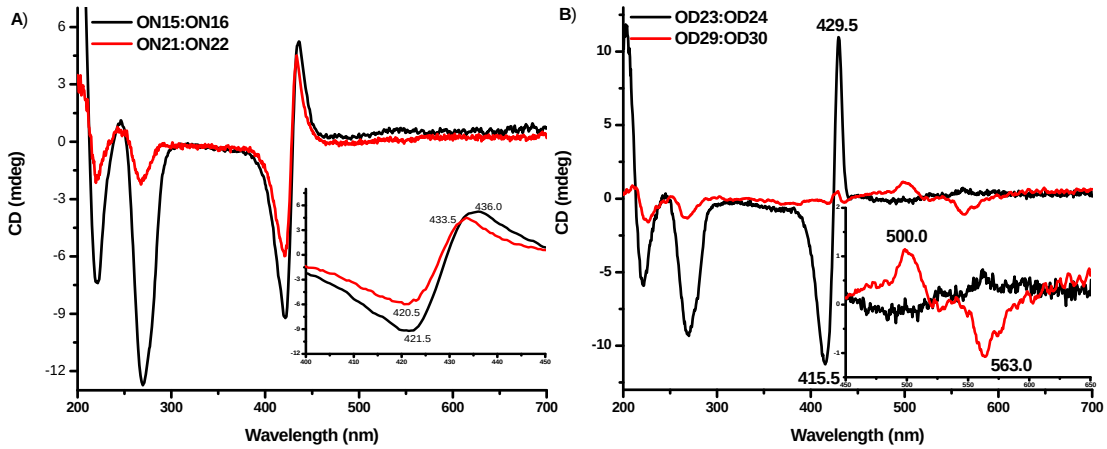

Figure 5.11 CD spectra of GNA strands. (A) **ON15**:**ON16** and **ON21**:**ON22**. (B) **ON23**:**ON24** and **ON29**:**ON30**. Conditions: 10 mM sodium phosphate, 100 mM NaCl, pH 7.0, and 12 μM of each strand.

As expected, the CD signals intensity of **ON21**:**ON22** in the GNA absorption was much lower than that of **ON15**:**ON16** (Figure 5.11A), there are only 4 natrual base

pairs in duplex. However, the intensity of CD signals of **ON21**:**ON22** in the Soret band was only slight lower of **ON15**:**ON16**. Accordingly, the conformation of **P-B-P** in **ON15**:**ON16** may be retained in **ON21**:**ON22**.

Figure 5.11B shows the CD spectra of **ON29:ON30**. In the porphyrin Soret band region, there is almost no bisignate CD signal, indicating there is no helical conformation of **P-B-P-B-P**. This revealed that natural bases played an important role in the formation of chromophore helical array and a certain amount of natural base pairs is needed for the formation of the helical array.

To explore the effect of natural bases on the **P** and **PBI** arrangements, the "duplexes" listed in Table 5.5 were synthesized and analyzed. Mixtures of modified strands with equal amounts of **P** and **B** moieties but with different natural bases were investigated by CD spectrometry to illustrate the conformation of **P-B-P-B-P**.

Table 5.5 Presentation of GNA strands used to study the effect of natural bases on the porphyrin and **PBI** arrangements.

Entry	Mixtures of GNA strands		Bisignate CD spectra in Soret band	T_m*[°C][a]
1	3′-TAAAAA**HBHBH**ATATT-2′ 2′-ATTTTT**PHPHP**TATAA-3′	(**ON23**) (**ON24**)	(–/+)	79
2	3′-TAAAAA**HBHBH**ATATT-2′ 2′-TT**PHPHP**TA-3′	(**ON23**) (**ON30**)	(–/+)	50
3	3′-AA**HBHBH**AT-2′ 2′-ATTTTT**PHPHP**TATAA-3′	(**ON29**) (**ON24**)	(–/+)	50
4	3′-AA**HBHBH**AT-2′ 2′-TT**PHPHP**TA-3′	(**ON29**) (**ON30**)	No	
5	3′-**HBHBC$_3$**-2′ 2′-**C$_3$PHPHP**-3′	(**ON34**) (**ON31**)	×	
6	3′-AA**HBHBH**AT-2′ 2′-**C$_3$PHPHP**-3′	(**ON29**) (**ON31**)	×	
7	3′-**HBHBC$_3$**-2′ 2′-TT**PHPHP**TA-3′	(**ON34**) (**ON30**)	(+/–)	50
8	3′-**HBHBC$_3$**-2′ 2′-ATTTTT**PHPHP**TATAA-3′	(**ON34**) (**ON24**)	(+/–)	45

*See details in the next chapter.

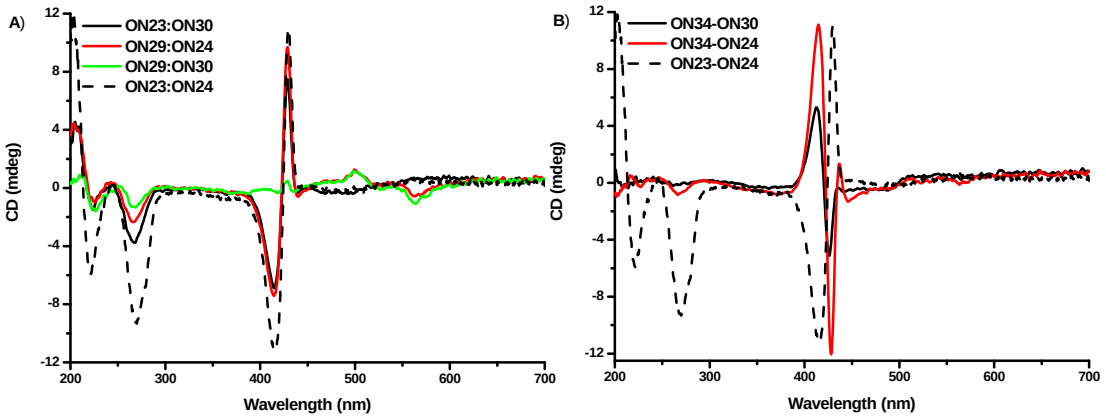

Figure 5.12 CD spectra of mixtures of GNA strands. Conditions: 10 mM sodium phosphate, 100 mM NaCl, pH 7.0, and 12 μM of each strand. (A) **ON23**:**ON30**, **ON29**:**ON24**, **ON29**:**ON30**, and **ON23**:**ON24**. (B) **ON34**:**ON30**, **ON34**:**ON24,** and **ON23**:**ON24**.

Interestingly, as shown in Figure 5.12A, **ON23**:**ON30** or **ON29**:**ON24** containing a natural overhang in one strand displayed a similar bisignate CD spectra (–/+) in the Soret band compared with **ON23**:**ON24**.

The possibility of a pure **P-B-P-B-P** array existing without the assistance of flanking natural base pairs was also investigated. Unfortunately, a porphyrin-GNA strand **ON31**without the natural base cannot be purified given its poor water solubility. However, Figure 5.12B shows that **ON34**:**ON30** or **ON34**:**ON24** exhibited an opposite bisignate CD signal (+/–) in the porphyrin Soret band although there were no flanking natural base pairs. This result suggested a different aggregation of **P-B-P-B-P** compared with **ON23**:**ON24**.

Overall, flanking natural base pairs or natural overhangs play a key role in affording helical structures. This was consistent with the report of Leumann et al., where they demonstrated that a few natural base pairs at the end of the duplex DNA is apparently required to align two strands in a defined structural register and to prevent undefined aggregation.[9] In addition, the conformation of porphyrin and **PBI** aggregates could be switched by adjusting natural overhangs in a GNA strand, although the function of this switching is still unknown.

Thermal stability of chromophore helical array

It is necessary to obtain the thermal stability of chromophore helical array. Unfortunately, our attempt to monitor the changes in absorbance upon heating at 260 nm failed to offer T_m of such chromophore array, because the low hyperchromicity of the short duplex with few natural base pairs. However, Figure 5.13 shows obvious changes in the Soret band of short duplexes upon heating from 10 °C to 90 °C, which give access to investigate the thermal stabilities of those arrays through monitoring the temperature-dependent changes in CD absorbance at porphyrin Soret band.

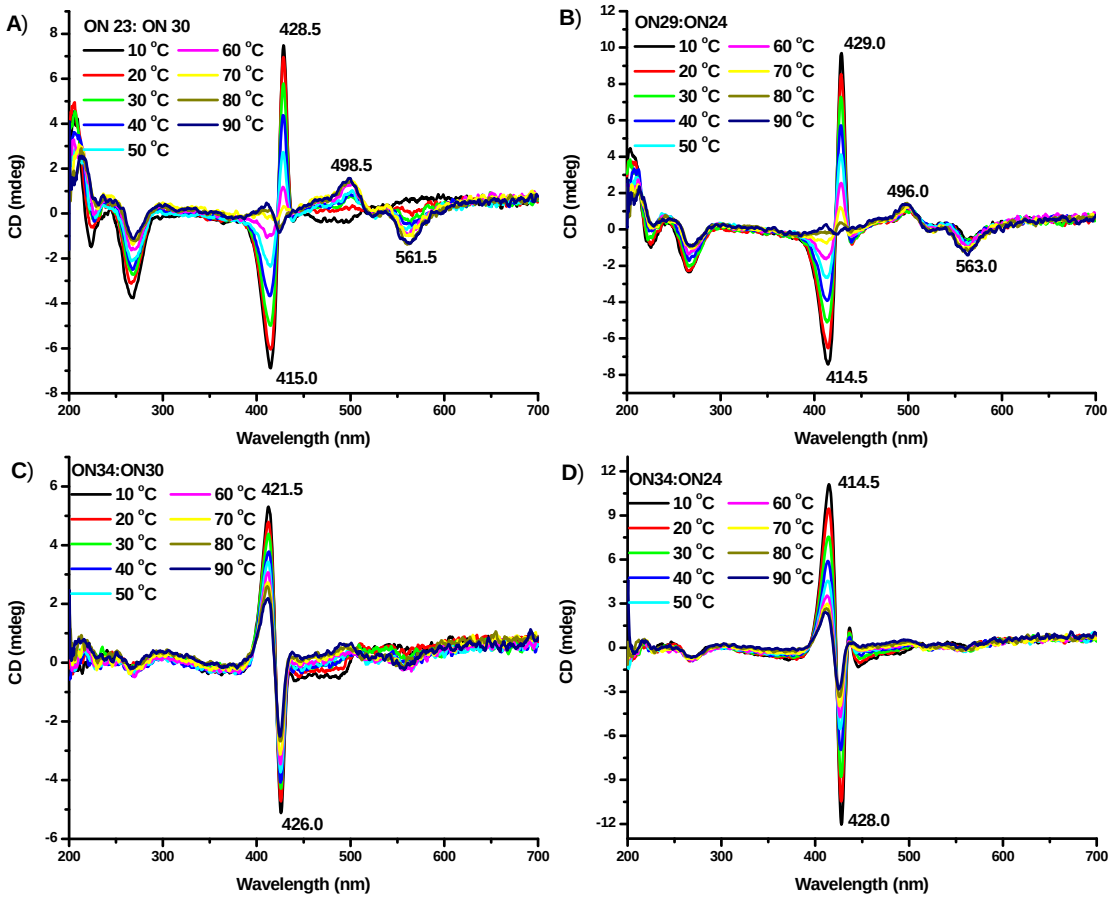

Figure 5.13 Temperature-dependent CD spectra of chromophore helical arrays. A) **ON23**:**ON30**; B) **ON29**:**ON24**; C) **ON34**:**ON30**; D) **ON34**:**ON24**. Conditions: 10 mM sodium phosphate, 100 mM NaCl, pH 7.0, and 12 μM of each strand.

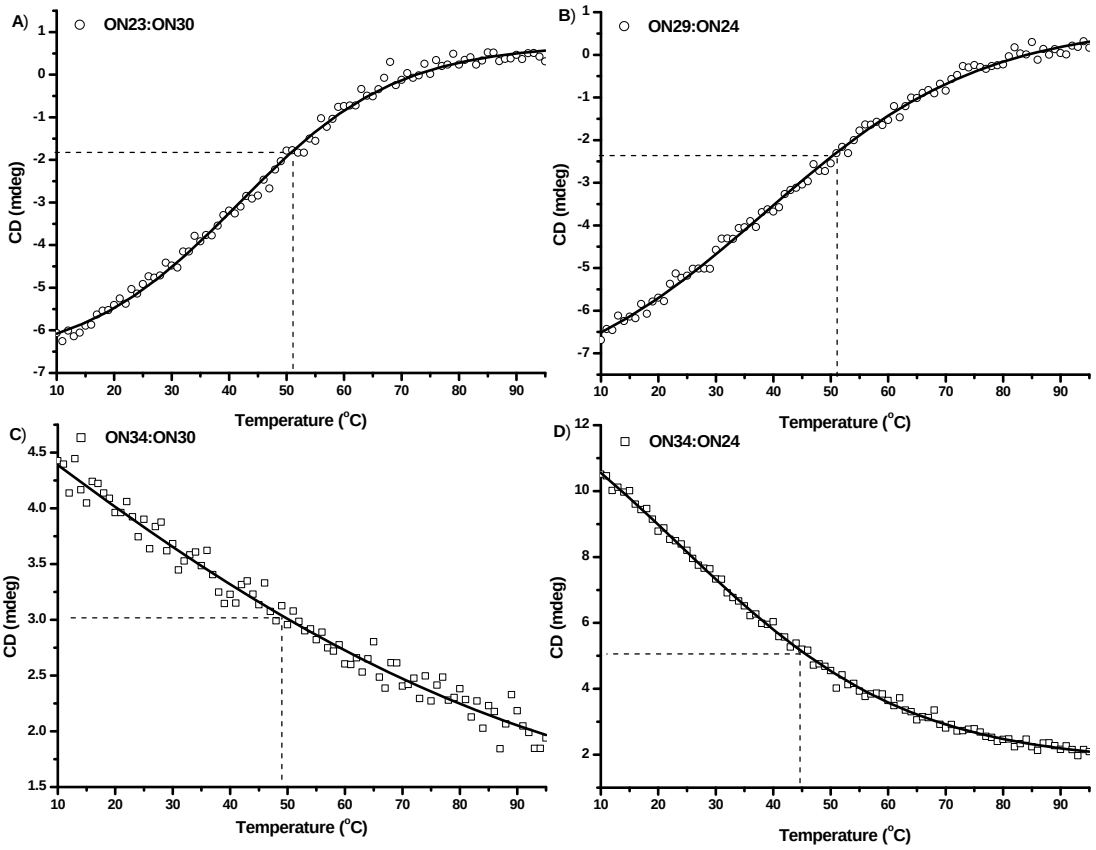

Figure 5.14 Melting curves of chromophore helical array. Temperature-dependent changes in CD absorbance as monitored at porphyrin Soret band. *Conditions (T_m*): 10 mM sodium phosphate, 100 mM NaCl, pH 7.0, and 12 μM of each strand. A) **ON23**:**ON30**; B) **ON29**:**ON24**; C) **ON34**:**ON30**; D) **ON34**:**ON24**.

The thermal stabilities of **ON23**:**ON30**, **ON29**:**ON24**, **ON34**:**ON30** and **ON34**:**ON24** were investigated by temperature-dependent CD spectrometry. The melting curves were obtained by monitoring changes in CD absorbance of porphyrin Soret band. As shown in Figure 5.14, the melting curves suggested that the melting point of those chromophore helical array ranged from 45 to 50 ^{o}C, thus dominated the stabilities of **ON23**:**ON30**, **ON29**:**ON24**, **ON34**:**ON30** and **ON34**:**ON24** at room temperature.

Crystallography of modified GNA duplexes

To understand better the conformation of porphyrin and **PBI** based on the GNA backbone, we attempted to obtain the crystals of the modified GNA duplexes listed Table 5.5.

The purification of the GNA oligonucleotides for crystallization was generally followed by desalting over Sep-Pak C18 columns in order to remove residual buffer and/or excess metal cations. After desalting, a single strand GNA was concentrated and then redissolved in water to prepare a 2 mM stock solution. The GNA duplex samples were prepared as a 1 mM stock solution (considering the poor water solubility of porphyrin-GNA strands), and were then denatured on a thermal heater. After cooling down to room temperature, the stock solution was finally filtered to remove insoluble particles.

Afterward, the oligonucleotide stock solution was placed in a 4 °C cold room for several hours prior to use. The coldness ensured the equilibration of the solution.

Crystallization buffers were obtained using the Nucleic Acid Mini Screen (Hampton Research, HR2-118). This screen consisted of 24 buffers with various pH, salt, and polyamine conditions. The crystallization buffers were also equilibrated (by storage in a cold room) at 4 °C overnight to reduce temperature fluctuation during the crystallization setup. The hanging drop vapor diffusion technique was initially used for crystallization. The sitting drop vapor diffusion method was later used because of its easier procedure.

Finally, the modified GNA duplex stock solution (2 μL) was mixed with the crystallization buffers (2 μL) at 4 °C. The mixture was equilibrated against a well of 35% 2-methyl-2,4-pentanediol (1 mL) after the plate was sealed with a clear, transparent tape.

Unfortunately, our attempt to crystallize the modified GNA duplex samples in a buffer failed. No crystal was obtained from the system because the samples easily precipitated directly from the buffer within half an hour at 4 °C. Crystallization at lower duplex concentrations (0.25 and 0.125 mM) was also tried, but to no avail.

Chapter 5.3 Conclusions

In this chapter, GNA duplexes containing two different chromophores such as **B-Pyr**, **B-Pyr′**, **B-Pe′** and **B-P** were investigated. Porphyrin (**P**) and **PBI** (**B**) stabilized the GNA duplex most significantly among all the tested chromophores. Accordingly, a zipper-like **P-B-P-B-P** was organized in the middle of a 16mer duplex GNA, which was examined by UV-vis and CD spectrometry. Flanking natural base pairs and natural overhangs helped chromophores to form a helical conformation in GNA duplex. Future works will be focused on the light harvesting and charge transport of porphyrin and **PBI** in GNA.

Chapter 5.4 Experimental

GNA oligonucleotide synthesis and purification

All the oligonucleotides were prepared on an ABI 394 DNA/RNA synthesizer on a 1 micromole scale according to previous method. After the steps of detritylation and purification, the identities of all oligonucleotides were confirmed by MALDI–TOF MS (Table 5.6).

Thermal denaturation

The melting studies were carried out in 1 cm path length quartz cells (total volume 325 μL; 200 μL sample solutions were covered by mineral oil) on a Beckman 800 UV-VIS spectrophotometer equipped with a thermo-programmer. Melting curves were monitored at 260 nm with a heating rate of 1 ^{o}C/min. Melting temperatures were calculated from the first derivatives of the heating curves. Experiments were performed in duplicate and mean values were taken.

CD spectroscopy

CD measurements were performed on a JASCO J-810 spectrometer in a 1 mm path length quartz cuvette. The GNA single strands or duplexes were prepared in 10 mM sodium phosphate, 100 mM NaCl, pH 7.0, and the concentration of each strand was 8 μM. Each measurement was repeated 5 times and the average taken.

Table 5.6 MALDI-TOF MS data of used GNA oligonucleotides.

Name	Oligonucleotides	M_{calcd}	M_{found}
ON 1	3′-TAAAAATTAATATT-2′	3951.5($C_{120}H_{157}N_{57}O_{70}P_{14}$)	3949.3
ON 2	3′-AATATTAATTTTTA-2′	3924.5($C_{120}H_{160}N_{48}O_{76}P_{14}$)	3923.2
ON 3	3′-TAAAAATAATAATATT-2′	4222.7($C_{128}H_{167}N_{62}O_{74}P_{15}$)	4223.3
ON 4	3′-AATATTATTATTTTTA-2′	4186.6($C_{128}H_{171}N_{50}O_{82}P_{15}$)	4185.5
ON 6	3′-AATATTAPyrHATTTTTA-2′	$C_{134}H_{171}N_{46}O_{78}P_{15}$(4136.7)	4137.7
ON 7	3′-AATATTAPyr′HATTTTTA-2′	$C_{135}H_{169}N_{46}O_{78}P_{15}$(4146.7)	4147.1
ON 8	3′-TAAAAATBHTAATATT-2′		
ON 9	3′-AATATTAPe′HATTTTTA-2′	4198.8($C_{139}H_{171}N_{46}O_{78}P_{15}$)	4198.2
ON 10	3′-AATATTAPHATTTTTA-2′	4408.9($C_{151}H_{181}N_{50}O_{78}P_{15}$)	4416.9
ON 11	3′-TAAAAATPHTAATATT-2′	4427.0($C_{151}H_{179}N_{56}O_{74}P_{15}$)	4434.2
ON 12	3′-AATATTABHATTTTTA-2′		
ON 13	3′-TAAAAAHPHTAATATT-2′	4288.8($C_{145}H_{173}N_{54}O_{72}P_{15}$)	4289.5
ON 14	3′-AATATTABHBTTTTTA-2′		
ON 15	3′-TAAAAAHBHTAATATT-2′		
ON 16	3′-AATATTAPHPTTTTTA-2′	6027.0($C_{199}H_{242}N_{77}O_{104}P_{21}$)	6025.8
ON 17	3′-TAAAAAHPHPAATATT-2′	6008.9($C_{199}H_{244}N_{71}O_{108}P_{21}$)	6006.6
ON 18	3′-AATATTHBHBTTTTTA-2′		
ON 19	3′-TAAAAAHBHBAATATT-2′		
ON 20	3′-AATATTHPHPTTTTTA-2′	4613.3($C_{174}H_{193}N_{44}O_{78}P_{15}$)	4613.6
ON 21	3′-AAHBHTA-2′	1948.4($C_{71}H_{83}N_{19}O_{35}P_6$)	1949.3
ON 22	3′-TAPHPTT-2′	2364.9($C_{108}H_{103}N_{19}O_{32}P_6$)	2366.4
ON 23	3′-TAAAAAHBHBHATATT-2′	4630.2($C_{164}H_{192}N_{47}O_{84}P_{15}$)	4631.5
ON 24	3′-AATATPHPHPTTTTTA-2′	4973.7($C_{203}H_{209}N_{46}O_{76}P_{15}$)	4975.7
ON 25	3′-TAAAAAHBBHAATATT-2′	4777.3($C_{170}H_{197}N_{52}O_{84}P_{15}$)	4778.4
ON 26	3′-AATATTPHHPTTTTTA-2′	4613.3($C_{174}H_{193}N_{44}O_{78}P_{15}$)	4614.5
ON 27	3′-TAAAAAHPPHAATATT-2′	4649.3($C_{174}H_{189}N_{56}O_{70}P_{15}$)	4650.5
ON 28	3′-AATATTBHHBTTTTTA-2′	4741.2($C_{170}H_{201}N_{40}O_{92}P_{15}$)	4740.5
ON 29	3′-AAHBHBHAT-2′	2759.0($C_{108}H_{119}N_{21}O_{50}P_8$)	2760.4
ON 30	3′-ATPHPHPTT-2′	3111.6($C_{147}H_{135}N_{23}O_{40}P_8$)	3110.7
ON 31	3′-HBHBC$_3$-2′	1697.36($C_{77}H_{80}N_4O_{32}P_4$)	1697.3

(**ON8**, **ON12**, **ON14**, **ON15**, **ON18** and **ON19** were provided by Yonggang Xiang.)

Chapter 5.5 References

1. Bouquin, N.; Malinovskii, V. L.; Haner, R. *Chemical Communication* **2008**, 1974-1976.
2. (a) Giaimo, J. M.; Gusev, A. V.; Wasielewski, M. R. *Journal of the American Chemical Society* **2002**, *124*, 8530–8531. (b) Fuller, M. J.; Sinks, L E.; Rybtchinski, B.; Giaimo, J. M.; Li, X.; Wasielewski, M. R. *The Journal of Physical Chemistry A* **2005**, *109*, 970–975.
3. (a) Muthukumaran, K.; Schwartz, J. K.; Sazanovich, I. V.; Kirmaier, C.; Hindin, E.; Diers, J. R.; Taniguchi, M.; Bocian, D. F.; Holten, D.; Lindsey, J. S. *The Journal of Physical Chemistry B* **2003**, *107*, 3443–3454. (b) Muthukumaran, K.; Loewe, R. S.; Kirmaier, C.; Hindin, E.; Schwartz, J. K.; Sazanovich, I. V.; Diers, J. R.; Bocian, D. F.; Holten, D.; Lindsey, J. S. *The Journal of Physical Chemistry B* **2003**, 1*07*, 3431–3442.
4. (a) Brotschi, C.; Häberli, A.; Leumann, D. J. *Angewandte Chemie International Edition* **2001**, *40*, 3012-3014; (b) Brotschi, C.; Leumann, D. J. *Angewandte Chemie International Edition* **2003**, *42*, 1655-1658; (c) Brotschi, C.; Mathis, G.; Leumann, D. J. *Chemistry-A European Journal* **2005**, *11*, 1911-1923; (d) Zahn, A.; Leumann, C. J. *Chemistry-A European Journal* **2008**, *14*, 1087-1094; (e) Johar, Z.; Zahn, A.; Leumann, C. J.; Jaun, B. *Chemistry-A European Journal* **2008**, *14*, 1080-1086.
5. Kasha, M.; Rawls, H.R.; El-Bayoumi, M. A. *Pure and Applied Chemistry* **1965**, *11(3-4)*, 371-392.
6. Kashida, H.; Asanuma, H.; Komiyama, M. *Angewandte Chemie International Edition* **2004**, *43*, 6522-6525.
7. Bouquin, N.; Malinovskii, V. L.; Guegano, X.; Liu, S. X.; Decurtins, S.; Haner, R. *Chemistry-A European Journal* **2008**, *14*, 5732-5736.
8. (a) McMillin, D. R.; Shelton, A. H.; Bejune, S. A.; Fanwick, P. E.; Wall, R. K. *Coordination Chemistry Review* **2005**, *249(13-14)*, 1451; (b) Nitta, Y.; Kuroda, R.

Biopolymers **2006**, *81*, 376.

9. Brotschi, C.; Mathis, G.; Leumann, D. J. *Chemistry-A European Journal* **2005**, *11*, 1911-1923.

Chapter 6 Photochemical Ligation of GNA via Anthracene Cyclodimer Formation

Chapter 6.1 Introduction

Anthracene is a polycyclic aromatic hydrocarbon consisting of three fused benzene rings. Due to their unique photophysical and photochemical properties, anthracenes have been used in DNA in serveal areas.

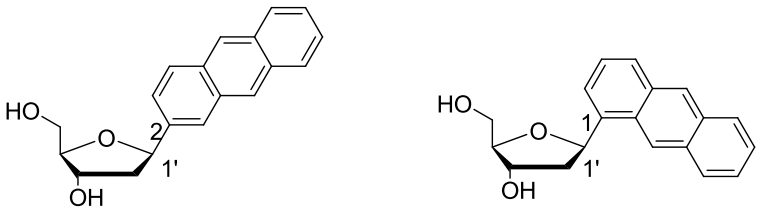

Figure 6.1 Artificial anthracene C-nucleosides.[4]

As efficient photosensitizers, anthracenes and their derivatives have been widely used as cleaving agents in the study of DNA photocleavage.[1] Nevertheless, the fluorescence characteristics of anthracene monomers and excimers have been explored in the development of potential probes for detecting single DNA base-pair mismatches[2] and single nucleotide polymorphisms.[3] Anthracenes have also been introduced into DNA as nonpolar artificial bases for the development of potential van der Waals probes (Figure 6.1).[4]

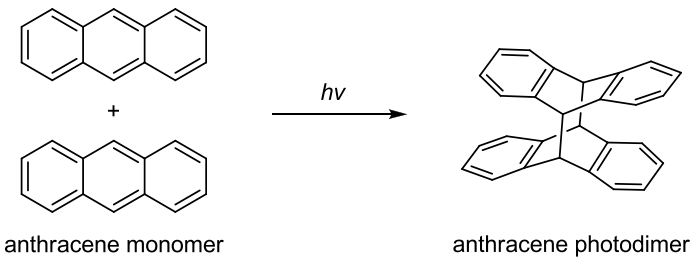

Figure 6.2 Photodimerization of anthracenes.[5]

Aside from the application for photosensitizer and probe, anthracenes had been used as a phototriggered joint for DNA. Two anthracenes are known to form a dimer by the [4π + 4π] photoreaction (Figure 6.2).[5] The photochemical properties of anthracenes are the base of their potential applications. Over the past several years,

anthracene cyclodimer formation has been applied in the DNA photoligation.[6] Ihara et al. investigated the photochemical ligation of DNA conjugates via the cycloaddition of anthracenes. Anthracene-DNA conjugates were synthesized by linking the 5′- or 3′-end of oligodeoxyribonucleotides to anthracene (1-, 2-, or 9-positions) using multi-methenylene linkers.[6] The use of such multi-methenylene linkers enables appropriate slacking in the chains, which is always required for efficient dimerization by the entropic demand in terms of statics.[6a] However, the cycloaddition of anthracenes without multi-methenylene linkers in interior of DNA was rarely investigated, probably due to inefficient dimerization of anthracenes in duplex DNA.

Considering the significantly decreased yield of modified GNA strand with multi-incorporated chromophores, photochemical ligation of GNA was developed in order to address this problem. In the chapter, we describe the incorporation of anthracenes as artificial bases into GNA and the photochemical ligation of GNA *via* anthracene cyclodimer formation.

Chapter 6.2 Results and Discussion

Chapter 6.2.1 Synthesis of anthracene-GNA

The propane-1,2-diol-modified anthracene building block (**An**) was selected to use in the ligation of GNA (Figure 6.3B), because the ligation of DNA conjugates with 2-substituted anthracenes have been reported to proceed more efficiently than that with 9-substituted anthracenes.[6f] The phosphoramidite **9a** was used to synthesize GNA strands with incorporated anthracene nucleotides (**An**, Figure 6.3A). The anthracene-GNA strands were prepared according to the previous method.

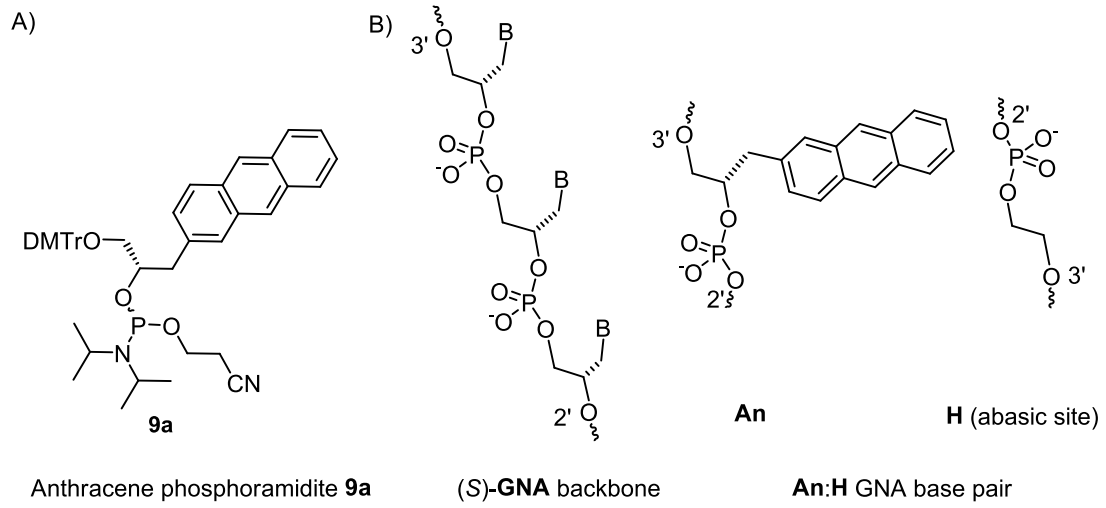

Figure 6.3 (A) Structure of anthracene phosphoramidite **9a**. (B) Constitution of the (*S*)-GNA backbone. **An**:**H** base pair used in the present study.

Chapter 6.2.2 Photochemical ligation of GNA

Subsequently, the photochemical ligation of GNA *via* anthracene cyclodimer formation was investigated in terms of three aspects, namely, template-supported GNA ligation, interstrand crosslinking in the middle of the GNA duplex, and end capping of the GNA duplex.

A. Template-supported GNA ligation

The structures and sequences of the GNA strands used in the present study are shown in Figure 6.4. **ON3** and **ON4** were 8-mer and 14-mer GNA nucleotides containing anthracene nucleotides on their 3′ and 2′ termini. The sequences of the strands were designed to be complementary to the neighboring sites of the template strand **ON2**. A pair of the strands were hybridized to the template with their anthracene units facing each other to form a tandem duplex. The model template **ON2** was a 22-mer sequence containing two adjacent abasic sites, which are supposed to offer the space for the anthracenes upon the formation of the tandem duplex.

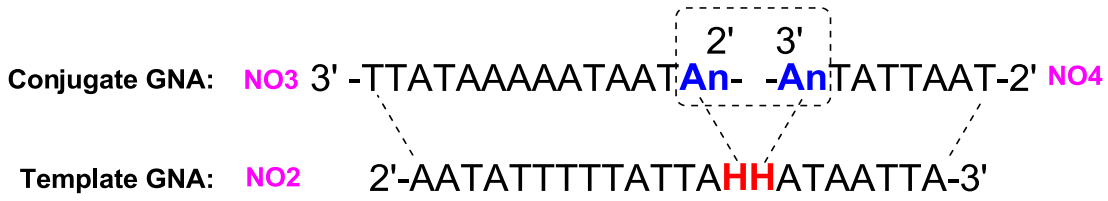

Figure 6.4 Structures and sequences of the conjugate and template GNAs used in the present study.

Table 6.1 Properties of the anthracene-containing GNA duplexes.[a]

Entry	Sequence		T_m (°C)	T_m (°C)*	Excimer
1	3′-TTATAAAAATAAT**An**A**n**TATTAAT-2′	(**ON1**)	52		Weak
	2′-AATATTTTTATTA**HH**ATAATTA-3′	(**ON2**)			
2	3′-**An**TATTAAT-2′	(**ON4**)	53	53	No
	3′-TTATAAAAATAAT**An**-2′	(**ON3**)			
	2′-AATATTTTTATTA**HH**ATAATTA-3′	(**ON2**)			

[a]Conditions: 10 mM sodium phosphate, 100 mM NaCl, and 2 μM individual strands. *After photoirradiation.

The thermal stabilities of the duplexes were first analyzed by UV melting experiments. Table 6.1 reveals that the T_m of the tandem duplex **ON4**:**ON3**:**ON2** (Table 6.1, entry 1) was only slightly higher than that of duplex **ON1**:**ON2** (Table 6.1, entry 2) by 1 °C.

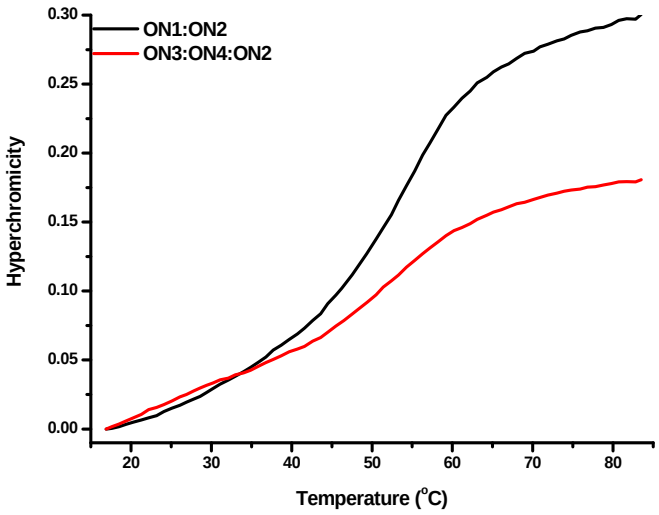

Figure 6.5 UV-melting curves of the GNA duplexes **ON1**:**ON2** and **ON3**:**ON4**:**ON2**. Changes in the absorbance upon heating were monitored at 260 nm. Conditions: 10 mM sodium phosphate, 100 mM NaCl, pH 7.0, and 2 μM of each strand.

Excimer formation is regarded as a prerequisite for the photodimerization of anthracenes,[6a] the fluorescence properties of the GNA strands containing anthracene were analyzed to explore whether the stacking anthracenes were formed in the tandem duplex **ON3**:**ON4**:**ON2**.

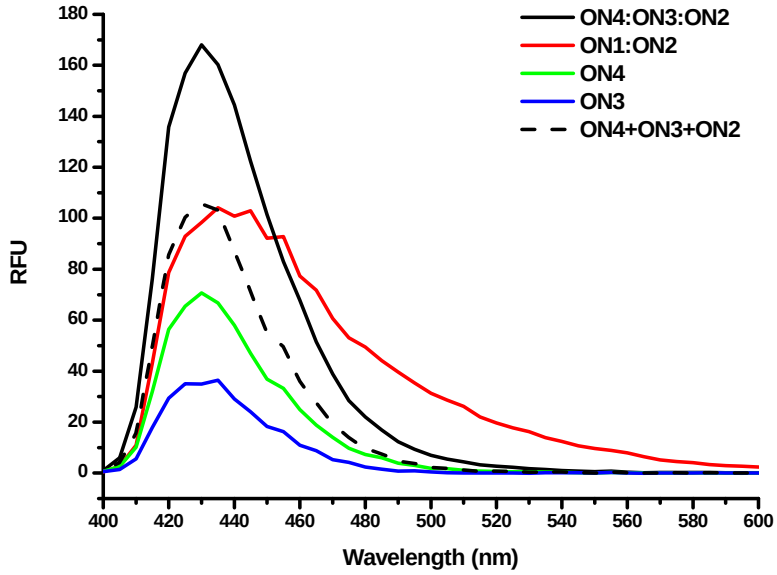

Figure 6.6 Fluorescence properties of anthracene nucleotides in GNA: **ON1:ON2**, **ON3:ON4:ON2**, **ON3**, and **ON4**. Conditions: 10 mM sodium phosphate, 100 mM NaCl, pH 7.0, and 2 μM of each strand of a duplex; excitation at 350 nm with a cutoff filter at 420 nm.

Upon excitation at 350 nm, duplex **ON1:ON2** containing two adjacent anthracene nucleobases in one strand yielded a weak fluorescence emission at around 500 nm (excimer emission). In contrast, the tandem duplex **ON4**:**ON3**:**ON2** only gave a strong fluorescence emission at 435 nm (regular emission), which was much higher in intensity than the simple sum of the spectra of each strand. This result together with the thermal stabilities might indicate no stacking of two anthracenes in the tandem duplex.

Although excimer emissions of anthracenes were not observed in the duplexes, the photochemical ligation of GNA in the tandem duplex **ON4**:**ON3**:**ON2** was examined. Solutions containing 8 μM GNA oligonucleotides of each strand were irradiated at 366 nm in an N_2 atmosphere at 0 °C for 3 min. A high-pressure mercury lamp equipped with longpass optical filters was used.

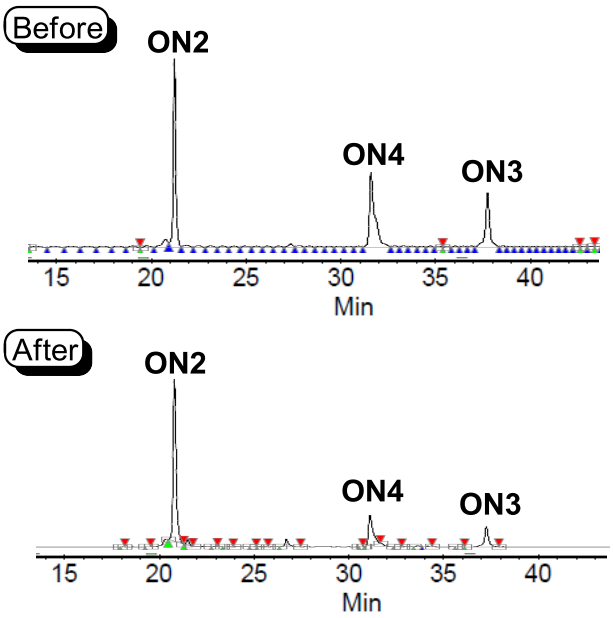

Figure 6.7 HPLC chromatograms of the reaction mixtures before and after 3 min of photoirradiation for the tandem duplex **ON3**:**ON4**:**ON2**. The chromatograms were obtained under the following conditions: Waters Xterra column (MS C18, 4.6 mm × 50 mm); solution A, 50 mM triethylamine-acetic acid buffer (pH 7); solution B, acetonitrile; linear gradient, 4%–20% in 40 min; flow rate, 1 mL/min.

The mixture of the photoreaction was analyzed by reversed-phase HPLC. Figure 6.7 shows the chromatograms of the reaction mixture for the tandem duplex **ON4**:**ON3**:**ON2** before and after photoirradiation. No new peak was observed in the chromatogram after photoirradiation, indicating no photochemical ligation of GNA in the tandem duplex. A new peak did not appear even after a prolonged irradiation time of 15 min.

B. Interstrand crosslinking in the middle of the GNA duplex

Anthracene nucleotides were introduced into the middle of a 16-mer GNA duplex. The duplexes **ON7**:**ON8** and **ON9**:**ON10** containing two adjacent anthracene nucleobases (Table 6.2, entries 2 and 3) were expected to form a hairpin structure as a result of the photoirradiation.

Table 6.2 reveals that duplexes **ON7**:**ON8** and **ON9**:**ON10** containing two adjacent anthracene nucleobases (Table 6.2, entries 2 and 3) yielded an overall low

melting temperature (T_m) of 31 and 35 °C, respectively, compared with 54 °C for an **A**:**T** base pair at the same position (Table 6.2, entry 1). On the other hand, duplexes **ON3**:**ON4** and **ON5**:**ON6** were stable at room temperature. Hence, they are suitable for use in the next studies.

Table 6.2 Thermal stabilities of the anthracene-containing GNA duplexes before and after photoirradiation.[a]

Entry	Sequence		T_m (°C)	T_m (°C)*
1	3′-TAAAAATAATAATATT-2′ 2′-ATTTTTATTATTATAA-3′	(**ON5**) (**ON6**)	54	
2	3′-TAAAAAT**HAn**TAATATT-2′ 2′-ATTTTTA**AnH**ATTATAA-3′	(**ON7**) (**ON8**)	31	72
3	3′-TAAAAAT**AnH**TAATATT-2′ 2′-ATTTTTA**HAn**ATTATAA-3′	(**ON9**) (**ON10**)	35	77
4	3′-TAAAAAT**HA**TAATATT-2′ 2′-ATTTTTA**AnH**ATTATAA-3′	(**ON11**) (**ON8**)	30	30
5	3′-TAAAAAT**AnH**TAATATT-2′ 2′-ATTTTTA**HT**ATTATAA-3′	(**ON9**) (**ON12**)	32	31

[a]Conditions: 10 mM sodium phosphate, 100 mM NaCl, and 2 μM individual strands. *After photoirradiation.

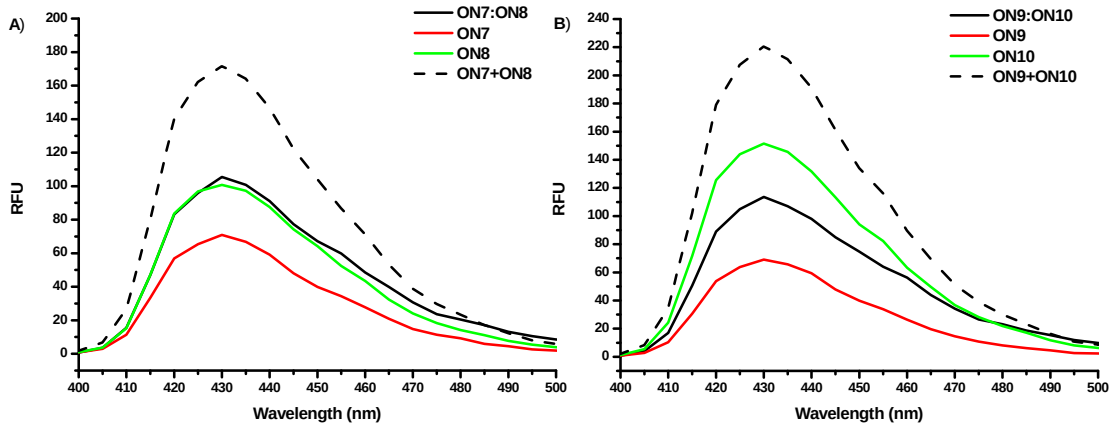

Figure 6.8 Fluorescence properties of anthracene nucleotides in GNA. Conditions: 10 mM sodium phosphate, 100 mM NaCl, pH 7.0, and 2 μM of each strand of a duplex (Table 6.2); excitation at 350 nm with a cutoff filter at 420 nm. (A) **ON7**, **ON8** and **ON7**:**ON8**. (B) **ON9**, **ON10** and **ON9**:**ON10**.

As shown in Figure 6.8, duplexes **ON7**:**ON8** and **ON9**:**ON10**, each containing two adjacent anthracene nucleobases, exhibited no excimer emission. However, they

showed much lower fluorescence intensity than the simple sum of the spectra of each strand, indicating the possible π-π stacking interactions of anthracenes in the duplexes.

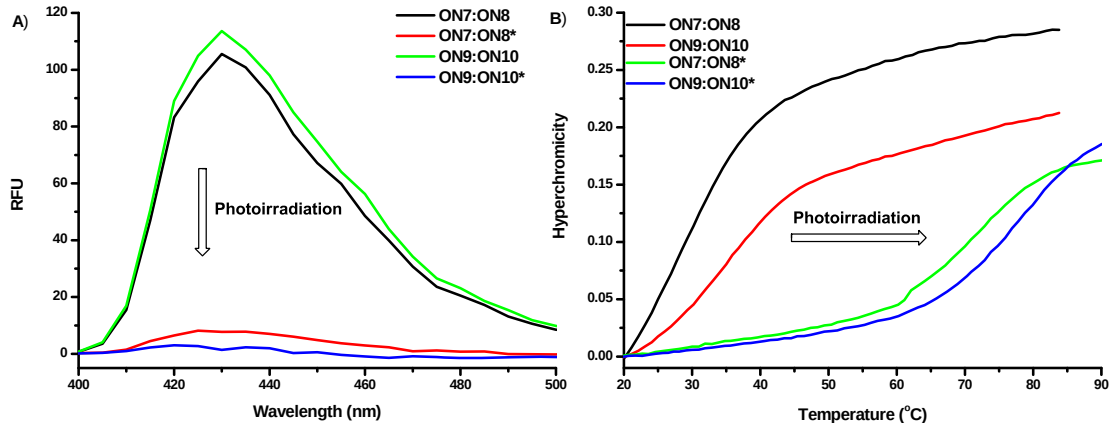

Figure 6.9 (A) The fluorescence properties of anthracene-GNA duplexes before and after photoirradiation: **ON7**:**ON8**, **ON9**:**ON10**, **ON7**:**ON8*** and **ON9**:**ON10***. (B) UV-melting curves of the GNA duplexes containing anthracene nucleotides: **ON7**:**ON8**, **ON9**:**ON10**, **ON7**:**ON8*** and **ON9**:**ON10***. Changes in the absorbance upon heating were monitored at 260 nm. Conditions: 10 mM sodium phosphate, 100 mM NaCl, pH 7.0, and 2 μM of each strand (Table 6.2; *after irradiation).

Figure 6.9A shows that the fluorescence emission of anthracene in the duplex was significantly decreased after photoirradiation. This result is due to the highly efficient crosslinking reaction of anthracenes, which could be used as a probe to monitor photoirradiation reactions.

Figure 6.9B reveals the high stability of the duplexes **ON7**:**ON8** and **ON9**:**ON10** after irradiation at 366 nm UV light for 3 min. Table 6.2 shows that **ON7**:**ON8*** and **ON9**:**ON10*** exhibited melting temperatures (T_m) at 72 and 77 °C, respectively. This increased duplex stability could be associated with the crosslinking reaction of anthracenes in the duplex after photoirradiation, but not with the undesired crosslinking reactions with nucleobases.[5] This was further supported by the un-increased duplex stabilities for the photoirradiated duplexes **ON11**:**ON8*** and **ON9**:**ON12*** each contained a single anthracene nucleotide (Table 6.2, entries 4 and 5; Figure 6.10B).

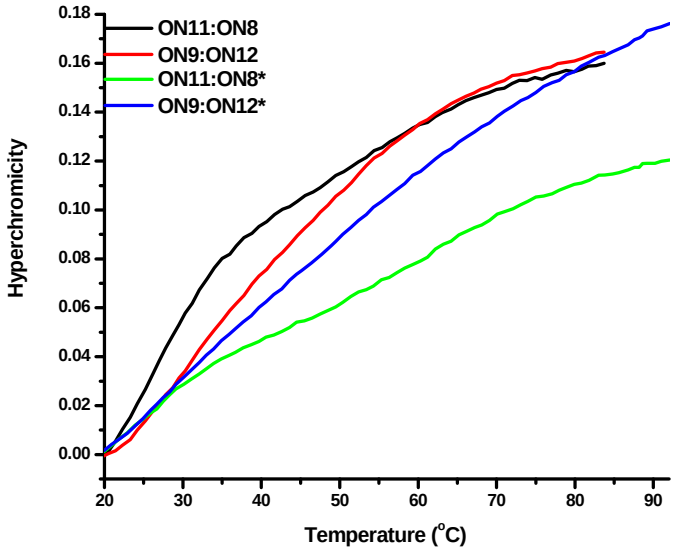

Figure 6.10 UV-melting curves of the GNA duplexes containing anthracene nucleotides: **ON11**:**ON8**, **ON9**:**ON12**, **ON11**:**ON8*** and **ON9**:**ON12***. Changes in the absorbance upon heating were monitored at 260 nm. Conditions: 10 mM sodium phosphate, 100 mM NaCl, pH 7.0, and 2 μM of each strand.

Unfortunately, our attempt to separate the photoproducts of **ON7**:**ON8*** and **ON9**:**ON10*** by HPLC failed.

C. End capping of the GNA duplex

To investigate whether the ends of a duplex were crosslinked by the photoreaction, anthracene-GNA **ON13** and **ON14** were designed. These duplexes contained two adjacent anthracene nucleotides dangling at the ends of the duplex. The sequences of **ON13** and **ON14** were complementary to each other, and the duplex **ON13**:**ON14** was expected to form a hairpin structure as a result of the photoirradiation.

Table 6.3 Thermal stabilities of the anthracene-containing GNA duplexes before and after photoirradiation.[a]

Entry	Sequence		T_m (°C)	T_m (°C)*
1	3′-TAAAAATAATAATATT-2′	(**ON5**)	54	
	2′-ATTTTTATTATTATAA-3′	(**ON6**)		
2	3′-**An**TAAAAATAATAATATT-2′	(**ON13**)	56	82
	2′-C_3**AnH**ATTTTTATTATTATAA-3′	(**ON14**)		
3	3′-**An**TAAAAATAATAATATT**Pyr′**C_3-2′	(**ON15**)	58	85
	2′-C_3**AnH**ATTTTTATTATTATAA**HPyr′**-3′	(**ON16**)		

[a]Conditions: 10 mM sodium phosphate, 100 mM NaCl, and 2 μM individual strands. *After photoirradiation.

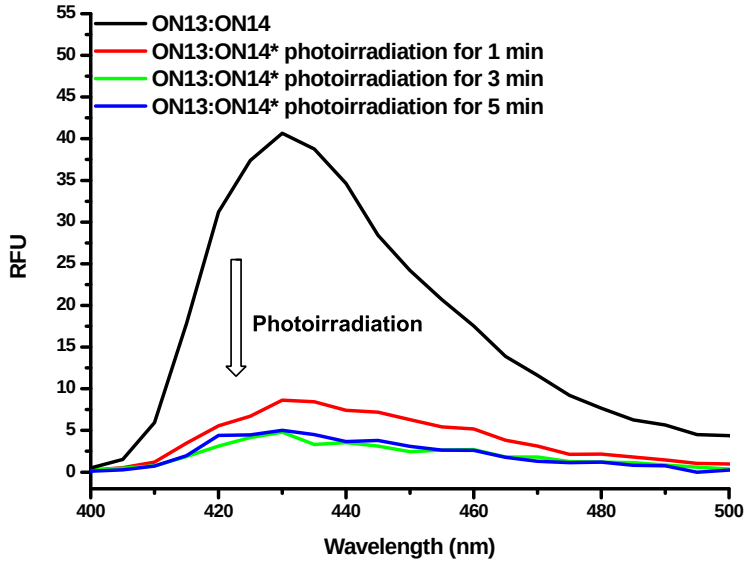

Figure 6.11 Fluorescence spectra of the duplex **ON13:ON14** before and after photoirradiation (Table 6.3; *after irradiation). Conditions: 10 mM sodium phosphate, 100 mM NaCl (pH 7.0), and 2 μM of each strand.

Figure 6.11 reveals that the fluorescence intensity of anthracenes decreased with a prolonged photoirradiation time of 3 min. Only a marginal reduction further occurred upon an increase in irradiation time. This finding indicated the nearly complete photodimerization of anthracenes in **ON13:ON14**. Thus, the photoirradiation time was set at 3 min.

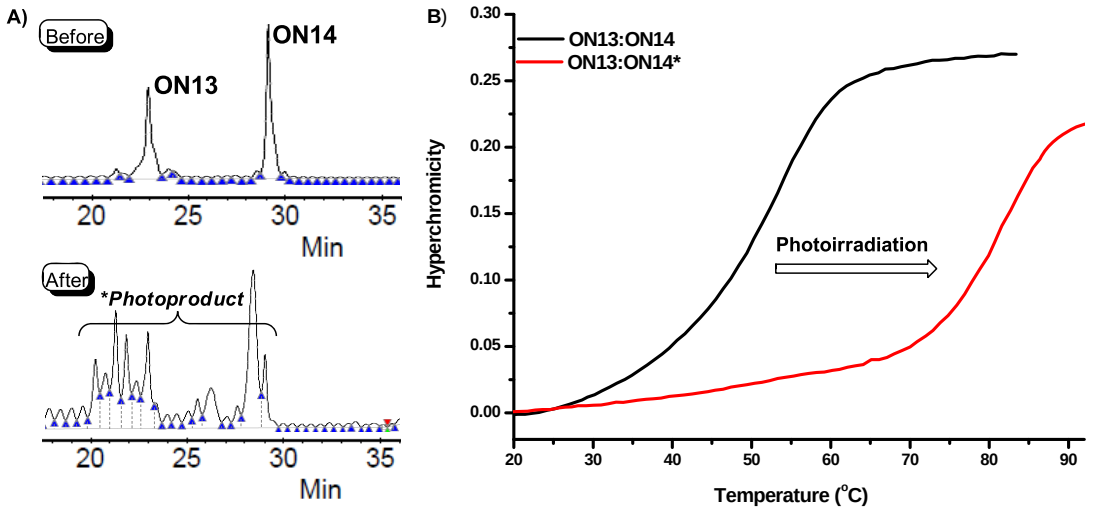

Figure 6.12 (A) HPLC chromatograms of the reaction mixtures before and after 3 min of photoirradiation for duplex **ON13**:**ON14**. The chromatograms were obtained under the following conditions: Waters Xterra column (MS C18; 4.6 mm × 50 mm); solution A, 50 mM triethylamine-acetic acid buffer (pH 7); solution B, acetonitrile; linear gradient, 10%–20% in 40 min; flow rate, 1 mL/min. (B) UV-melting curves of the duplex **ON13**:**ON14** and **ON13**:**ON14***. Changes in the absorbance upon heating were monitored at 260 nm. Conditions: 10 mM sodium phosphate, 100 mM NaCl (pH 7.0), and 2 μM of each strand.

The products of the photoreactions were analyzed by reversed-phase HPLC. Figure 6.12A shows the chromatograms of the reaction mixtures for the duplex **ON13**:**ON14** before and after photoirradiation for 3 min. The chromatograms show the appearance of new peaks, along with the disappearance of the starting strands. MALDI-TOF MS indicated that the asterisked peaks in HPLC chromatogram were the crosslinked products between the two corresponding strands (Figure 6.17 and 6.18). Duplex **ON13**:**ON14*** displayed several peaks in the HPLC chromatogram because it could form a maximum of eight isomers, including two pairs of enantiomers.

To evaluate the thermal stability of the dimerized structure, melting experiments were carried out using the photoproducts. Table 6.12B reveals that the photoproduct **ON13**:**ON14*** exhibited a melting temperature much higher than that of duplex **ON13**:**ON14** by 26 °C. This remarkable increase in melting temperature was consistent with the formation of an intramolecular duplex with a hairpin structure.

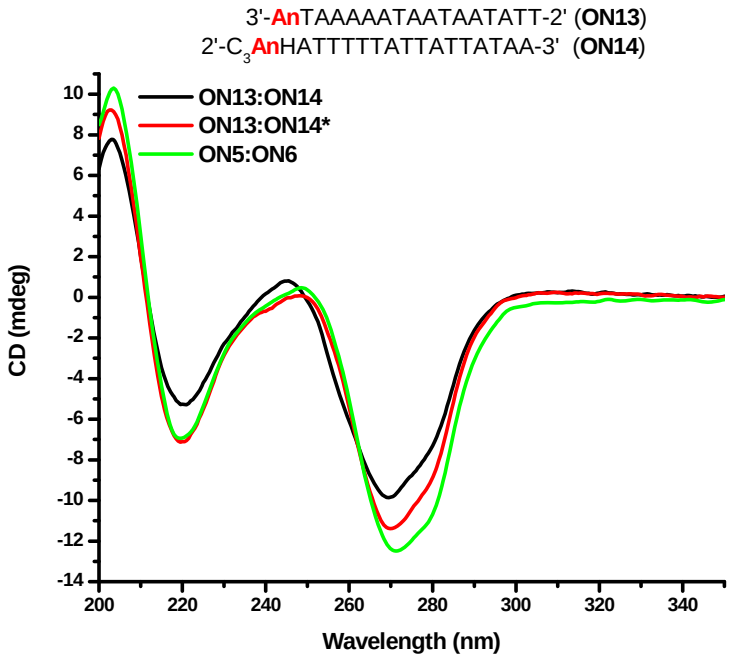

Figure 6.13 CD spectra of the GNA duplexes **ON13**:**ON14**, **ON13**:**ON14*** and **ON5**:**ON6** (Table 6.3). Conditions: 10 mM sodium phosphate, 100 mM NaCl, pH 7.0, and 8 μM of each strand; 25 °C.

Subsequently, the end-capped duplex **ON13**:**ON14*** was investigated by circular dichroism (CD) spectrometry. Figure 6.13 shows that the CD spectra of **ON13**:**ON14*** were identical to those of duplex **ON13**:**ON14** and native duplex **ON5**:**ON6**. This indicated that the photodimerization of anthracenes did not distort the overall GNA duplex structure.

Improvement in the analysis and separation of the photoproducts

Although reversed-phase HPLC is a convenient tool for analyzing the GNA mixture of photoirradiation, this method still exhibited several disadvantages in present study: (i) the attempt to separate the photoproduct of **ON7**:**ON8*** and **ON9**:**ON10*** by HPLC failed, indicating this purification method was deficient in this case; (ii) the conjugated GNA duplex exhibited several peaks in the HPLC chromatogram that always overlapped with the peaks of the anthracene-GNA strands. This overlapping affected the analysis and separation of the photoproduct (Figure 6.7A).

Denaturing urea polyacrylamide gel electrophoresis (PAGE) is widely used to analyze or purify single DNA or RNA fragments based on their molecular weights. DNA migrates through a gel toward the positive electrode in the presence of current. Shorter oligonucleotides migrate faster through the gel than longer ones, because shorter oligonucleotides more easily travel through the pores of the gel. DNA is only absorbed in the UV region, visualization is generally achieved by staining the oligonucleotides with a visible dye. However, fluorescent tags such as ethidium bromide do not stain GNA because they could not intercalate into GNA.

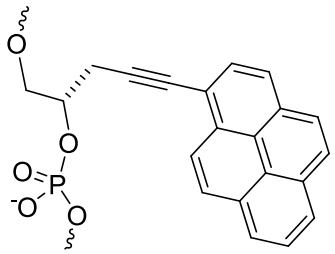

Figure 6.14 Pyrene acetylide GNA nucleotides (**Pyr′**).

To visualize the GNA used in the gel electrophoresis, pyrene acetylide nucleotides (**Pyr′**), expected to function as fluorescence tags, were introduced into GNA. In addition, pyrene acetylide GNA nucleotides enable to monitor duplex formation by excimer fluorescence detection, and this would be applied in sensing the GNA duplex denaturing. Accordingly, duplex **ON15**:**ON16** was designed to contain two adjacent pyrene acetylide nucleotides (**Pyr′**) in the duplex terminus (Table 6.3, entry 3).

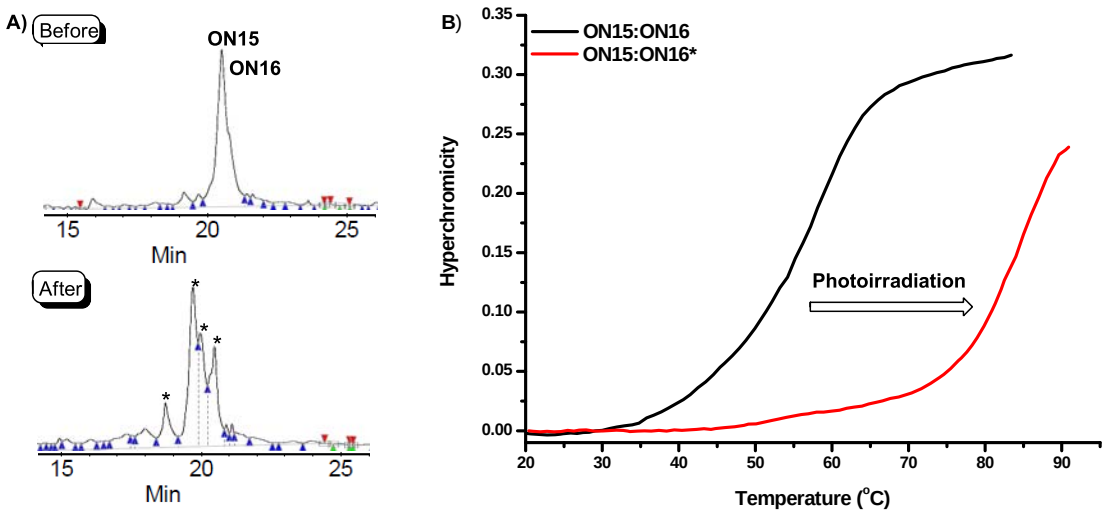

Figure 6.15 (A) HPLC chromatograms of the reaction mixtures before and after 3 min of photoirradiation for duplex **ON15**:**ON16**. The chromatograms were obtained under the following conditions: Waters Xterra column (MS C18; 4.6 mm × 50 mm); solution A, 50 mM triethylamine-acetic acid buffer (pH 7); solution B, acetonitrile; linear gradient, 10%–40% in 30 min; flow rate, 1 mL/min. (B) UV-melting curves of the duplex **ON15**:**ON16** and **ON15**:**ON16***. Changes in the absorbance upon heating were monitored at 260 nm. Conditions: 10 mM sodium phosphate, 100 mM NaCl (pH 7.0), and 2 μM of each strand.

After photoirradiation for 3 min, the reaction mixture of duplex **ON15**:**ON16** was first analyzed by reversed-phase HPLC. Figure 6.15A shows the chromatograms of duplex **ON15**:**ON16** before and after photoirradiation. Although the chromatogram shows the appearance of several new peaks, it cannot reveal the percent conversion of duplex **ON15**:**ON16** to photoproduct because of overlapping peaks.

Thus, denaturing urea PAGE was selected to analyze the conversion of this reaction. Before the denaturing urea PAGE, the fluorescence properties of duplex **ON15:ON16** with and without urea denaturation were analyzed. Figure 6.16A shows that **ON15:ON16** emitted a strong excimer emission of pyrenes in the buffer solution. In contrast, the denatured **ON15:ON16** only emitted a monomer emission of pyrene, indicating the dissociation of complementary strands.

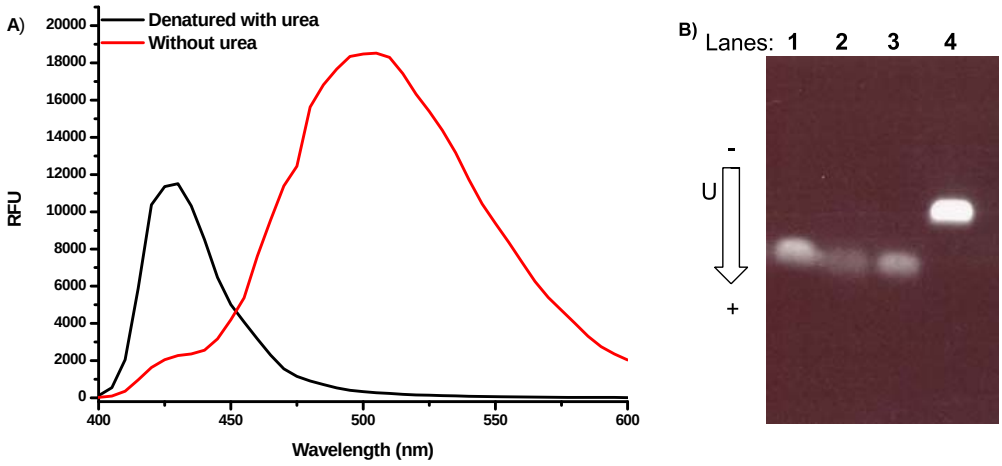

Figure 6.16 (A) Fluorescence spectra of **ON15:ON16** with and without urea denaturation (Table 6.3; *after irradiation). Conditions: 10 mM sodium phosphate, 100 mM NaCl (pH 7.0), and 8 μM of each strand; excitation at 365 nm with a cutoff filter at 420 nm; fluorescence at 500 nm taken as the indicator of excimer fluorescence. (B) A photograph of denaturing urea polyacrylamide gel (6%) electrophoresis mobility shift arrays showing the denatured **ON15:ON16** (lane 1), **ON15** (lane 2), and **ON16** (lane 3), as well as the photoreaction mixture of **ON15:ON16*** (lane 4).

Subsequently, the GNA mixture of the photoreaction was analyzed by denaturing urea PAGE. Figure 6.16B shows a photograph of the denaturing urea PAGE mobility shift arrays of **ON15**:**ON16** before and after irradiation. The denaturing urea PAGEs of **ON15**:**ON16**, **ON15,** and **ON16** (Figure 6.16B, lanes 1–3) indicates duplex **ON15**:**ON16** was dissociated complementary, which was consistent with the fluorescence experiment (Figure 6.16A). After photoirradiation for 3 min, the conversion of **ON15**:**ON16** (lane 1) to the crosslinking product **ON15**:**ON16*** (lane 4) was complete.

Thus, the photoproduct **ON15**:**ON16*** can be collected according to the asterisked peaks in HPLC chromatograms (Figure 6.15A). MALDI-TOF MS indicated that the collected peaks are the crosslinked products between the two corresponding strands (Figure 6.19 and 6.20). Figure 6.15B shows that the photoproduct **ON15**:**ON16*** exhibited a melting temperature much higher than that of duplex **ON15**:**ON16** by 27 °C (T_m = 85 °C; Table 6.3, entry 3). This significant increase in the melting temperature revealed the formation of a crosslinked duplex via the photodimerization of anthracenes.

Chapter 6.3 Conclusions

In this chapter, we introduced anthracene as an artificial nucleosidic base into GNA, and investigated the photochemical ligation of GNA through anthracene cyclodimer formation. The photoreaction of GNA was analyzed by HPLC, UV-vis, CD, MALDI-TOF MS and denaturing urea PAGE. The template-supported GNA photoligation did not occur, probably due to the inefficient dimerization of anthracenes in tandem duplex. In contrast, both the interstrand crosslinking in middle of duplex and the end capping of duplex proved to be feasible. The photochemical ligation of GNA *via* anthracene cyclodimer formation is a useful method for the crosslinking of interstrand GNA, which may be applied in the construction of functional GNA-supramolecules in the future.

Chapter 6.4 Experimental

GNA oligonucleotide synthesis and purification

All the GNA oligonucleotides were prepared according to previous method. The MALDI–TOF MS data of used GNA oligonucleotides and photoproducts were shown in Table 6.4. Figure 6.17-6.20 presented the MALDI–TOF MS spectrums of conjugated GNA strands **ON13**:**ON14*** and **ON15**:**ON16***.

Table 6.4 MALDI-TOF MS data of used GNA oligonucleotides.

Name	Oligonucleotides	M_{calcd}	M_{found}
ON 1	3′-TTATAAAAATAAT**AnAn**TATTAAT-2′	5908.9($C_{194}H_{240}N_{73}O_{104}P_{21}$)	5910.2
ON 2	2′-AATATTTTTATTA**HH**ATAATTA-3′	5510.4($C_{164}H_{222}N_{67}O_{108}P_{21}$)	5510.7
ON 3	3′-TTATAAAAATAAT**An**C_3-2′	3870.5($C_{124}H_{158}N_{50}O_{68}P_{14}$)	3870.5
ON 4	3′-**An**TATTAAT-2′	2114.4($C_{73}H_{90}N_{23}O_{38}P_7$)	2114.3
ON 5	3′-TAAAAATAATAATATT-2′	4222.7($C_{128}H_{167}N_{62}O_{74}P_{15}$)	4223.3
ON 6	3′-AATATTATTATTTTTA-2′	4186.6($C_{128}H_{171}N_{50}O_{82}P_{15}$)	4185.5
ON 7	3′-TAAAAAT**HAn**TAATATT-2′	4188.7($C_{131}H_{167}N_{57}O_{74}P_{15}$)	4194.1
ON 8	2′-ATTTTTA**HAn**ATTATAA-3′	4100.6($C_{131}H_{169}N_{46}O_{78}P_{15}$)	4101.1
ON 9	3′-TAAAAAT**AnH**TAATATT-2′	4188.7($C_{131}H_{167}N_{57}O_{74}P_{15}$)	4193.1
ON 10	2′-ATTTTTA**AnH**ATTATAA-3′	4100.6($C_{131}H_{169}N_{46}O_{78}P_{15}$)	4100.0
ON 11	2′-ATTTTTA**H**TATTATAA-3′	$C_{122}H_{165}N_{48}O_{80}P_{15}$(4046.6)	4048.2
ON 12	3′-TAAAAAT**H**ATAATATT-2′	$C_{122}H_{162}N_{57}O_{74}P_{15}$(4073.7)	4076.0
ON 13	3′-**An**TAAAAATAATAATATT-2′	4536.9($C_{145}H_{182}N_{62}O_{78}P_{16}$)	4536.5
ON 14	2′-C_3**AnH**ATTTTTATTATTATAA-3′	4772.0($C_{150}H_{197}N_{53}O_{92}P_{18}$)	4764.5
ON 15	3′-**An**TAAAAATAATAATATTPyr′C_3-2′	5037.3($C_{169}H_{204}N_{62}O_{86}P_{18}$)	5037.7
ON 16	2′-C_3**AnH**ATTTTTATTATTATAAHPyr′-3′	5249.3($C_{173}H_{218}N_{50}O_{102}P_{20}$)	5249.7
ON13: **ON14***	3'-**An**TAAAAATAATAATATT-2' 2'-C_3**AnH**ATTTTTATTATTATAA-3'	9308.9 ($C_{295}H_{370}N_{115}O_{170}P_{34}$)	9305.5
ON15: **ON16***	3'-**An**TAAAAATAATAATATTPyr'C_3-2' 2'-C_3**AnH**ATTTTTATTATTATAAHPyr'-3'	10286.7 ($C_{342}H_{422}N_{112}O_{188}P_{38}$)	10286.4

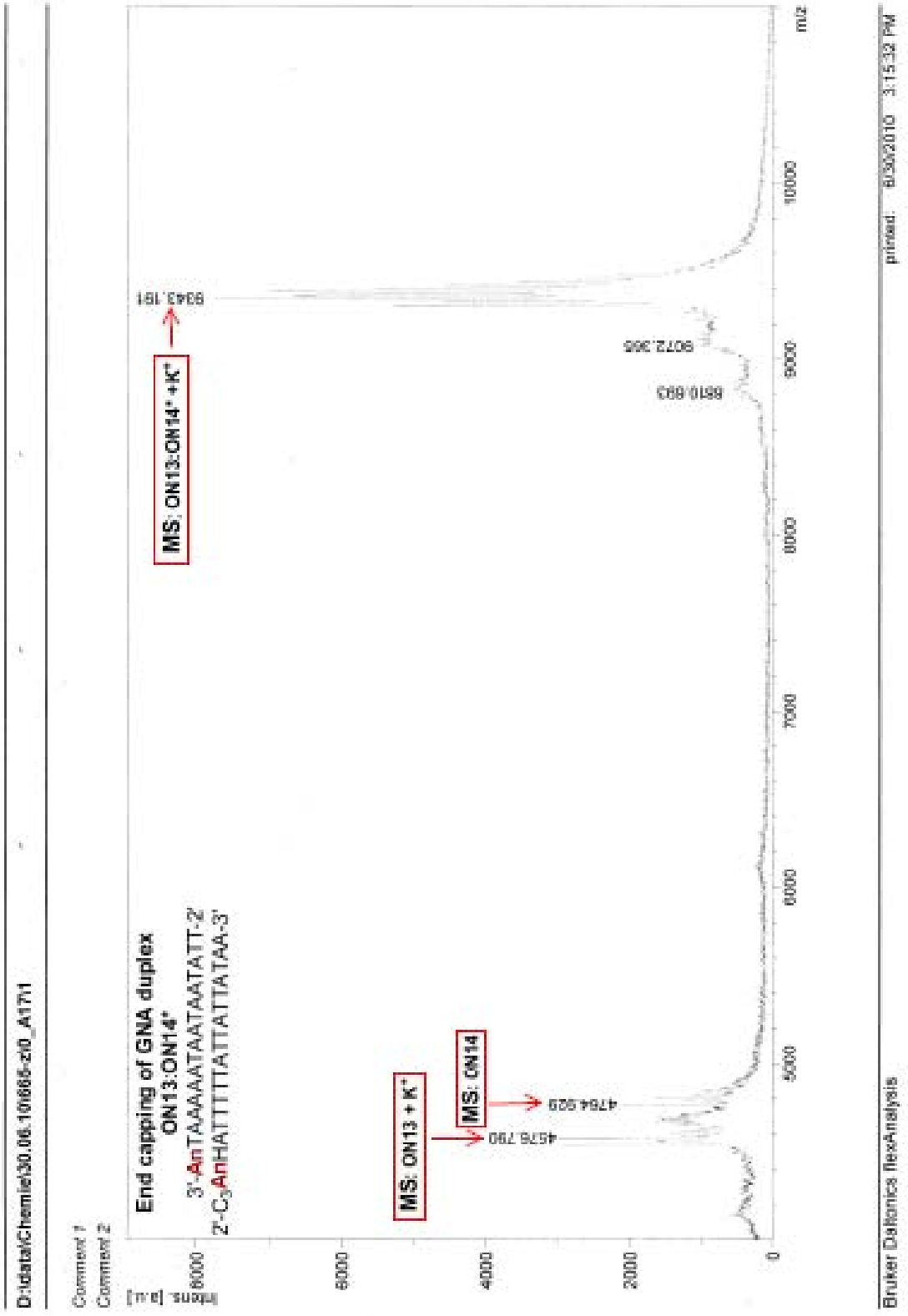

Figure 6.17 MALDI-TOF MS of the photoproduct **ON13**:**ON14***.

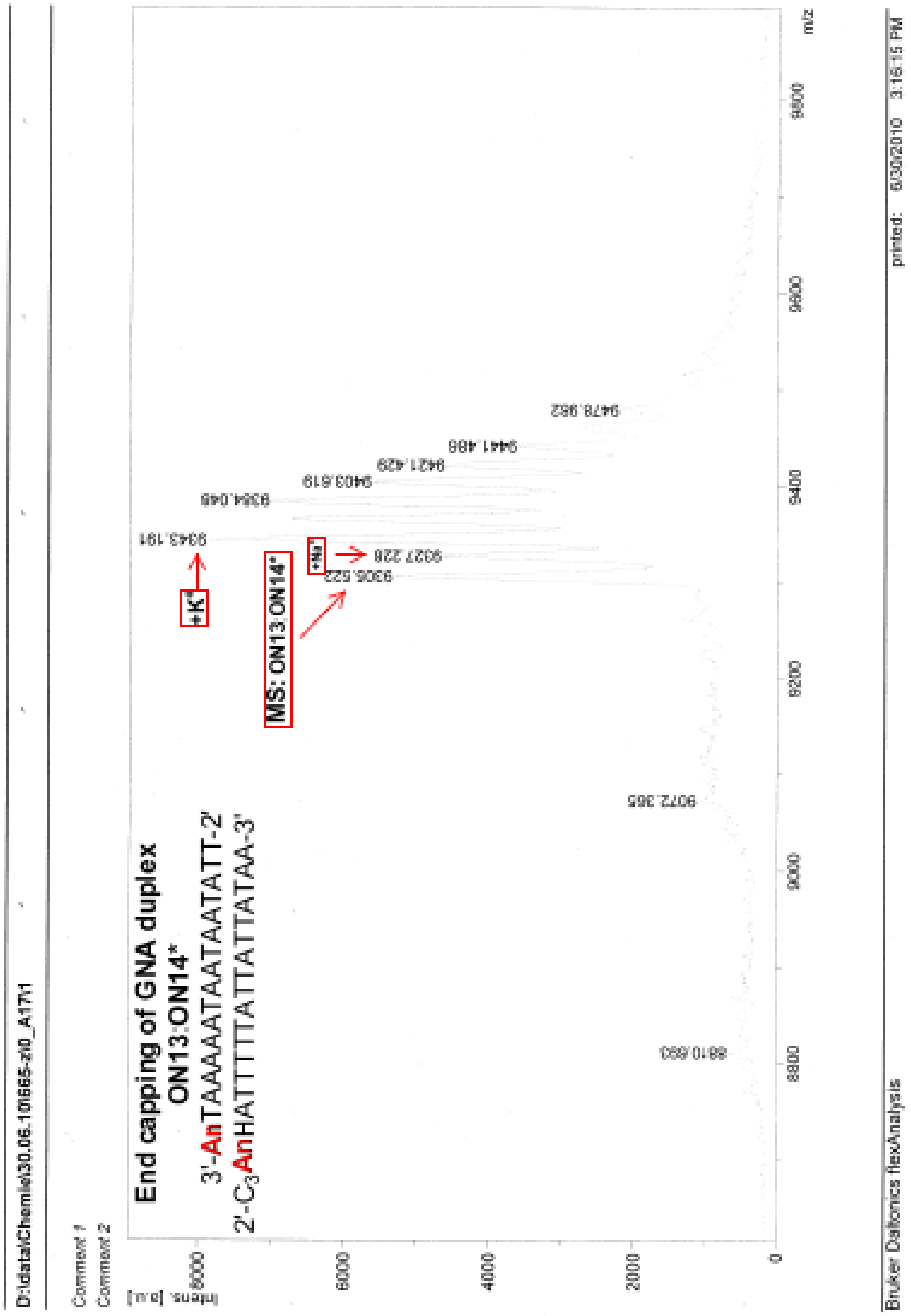

Figure 6.18 MALDI-TOF MS of the photoproduct **ON13**:**ON14***.

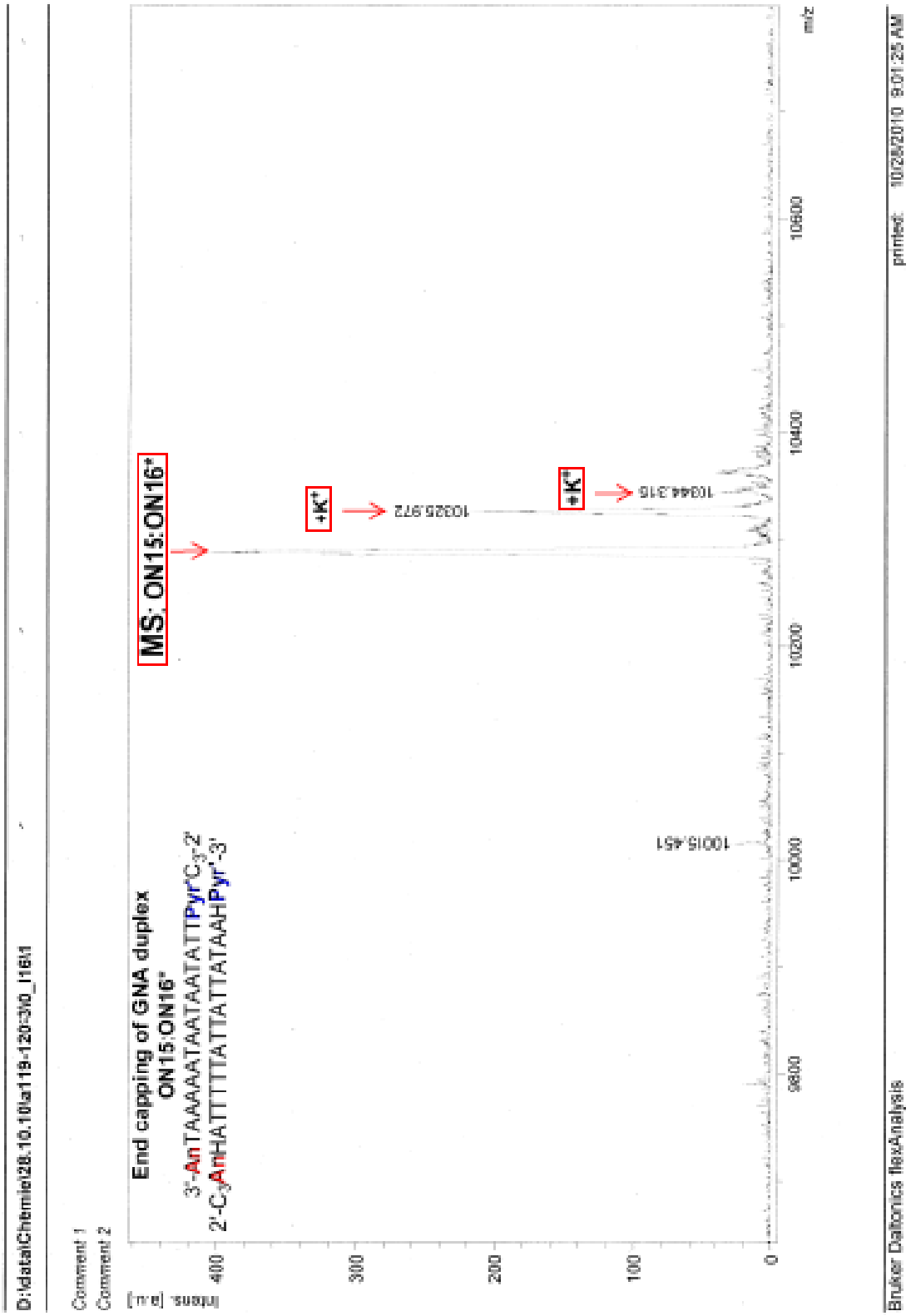

Figure 6.19 MALDI-TOF MS of the photoproduct **ON15**:**ON16***.

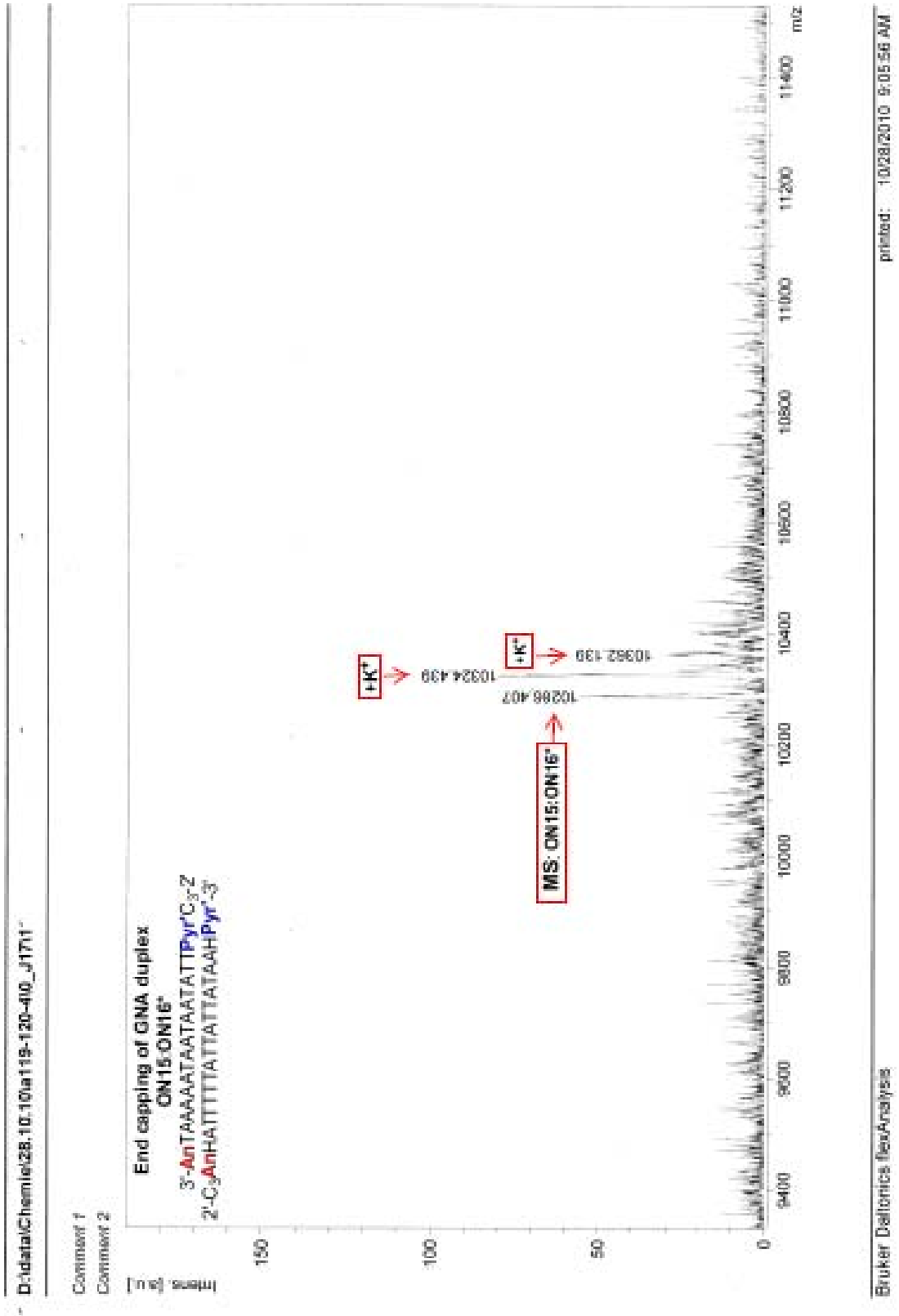

Figure 6.20 MALDI-TOF MS of the photoproduct **ON15**:**ON16***.

Photoirradiation experiments

The anthracene-GNAs (8 μM of each strand) were irradiated in buffer solution containing 10 mM sodium phosphate and 100 mM NaCl. Prior to irradiation, reaction mixtures were heated to 80 ^{o}C and then annealed with slow cooling to 0 ^{o}C on a heating block. Reaction mixtures were irradiated in an N_2 atmosphere with a high-pressure mercury lamp (200 W) equipped with longpass optical filters (330 nm). The products formed after photoirradiation were analyzed using RP-HPLC on a Waters Xterra column (MS C18, 4.6 × 50mm): solution A, 50 mM TEAA (triethylamine-acetic acid) buffer (pH 7.0); solution B, acetonitrile; linear gradient, depending on the anthracene-GNA, for example, 4-20% in 40 min for tandem duplex **ON4**:**ON3**:**ON2**; flow rate, 1 mL/min. Elution of the reaction products was monitored by absorption at 260 nm. All peaks were identified by MALDI–TOF MS.

Denaturing urea polyacrylamide gel electrophoresis

The denaturing urea polyacrylamide gel (6%) was used in the electrophoresis experiment for present study, which was prepared as follows: combine 16.8 g urea, 4 mL 10 × TBE buffer and 10 mL 30% acrylamide : N,N′-methylenbisacrylamide (19:1) in a beaker. Bring the volume of the solution to 35 mL using deionized water. Place the beaker in a hot water bath, once the urea has dissolved, bring the solution to a final volume of 50 mL with deionized water. To finalize the gel solution, first add 250 μL of 10% ammonium persulfate (APS) to the 6% acrylamide solution. Then add 25 μL of TEMED and quickly but gently mix. Upon the addition of APS and TEMED, carefully pipet the gel between the galss plates using a sterile plastic pipet. After gel prerunning in buffer solution (1 × TBE, 7 M urea) for half an hour, the denatured GNA sample was loaded into the wells. Then adjust the settings to approximately 20 watts, the other setting read 50 milliamps and 120 volts. Once the gel has run to experimental specifications, cut off the power source and disconnect the leads.

Thermal denaturation

The melting studies were carried out in 1 cm path length quartz cells (total volume 325 μL; 200 μL sample solutions were covered by mineral oil) on a Beckman 800 UV-VIS spectrophotometer equipped with a thermo-programmer. Melting curves were monitored at 260 nm with a heating rate of 1 ^{o}C/min. Melting temperatures were calculated from the first derivatives of the heating curves. Experiments were performed in duplicate and mean values were taken.

Fluorescence measurements

The experiments were performed in 96-well plates on a Molecular Devices SpectraMax M5.

CD spectroscopy

CD measurements were performed on a JASCO J-810 spectrometer in a 1 mm path length quartz cuvette. The GNA single strands or duplexes were prepared in 10 mM sodium phosphate, 100 mM NaCl, pH 7.0, and the concentration of each strand was 8 μM.

Chapter 6.5 References

1. (a) Gude, L.; Fernández, M.-J.; Grant, K. B.; Lorente, A. *Tetrahedron Letter* **2002**, *43*, 4723-4727; (b) Bhattacharya, S.; Mandal, S. S. *Chemical Communication* **1996**, 1515-1516; (c) Gude, L.; Fernández, M.-J.; Grant, K. B.; Lorente, A. *Organic & Biomoleculor Chemistry* **2005**, *3*, 1856-1862; (d) Dong, S.; Hwang, H.-M.; Harrison, C.; Holloway, L.; Shi, X.; Yu, H. *Bulletin of Environmental Contamination and Toxicology* **2000**, *64*, 467-474; (e) Dong, S.; Fu, P. P.; Shirsat, R. N.; Hwang, H.-M.; Leszczynski, J.; Yu, H. *Chemical Research in Toxicology* **2002**, *15*, 400-407.
2. Moran, N.; Bassani, D. M.; Desvergne, J.-P.; Keiper, S.; Lowden, P. A. S.; Vyle, J. S. V.; Tucker, J. H. R. *Chemical Communication* **2006**, 5003-5005.
3. Granzhan, A.; Teulade-Fichou, M.-P. *Chemistry-A European Journal* **2009**, *15*, 1314-1318.
4. Coleman, R. S.; Mortensen, M. A. *Tetrahedron Letter* **2003**, *44*, 1215-1219.
5. (a) Bouas-Lauren, H.; Castellan, A.; Desvergne, J-P.; Lapouyade, R. *Chemical Society Reviews* **2000**, *29*, 43-55; (b) Backer, H.-D. *Chemical Reviews* **1993**, *93*, 145-172.
6. (a) Ihara, T.; Fujii, T.; Mukae, M.; Kitamura, Y.; Jyo, A. *Journal of American Chemical Society* **2004**, *126*, 8880-8881; (b) Ihara, T., Mukae, M.; Fujii, T.; Kitamura, Y.; Jyo, A. *Nucleic Acids Symposium Series* **2004**, *48*, 125-126; (c) Ihara, T.; Mukae, M.; Tabara, M.; Kitamura, Y.; Jyo, A. *Nucleic Acids Symposium Series* **2005**, *49*, 41-42; (d) Arslan, P.; Ihara, T.; Mukae, M.; Jyo, A. *Nucleic Acids Symposium Series* **2007**, *51*, 237-238; (e) Arslan, P.; Ihara, T.; Jyo, A. *Nucleic Acids Symposium Series* **2008**, *52*, 389-390; (f) Mukae, M.; Ihara, T.; Tabara, M.; Jyo, A. *Organic & Biomoleculor Chemistry* **2009**, *7*, 1349-1354.; (g) Arslan, P.; Jyo, A.; Ihara, T. *Organic & Biomoleculor Chemistry* **2010**, *8*, 4843-4848.

Chapter 7 Summary and Outlook

In this thesis, GNA is explored as a simplified duplex scaffold for arranging different chromophores and the properties of the resulting chromophore assemblies are investigated.

Chromophore nucleotides were incorporated into GNA by automated solid phase synthesis of oligonucleotides. The synthesis of different chromophore glycol nucleoside GNA building blocks was presented in chapter 2. The key step for synthesizing these glycol nucleosides was the regioselective and stereospecific ring-opening of dimethoxytrityliated (*S*)-glycidol (**3**). As shown in Scheme 7.1A, compounds **5**, **9**, **14** and **17** were synthesized by three efficient methods, namely, the application of Grignard reagents, Grignard reagents containing a metallation/transmetallation protocol, and organolithum reagents. Among these compounds, compound **17c** can be also synthesized by Pd-catalyzed Sonogashira coupling reaction of compound **30** with compound **17d** (Scheme 7.1 B), thus any chromophore with alkyne groups can be introduced to GNA by this method.

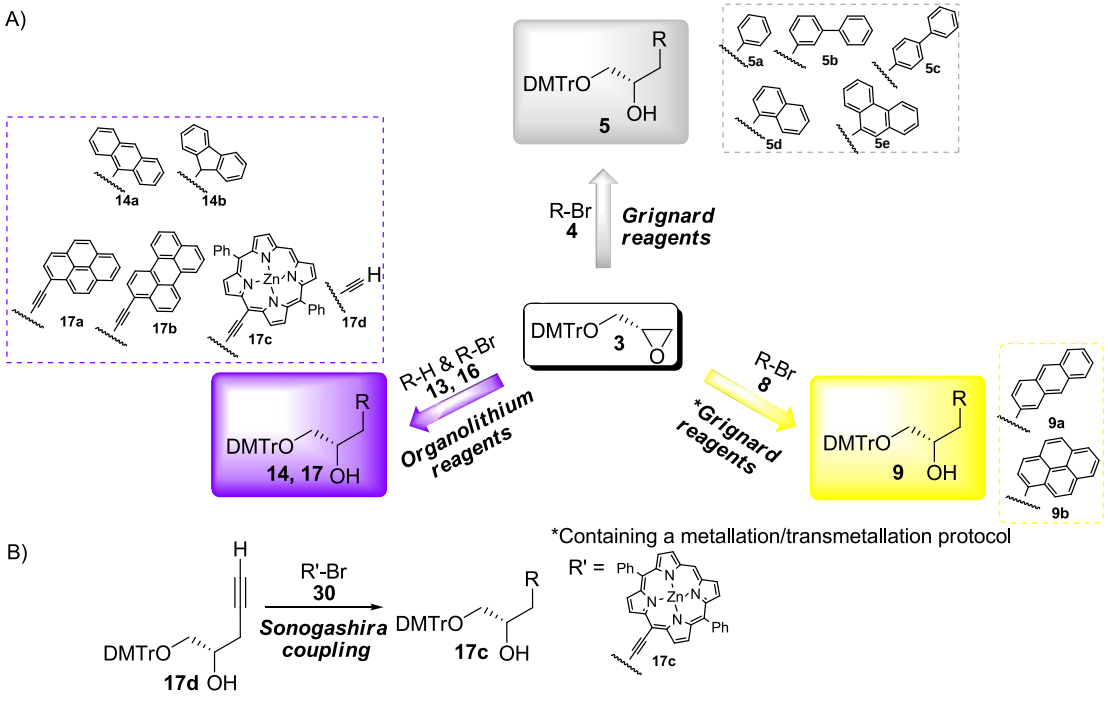

Scheme 7.1 (A) The synthesis of compounds **5**, **9**, **14** and **17** based on nucleophilic ring-opening of dimethoxytrityliated (*S*)-glycidol **3** by carbon nucleophiles. (B) The synthesis of compound **17c** through Sonogashira coupling reaction.

Subsequently, compounds **5**, **9**, **14** and **17** were converted to glycol nucleoside phosphoramidites in high yields, which were successfully used to synthesize modified GNA strands.

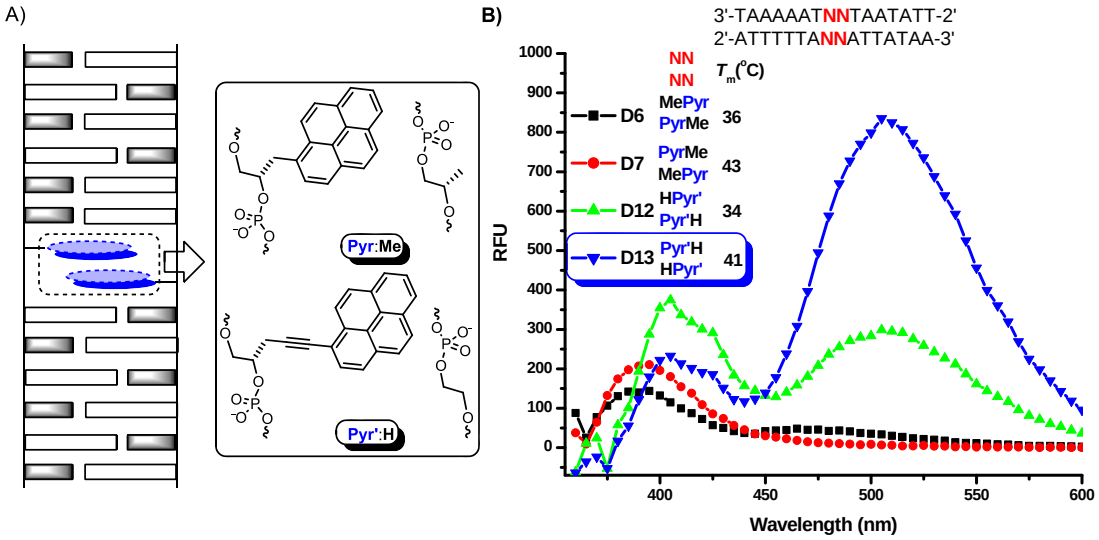

Figure 7.1 (A) Structure of **Pyr**:**Me** and **Pyr′**:**H** base pairs used in chapter 3. (B) Fluorescence properties of pyrene nucleotides (**Pyr**) and pyrene acetylide nucleotides (**Pyr′**) in GNA duplexes.

In chapter 3, we investigated GNA duplexes containing fluorescent pyrene (**Pyr**) and pyrene acetylide nucleotides (**Pyr′**) (Figure 7.1A). Duplexes with one or two adjacent **Pyr**:**Me** or **Pyr′**:**H** base pairs were synthesized, all resulting in thermally stable duplexes at room temperature. The incorporation of pyrene or pyrene acetylide to GNA duplexes did not distort the overall GNA duplex structure.

Interestingly, only the pyrene acetylides but not the related pyrene nucleotides, could form strong excimers upon interstrand stacking within the GNA duplexes (Figure 7.1B). The reason for this may be a combination of structural effects, influence of the stacking of adjacent pyrene acetylides nucleobases, and electronic effects due to the conjugation of the aromatic pyrene with the acetylide π-system.

As an application of excimer emission upon duplex formation with pyrene acetylide containing GNA strands, we developed a metal ion sensor by additionally incorporating a metal-mediated base pair: hydroxypyridone homo-base pair (**M**:**M**) or

hydroxypyridone-pyridylpurine hetero-base pair (**M**:**P**). As shown in Figure 7.2, **D15** and **D19** are very sensitive and selective Cu^{2+} "turn-on" fluorescent sensors. Unfortunately, our attempt to develop a Cu^{2+} sensor for a complex biological environment failed.

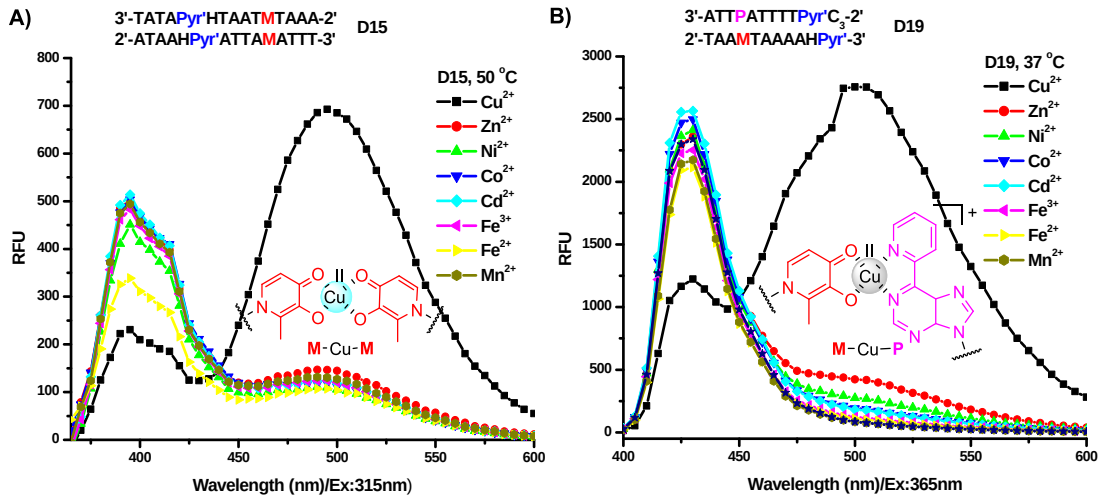

Figure 7.2 (A) Metal ion-selectivity of sensor **D15**. (B) Metal ion-selectivity of sensor **D19**.

In chapter 4, the porphyrin acetylide nucleotide (**P**) was incorporated into GNA duplexes opposite ethylene glycol abasic sites and the duplexes were analyzed by UV-melting, UV-vis, fluorescence spectroscopy, and circular dichroism.

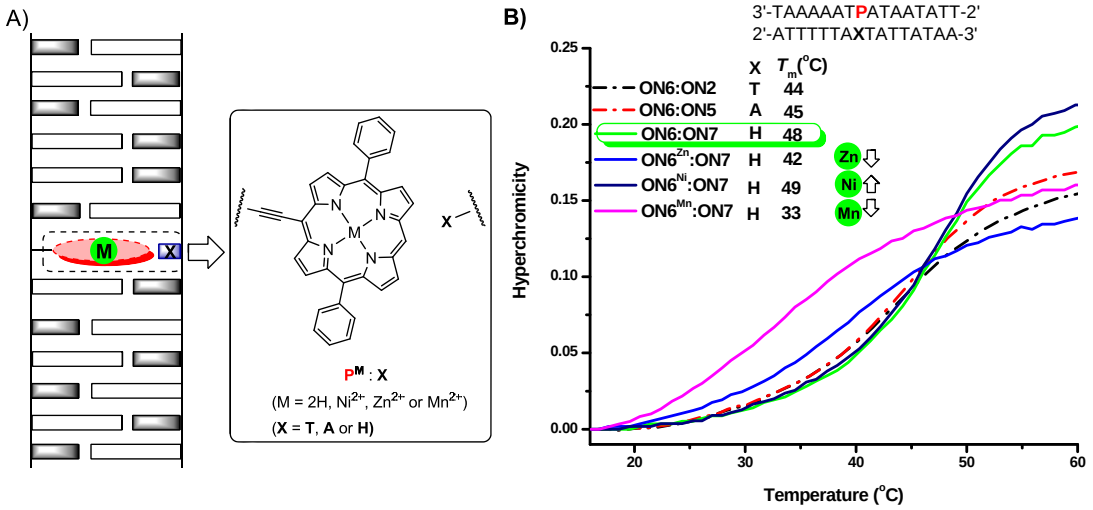

Figure 7.3 (A) Structure of $\mathbf{P^M}$:**X** base pair used in chapter 4. (B) UV-melting curves of GNA duplexes containing $\mathbf{P^M}$:**X** base pair.

The modified duplexes display lower thermal stabilities, however the thermal stabilities of duplex containing **P**:**H** base pairs could be modulated by the incorporation of zinc(II), manganes(II) or nickel(II) ions into **P** (Figure 7.3B). The incorporation of zinc(II) or manganes(II) ion led to a decrease in duplex stability, but the incorporation of nickel(II) resulted in increased duplex stability. These modulations of duplex stabilities by the nature of the metal ion can be interpreted by their differenct coordination behavior. Zn^{2+} or Mn^{2+} prefers to coordinate to axial ligands when incorporated into a porphyrin in an octahedral fashion and needs to dissociate these ligands if it wants to stack within GNA between neighboring base pairs. In contrast, Ni^{2+} prefers square planar coordination and can therefore be accommodated easily in the base stacking.

Furthermore, GNA duplexes provided a suitable scaffold to bring two porphyrins into close contact and to allow the interaction of porphyrins with different coordinated metal ions. The obvious change of the Soret bands accompanied by a blue shift (Figure 7.4B), together with the decrease of fluorescence intensity upon duplex formation revealed that a ground state interaction between two porphyrin moieties occurred in GNA, performing in face-to-face (H-dimer) fashion.

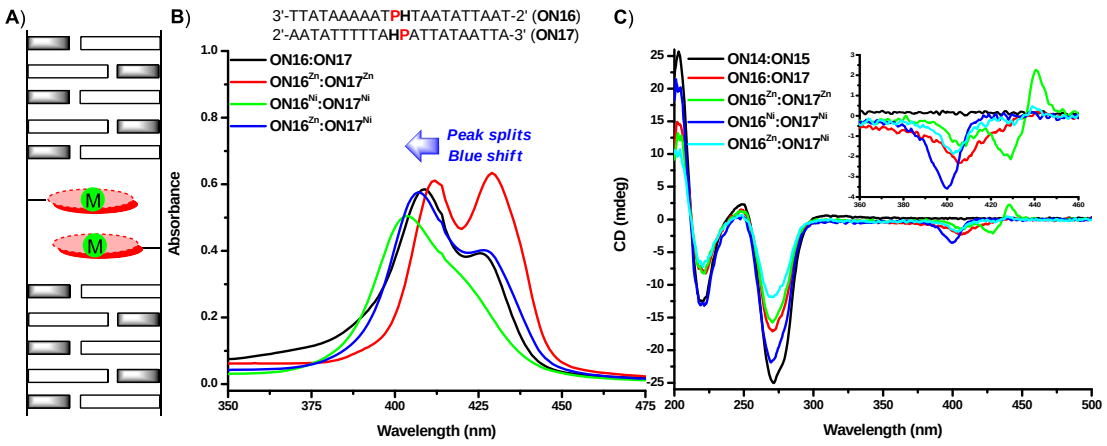

Figure 7.4 (A) Position of two $\mathbf{P^M}$:**H** base pair in the middle of GNA duplex **ON16**:**ON17**. (B) UV-vis spectra of porphyrin Soret band regions for GNA duplexes. (C) CD spectra of GNA duplexes. The insert shows expanded porphyrin Soret band regions.

In chapter 5, Electron donor-acceptor chromophores systems, mainly composed of perylene bisimide (**PBI**) and porphyrin (**P**) units were organized in duplex GNA (Figure 7.5A).

The GNA duplexes which contain **B-Pyr**, **B-Pyr′**, **B-Pe′** and **B-P** were investigated. The thermal stabilities revealed that **B-P** pair stabilizes the GNA duplex the most significantly, exceeding the stability of the native GNA duplex by additional 10 °C. The significantly increased duplex stability together with the red-shifted absorption band and induced CD signal at Soret band indicated the interstrand π-π stacking of **B-P** pair in the duplex.

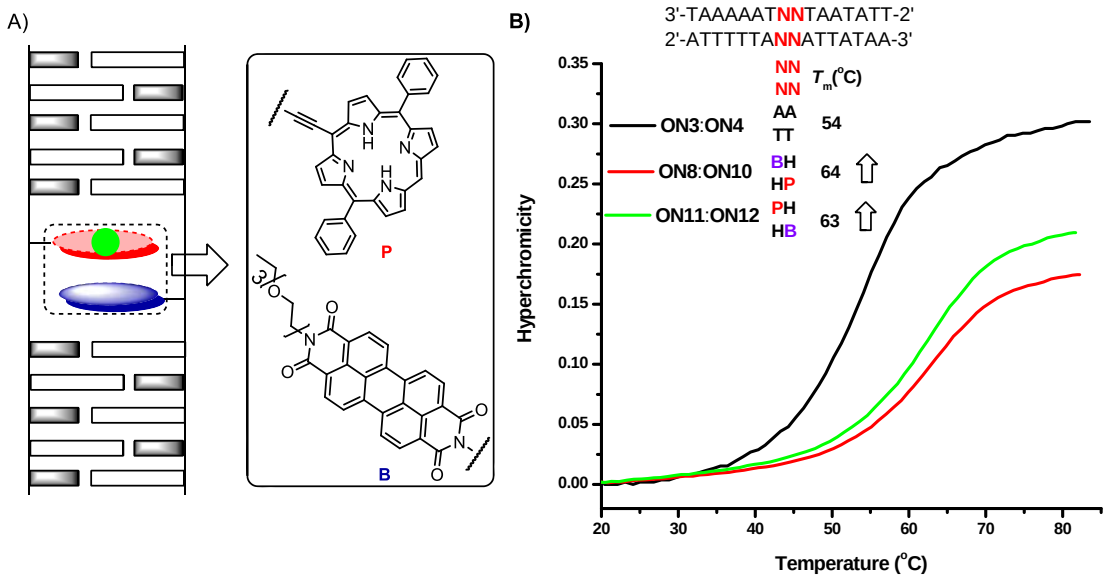

Figure 7.5 (A) Structure of **P**:**B** base pair used in chapter 5. (B) UV-melting curves of GNA duplexes containing one **P**:**B** base pair.

Subsequently, we investigated the systems which contain a couple of porphyrin and **PBI** building blocks. As shown in Figure 7.6B, the intensity of the CD signal accompanying the blue-shift of the bisignate CD spectra in the Soret band increased with the increasing amount of chromophore moieties. This continuous shift in a CD spectrum with increased amounts of chromophores indicated the interaction between **PBI** and porphyrin resulted in a highly ordered helical structure.

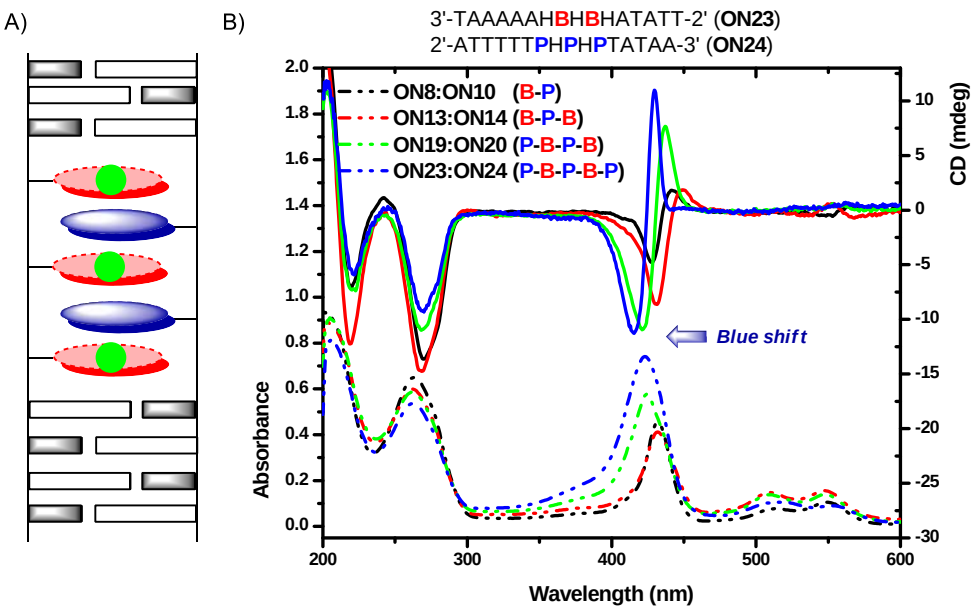

Figure 7.6 (A) Position of **B** and **P** in the middle of GNA duplex **ON23**:**ON24**. (B) CD and UV-vis spectra of GNA duplexes containing central chromophore cores: **B-P**, **B-P-B**, **P-B-P-B** and **P-B-P-B-P**.

In addition, we also synthesized some single strands which consisted of entirely **PBI**s or porphyrins. However, combining these single strands did not give us desired helical structure according to CD analysis. It seems that flanking natural base pairs or natural overhangs play a key role in affording helical structures.

Considering the significantly decreased yield of modified GNA strand with multi-incorporated chromophores, photochemical ligation of GNA was developed in order to address this problem. In chapter 6, the photochemical ligation of GNA via anthracene cyclodimer formation was explored. Anthrancenes were introduced into GNA not only as artificial nucleosidic bases but also as phototriggered joints (Figure 7.7A). Upon the duplex formation, the two adjacent anthracene nucleobases get close to each other, and the duplex was expected to generate a hairpin structure via anthracene cyclodimer formation as a result of the photoirradiation (366 nm).

The photochemical ligation of GNA via anthracene cyclodimer formation was investigated in terms of three aspects, namely, template-supported GNA ligation, interstrand crosslinking in the middle of the GNA duplex, and end capping of the GNA duplex.

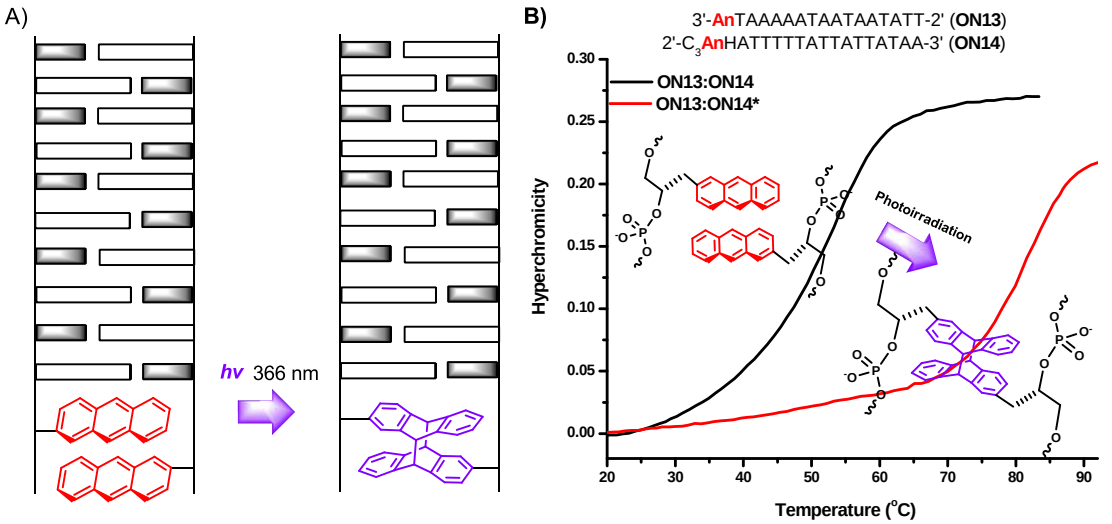

Figure 7.7 (A) Photochemical ligation of GNA *via* anthracene cyclodimer formation. (B) UV-melting curves of the duplexes before and after end-capping of duplex.

The template-supported GNA photoligation did not occur, probably due to the inefficient dimerization of anthracenes in tandem duplex. However, both the crosslinking in the middle of duplex and end capping of duplex proved to be feasible. Resulting intramolecular duplexes exhibited high melting temperature (Figure 7.7B), which was consistent with the formation of an intramolecular duplex with a hairpin structure. In addition, the CD spectra suggested that end capping did not disrupt overall GNA duplex structure.

In this study, the GNA duplex was employed as scaffold for the design of self-assembled and self-organized architectures. Several chromophores had been successfully introduced into the interior of GNA duplexes. GNA as a simplified general duplex scaffold proves to be useful for the defined chromophores organization.

Future work will be focused on applications of porphyrin-GNA conjugates as well as modified GNA containing porphyrin and **PBI** for light harvesting and charge transport. In addition, the photochemical ligation of GNA via anthracene cyclodimer formation is a useful tool for the interstrand crosslinking of GNA, which may provide a new method for the construction of functional GNA-supramolecules.

Kapitel 8 Zusammenfassung

In dieser Dissertation wurde GNA als ein einfaches Duplexgerüst für die Anordnung verschiedener Chromophoren verwendet und die Eigenschaften der resultierenden Chromophoreinheiten wurden untersucht.

Durch automatisierte Festphasensynthese von Oligonukletioden wurden Chromophornukleotide in GNA eingebaut, die Synthese der verschiedenen Chromophorglykolnukleosidbausteinen wurde bereits in Kapitel 2 vorgestellt. Dabei war die regioselektive und stereospezifische Ringöffnungsreaktion von dimethoxytrityliertem (*S*)-Glycidol (**3**) entscheidend. Verbindungen **5**, **9**, **14** und **17** wurden unter Verwendung drei effektiver Methoden synthetisiert: durch Anwendung von Grignard-Reagenzien, Grignard-Reagenzien in Verbindung mit Metallierung/ Transmetallierung und Organolithum-Verbindungen (Schema 8.1 A).

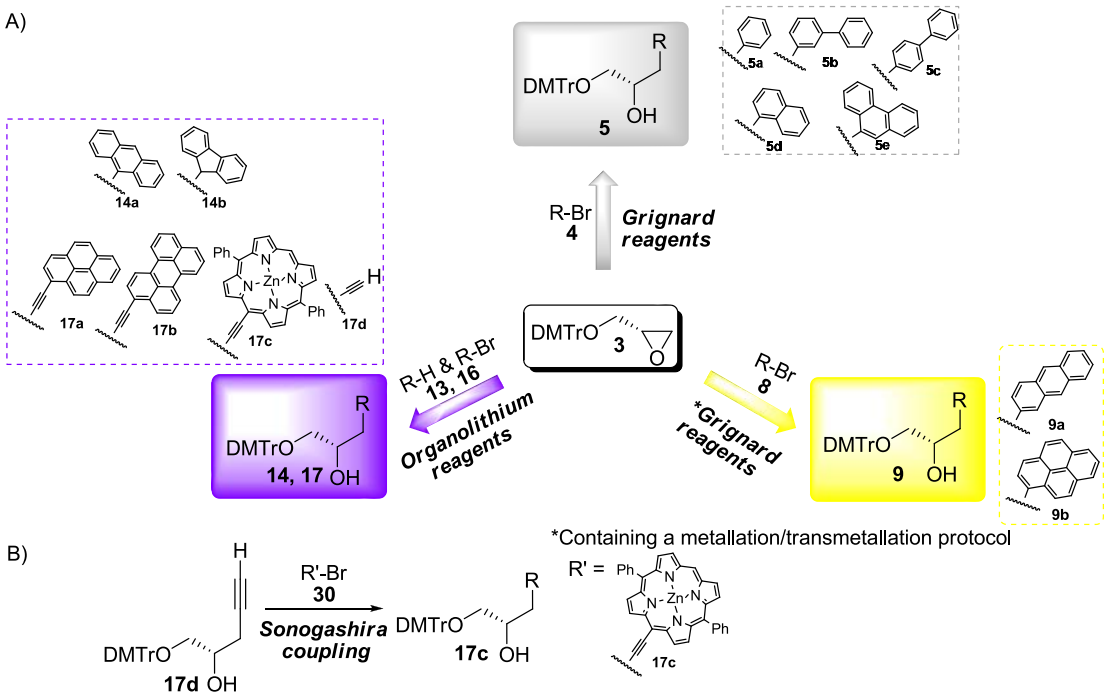

Schema 8.1 (A) Synthesen von Verbindungen **5**, **9**, **14** und **17** basierend auf nukleophiler Ringöffnung von dimethoxytritylierten (*S*)-Glycidol **3**. (B) Synthese von Verbindung **17c** durch eine Sonogashira-Kupplungsreaktion.

Anschließend wurden die Verbindungen **5**, **9**, **14** und **17** mit hoher Ausbeute zu Glykolnukleosidphosphoramidite umgesetzt, die für die weitere Synthese von modifizierten GNA-Strängen verwendet wurden.

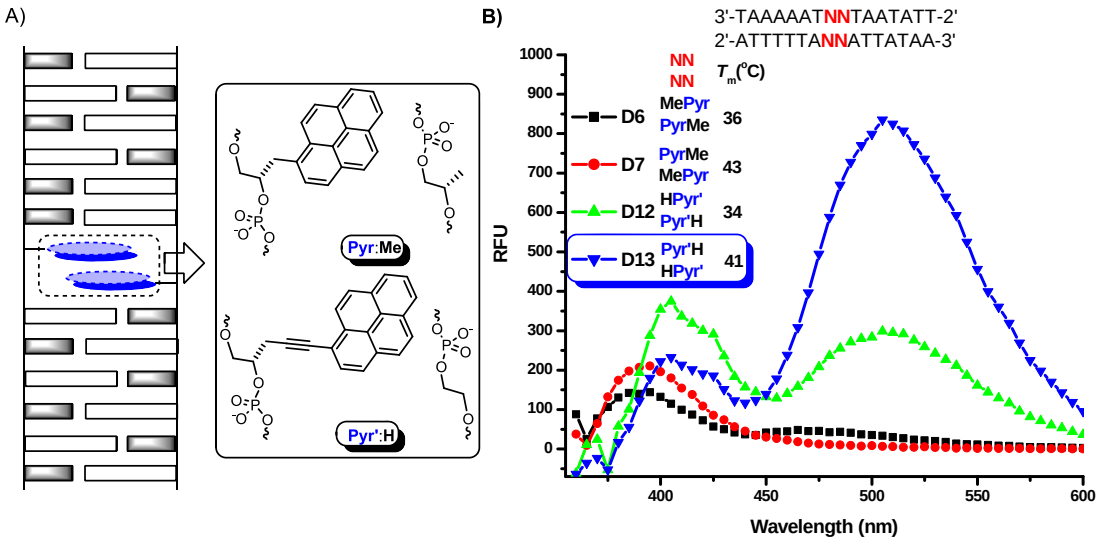

Abbildung 8.1 (A) Struktur des in Kapitel 3 verwendeten Basenpaares: **Pyr**:**Me** and **Pyr′**:**H**. (B) Fluoreszenzspektroskopie von Pyrennukleotid (**Pyr**) und Pyrenacetylidnukleotide (**Pyr′**) in GNA Duplexeinheiten.

In Kapitel 3 wurden GNA Duplexeinheiten mit fluoreszierenden Pyrennukleotide (**Pyr**) und Pyrenacetylidnukleotide (**Pyr′**) untersucht (Abbildung 8.1A). Zusätzlich wurden Duplexeinheiten mit ein oder zwei benachbarten **Pyr**:**Me** oder **Pyr′**:**H** Basenpaare synthetisiert. Diese Duplexeinheiten waren bei Raumtemperatur waren thermisch stabil.

Interessanterweise konnten nur die Pyrenacetylidnukleotide, aber nicht die entsprechenden Pyrennukleotide durch "interstrand-stacking" innerhalb der GNA-Duplexeinheit einen starken Excimer bilden (Abbildung 8.1B). Dieser wurde als Metallionensensor verwendet, indem ein Metall-vermittelten Basenpaar eingebaut wurde. Dabei wurde ein Hydroxypyridon homo-Basenpaar (**M**:**M**) oder ein Hydroxypyridon-pyridylpurine hetero-Basenpaar (**M**:**P**) verwendet. Abbildung 8.2 zeigt, dass mit **D15** und **D19** sehr empfindliche und selektive Cu^{2+} "turn-on" Fluoreszenzsensoren erhalten wurden.

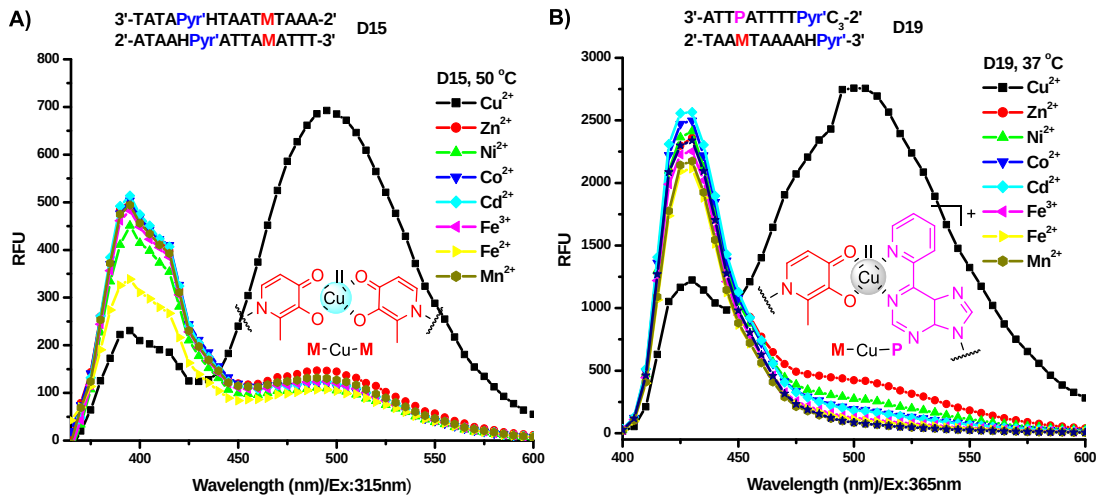

Abbildung 8.2 (A) Metallionen-Selektivität des Sensors **D15**. (B) Metallionen-Selektivität des Sensors **D19**.

Kapitel 4 beschäftigt sich mit dem Einbau von Porphyrinacetylidnukleotid (**P**) in GNA-Duplexeinheiten gegenüber von nichtbasischem Ethylenglykol. Die Verbindungen wurden durch UV-Schmelzkurvenanalyse, UV-Vis Spektroskopie, Fluoreszenzspektroskopie und Circulardichroismus analysiert.

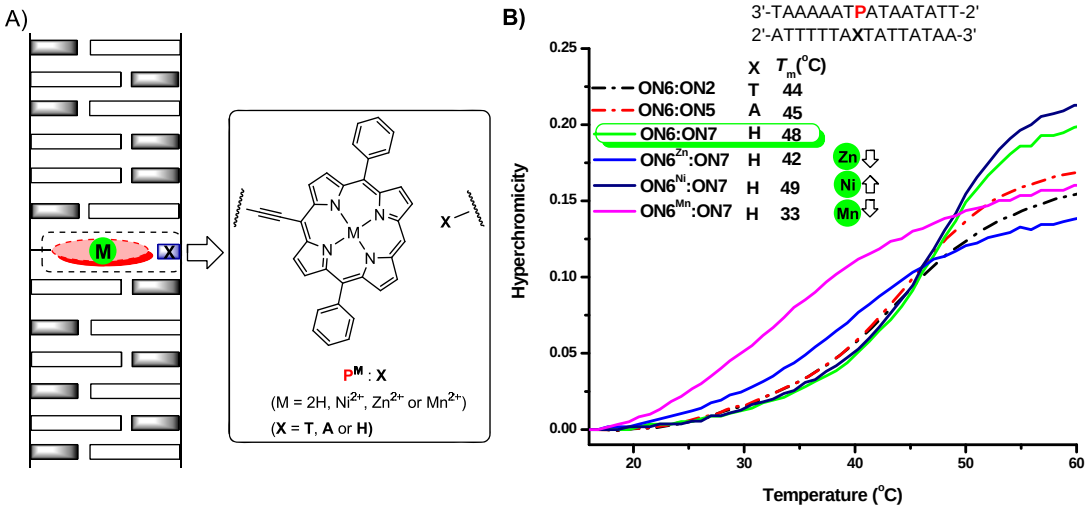

Abbildung 8.3 (A) Struktur des in Kapitel 4 verwendeten $\mathbf{P^M}$:**X** Basenpaars. (B) UV-Schmelzkurven von GNA-Duplexeinheiten mit $\mathbf{P^M}$:**X** Basenpaar.

Die modifizierten Duplexeinheiten zeigten geringe thermische Stabilität, diese konnte aber durch Koordination an Zink(II)-, Mangan(II)- oder Nickel(II)ionen in **P** gesteigert werden (Abbildung 8.3B).

Darüber hinaus boten die GNA-Duplexeinheiten ein geeignetes Gerüst um zwei Porphyrine in engen Kontakt zu bringen, woraus Wechselwirkungen zwischen den beiden Porphyrinen resultierten, die jeweils an verschiedenen Metallionen gebunden waren. Die klare Änderung der Soretbanden, die von einer Blauverschiebung begleitet war und die Abnahme der Fluorenzintensität durch Bildung einer Duplexeinheit (Abbildung 8.4B) zeigte, dass eine Wechselwirkung im Grundzustand zwischen zwei Porphyrineinheiten in der GNA auftrat. Dabei handelte es sich um eine "face-to-face" (H-dimer) Wechselwirkung.

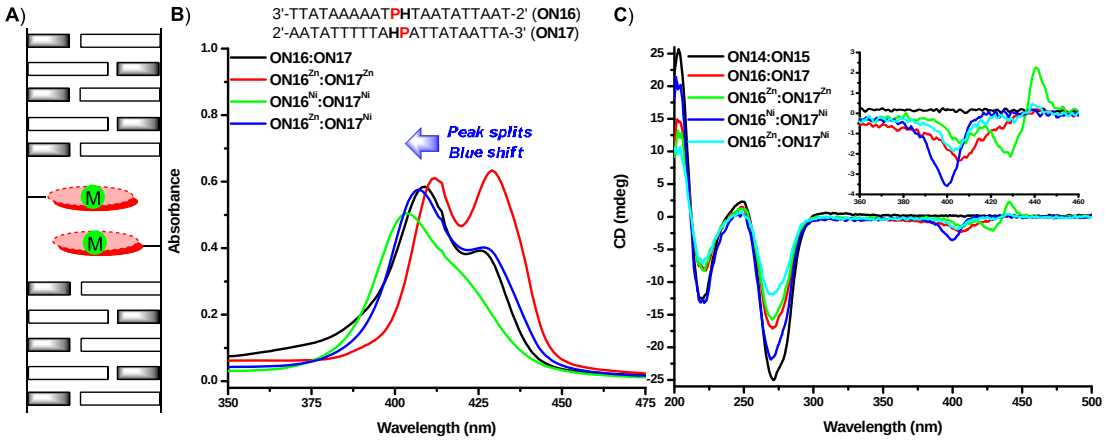

Abbildung 8.4 (A) Position von zwei $\mathbf{P^M}$:**H** in der Mitte der GNA-Duplexeinheit **ON16**:**ON17**. (B) UV-Vis-Spektren der Soretbande Region von Porphyrin in GNA-Duplexeinheit. (C) CD-Spektren von GNA-Duplexeinheiten. Der Einschub zeigt die vergrößerte Soretbanden Region von porphyrin.

In Kapitel 5 wurden die Donor-Akzeptor enthaltenden Chromophorsysteme, die hauptsächlich aus Perylenbisimid- (**B**) und Porphyrinbausteinen (**P**) bestehen, in GNA-Duplexeinheiten eingebunden (Abbildung 8.5A).

GNA-Duplexeinheiten mit **B-Pyr**, **B-Pyr′**, **B-Pe′** und **B-P** wurden thermisch untersucht. Dabei zeigte sich, dass das **B-P** Paar die GNA-Duplexeinheiten um zusätzlich 10 °C im Vergleich zur Schmelztemperatur der nativen GNA-Duplexeinheit stabilisieren konnte. Die deutlich erhöhte Stabilität der Duplexeinheit, zusammen mit der rotverschobenen Absorptionsbande und das induzierte CD-Signal bei der Soretbande deuteten auf eine "π-π stacking" Wechselwirkung der **B-P** Paaren zwischen beiden Strängen in der Duplexeinheit.

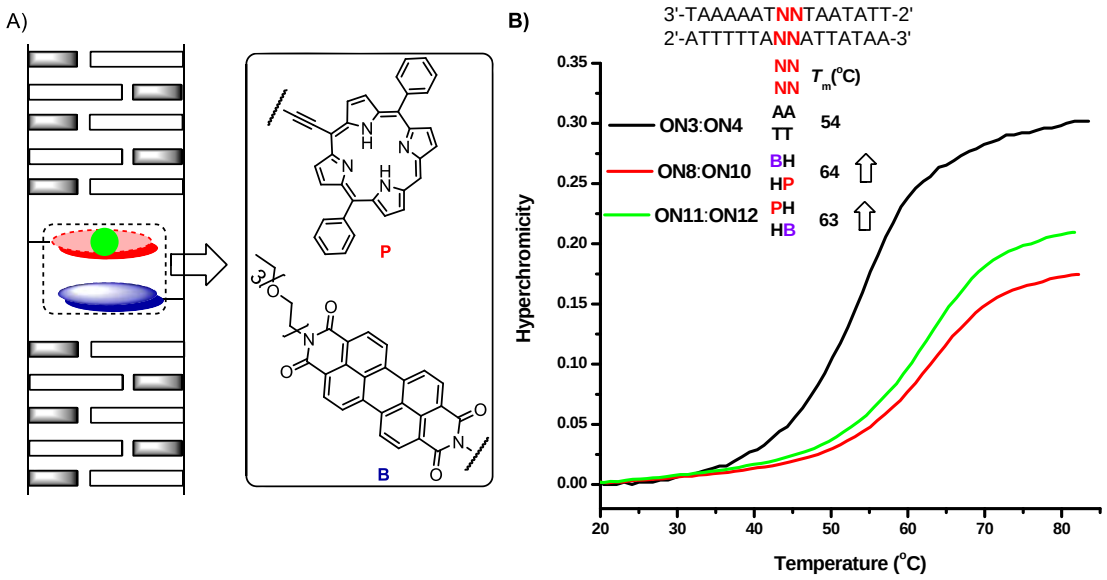

Abbildung 8.5 (A) Struktur des in Kapitel 5 verwendetem **B**:**P** Basenpaares. (B) UV-Schmelzkurven von GNA-Duplexeneinheiten mit einem **B**:**P** Basenpaar.

Anschließend wurden die Systeme mit Porphyrin und **PBI** Bausteine untersucht. Wie Abbildung 8.6 B zeigt, erhöhte sich die Intensität des CD-Signals mit der zunehmenden Anzahl von Chromophoreinheiten. Diese kontinuierliche Verschiebung resultiert aus der Wechselwirkung zwischen **PBI** und Porphyrin, was eine hochgeordnete Helixstruktur zur Folge hat.

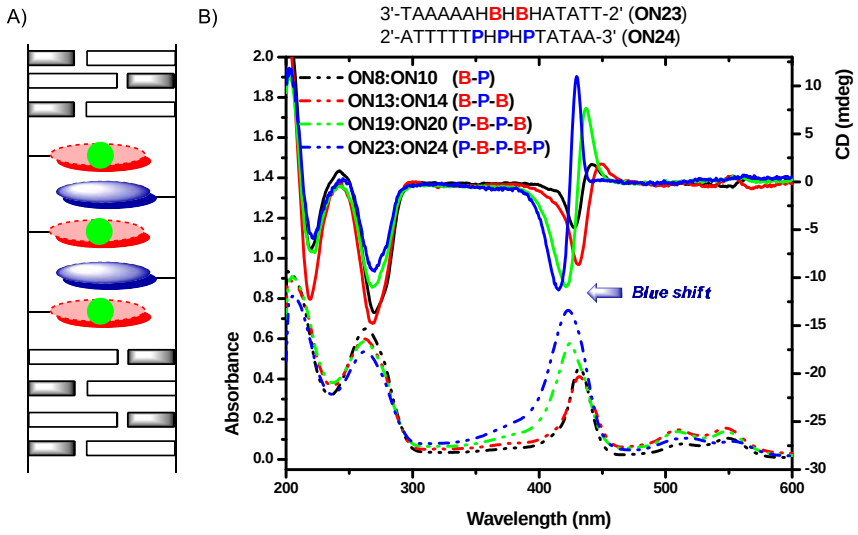

Abbildung 8.6 (A) Position von **B** und **P** in der Mitte der GNA-Duplexeinheit **ON23**:**ON24**. (B) CD-und UV-Vis-Spektren der Duplexeinheiten mit zentralen Chromophorkernen: **B-P**, **B-P-B**, **P-B-P-B** und **P-B-P-B-P**.

Angesichts der deutlich verringerten Ausbeute an modifiziertem GNA-Strang mit dem mehrfach eingebauten Chromophor, wurde photochemisches Anbinden von GNA entwickelt. In Kapitel 6 wurde Anthracen in GNA als photoreaktives Zentrum eingeführt (Abbildung 8.7A). Bei der Duplexbildung, näherten sich die beiden angrenzenden Anthracen-Nucleobasen einander und es wurde erwartet, dass die Duplexeinheit eine Haarnadelstruktur durch Anthracencyclodimerisierung als Folge der Bestrahlung von Licht (366 nm) erzeugt hat.

Die Reaktion wurde im Hinblick auf drei Aspekte untersucht, nämlich templatgestütztes GNA-Anbinden, Crosslinking zwischen den Strängen in der Mitte der GNA-Duplexeinheit und "end capping" der Duplexeinheit.

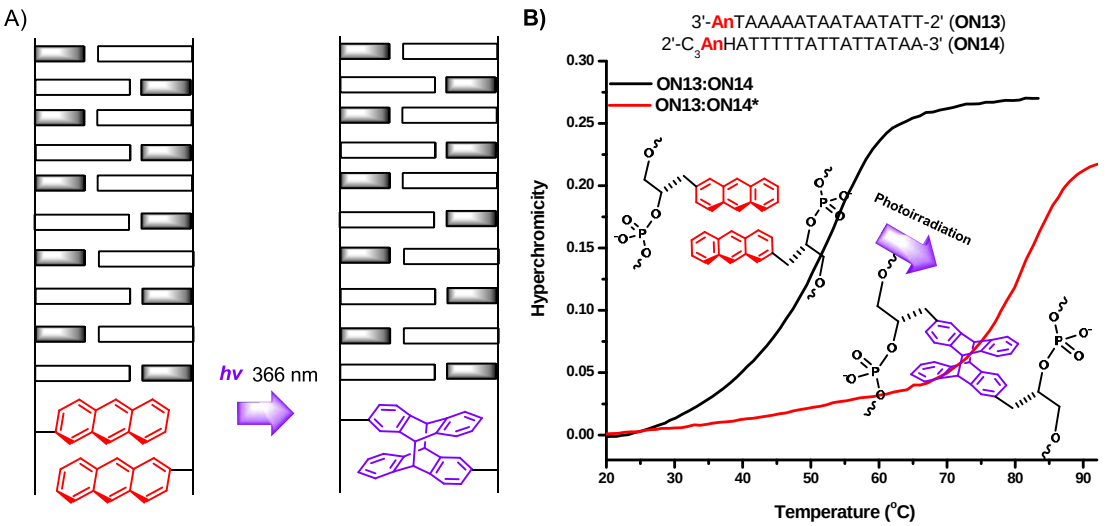

Abbildung 8.7 (A) Photochemische Reaktion von GNA über Anthracen-cyclodimerisierung. (B) UV-Schmelzkurven der GNA-Einheiten vor bzw. nach dem "end-capping".

Die templatgestützte Photoreaktion hat aufgrund ineffizienten Dimerisierung von Anthracen in Tandemduplexeinheiten der nicht stattgefunden. Allerdings erwiesen sich sowohl das Crosslinking in der Mitte des Duplexes, als auch "end-capping" des Duplexes als möglich. Die erzeugten intramolekularen Duplexeinheiten zeigten eine hohe Schmelztemperatur (Abbildung 8.7B), was im Einklang mit der Bildung eines intramolekularen Duplex mit einer Haarnadelstruktur steht.

In dieser Studie wurden GNA-Duplexeinheiten als Gerüst für das Design von

selbstangeordneten und selbstorganisierten Architekturen verwendet. Mehrere Chromophore wurden erfolgreich in GNA-Duplexeinheiten eingeführt. GNA erwies sich als und generelles Duplexgerüst für die definierte Chromophororganisation.